



SCHOOL of
GRADUATE STUDIES
EAST TENNESSEE STATE UNIVERSITY

East Tennessee State University
Digital Commons @ East
Tennessee State University

Electronic Theses and Dissertations

Student Works

5-2011

On The Cranial Osteology of *Eremiascincus* and Its Use For Identification.

William B. Gelnaw
East Tennessee State University

Follow this and additional works at: <https://dc.etsu.edu/etd>



Part of the [Paleontology Commons](#)

Recommended Citation

Gelnaw, William B., "On The Cranial Osteology of *Eremiascincus* and Its Use For Identification." (2011). *Electronic Theses and Dissertations*. Paper 1294. <https://dc.etsu.edu/etd/1294>

This Thesis - Open Access is brought to you for free and open access by the Student Works at Digital Commons @ East Tennessee State University. It has been accepted for inclusion in Electronic Theses and Dissertations by an authorized administrator of Digital Commons @ East Tennessee State University. For more information, please contact digilib@etsu.edu.

On the Cranial Osteology of *Eremiascincus*, and Its Use for Identification

A thesis
presented to
the faculty of the department of Biological Sciences
East Tennessee State University

In partial fulfillment
of the requirements for the degree
Master of Sciences in Biology

by
William B. Gelnaw
May 2011

James Mead, Chair
Blaine Schubert
Stephen Wallace

Keywords: Squamata, Morphometrics, Lizards, Skull

ABSTRACT

On the Cranial Osteology of *Eremiascincus*, and Its Use for Identification

by

William B. Gelnaw

A persistent problem for Australian paleontology has been a lack of diagnostic characters for identifying lizard fossils. *Eremiascincus* is one of the most widespread genera in Australia, so it was examined for distinguishing features and how it fits into a model of skink evolution. Skulls of *Eremiascincus* were examined within five separate contexts: 1) a description of the cranial osteology, 2) a qualitative comparison of individual cranial elements of *Eremiascincus* to closely related *Ctenotus*, 3) a description of the cranial allometry in *Eremiascincus* using linear morphometrics, 4) using cranial morphometrics of skinks to deduce their phylogeny, and 5) using geometric morphometrics to distinguish between individual elements of *Eremiascincus* and *Ctenotus*. Although linear morphometrics is adept at describing allometric changes to the skull during ontogeny, it only displayed a phylogenetic signal for small, closely related groups. Also, geometric morphometrics was just as capable distinguishing *Eremiascincus* from *Ctenotus* as qualitative characters.

CONTENTS

	Page
ABSTRACT	2
LIST OF TABLES	6
LIST OF FIGURES	7
Chapter	
1. INTRODUCTION	9
A Historical Review of Australian Fossil Skinks and the Systematic Status of <i>Eremiascincus</i> (Squamata: Scincidae).....	9
2. THE CRANIAL OSTEOLOGY OF <i>EREMIASCINCUS</i>	18
Introduction.....	18
Materials and Methods.....	21
Results.....	24
Skull Roof and Suspensorium	24
Palatal Complex	47
Neurocranium	56
Teeth	64
Lower Jaw	66
Discussion	78
Acknowledgements.....	79
Literature Cited	80
3. COMPARING THE CRANIAL OSTEOLOGY OF TWO AUSTRALIAN SPHENOMORPHUS GROUP SKINKS: <i>EREMIASCINCUS</i> AND <i>CTENOTUS</i>	83
Introduction	84
Materials and Methods	86
Results	110
Discussion	120
Literature Cited	122
4. ANALYZING SKULL SHAPE THROUGH ONTOGENY IN <i>EREMIASCINCUS</i> USING TRADITIONAL MORPHOMETRICS	124

Introduction	124
Methods	126
Results and Discussion	129
Literature Cited	135
5. ASSESSING THE PHYLOGENETIC SIGNAL OF SKULL SHAPE IN SKINKS FROM A MORPHOMETRIC DATASET	138
Introduction	138
Materials and Methods	142
Results	148
Discussion	164
Literature Cited	168
6. USING GEOMETRIC MORPHOMETRICS TO DISTINGUISH INDIVIDUAL ELEMENTS OF <i>EREMIASCINCUS</i> FROM <i>CTENOTUS</i>	174
Introduction	174
Materials and Methods	176
Landmark Placement	177
Statistical Analyses	189
Results	191
Discussion	205
Literature Cited	213
REFERENCES	216
APPENDIXES.....	227
APPENDIX A: Key to Abbreviations	227
APPENDIX B: Dataset Used in the Cladistic Analysis	231
APPENDIX C: Linear Measurements of Lizard Skulls	236
VITA.....	251

LIST OF TABLES

Table	Page
2.1 Specimens of <i>Eremiascincus</i> that were examined	22
3.1 List of the specimens used for comparison.....	87
3.2 Characters selected by Bayesian analysis.....	119
4.1 Specimens of <i>Eremiascincus</i> that were examined.....	127
4.2 Test for differences between <i>Eremiascincus fasciolatus</i> and <i>E. richardsonii</i>	129
4.3 Slope, y-intercept, and coefficients of correlation of each of lines of best fit for all 15 dimensions of skull shape.....	130
5.1 List of species used in the analysis with their respective substrate use classification and the literature source of that classification.....	150
5.2 Individual loading of each variable on the first four principal components	161
6.1 Specimens used for comparison, with snout-vent length where available.	178
6.2 Regression coefficients (B) and coefficients of determination (R^2) for the stepwise discriminant scores correlated with the length of the frontal in mm.	191

LIST OF FIGURES

Figure	Page
1.1 <i>Eremiascincus richardsonii</i>	10
1.2 Map of sites in Australia where skink fossils have been found.	15
2.1 Skull of <i>Eremiascincus richardsonii</i>	23
2.2 Left nasal bone	25
2.3 Frontal of <i>Eremiascincus richardsonii</i>	27
2.4 Parietal of <i>Eremiascincus richardsonii</i>	30
2.5 Left premaxilla of <i>Eremiascincus richardsonii</i>	33
2.6 Left maxilla of <i>Eremiascincus richardsonii</i> in medial view.	36
2.7 Left maxilla of <i>Eremiascincus richardsonii</i> in dorsal view	37
2.8 Right jugal of <i>Eremiascincus richardsonii</i>	39
2.9 Right postfrontal with a fused postorbital of <i>Eremiascincus richardsonii</i>	41
2.10 Left quadrate of <i>Eremiascincus richardsonii</i>	44
2.11 Left prefrontal of <i>Eremiascincus richardsonii</i>	46
2.12 Vomer of <i>Eremiascincus richardsonii</i>	48
2.13 Left palatine of <i>Eremiascincus richardsonii</i>	50
2.14 Left pterygoid of <i>Eremiascincus richardsonii</i>	53
2.15 Left ectopterygoid of <i>Eremiascincus richardsonii</i>	55
2.16 Braincase of <i>Eremiascincus richardsonii</i>	57
2.17 Lower jaw of <i>Eremiascincus richardsonii</i>	68
2.18 Left articular complex of <i>Eremiascincus richardsonii</i>	69
2.19 Left coronoid of <i>Eremiascincus richardsonii</i>	73
2.20 Left dentary of <i>Eremiascincus richardsonii</i>	77
3.1 Distinguishing characters on a left articular complex	91
3.2 Distinguishing characters on a left coronoid	93
3.3 Distinguishing characters on a left dentary.	95
3.4 Distinguishing characters on a frontal.. ..	97
3.5 Distinguishing characters on a maxilla.. ..	100
3.6 Distinguishing characters of a left palatine.	102
3.7 Distinguishing characters of the parietal.	104

3.8 Distinguishing characters of a postfrontal.....	106
3.9 Distinguishing characters of a pterygoid.....	108
3.10 Distinguishing characters of the quadrate.....	110
3.11 Shortest tree derived from analysis of all characters for all elements and specimens.	111
4.1 Linear measurements of the whole skull of a lizard.....	128
4.2 Relative widths of the skull of <i>Eremiascincus</i> at the quadrates and jugals, as well as depths of the skull measured at the orbit, pterygoid and quadrate.....	131
4.3 Relative lengths of facial and cranial portions of the skull, showing allometric growth with a faster growing facial region.....	132
4.4 Relative lengths of the orbital, temporal and rostral regions of the skull compared to the total length of the skull.....	133
4.5 Proportions of the lower jaw	134
5.1 Linear measurements of the whole skull of a lizard.....	143
5.2 Plot of the first two principle component scores for all anguids, teiids and skinks measured.....	151
5.3 Plot of the first two principal component scores for all skinks measured.....	152
5.4 Separating groups of skinks on the basis of discriminant scores.....	153
5.5 Separating the species of <i>Eremiascincus</i> on the basis of discriminant scores	154
5.6 Combined phylogenetic tree of skinks used in the morphometric analysis.....	156
5.7 Phylogeny of skinks plotted onto the first two principal components of the cranial measurements.....	157
5.8 Phylogeny of the Lygosominae plotted onto the first two principal components of their cranial measurements.....	158
5.9 Phylogeny of <i>Plestiodon</i> plotted over the first two principal components of their cranial measurements.....	159
5.10 Phylogeny of the Afro- Eurasian skinks plotted over the first 2 principal components of their cranial measurements.....	160
6.1 Coronoid landmarks.....	180
6.2 Dentary landmarks	181
6.3 Frontal landmarks.....	182

6.4 Maxilla landmarks	183
6.5 Palatine landmarks	184
6.6 Parietal landmarks.....	185
6.7 Postfrontal landmarks.....	186
6.8 Pterygoid landmarks.....	187
6.9 Quadrate landmarks.....	188
6.10 Discriminant scores of <i>Eremiascincus</i> and <i>Ctenotus</i> for each of the 9 elements examined	189
6.11 Stepwise discriminant scores of <i>Eremiascincus</i> and <i>Ctenotus</i> for each of the 9 elements examined.....	190
6.12 Plot of the first two principal components of coronoid landmark data	192
6.13 Plot of the first two principal components of dentary landmark data.....	194
6.14 Plot of the first two principal components of frontal landmark data.....	195
6.15 Plot of the first two principal components of maxilla landmark data.....	196
6.16 Plot of the first two principal components of palatine landmark data.....	198
6.17 Plot of the first two principal components of parietal landmark data.....	200
6.18 Plot of the first two principal components of postfrontal landmark data.....	201
6.19 Plot of the first two principal components of pterygoid landmark data.....	202
6.20 Plot of the first two principal components of quadrate landmark data.....	203

CHAPTER 1

INTRODUCTION

A Historical Review of Australian Fossil Skinks and the Systematic Status of *Eremiascincus*

(Squamata: Scincidae)

Skinks (Scincidae) are a group of typically small, armored lizards (Reptilia: Squamata), found on every continent except Antarctica. In Australia, skinks are ubiquitous. The most recent review of Australian lizard fauna (Wilson and Swan 2003) recognizes more than 370 species of skinks. Australian skinks occupy a wide range of ecological roles and habitats, from fully arboreal forms with strong limbs, to legless burrowers; from moist tropical habitats, to arid desert. As such, Australian skinks represent an excellent model for the study of evolution in squamates as a whole. Understanding the evolution of skinks in Australia requires an understanding of the modern diversity of the group, and of how deep the branches within the lineage extend into the past, which requires the ability to identify members of the group in the fossil record. Unfortunately, there is a dearth of information on the identification of fossil skinks. This thesis will focus on one genus of Australian skink, *Eremiascincus* (Figure 1.1), and explore the osteology of its skull through several avenues. The chapters here will examine the detailed osteology of each element and develop discrete, qualitative and quantitative characters for differentiating *Eremiascincus* from other Australian skinks, as well as examine the growth of the skull and how the shape of the skull relates to the ecology of the lizard.



Figure 1.1 *Eremiascincus richardsonii*, illustrated by Rebecca Caviness for this thesis.

First though, it is important to explore how *Eremiascincus* fits within the current knowledge of skinks. The diversity of skinks is almost unparalleled among the tetrapods, only rivaled in number of species by rodents and bats. Worldwide, there are four recognized subfamilies of skinks, the: Scincinae, Acontinae, Lygosominae and Feylininae (Greer 1970). The Scincinae has long been recognized as a paraphyletic group that gave rise to the other three subfamilies (Greer 1970; Whiting et al. 2003; Brandley 2005). All skinks in the Australian region are in the subfamily Lygosominae, which was erected by Mittleman (1952) and later rediagnosed by Greer (1970). Originally, the single genus *Lygosoma* (Boulenger, 1887) encompassed all of what is now the Lygosominae, with finer classifications at the subgeneric level. Since then, smaller groups were raised to the generic level and separated from the core group, including *Lygosoma* itself. The remaining core became known as *Sphenomorphus*, and subsequent taxonomic revision further split away genera, so that because of continual subdivision, there are no skinks in Australia still attributed to the genus *Sphenomorphus* (Storr 1964; Greer 1979a, 1983, 1990).

Greer (1979b) subdivided the Lygosominae into the *Egernia*, *Eugongylous* and *Sphenomorphus* groups based on morphology of the palate and scutellation patterns, and hypothesized two separated colonizations of Australia by skinks from the north. Genetic work (Honda et al. 1999; Honda et al. 2000) further subdivided the Lygosominae to include a *Lygosoma* group and a *Mabuya* group. Neither of the new groups occur in Australia, but do support the hypothesis of a separate invasion of Australia for each of the groups that do occur there. The molecular work of Baverstock and Donnellan (1990) support a Paleocene split of the *Sphenomorphus* group from the common ancestor of the *Egernia* and *Eugongylous* groups, and suggest a latest Mesozoic or early Cenozoic arrival and

diversification of skinks in Australia. Furthermore, molecular work by Gardner et al. (2008) supports a long history of *Egernia* in Australia.

Eremiascincus belongs to the Australian clade within the *Sphenomorphus* group, which is monophyletic (Reeder 2003; Skinner 2007) and currently made up of 13 genera: *Anomalopus*, *Calyptotis*, *Coeranoscincus*, *Coggeria*, *Ctenotus*, *Eremiascincus*, *Eulamprus*, *Glaphyromorphus*, *Hemiergis*, *Lerista*, *Ophioscincus*, and *Saiphos* (Pianka and Vitt, 2003). The primary method of identification for each of these has been the differences in color patterns and the arrangement of head scales (Storr 1964; Greer 1979a & b, 1990).

The genus was expanded to include one newly discovered species and eight species that had previously composed the *Glaphyromorphus isolepis* species group (Mecke et al. 2009). However, the study here is concerned only with the two species originally included by Greer in the 1979 diagnosis of the genus. The newly included species have a much smaller geographic distribution, and those that were previously included in *Glaphyromorphus* have a distinct physical appearance and ecology. The species that were previously in *Glaphyromorphus* are smaller, live in the tropics and tend to burrow through leaf litter.

Among Australian skinks, *Eremiascincus richardsonii* and *E. fasciatus* are the two most geographically widespread species, occurring throughout the arid and semi-arid regions of the interior of the continent, in all six territories (Wilson and Swan 2003). They are ambush predators that bury themselves in the sand to wait for passing insects or smaller lizards. To evade predators, they also employ a sand-swimming behavior whereby they dives head first into the soft sand and uses lateral undulations of the body to swim

through the sand the same way another lizard might swim through water (Greer 1979a). Until recently, *Eremiascincus* included only two species: *E. fasciolatus* and *E. richardsonii*.

Eremiascincus is well nested within a phylogeny of the *Sphenomorphus* group of skinks (Reeder 2003; Skinner 2007), meaning that the occurrence of the genus in the fossil record would serve as a valuable calibration point for molecular clock estimates of the divergence of nodes within the group. However, there is no current method for differentiating the skeletal remains of *Eremiascincus* from other members of the Lygosominae. Greer (1970) diagnosed the Lygosominae on the basis of a combination of 16 osteological characters of the dermatocranium, palatal region, and the lower jaw. Of these though, among skinks, only the characters related to the formation of the secondary palate and the fusion of the frontals are unique to the Lygosominae. The others are mosaically distributed through the other subfamilies. Below the level of the Lygosominae, few taxa have had osteological characters identified for differentiating them from their close relatives (Williams 1999; Hutchinson and Scanlon 2009; Hollenshead 2010)

Eremiascincus fasciolatus and *E. richardsonii* are characterized by Greer (1979) as having a series of low, longitudinal ridges along the dorsum, though these may be reduced. The color pattern is highly variable, but both species have a pale yellow or off-white to medium brown ground color with darker cross bands. *Eremiascincus richardsonii* has fewer than 13 dark bands across the body that are about as wide as the light ground colored bands, while *E. fasciolatus* is distinguished from *E. richardsonii* by having “more numerous, less regular and narrower body bands, and more numerous, more regular and narrower caudal bands” (Storr 1967: 13).

Patterns of squamation are however of no use in the identification of fossil taxa. Although skinks do have a bony osteoderm in each scale, lizards readily disarticulate after death and the process of screen washing, by which small fossils are recovered, is not conducive to discovering the articulation between skeletal elements (J. I. Mead pers. com.; Price and Webb 2006). Furthermore, within the Lygosominae, there is a mosaic distribution of osteological characters throughout the skeletons so that many of the characters are most informative in combination and are much less useful when regarding an isolated bone. Greer (1979) included 12 osteological characters in his description of *Eremiascincus*, but not in the diagnosis because most of them are variably shared with other taxa. For these reasons, isolated bones will be assessed for a large number of character states, so that the likelihood of another skink having the same combination of characters becomes infinitesimal. Greer (1979a, 1989) also comments that the dorsoventral depth of the skull is variable and appears dependant on the substrate in which the lizard lives. *Eremiascincus* typically has a deep head, but it is flattened when the lizard lives in open habitats with fine-grained sand. The variability of head shape, and its bearing on fossoriality will be examined in the third and fourth chapters of this thesis.

There are several localities in Australia that have produced fossils attributed to skinks (Figure 1.2). However, the scarcity of diagnostic osteological characters for most elements in the skulls of Australian skinks, has led to a disproportionate representation of members of the *Egernia* group in the fossil record. *Sphenomorphus* group skinks account for about 60% of the modern taxonomic diversity, yet their fossils are largely absent from the literature. The majority of characters developed for identifying the lower taxonomic levels of Australian skinks apply to the *Egernia* group (Williams 1999; Hutchinson and

Mackness 2002; Hutchinson and Scanlon, 2009), and concurrent with that, the majority of fossils identified also belong to the *Egernia* group.

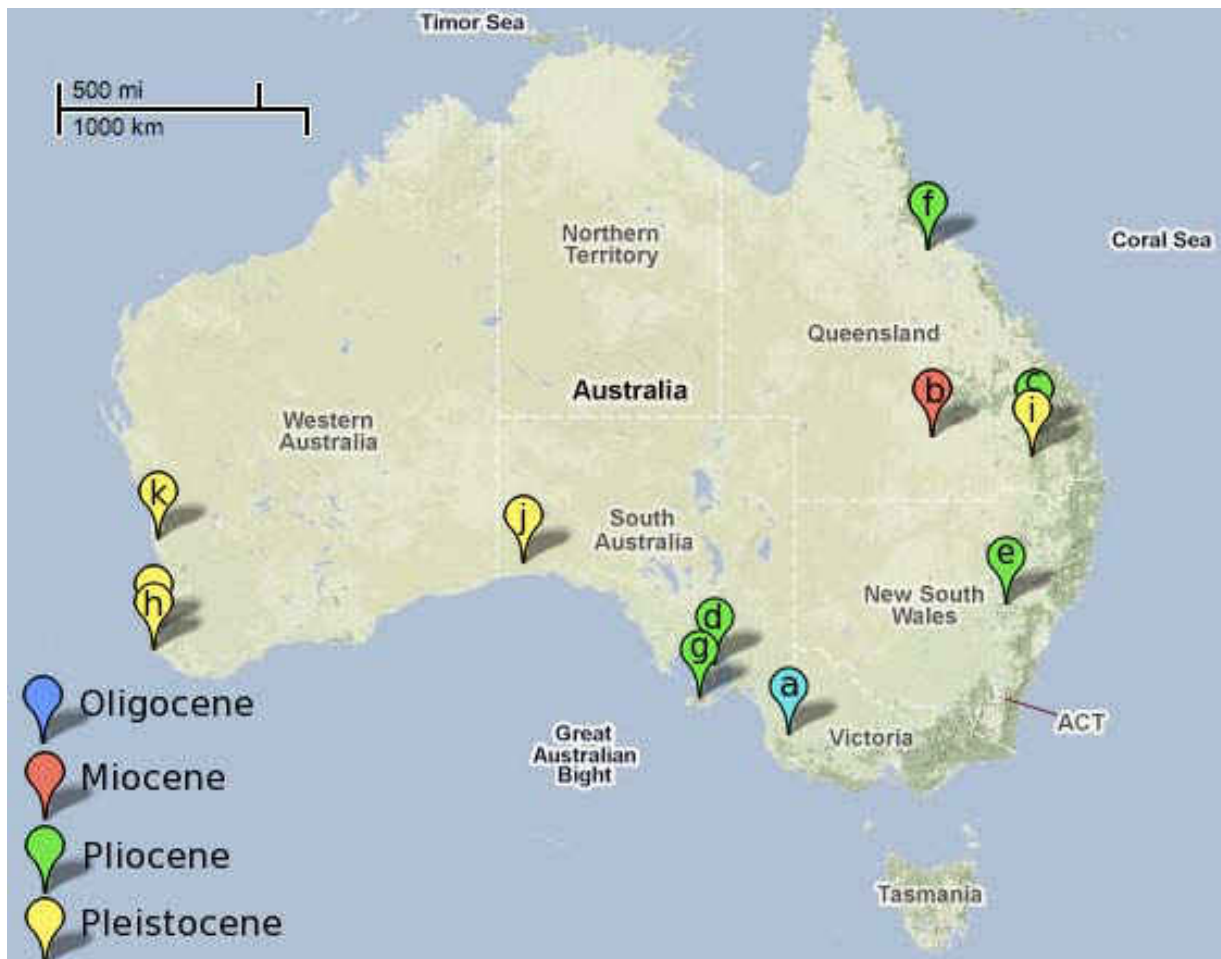


Figure 1.2. Map of sites in Australia where skink fossils have been found. A) Etadunna Formation and Victoria Cave, b) Riversleigh, c) Chinchilla local fauna, d) Curramulka local fauna, e) Wellington Cave, f) Bluff Downs local fauna, g) Kangaroo Island, h) Devil's Lair and Yallingup Caves, i) Darling Downs local fauna, j) Horseshoe Cave, and k) Hastings Cave.

The oldest lacertilian fossil in Australia is a femur tentatively attributed to a skink from the Eocene Trundle Formation of Queensland (Hocknull 2000). The oldest definitive skink on the continent was reported by Martin and colleagues (2004) and attributed to the *Egernia* group from the Oligocene of the Etadunna Formation, South Australia. Estes (1984) had earlier reported *Egernia* from the Miocene of the same formation. Miocene

scincid material from Riversleigh (Queensland) is relatively abundant, but only preliminarily described (Hutchinson 1992; Shea and Hutchinson 1992). According to these studies, the Riversleigh material includes a gracile and robust morph within the *Sphenomorphus* group, four different morphs within the *Egernia* group, and one morph of the *Eugongylous* group. There are records of Pliocene *Tiliqua* spp. from the Chinchilla local fauna of Queensland (Hutchinson and Mackness 2002), the Curramulka local fauna (Pledge 1992), and Wellington caves (Hand et al. 1988). *Egernia* and *Eulamprus* have been documented from the Bluff Downs local fauna (Mackness and Hutchinson 2000), and fossil *Cyclodomorphus* are known from several localities in eastern Queensland (Hutchinson and Mackness 2002; Hocknull 2005). Pleistocene *Tiliqua* spp. have been found at Victoria Cave, (Smith 1976), Kangaroo Island (Smith 1982), Tantanoola Cave (Tindale 1933), Cement Hills (Bartholomai 1977), caves throughout eastern Queensland (Hocknull 2005), and Devil's Lair cave (Hollenshead et al. 2010). Pleistocene *Egernia* and *Eulamprus* have also been reported from Victoria cave (Smith 1976; Williams 1999), *Egernia* at Kangaroo Island (Smith 1982), and *Liopholis* spp., *Egernia* spp. and *Lissolepis* spp. at Devil's Lair cave (Hollenshead et al., in press). Fossil lizard material has been attributed to the *Sphenomorphus* group from Quaternary deposits throughout Australia (Price and Webb 2006; Molnar 1991) but so far have not received more refined identifications.

It is the aim of this thesis that fossils of *Eremiascincus* be discernable from other taxa. Furthermore, the reader should take away methods that are applicable to other taxa, so that the osteological information on poorly understood groups may grow into a wealth of understanding. It is only once the most basic problem of identifying material of each taxon has been solved, that the higher order questions about the tempo and mode of

evolution may be addressed. I look forward to a day when, using skinks as a model, predictive hypotheses about biogeography and evolution can be tested on datasets culled from both modern and fossil representatives.

CHAPTER 2

The Cranial Osteology of *Eremiascincus*

William B. Gel naw

The Don Sundquist Center for Excellence in Paleontology, East Tennessee State University,
Johnson City, Tennessee 37614, United States

Abstract - The skull, lower jaw and each of their constituent elements are described in detail for *Eremiascincus richardsonii* and *E. fasciolatus*. The description includes the arrangement of elements, their shape, including some observed variations, and the placement of important structures on those elements.

Introduction

Among Australian skinks, *Eremiascincus* is the most widespread genus, occurring throughout the arid and semi-arid regions of the continent's interior (Greer 1979a; Wilson and Swan 2003). *Eremiascincus* is an ambush predator that buries itself in the sand to wait for passing insects or smaller lizards. To evade predators, it employs a sand-swimming behavior whereby it dives head first into loose sand and uses lateral undulations of its body to swim through the sand the same way another lizard might swim through water. Until recently (Mecke et al. 2009), *Eremiascincus* included only two species: *E. fasciolatus* and *E. richardsonii*. The genus was expanded to include one new species and eight species that had been previously included in the genus *Glaphyromorphus*. However, the description

here will deal only with the two species originally included by Greer's (1979a) diagnosis of the genus. The new species described by Mecke and colleagues (Mecke et al. 2009) has a very small range, and those that were previously included in *Glaphyromorphus* have a very different appearance and ecology from *E. richardsonii* and *E. fasciolatus*. It is for these reasons that the description of the cranial osteology of *Eremiascincus* presented here, will only include the two species originally included in the genus (Greer 1979a). *Eremiascincus musivus*, which was recently named and described by Mecke and colleagues (2009) was not available for osteological study. On the basis that *E. musivus* is similar in size and ecology to *E. richardsonii* and *E. fasciolatus*, it would be anticipated that *E. musivus* would be very similar to the other two. Future work on *E. musivus* should confirm or refute this assertion.

Within the family Scincidae, *Eremiascincus* belongs to the subfamily Lygosominae (Mittleman 1952). Greer (1979b) formally subdivided the Lygosominae into the *Egernia*, *Eugongylous* and *Sphenomorphus* groups, to which *Eremiascincus* belongs. Within the *Sphenomorphus* group there are currently 13 genera in Australia: *Anomalopus*, *Calyptotis*, *Coeranoscincus*, *Coggeria*, *Ctenotus*, *Eremiascincus*, *Eulamprus*, *Glaphyromorphus*, *Hemiergis*, *Lerista*, *Ophioscincus* and *Saiphos*. However, few of these genera have received any osteological description whatsoever. The primary method of classification so far has been the differences in patterns of head scales (Storr 1964; Greer 1979a, 1979b, and 1990).

Both *Eremiascincus fasciolatus* and *E. richardsonii* are characterized by Greer (1979a) as having a series of low, longitudinal ridges along the dorsum, though these may be reduced. The color pattern is highly variable, but both species have a pale yellow or off-white to medium brown ground color with darker cross bands. *Eremiascincus richardsonii* has fewer than 13 dark bands across the body, which are about as wide as the light ground

colored bands. *Eremiascincus fasciolatus* is distinguished from *E. richardsonii* by having “more numerous, less regular and narrower body bands, and more numerous, more regular and narrower caudal bands” (Storr 1967: pg 13). Storr (1964) stated that within Western Australia, there is no variation in the color pattern related to geography. However, the discovery and description of *Eremiascincus musivus* on the Pilbara coast of Western Australia, shows that there is definitely more variation in *Eremiascincus* than Storr had thought. *Eremiascincus musivus* (Mecke 2009) was diagnosed on the basis of its spotted pattern and it seems likely that the variation seen in other populations of *Eremiascincus* will result in further subdivision of the genus. The description presented here is not intended to represent the total variation in *Eremiascincus*, but rather to provide a detailed general description that future work may be compared to. The specimens studied here were taken from two localities. Articulated skulls of both species came from specimens from central South Australia, and the disarticulated *E. richardsonii* came from a single location at the Mt Gibson station, Western Australia. As such, specific identity is certain, but regional variation may not be fully represented.

Greer (1979a) included 12 osteological characters in his description and the work presented here is intended to fill out the osteological information to the fullest extent possible. This paper will be composed of a description of the cranial osteology, both of the skull form and arrangement as well as a detailed individual descriptions of 25 elements within the skull. For the sake of organization, the skull is here divided into the dermal roof with the suspensorium, the palatal region, neurocranium, and lower jaw.

Materials and Methods

Study was conducted on the articulated skulls of 14 members of both species of *Eremiascincus* came from specimens collected in central South Australia, and 15 disarticulated *E. richardsonii* came from a single well at the Mt. Gibson station, Western Australia. The specimens represent a broad size series, and by inference, an ontogenetic series as well. Specimens of *Eremiascincus* used in this description are listed in Table 2.1. Additionally, the following skinks were used for comparison and to confirm previously published accounts:

Skincinae

Scincus scincus

Acontinae

Acontias

Lygosominae

Mabuya fasciata

Ctenotus mimetes, *C. robustus*, *C. severus* and *C. schomburgkii*

Egernia multiscutata (from photographs) and *E. whitii* (from photographs)

Measurements of the frontal and parietal were taken by photographing the elements and then digitally measuring them using the GIMP graphics suite. Terminology predominantly follows Evans (2008), and is supplemented by terms from Conrad (2004) where the first is lacking.

Table 2.1. Specimens of *Eremiascincus* that were examined to produce this description (ETVP = East Tennessee State University Laboratory of Vertebrate Paleontology; WAMR = Western Australia Museum; SAMR = South Australia Museum):

Species	Specimen number	Articulation
<i>Eremiascincus richardsonii</i>	WAMR 146922	disarticulated
<i>Eremiascincus richardsonii</i>	WAMR 146923	disarticulated
<i>Eremiascincus richardsonii</i>	WAMR 146924	disarticulated
<i>Eremiascincus richardsonii</i>	ETVP 7127	disarticulated
<i>Eremiascincus richardsonii</i>	ETVP 7128	disarticulated
<i>Eremiascincus richardsonii</i>	ETVP 7129	disarticulated
<i>Eremiascincus richardsonii</i>	ETVP 7130	disarticulated
<i>Eremiascincus richardsonii</i>	ETVP 7131	disarticulated
<i>Eremiascincus richardsonii</i>	ETVP 7132	disarticulated
<i>Eremiascincus richardsonii</i>	ETVP 7133	disarticulated
<i>Eremiascincus richardsonii</i>	ETVP 7134	disarticulated
<i>Eremiascincus richardsonii</i>	ETVP 7135	disarticulated
<i>Eremiascincus richardsonii</i>	ETVP 7136	disarticulated
<i>Eremiascincus richardsonii</i>	ETVP 7136	disarticulated
<i>Eremiascincus richardsonii</i>	WAMR 24144	articulated
<i>Eremiascincus fasciolatus</i>	WAMR 156826	articulated
<i>Eremiascincus richardsonii</i>	SAMR 12717B	articulated
<i>Eremiascincus fasciolatus</i>	SAMR 19862	articulated
<i>Eremiascincus richardsonii</i>	SAMR 14878	articulated
<i>Eremiascincus richardsonii</i>	SAMR 9302	articulated
<i>Eremiascincus fasciolatus</i>	SAMR 11125	disarticulated
<i>Eremiascincus richardsonii</i>	SAMR 9301	articulated
<i>Eremiascincus richardsonii</i>	WAMR 146921	disarticulated
<i>Eremiascincus fasciolatus</i>	SAMR 9411	articulated
<i>Eremiascincus richardsonii</i>	SAMR 14866	articulated
<i>Eremiascincus richardsonii</i>	SAMR 1787	articulated
<i>Eremiascincus fasciolatus</i>	SAMR 9333	articulated
<i>Eremiascincus richardsonii</i>	SAMR 24638	articulated
<i>Eremiascincus richardsonii</i>	SAMR 1279A	articulated
<i>Eremiascincus richardsonii</i>	SAMR 24729	articulated

Results

The skull of *Eremiascincus* is about twice as long as it is wide, with its widest points measured across either the quadrates or the jugals (Figure 2.1). The eyes are large and take up about 30% of the length of the skull in profile. The cranium is slightly domed and

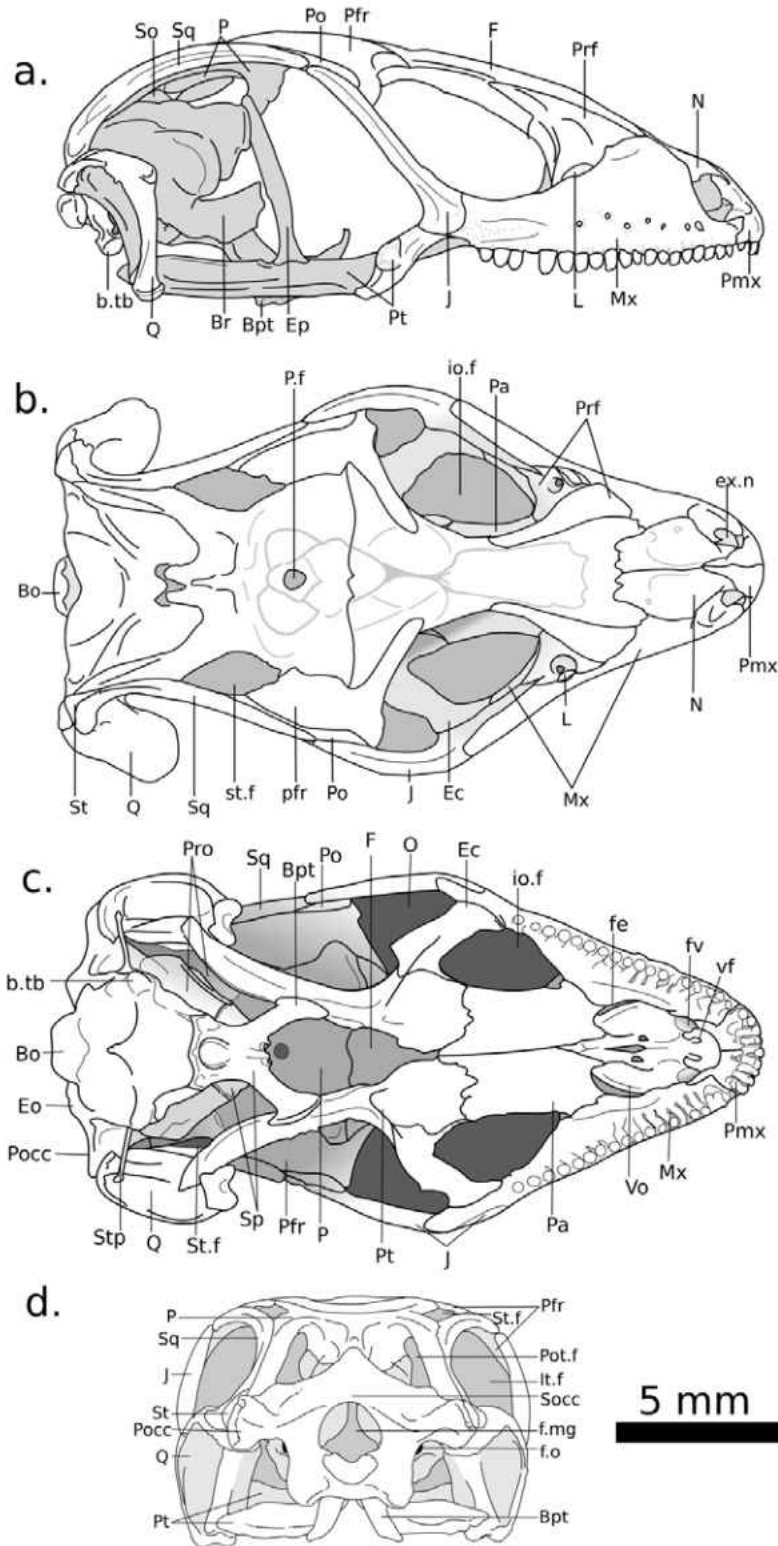


Figure 2.1. Skull of *Eremiascincus richardsonii* in a) lateral, b) dorsal, c) ventral, and d) posterior views.

accounts for about 40% of the skull length, and the wedge-shaped rostrum accounts for the remaining 30% of the skull length. Although the rostrum is somewhat wedge shaped to facilitate face-first burrowing through sand, the tip of the snout is still rounded, rather than sharp, and lacks any additional rostral process like the one seen in the ecologically very similar *Scincus scincus*.

Skull Roof and Suspensorium:

The dermal roof is composed of the premaxillae, nasals, frontal, maxillae, prefrontals, parietal, postorbitofrontals, and palpebral. The suspensorium is the portion of the skull connecting the cranium to the lower jaw. The suspensorium on each side of the skull is composed of the posterior processes of the parietal, the posterior processes of the postfrontal, the supratemporal, squamosal and quadrate. The skull roof contains the external nares and orbits, while the suspensorium is pierced by the supratemporal fenestra and forms the dorsal margin of the posttemporal fenestra. The foraminae that pierce each bone are described below. Although the epipterygoid and quadrate are both derivatives of the palatoquadrate cartilage, only the quadrate is included here since it is directly involved in suspension of the lower jaw, while the epipterygoid is included in the palatal region.

Nasals:

The external nares are large and are oriented dorsolaterally. They are bordered rostrally by the premaxillae, posterolaterally by the maxillae and posteromedially by the nasals. The nasals are short, paired, narrow and in medial contact for about 75% of their total length, only separated by the nasal processes of the premaxillae. Paired nasals are characteristic of the Lygosominae (Greer 1970). Each nasal is trapezoidal in shape, widest where it enters the posteromedial margin of the external naris, and tapering to a point anteriorly (Figure 2.2). The posterior edge is somewhat serrated and overlaps the anterior margin of the frontals. The edge of the posterior margin is curved, but overall is roughly perpendicular to the line of symmetry of the skull. The frontonasal border appears W-shaped and the frontal sends a broad shelf underneath each nasal, forming a broad lap joint.

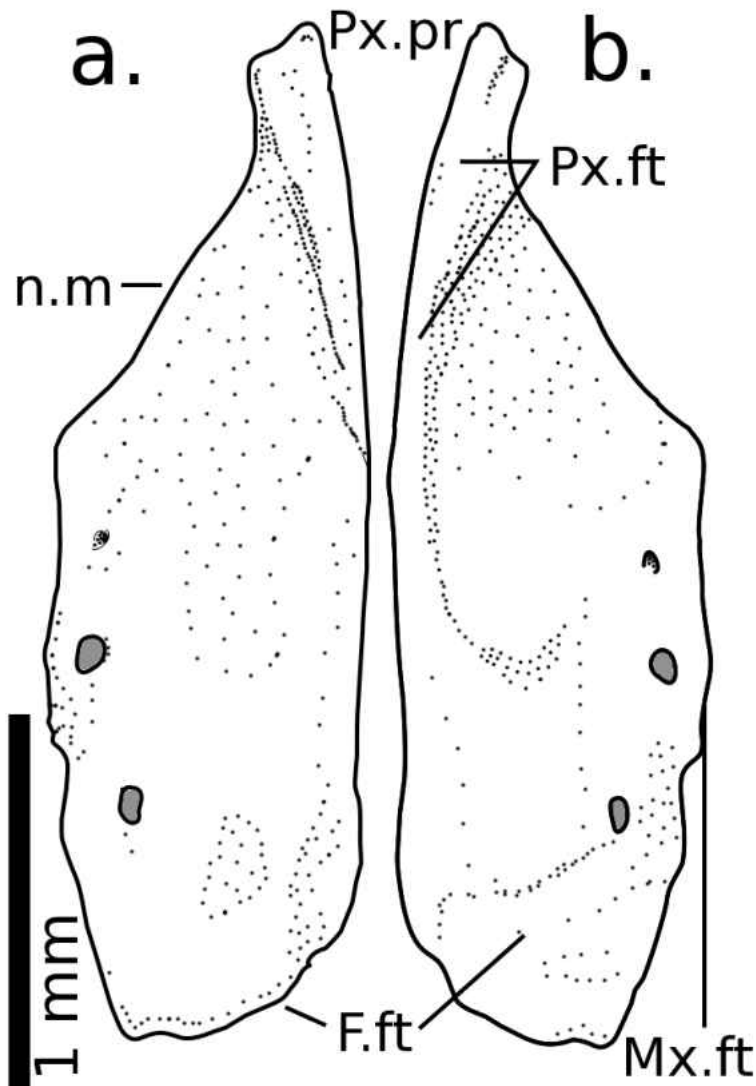


Figure 2.2. Left nasal bone in a) dorsal and b) ventral views.

Frontal:

The frontal contacts the parietal, postorbitofrontal, maxilla, prefrontal and nasals and forms part of the dorsomedial margin of the orbit. In *Eremiascincus*, as is typical of lygosomines (Greer 1970), the two sides of the frontal are fused into a single element and thickened along their midline, even in the smallest individuals examined. The frontal is widest at its contact with parietal, then constricts between the orbits, and expands again anteriorly (Figure 2.3). In lateral profile, the frontal is slightly dorsally arched overall. The

frontal has a triradiate anterior margin that contacts the maxillae at the widest point of the anterolateral processes and the nasals on the anteromedial process. As in other members of Scincomorpha (Camp 1928) the nasals are separated from the prefrontal by the frontomaxillary contact (Estes et al. 1988). There is typically some degree of dermal sculpting but this ranges from a few small grooves, to fusion of the overlying dermal ossicles.

When disarticulated, it is on average ($n = 13$) about 140% longer than the parietal table, and about 15% longer than the entire parietal. In an articulated skull, the frontal would appear shorter due to overlap by the nasals. Through ontogeny, the frontal becomes proportionately shorter, decreasing from about 25% longer than the parietal on the juvenile with the greatest ratio measured, to about 6 % larger than the parietal table in the adult with the smallest ratio measured.

There are two descending flanges (the cristae cranii) that extend the length of the lateral margins of the frontal. These are short and hang vertically posteriorly but increase in length and are medially inflected to increasing degrees further anteriorly so as to partly enclose the olfactory bulbs of the brain. While the medial inflections of the cristae cranii approach each other, they do not contact. In life, the gap between them is bound ventrally by a tough fibrous ligament. The point of greatest inflection is about 33-40% the length of the frontal posterior to its anterior margin. Behind this point of greatest inflection, the flanges become less inflected and lower so that they become nearly flush with the rest of the frontal table by the point where they reach the parietal suture. The lateral margin of the frontal does not extend noticeably beyond the lateral margin of the cristae cranii.

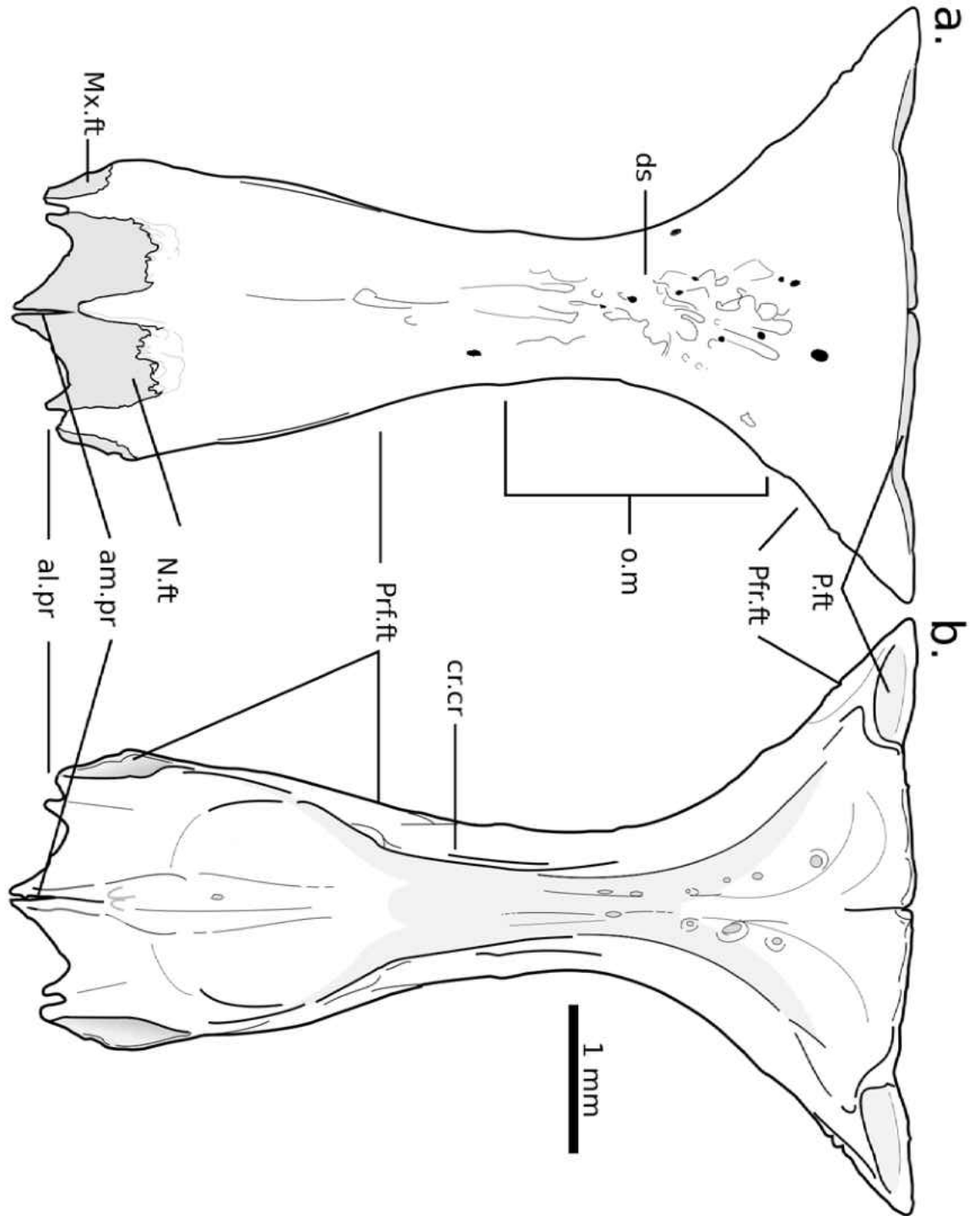


Figure 2.3. Frontal of *Eremiascincus richardsonii* in a) dorsal, and b) ventral views.

The frontal contact with the parietal is broad and roughly straight. In dorsal view, the parietal contact has a small facet for the overlap of the anterior margin of the parietal. In ventral view, each of the lateral corners of the parietal contact has a semilunar facet that overlaps the frontal lapets of the parietal. Around the orbital margin, the frontal has facets for the postfrontal posteriorly and the prefrontal anteriorly. These facets are shallowly concave and are separated by the frontal's contribution to the orbital margin. These facets are subtle and difficult to see except by the slight change in curvature of the lateral margin. At the rostral end of the frontal, on the dorsal surface, there are large semielliptical facets, on which rest the posterior margins of the nasals.

Parietal:

The two sides of the parietal are fused into a single element which is made up of: the broad, flat, trapezoidal plate of the parietal table; the long, laterally placed, posteriorly projecting supratemporal processes; and two triangular, medially placed posterior processes (Figure 2.4). The supratemporal processes are somewhat ventrally inflected, so that the whole parietal is dorsally arched. The parietal contacts the frontal, postorbitofrontal, prootic, supraoccipital, exoccipital, epipterygoids, supratemporals, and squamosals. The frontal and parietal are held together with a lap joint that looks straight in articulation. On the ventral side of the frontal contact, there is a medial facet that overlaps the corresponding facet on the dorsal side of the frontal. At the lateral ends of the frontal contact, the parietal extends forward a parietal lappet on each side, which underlies the frontal. This type of suture possibly reduces the mobility of the mesokinetic line of the amphikinetic skull. Dermal sculpting covers most of the dorsal surface of the parietal and ranges from mere impressions of blood vessels in the smallest individuals, to fusion of the

three largest overlying dermal ossicles anterior and lateral to the parietal foramen in medium to large individuals. Although osteoderms fuse to the skull in adults, they do not appear to cross the frontal-parietal suture and therefore do not themselves restrict movement of the frontoparietal hinge.

As in other lygosomines (Greer 1970), the pineal foramen is located in the anterior half of the parietal table. The pineal foramen however remains relatively close to the middle of the parietal table. In the smallest juveniles, the midline of the parietal is unossified anterior to the pineal foramen, so that the foramen is open to a narrow notch leading from the frontoparietal suture. As the animal grows, the notch closes around the foramen first and then seemingly zippers closed anteriorly.

Between the supratemporal processes, the two small posterior processes extend around the lateral edges of the processus ascendens of the supraoccipital and connect to it via a ligamentous sheet. The parietal table overlaps the tip of the processus ascendens, which fit into a pit on the ventral side of the posterior margin of the parietal. The anterior margin of the pit for the processus ascendens ranges from an acute V-shape to a broad, gently rounded U. On the ventral surface of the parietal, between the posterior process and the supratemporal process and the ventromedial side of the supratemporal process itself, there is an elliptic fossa for the attachment of the anterior dorsal neck musculature. On the dorsal side, there is another set of fossae for the attachment of dorsal neck musculature. These fossi extend onto both the supratemporal and posterior processes. At about the point during growth when the parietal midline suture closes completely, the dorsal posterior fossa expands from a triangular depression limited by the lateral margin of the

posterior process, to a large ovoid or squared off fossa that extends all the way to the midline between the two posterior processes.

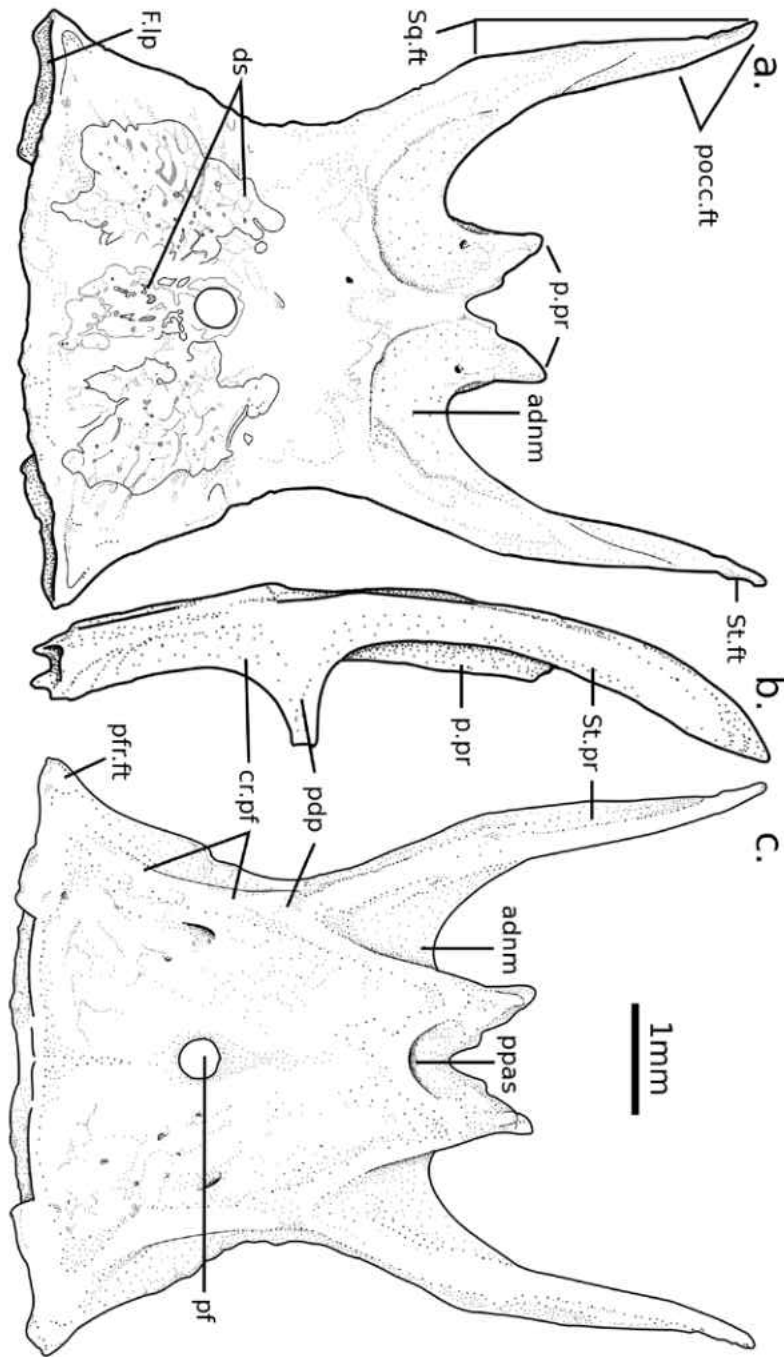


Figure 2.4. Parietal of *Eremiascincus richardsonii* in a) dorsal, b) left lateral, and c) ventral views.

Running lengthwise along the lateral margins of the parietal table are two low descending flanges (*cristae postfovealis*), which extend from the anterolateral corners to the supratemporal process where they each become confluent with the margins of the ventral fossa for the dorsal neck musculature. At the anterolateral corners of the parietal, the *crista postfovealis* becomes wider but more flush with the rest of the parietal and becomes contiguous with the slight general thickening of the anterior edge of the bone. At the confluence of the crest and the fossa for the dorsal neck musculature, roughly parallel with the point of maximum width of the supratemporal fenestra and minimum width of the parietal table, there is a short, pointed triangular process that descends from each *crista postfovealis*. This process is the *processus decensus parietalis*. In *Eremiascincus*, they descend to the level of the anterior most point of the alar process of the prootic. By comparison, the *processus descendens parietalis* in *Eremiascincus* is proportionately smaller than that in *Scincus scincus*., but larger than those of *Ctenotus*, *Mabuya*, *Lygosoma*, and *Acontias* observed. As in other members of Scincomorpha, the *processus descendens parietalis* has a contact with the epipterygoid (Camp 1928), which is limited to the dorsal tip of the epipterygoid in *Eremiascincus*. Greer (1970) remarks that in lygosomines, the ventral process is reduced to only the small, finger-like projection and is not laterally expanded. In *Eremiascincus* however, the *processus descendens* is confluent with the *crista postfovealis*, which expands the base of the process into something more triangular than finger-like.

The lateral margin of the supratemporal process has a distinct medial inflection marking the anterior extent of the squamosal facet. On the posteromedial end of the supratemporal process, there is a ventromedial expansion and a flat edge for the

articulation of the paroccipital process of the otooccipital. The posterolateral edge of the supratemporal process has a facet for the supratemporal. On the lateral edges of the parietal table, there are expanded flanges for the origin of the muscularis pseudotemporalis and form the medial margin of the supratemporal fenestra. Anterior to the fenestral margin, the lateral expansion continues and forms the overlapping contact with the postfrontal.

The parietal table is about an average ($n=13$) 62.5% longer than it is wide at its anterior margin, though ontogenetically the parietal increases in width faster than length ($r^2=0.31$). The width of the parietal at its posterior, between the tips of the supratemporal processes, is about equal to that of the anterior margin. The parietal table comprises an average ($n=12$) of about 51.6% of the total parietal length. However, the parietal table ranges from 40.2% of the total length in the smallest individual measured up to 58.9% of the total length in one adult near the upper limit of the size range. Thus, adults have a parietal table that is proportionately wider and supratemporal processes that are proportionately shorter.

Premaxilla:

The premaxillae are paired and unfused even in the largest individuals examined (Figure 2.5), characteristic of the Lygosominae (Greer 1970). The left element always contained 4 tooth positions and the right element bore sometimes 4, but more often 5 tooth positions so that a total of 8 teeth is possible, but 9 is more common. In no case observed did the left element have more tooth positions than the right. Each has a nasal process that together, divide the anterior of the nasals and extend about 50% of the way up the medial margin of the external nares and then about 25% of the way up the medial margins

between the nasals. Each has a strong palatal shelf that clasp the anterolateral margin of the vomer, and a posterior process that rests in a facet on the premaxillary process of the maxilla. The premaxillae have a broad arching contact with the maxilla on both the lateral and palatal sides of the skull. The premaxillae of *Eremiascincus* each have a very small incisive process, much smaller than found in *Mabuya*, *Scincus*, or *Eumeces*. The premaxilla also lacks the rostral expansion that is seen as an adaptation for sand swimming as in *Scincus scincus*.

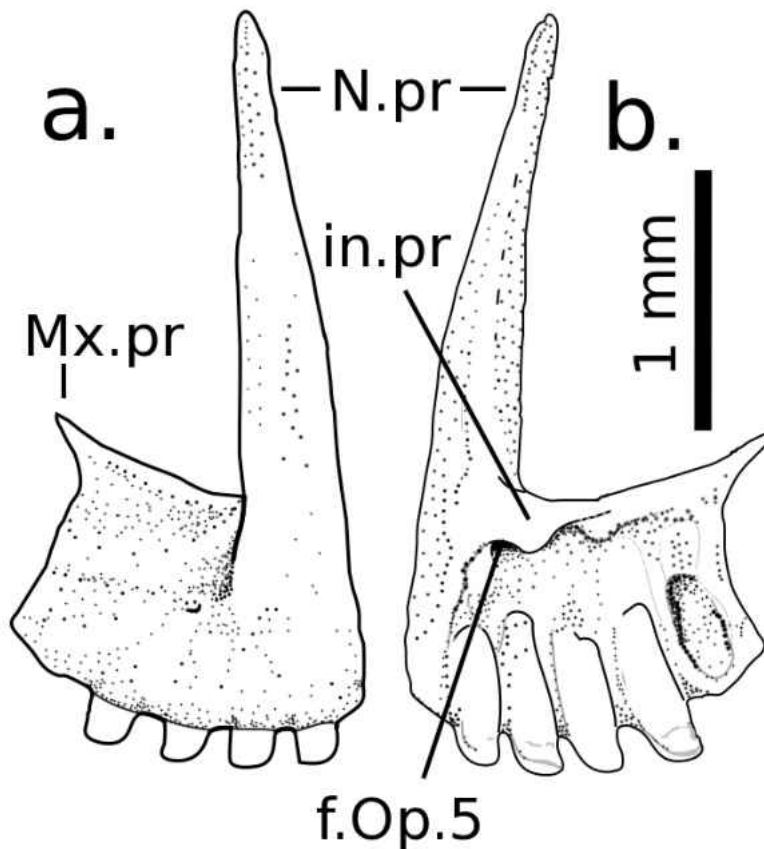


Figure 2.5. Left premaxilla of *Eremiascincus richardsonii* in a) labial and b) lingual views.

Maxilla:

The maxilla contacts the premaxilla, nasal, septomaxilla, vomer, palatine, jugal, ectopterygoid, prefrontal, and frontal. The maxilla has a large, triangular ascending nasal process that tapers to a dorsal apex at the juncture of the frontal and prefrontal contacts (Figure 2.6). There are two processes anteriorly that grip the premaxilla, vomer and septomaxilla. Posteriorly there are two processes that grip the jugal. Medially, there is an elongate, subtriangular choanal shelf that contacts the palatine. Below the choanal shelf, there is a row of teeth that extends from just behind the premaxillary process anteriorly, to just ahead of the ectopterygoid facet on the posterior process at the rear. In *Eremiascincus*, there are from 16 to 21 tooth positions, with 19 or 20 as the most common number.

The ascending nasal process curves medially to form the dorsolateral surface of the rostrum. Posterior to the junction of the premaxillary and septomaxillary processes, the anterior surface of the maxilla is gently concave and slopes posterodorsally to form the posteroventral margin of the external naris. The maxilla is contacted anterodorsally by the nasal, which fits onto the flat anterior surface of the ascending nasal process. Contrary to Greer's (1979a) diagnosis of *Eremiascincus*, which characterized the maxilla-frontal contact as broad, that contact in specimens examined here was typically narrow, occurring only at the apex of the ascending nasal process. The anterior half of the posterodorsal margin of the ascending nasal process is occupied by the prefrontal facet. The shape of the prefrontal facet is variable, but there is universally a recess behind the apex of the nasal process and a secondary ascending process that has secondary apices on it. Posterior to the prefrontal articulation, the maxilla composes the anterior half of the ventral margin of the orbit along with the maxillary process of the jugal, which lies in an elongate triangular groove on the

dorsal side of the posterior process of the maxilla. The jugal facet does not completely close anteriorly, but instead opens up onto the dorsal surface of the choanal shelf (Figure 2.7).

Laterally, the maxilla is pierced by from 4 to 7 nutritive foramina, most frequently 5 or 6, arranged in a longitudinal row above the labial margin. The ethmoid foramen perforates the maxilla mid way between the choanal shelf and the nasal facet, straight through to the lateral side of the maxilla, above the nutritive foramina. At the junction of the choanal shelf and the main body of the maxilla, there are the openings of the maxillary branch of the trigeminal nerve and the superior alveolar canal. The opening for the trigeminal nerve and the superior alveolar canal range from being widely separated on the choanal shelf, to being co-located in a single pit (Figure 2.7). These two foramina are typically located adjacent to the apex of the triangle formed by the choanal shelf, which is mediolaterally widest point on the maxilla.

The maxilla also plays an important role in connecting the dermal roof of the skull to the palatal complex via its contacts with the ectopterygoid, palatine and vomer. On the anterior end of the palate, the maxilla has a narrow contact with the vomer directly behind the premaxillary contact, being mostly separated from the vomer by the maxillary process of the premaxilla. There is a septomaxillary process of the maxilla that rises above the vomer to contact the septomaxilla within the nasal capsule. Between palatine and ectopterygoid, the maxilla also contributes to approximately half the length of the infraorbital fenestra. The maxilla has a long, oblique contact with the anterolateral edge of the palatine via the choanal shelf. Posterior to the end of the tooth row and ventral to the

jugal contact, the maxilla connects to the palatal complex via its contact with the expanded lateral process of the ectopterygoid.

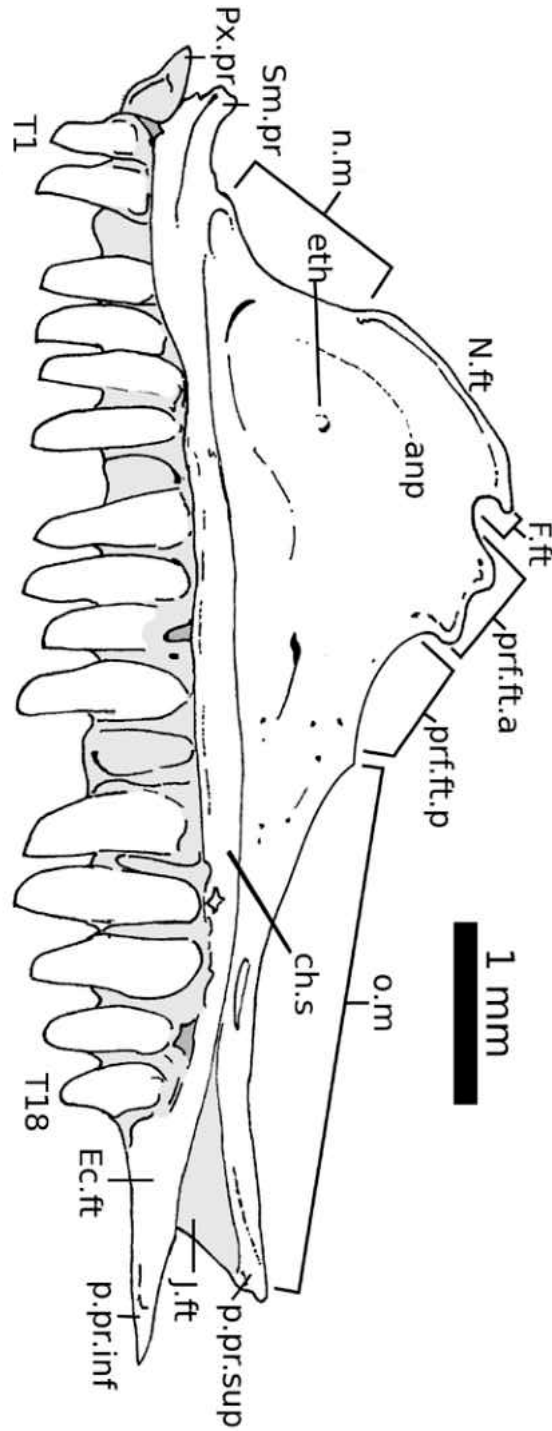


Figure 2.6. Left maxilla of *Eremiascincus richardsonii* in medial view.

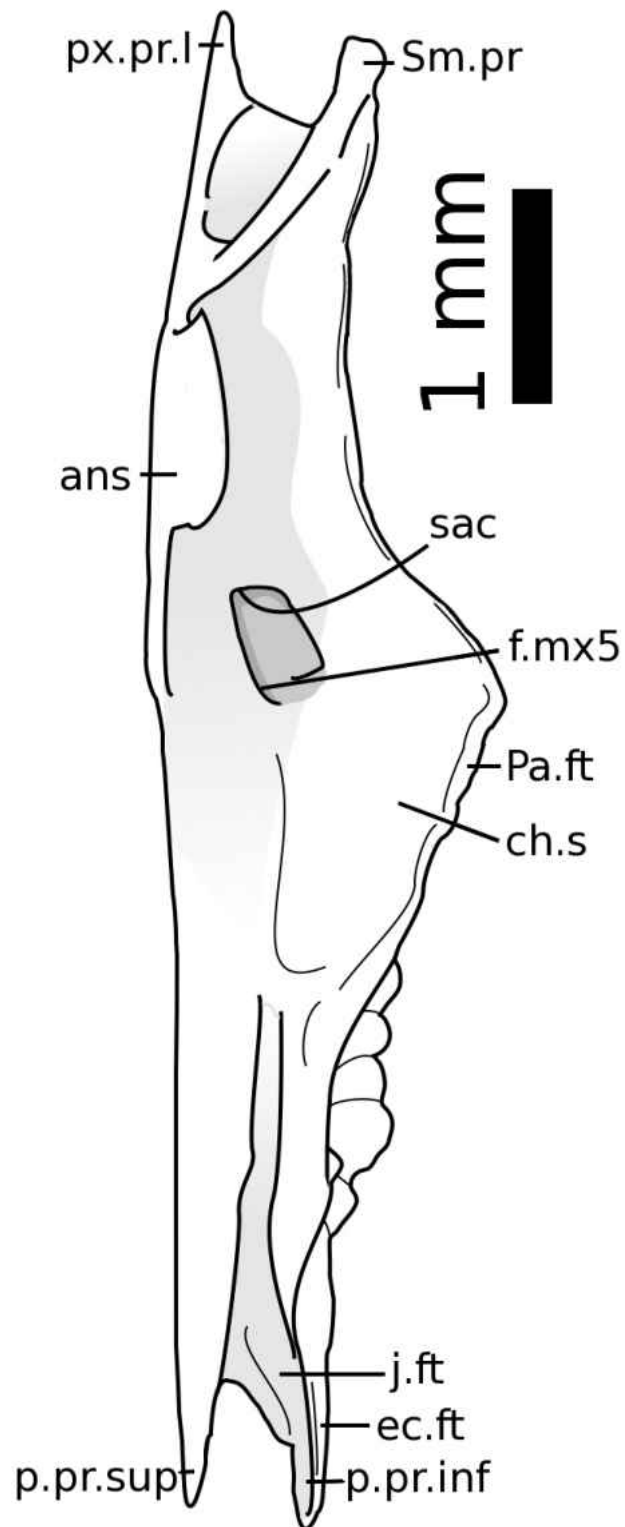


Figure 2.7. Left maxilla of *Eremiascincus richardsonii* in dorsal view.

Jugal:

The jugal is composed of three unequal processes (Figure 2.8). The anterior and ascending processes are long, thin and taper to a point. The posteroventral process is short and is hardly distinguishable from the angle between the other two processes. The jugal contacts the maxilla, ectopterygoid and the tip of the orbitonasal flange of the prefrontal anteriorly. Posteriorly, it contacts the lateral tip of the postfrontal, the anterior half of the postorbital and the anterior tip of the squamosal. The anterior process has facets medially and ventrally for contact with a groove on the dorsal surface of the posterior process of the maxilla. The anterior process also has a broad contact with the ectopterygoid and a narrow contact with the orbitonasal flange of the prefrontal. In lateral view of an articulated skull, the anterior process of the jugal is a short exposure between the dorsal and ventral posterior processes of the maxilla that possesses the jugal foramen. Immediately behind this exposure, at the junction between the anterior and ascending processes of the jugal, there is a small posteroventral process for the attachment of the quadrato-maxillary ligament (Haas 1973). The ascending process of the jugal forms most of the postorbital bar, with a small contribution from the postfrontal to which the jugal articulates over a narrow span. There is a subtle facet on the ascending process for articulation with the postorbital. The existence of a jugal-squamosal contact on the supratemporal bar is characteristic of the Scincidae (Estes et al. 1988).

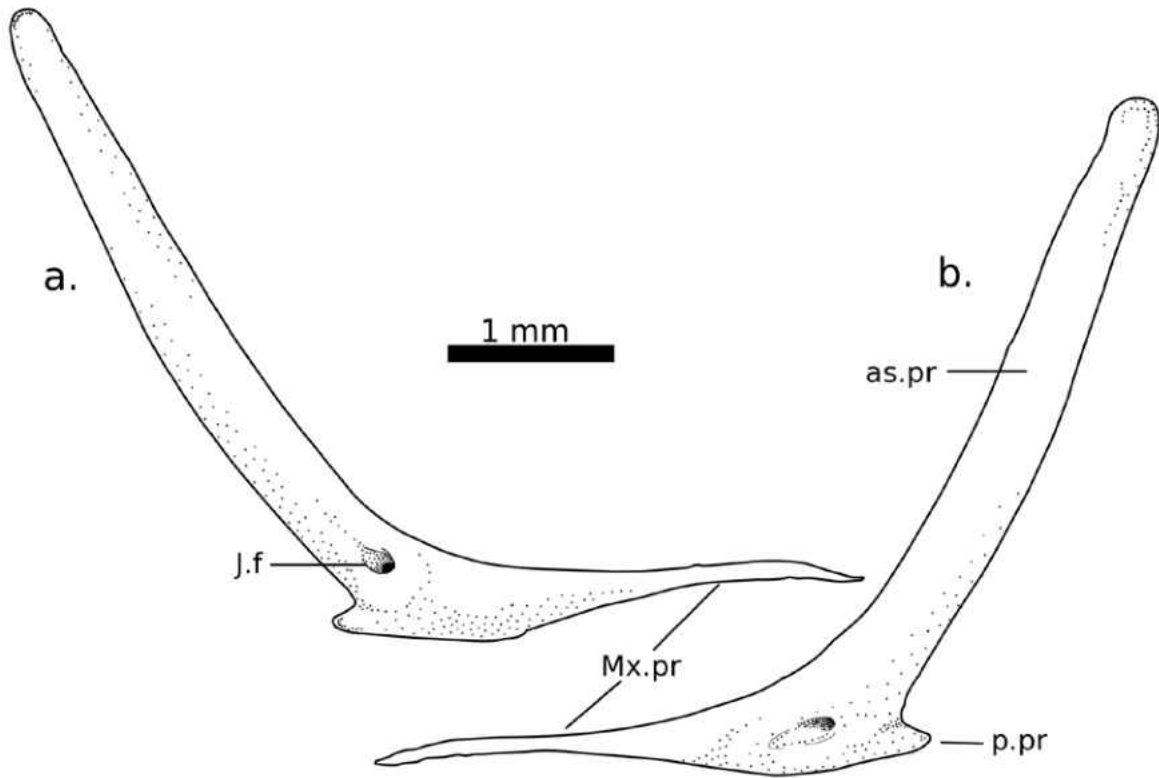


Figure 2.8. Jugal of *Eremiascincus richardsonii* in a) lateral and b) medial views.

Postorbital and Postfrontal:

The postorbital and postfrontal usually remain separate elements in *Eremiascincus*, though fuse in a few cases. The postfrontal forms a sharply angled chevron with two anterior processes and one posterior process (Figure 2.9). The postfrontal contacts the frontal, parietal, postorbital, squamosal, and jugal. Posterior and medial processes taper to sharp points. The element is gently, dorsally convex in both lateral and anterior views. The anterior and lateral margins are shallowly concave in dorsal view and form the posterior orbital margin anteriorly and squamosal and postorbital facets laterally. At the anteromedial angle, there is a facet for the overlap of the lateral edges of the parietal and frontal. Posterior to the facet for the frontal and parietal, is a broad thin lamina,

articulating with the lateral margin of the parietal and covering the dorsal surface of the supratemporal fenestra. The posteromedial margin of the postfrontal forms the anterolateral margin of the supratemporal fenestra. The supratemporal fenestra varies in shape from linear, with parallel sides, to acuminate, rounded anteriorly and pointed posteriad to lanceolate, pointed at both ends. The length of the posterior process of the postfrontal is variable and affects the size of the supratemporal fenestra.

The postorbital is small, thin, lanceolate and varies greatly in length. Variation in the length of the postorbital was noted by Greer (1979a) in the diagnosis of the genus. In all cases, the postorbital is excluded from the actual orbital margin by the anterolateral process of the postfrontal. The postorbital starts directly behind this anterolateral process and extends some length down the lateral side of the postfrontal. The postorbital varies in length from extending only about 33% of the length of the postfrontal, to greater than the length of the postfrontal, entering the margin of the supratemporal fenestra and completely excluding the postfrontal from contact with the squamosal. None of the variability in the supratemporal arch and fenestra appears to be taxonomically significant as it varies widely within the species, and occurs asymmetrically in some individuals.

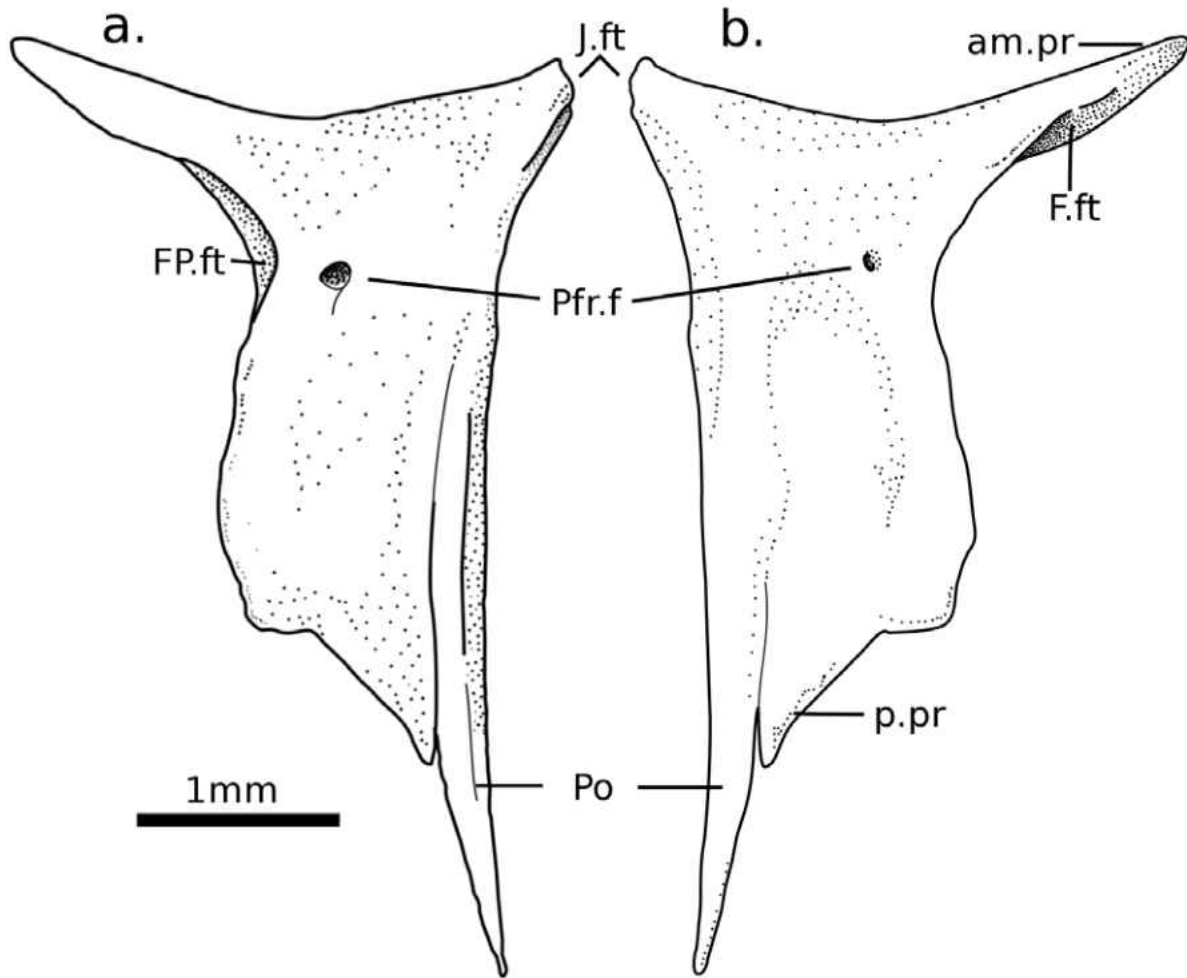


Figure 2.9. Postfrontal with a fused postorbital of *Eremiascincus richardsonii* in a) dorsal, and b) ventral views.

Squamosal and Supratemporal:

The squamosal is a long thin single bar that forms the posterolateral margin of the skull. It ranges from having a wide entry into the posterolateral margin of the supratemporal fenestra to complete exclusion by the postfrontal. In lateral view, it hooks posteroventrally and forms a rounded distal head that contacts the cephalic condyle of the quadrate. However, it is more curved throughout its length than the “hockey-stick” appearance described by Evans (2008) for skinks in general. Along the length of its lateral side, there is a shallow groove for the attachment of the muscularis adductor mandibulae

externus superficialis. Medially, the posterior half of the squamosal has a broad flat surface for the articulation with the parietal and distal facet for the supratemporal articulation.

The supratemporal is present, but is reduced to an extremely small splint of bone that primarily contacts the dorsolateral edge of the paroccipital process of the braincase and the squamosal. Only the very anterior tip of the supratemporal contacts the parietal.

Temporal Fenestrae:

As in other lygosomines and scincines (Greer 1970), the supratemporal arch is complete. The supratemporal fenestrae are present but reduced by posterior expansion of the postfrontal, characteristic of the Scincidae as a whole (Estes et al. 1988). These fenestrae vary in shape from linear (having long, parallel margins and pointed at both ends) to lanciolate (pointed at both ends and widest in the middle) to acuminate (rounded and widest anteriorly and tapering to a point posteriorly). The post-temporal fenestrae are present, acuminate in shape and proportionately larger than those in *Mabuya*. This appears to be owing to a higher domed dermatocranium in *Eremiascincus* rather than a difference in relative braincase size. The post-temporal fenestra is bound medioventrally by the supraoccipital and dorsolaterally by the parietal only. The infratemporal vacuity is bound anteriorly by the jugal, dorsally by the squamosal, posteriorly by the quadrate and has a falcate (pointed at both ends and a wide, sinusoidal midlength) shape. The suborbital fenestrae are about half the length of the orbit, are bound by the maxilla anteriorly and laterally, the palatine and pterygoid medially, the ectopterygoid posteriorly, and have a medially flattened lanciolate shape.

Quadrate:

The quadrate dorsally contacts, from medial to lateral, the otooccipital, supratemporal, and squamosal, and ventrally contacts the pterygoid on the medial side and the articular on the lower jaw. The quadrate has a cephalic and mandibular condyle at its dorsal and ventral ends respectively (Figure 2.10). These condyles are connected by a long and gently anteriorly arched central column and the deeply D-curved tympanic crest on the lateral edge. The tympanic crest is not reduced significantly compared to non-burrowing skinks as would be predicted for a burrower (Rieppel 1981). Medial to the central column there is a much smaller crest, the pterygoid lappet, which extends up from the mandibular condyle and variably tapers out along the length of the central column or sometimes reaches the cephalic condyle. As in other lygosomines, the pterygoid lappet is relatively broad, which helps distinguish them from scincines (Greer 1970). There is a quadrate foramen on the pterygoid lamina.

The surface of the quadrate is dorsally convex, with the medial edge of the cephalic condyle oriented posteroventrally. The cephalic condyle itself is wider posteriorly than anteriorly. At the top of the quadrate, an apical foramen is formed by the junction of the cephalic condyle, the central column and the tympanic crest. The tympanic crest curls over the cephalic condyle to varying degrees. In some specimens, it leaves an open channel from the apical foramen to the posterior margin of the tympanic crest, while in others it completely closes the margin of the foramen but remains unfused or else fuses to the cephalic condyle. The junction between the tympanic crest and the cephalic condyle typically leaves at least a slight notch between the two, as described by Evans (2008) for skinks in general. In articulation the apical foramen is completely covered by the elements

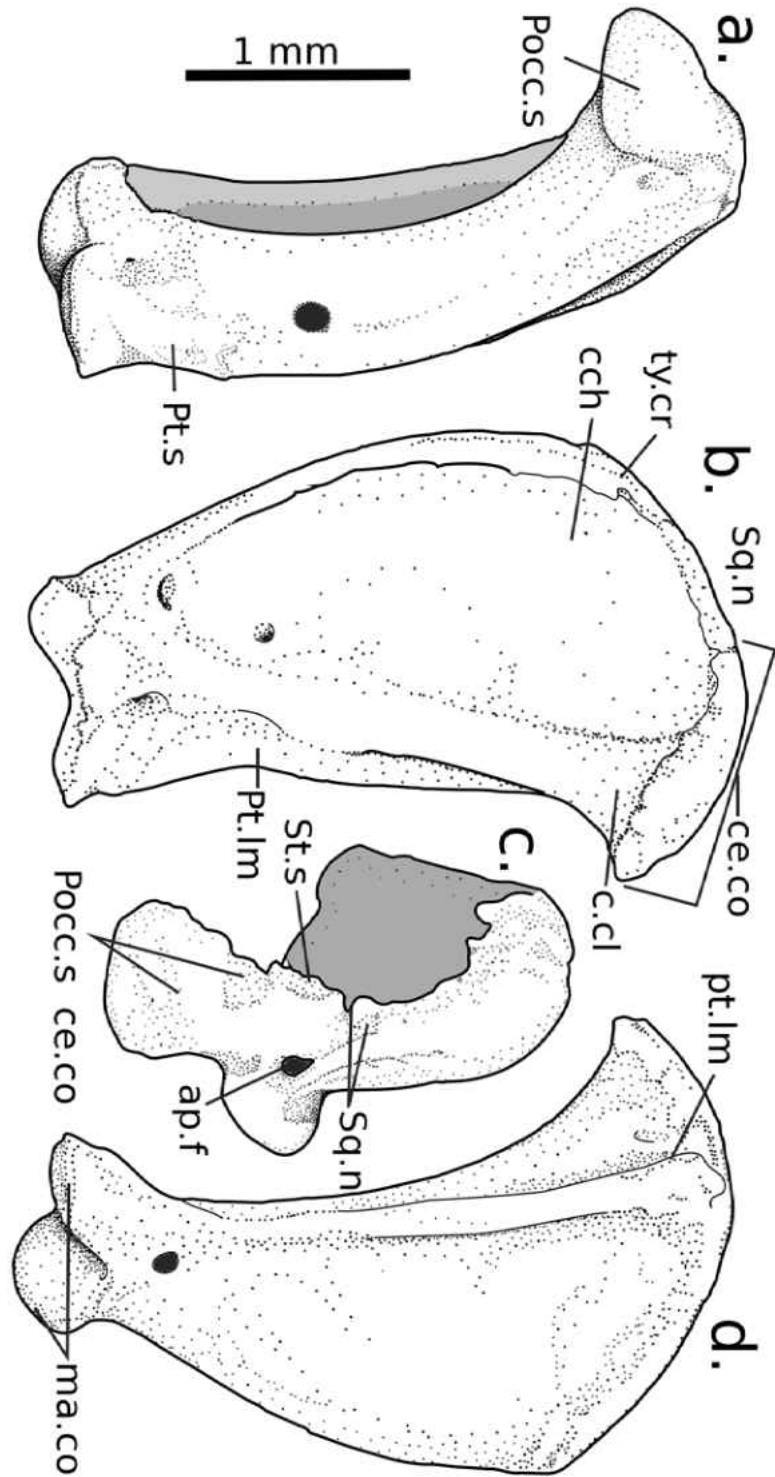


Figure 2.10. Left quadrate of *Eremiascincus richardsonii* in a) medial, b) posterior, c) dorsal, and d) anterior views.

of the supratemporal arch. The paroccipital process and supratemporal occupy most of the space on the cephalic condyle and these are separated from the squamosal articulation by a small triangular gap. The squamosal curls somewhat laterally so that its tip articulates at the notch between the cephalic condyle and the tympanic crest and is likely the element that directly covers the apical foramen.

The quadrate is broadest about 33% of the way down from the top of the cephalic condyle in lateral view and at about the same point mediolaterally. In lateral view, the conch and the central column are posteriorly concave. Along the lateral margin of the conch, there is an indentation that breaks the smooth contour of the posterior margin. This occurs at the level of the widest part of the conch and can be as deeply expressed as a sharp hook. Along the anterior face of the conch at this level, there is also a thickened band crest that breaks the gentle curvature of the conch. The horizontal thickening is met by two vertical thickenings and together they form an anterodorsally directed flattened surface on the front of the tympanic crest.

The mandibular condyle, confluent with a ventral expansion of the central column, has two rounded articular surfaces and a narrowed portion in between. The lateral surface is larger in ventral view than the medial one. The tympanic crest and the pterygoid crest both become flush with the thickened central column above the mandibular condyles.

Prefrontal:

The prefrontals are large, making up the anterior and anterodorsal margin of the orbit. It has a long, thin, triangular frontal process, a wide anterior maxillary process and a broad, transverse orbitonasal flange (Figure 2.11). The prefrontal contacts the maxilla, frontal, palatine, jugal, lacrymal and palpebral. Roughly the anterior half of the maxillary

process is hidden by the overlapping ascending nasal process of the maxilla. Posterior to its contact with the maxilla, the maxillary process has a small, shallow facet for the lacrymal. Dorsally, the frontal process extends posteriorly over the top of the orbit, contacting the cristae cranii of the frontal. At the junction of the maxillary and frontal processes, there is the broad orbitonasal flange, which extends medially to contact the entire width of the dorsal lamina of the palatine. At the base of the orbitonasal flange, where it contacts the posterior process of the maxilla and the anterior tip of the jugal, there is a deep notch the suborbital canal. The palpebral is suspended in a notch at the base of the frontal process.

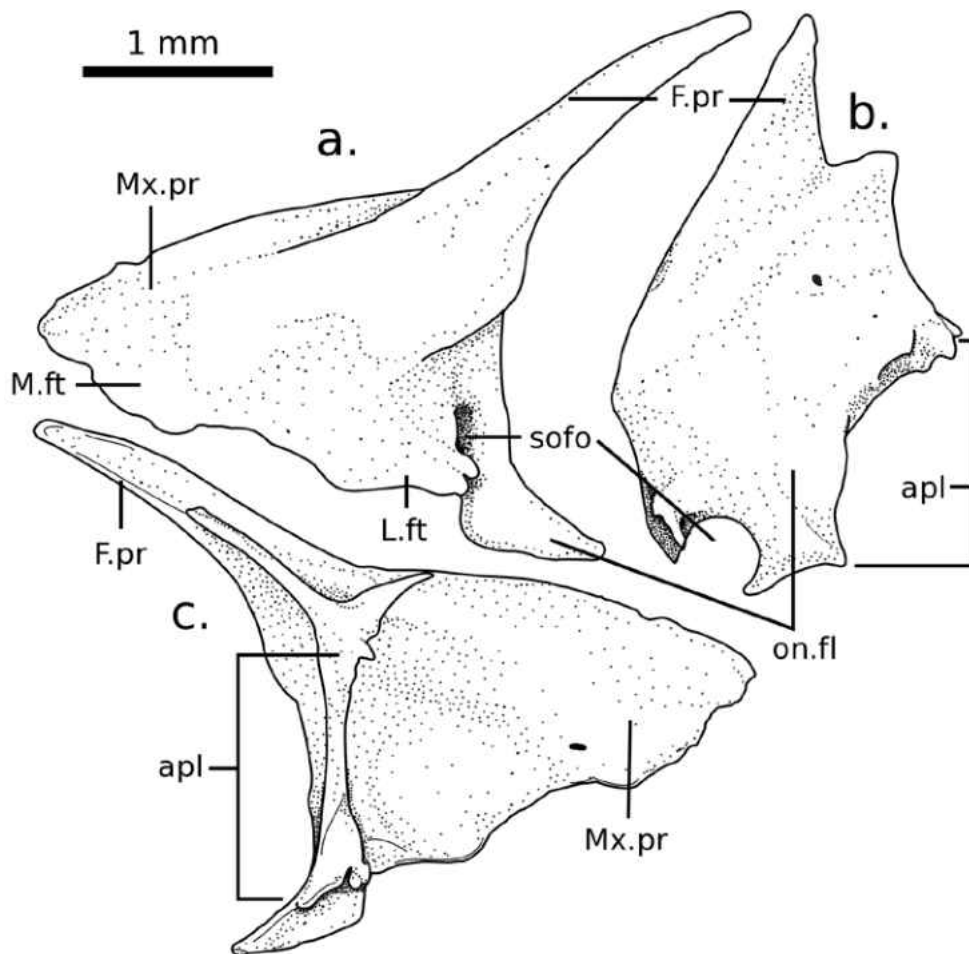


Figure 2.11. Left prefrontal of *Eremiascincus richardsonii* in a) lateral, b) posterior, and c) medial views.

Palpebral & Lacrymal:

The palpebral is a small, mediolaterally flattened, equilateral triangle of dense bone that forms the anterolateral margin of the orbit. The anterior surface is slightly convex for articulation with the prefrontal. The palpebral is about 15% of the length of the orbit.

The lacrymal of *Eremiascincus* is extremely small. It is ovate in shape and articulates only with the prefrontal, near the edge of the maxilla. It is typically smaller than most of the osteoderms and is held to the skull only by connective tissue and no sutures. Therefore, even in articulated skulls, the lacrymal is often lost during the process of skeletonizing the head. There is no separate lacrymal foramen, and it is presumed that the lacrymal duct passes through the suborbital foramen in the prefrontal.

Palatal Complex:

The palatal complex is composed of the single vomer and paired palatines, pterygoids, ectopterygoids, and epipterygoids.

Vomer:

The vomers are fused into a single element in even the smallest individuals examined, though in those, the anterior midline remains unfused (Figure 2.12). Anteriorly, the vomer is narrow and elliptical to fit between the premaxillae and it has a small lateral contact with the anteriormost corner of the palatal shelves of the maxillae. About 25% of the way from the anterior edge, the vomer expands dramatically, reaching its maximum width about 33% of the way back from the anterior edge. The lateral border of the vomer contacts the maxilla only at a slight dorsad curvature of the choanal shelf of the maxilla that separates the vomeronasal opening from the choana. This separation is not as pronounced as in *Mabuya*, *Acontias*, *Scincus* or *Egernia multiscutata*, but is comparable to that seen in

Egernia whitii. This separation of the vomeronasal opening from the choana, is consistent with the incompletely neochoanate condition described by Lakjer (1927) and by Rieppel and colleagues (2008). The vomer then tapers posteriorly until it forms one posterolateral and one shorter posteromedial processes on each side. These palatine processes interlock with the with the vomerine processes from the palatine. The posteromedial palatine process is folded medially so that it grasps the palatine from both above and below.

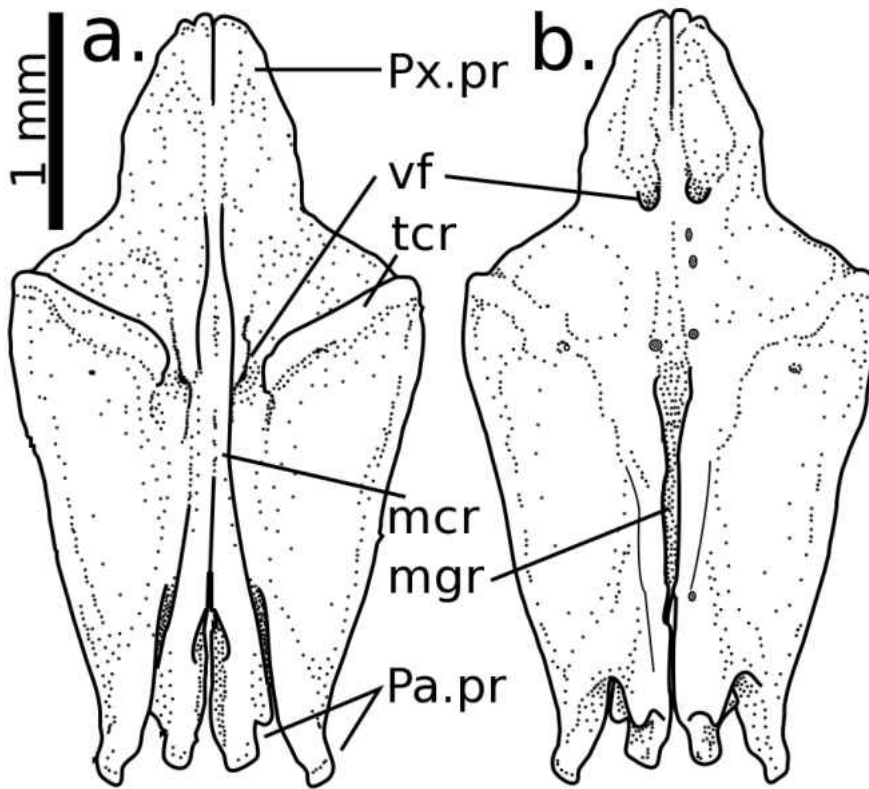


Figure 2.12. Vomer of *Eremiascincus richardsonii* in a) dorsal and b) ventral views.

In dorsal view, there is a strong ridge on the midline and two anterolaterally directed crests running from the midline to the corners at the bone's widest point. In ventral view, there is a deep median sulcus flanked by a ridge on each side. There is also a prominent notch into the ventral margin of the vomer between each posterolateral process

and its corresponding posteromedial process. On the ventral surface, the vomer is pierced anteriorly by a small vomerine foramen that opens into a channel running along the median groove. The channel opens again on the dorsal surface between the transverse crests.

Palatine:

The palatine contacts the vomer, pterygoid, maxilla, and sometimes a portion of the ectopterygoid, and comprises the majority of the medial margin of the suborbital fenestra. As in other skinks (Estes et al. 1988), *Eremiascincus* has a well-developed secondary palate, and as with other lygosomines (Greer 1970), palatine teeth are absent (Figure 2.13). The palatine is scrolled, with dorsal and ventral laminae enclosing the air passages, and the dorsal and ventral laminae of each palatine meet as a pinched lateral fold. The paired palatines contact ventrally along the midline for almost their entire length, only parting anteriorly to accommodate the vomer. In articulated specimens examined, there is, in some cases, slight overlap between the ventral laminae, but this appears to be related to contraction of the connective tissues associated with desiccation.

In ventral view, each palatine is an elongate parallelogram with a broad, triangular anterolateral process, a much smaller anteromedial vomerine process, as well as a long, broad, falcate posteromedial process and much smaller posterolateral process. With this arrangement, there is a deep concavity in the anterior margin and the posterior margin appears serrated. The anterolateral process has an oblique facet on its ventral surface for the overlap of the choanal shelf of the maxilla. Above the maxillary facet, there is an expanded prefrontal process composed of a dorsolaterally-inflected meeting of both laminae.

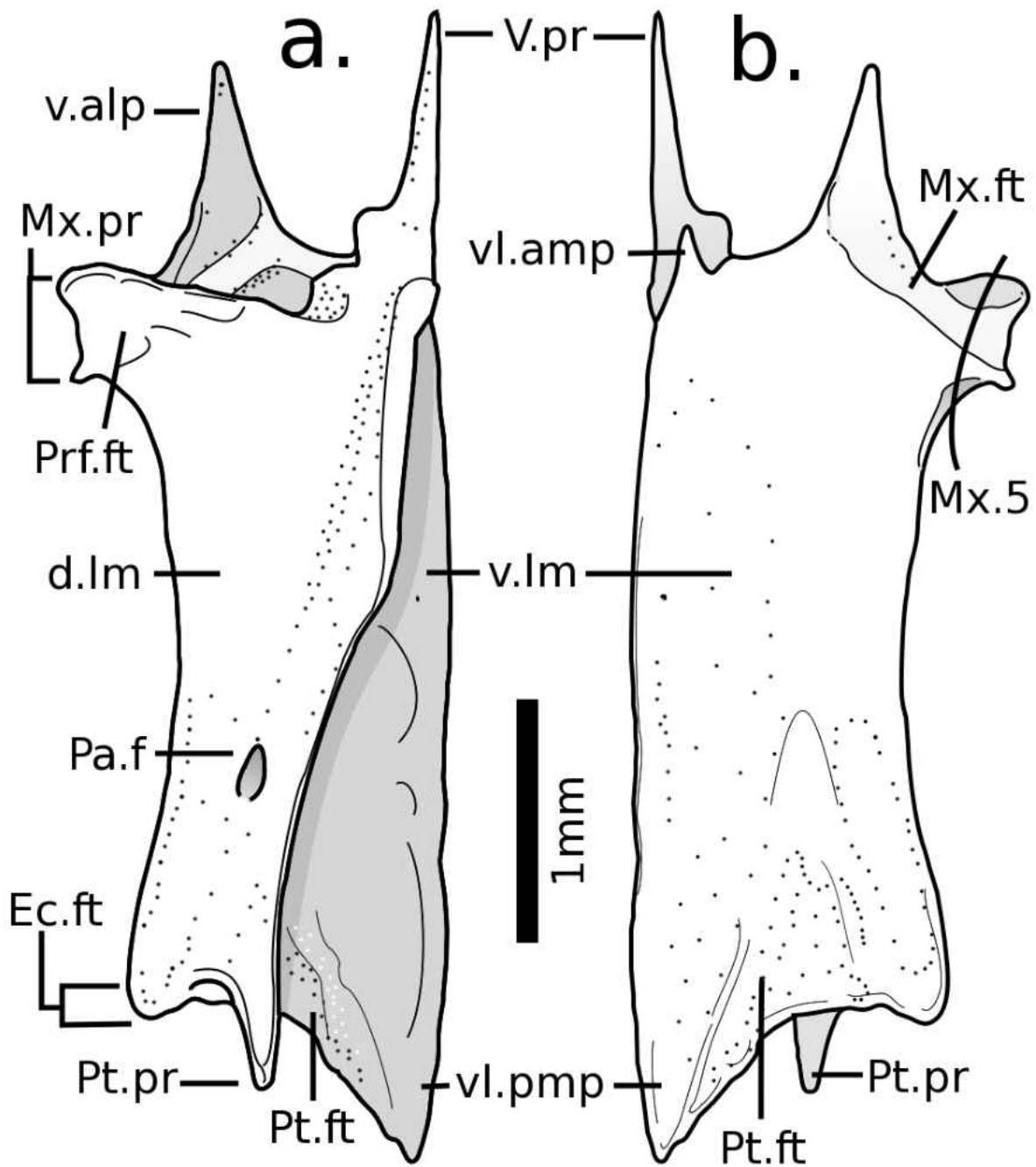


Figure 2.13. Left palatine of *Eremiascincus richardsonii* in a) dorsal and b) ventral views.

Along the midline, the dorsal laminae contact for about 33% of the total length of the palatine and then curve away from each other, sweeping concordant concave arcs and terminating in the dorsal pterygoid processes. The gap between them is spanned by a tough, fibrous sheet that encloses the airway and continues to enclose the airway along at least part of the length of the palatine flange of the pterygoid. At the front of the dorsal lamina, the vomerine process is a thin needle that extends onto the dorsal surface of the vomer. There is also an adjacent, much smaller secondary lateral vomerine process. Behind the vomerine processes, the dorsal lamina is upturned and thickened into a transverse ridge that extends from the prefrontal process to the anteromedial angle for the contact with the medial margin of the orbitonasal flange of the prefrontal. The prefrontal process itself is perforated from anterior to posterior by the foramen for the maxillary branch of the trigeminal nerve. The curvature of the anterior margin of the dorsal lamina varies, ranging from a gently concave sweep to an abrupt angle. In the portion of the dorsal lamina in which the medial margins diverge, just lateral to the midpoint of each of the diverging arcs, is a dorsolaterally directed palatine foramen.

The palatine articulation with the pterygoid is complex but unfused and permits motion, forming the hypokinetic joint. A posteromedial process of the ventral lamina of the palatine grips the medial border of the pterygoid, separating the pterygoids, while a posterior process from the medial border of the dorsal lamina fits into a groove on the dorsal side of the pterygoid. The anterior projection of the palatine flange of the pterygoid fits between the dorsal and ventral laminae into a corresponding facet that is partially exposed in the dorsal view of the disarticulated palatine. The lateral posterior process of

the palatine, formed by the combined dorsal and ventral laminae is connected to the pterygoid by the ligamentous sheet that covers the entire ventral side of the palate.

Pterygoid:

The pterygoids are paired, y-shaped elements composed of three sections: the broad anteriorly directed palatine process; the sharply angled and anterolaterally directed transverse process; and the elongate, posterolaterally directed quadrate process (Figure 2.14). Pterygoid teeth are absent. The palatine process is thin and flat in lateral view, and in ventral view tapers anteriorly to a sharp central point with two lateral accessory points, bearing a facet for the lap joint with the palatine. The two accessory points are variably developed, from virtually hidden to being better developed than the central cusp. The middle of the palatine process is also pierced by either one or two foramina.

Lateral to the palatine process is the well-developed transverse process. Descending from the ventral surface of the pterygoid is a short pterygoid flange, which crosses laterally from the posterior edge of the palatine process, along the posterior edge of the transverse process, to the ectopterygoid facet at its distal end. The pterygoid flange has a weak vertical component and inserts into a groove on the posterior of the ectopterygoid, but does not reach the maxilla. The ectopterygoid facet is thickened compared to the rest of the transverse process, anteriorly inflected and makes up about half of its posterior margin on the dorsal surface of the transverse process. The palatine process of the ectopterygoid also leaves an acute v-shaped shallow facet on the dorsal side of the transverse process, extending to the common base of the transverse and palatine processes.

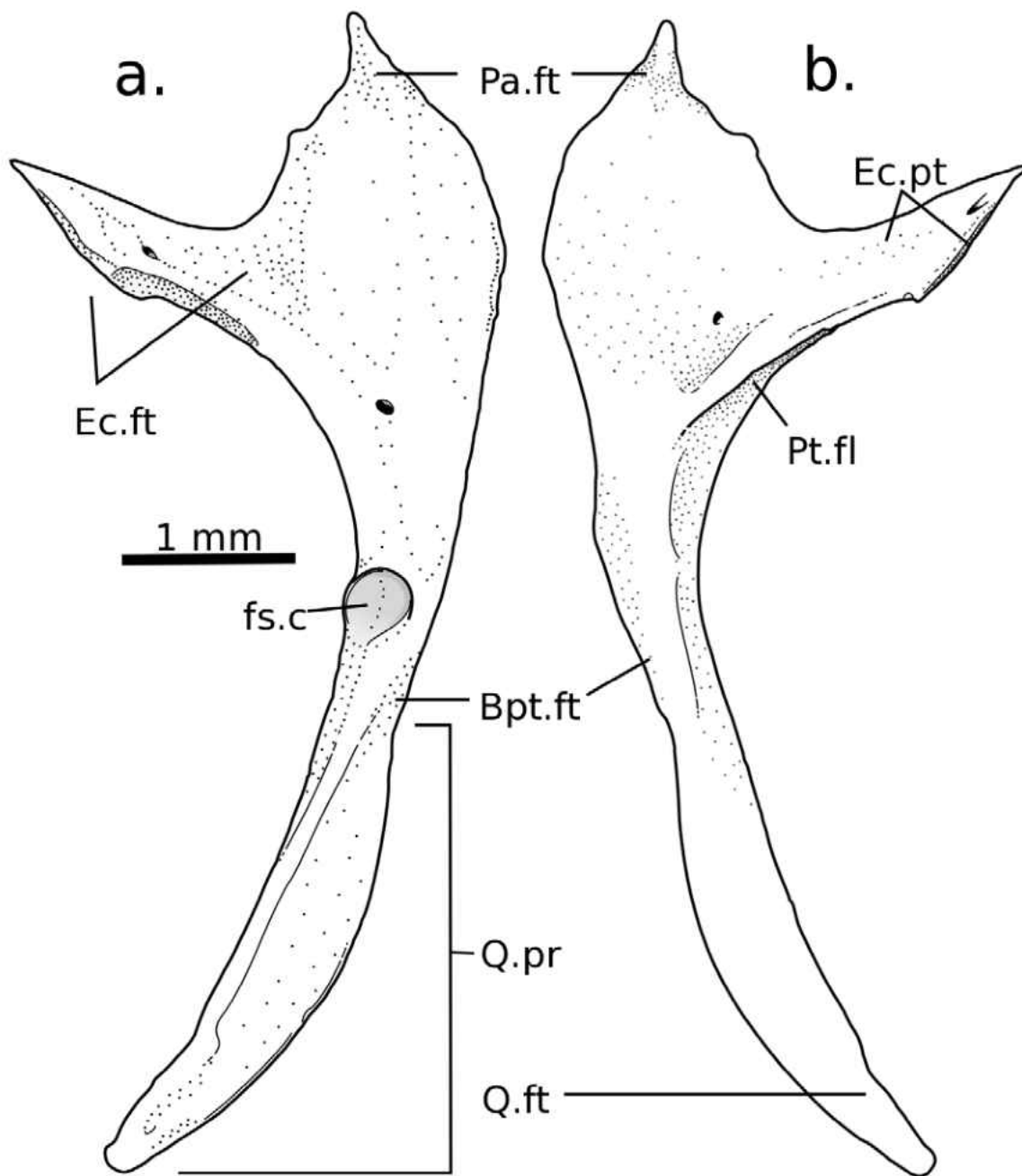


Figure 2.14. Left pterygoid of *Eremiascincus richardsonii* in a) dorsal and b) ventral views.

The quadrate process of the pterygoid is flat, spatulate, and defined here as all points on the pterygoid posterior to the anterior edge of the pit for the ventral head of the epipterygoid, (fossa columnellae). The fossa columnellae is an open, teardrop-shaped or ovoid pit and has a raised margin that becomes continuous with the lateral margin of the quadrate process via a counterclockwise twist in the left process and clockwise in the right. In this way, the raised medial wall of the pit continues posteriorly and twists to form the lateral margin of the process. Correspondingly, on the ventral side of the process, below the epipterygoid pit, there is a ventromedially directed flattened expansion of the quadrate process, called the pterygoid notch, that forms a butt joint with the basipterygoid processes of the braincase. This edge twists so that its medial margin becomes continuous with the medial margin of the rest of the process. The elongate posterior portion of the quadrate process is dorsally concave for the origin of the large pterygoideus musculature. Distally, the tips of the quadrate process are slightly flattened and dorsolaterally deflected to meet the pterygoid facets of the quadrates.

Ectopterygoid:

The ectopterygoid connects the jugal and maxilla to the pterygoid and has a morphology that is fairly typical of lygosomines (Greer 1970). The first of its two components is the maxillary process, which has a round, anterolaterally oriented central column that butts against the jugal at the posterior extent of its contact with the maxilla. It sends a thin chevron of bone forward along the jugal and overlaps the posterior process of the maxilla, forming the posterolateral wall of the infraorbital fenestra and the anteroventral margin of the infratemporal vacuity (Figure 2.15). The second is the palatine process, which grasps the transverse process of the pterygoid and sends a long thin

projection forward along the lateral margin of the palatine process of the pterygoid, contributing to the posteromedial margin of the infraorbital fenestra, sometimes reaching the palatine and excluding the pterygoid from the fenestral margin. The palatine process also sends a much shorter, broader expansion over the anterior of the dorsal surface of the transverse process, fitting into the shallow v-shaped groove there. The anterior projection of the palatine process was also observed in *Ctenotus*, but was absent from *Eumeces*, *Scincus*, *Mabuya* and *Sphenomorphus* examined, as would be expected per Greer (1967, 1970).

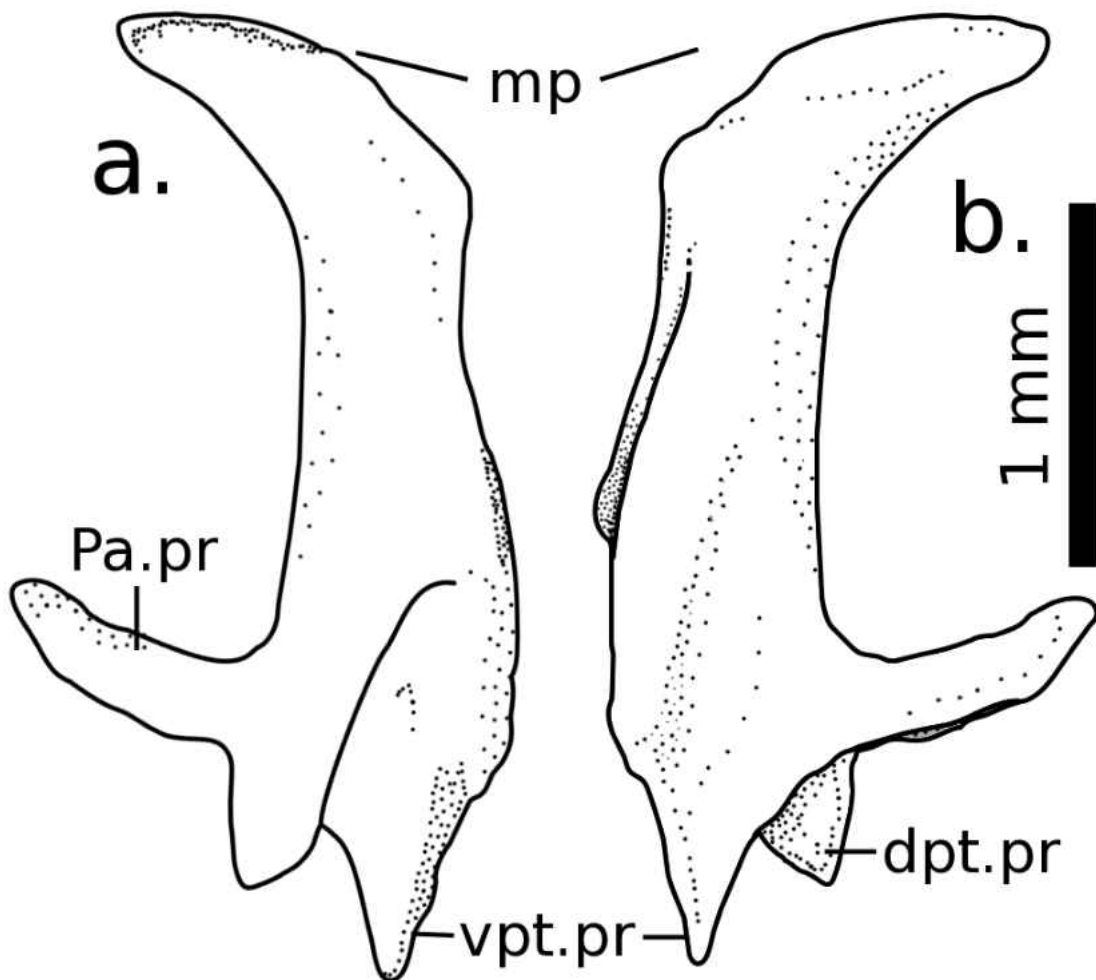


Figure 2.15. Left ectopterygoid of *Eremiascincus richardsonii* in a) dorsal and b) ventral views.

Epipterygoid:

The epipterygoid is a long thin column of bone extending from the pterygoid to the contact between the alar process of the prootic and the descending process of the parietal. The base, which fits into the fossa collumellae on the pterygoid, is round and slightly expanded relative to the shaft directly above it. The shaft thickens about midway up, but is constricted again abruptly at the top to form an oblique facet for the parietal and prootic contact. A well-developed epipterygoid is characteristic of lygosomines (Greer, 1970).

Neurocranium:

The general form of the braincase in *Eremiascincus* is very similar to other skink braincases that it was compared to, and may be considered typical of the group (Figure 2.16). The braincase is composed of the surpaoccipital, exoccipital, opisthotic, prootic, basioccipital, sphenoid, and basipterygoid. The components of the *Eremiascincus* braincase are completely fused only in the largest individuals examined, suggesting that full physical maturity is attained late in life. However, in all specimens examined, the exoccipital and opisthotic were fused into a single otooccipital. Although the stapes originates from branchial cartilage, not the neurocranium, it will be discussed with the neurocranium because of its placement and lack of contact with any other element.

Stapes:

The stapes is a minute, thin shaft, expanded at both ends. The medial end is wider than the lateral and flares out dramatically at its base to rest in, and cover up the foramen ovale. The shaft of the stapes then passes posterior to the quadrate to the external auditory meatus.

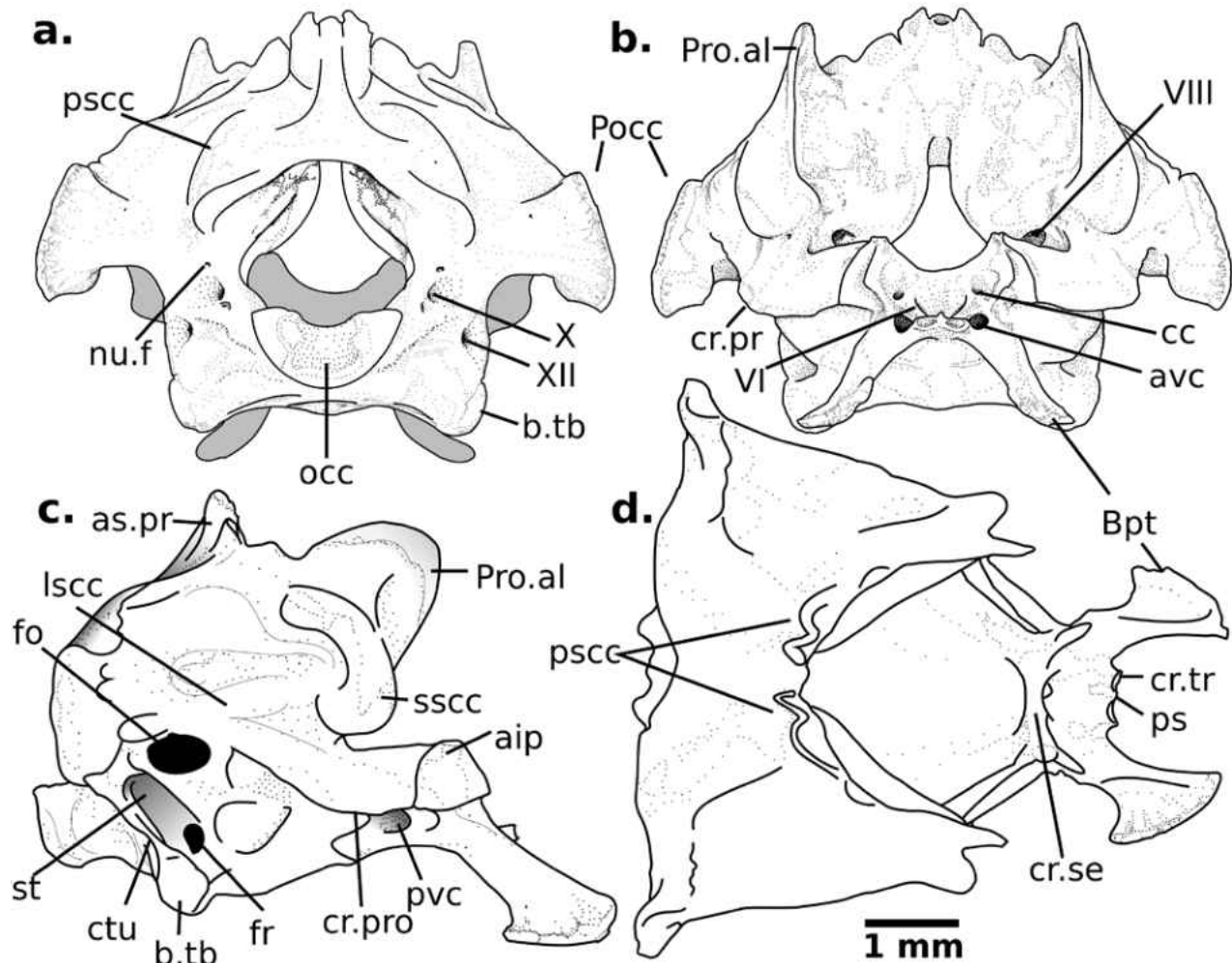


Figure 2.16. Braincase of *Eremiascincus richardsonii* in a) posterior, b) anterior, c) right lateral and d) dorsal views.

Supraoccipital:

The supraoccipital is gently dorsally arched to form the posterodorsal roof of the braincase. The supraoccipital has the same “inverted U” shape in anterior view as described for *Shinisaurus* by Conrad (2004). In dorsal view, it is sub-hexagonal in shape, with a concave posterior margin forming the dorsal margin of the foramen magnum, and an emarginated anterodorsal margin that contains the processus ascendens, which fits into a corresponding sulcus on the parietal. The processus ascendens is three-pronged; each one

short, close to the midline, and terminating in a concavity into which fit ligaments for the attachment to the parietal. The supraoccipital expands posterolaterally along its prootic contact and then contracts at its contact with the otooccipital posterolaterally. Its widest point is at the junction of those three bones. The narrowest dimension is along the midline. The posterolateral walls house the otic capsules, which are clearly visible in anterior view, pinching the sides of the "U." On the medial surface, the suture with the prootic forms a nearly vertical V on each side, but the ventral tip is laterally inflected to contribute to the ventral wall of the otic capsule.

The supraoccipital also has a pair of thickened crests forming a dorsally pointing arch from one posterior otooccipital contact to the other above the foramen magnum as well as another pair of thickened lines that run along the otooccipital sutures. At the intersection of the arc with the posterior otooccipital suture, the posterior semicircular canal is exposed in cross section. At the anterodorsal corner of the contact with the prootic, the anterior semicircular canal is exposed in cross section. Within the bone, the two canals unite and enter the otic capsule via the osseous common crus. On the anterior surface, the supratemporal concavities are large and dorsomedially directed. Well forward of them, nearly right below the anterodorsal corner of the prootic contact are the very small, anteriorly directed external foramina for the endolymphatic ducts.

Prootic:

The prootic is a triradiate element that forms the anterolateral wall of the braincase. It is composed of an ascending, broad alar process and an anteriorly directed anterior inferior process. These two processes have a common base, which projects posteriorly to form the otic process. The alar process is high, ovate and oriented almost vertically. The

anterior edge is slightly medially inflected. On the alar process, the anterior semicircular canal runs its course through a thickened crest that anteriorly projects anterolaterally away from the wall of the alar process and could be considered a separate process. Below the anterior semicircular canal, the alar process continues down for a short distance before it is emarginated by the notch for the trigeminal nerve. The trigeminal notch is deep and has sharp angles delineating its anterior extent. The trigeminal notch will also be used here as the arbitrary separation of the alar process and the anterior inferior process. Medially, posterior to the trigeminal notch, are the internal openings of the foramina for the facial and auditory nerves within the acoustic recess.

The anterior inferior process does not extend as far anteriorly as the alar process. It is trapezoidal in lateral view, with the narrower base on the ventral side. Its dominant lateral feature is the crista prootica, which extends from the anterior edge of the anterior inferior process posterodorsally to the contact with otooccipital on the otic process. The crista prootica changes slope twice. It increases slope to form a distinct angle posteroventral to the trigeminal notch and then decreases slope directly dorsal to the posteroventral corner of the anterior inferior process. Tucked into the fold of the crista prootica between these two changes in slope are two foramina for the exit of the branches of the facial nerve (CN VII). In lateral view, the posterior border of the process has a sharp angle ventrally and trends posterodorsally into the otic process. Immediately ventral to the transition to the otic process, ventral to the crista prootica, the posterolateral margin puts out two short processes that form the anterior margin of the fenestra ovalis. In posterior view, the anterior inferior process forms the mushroom-shaped anterior wall of the

cochlear cavity and the contact with the otooccipital. Medially, the anterior portion of the process contributes to the lateral supports of the dorsum sellae (crista sellaris).

The lateral view of the otic process of the prootic is fairly simple. It is a truncated triangle, tapering towards the otooccipital contact. The crista prootica continues its path up the ventral margin of the otic process and the posterolateral margin is serrated to interdigitate with the anterolateral margin of the otooccipital. Internally, the otic process forms the anterolateral wall of the otic capsule and the posterior extension has a broad facet to form a lap joint posteriorly.

Otooccipital:

The otooccipital is composed of the fused exoccipital and opisthotic. It forms the lateral margin of the foramen magnum, the posterolateral wall of the otic capsule and braincase as a whole and contains more foramina than any other bone in the braincase. Starting at the posterior end, one begins with the lateral contribution to the occipital condyle. The condyle is divided about evenly into thirds between the two otooccipitals laterally and the basioccipital ventrally. The contribution of each otooccipital is subtriangular in posterior view. Above the occipital condyle, the posterior margin of the otooccipital arcs to form the concave lateral and dorsolateral margins of the foramen magnum. The margin of the foramen magnum is thickened and round in cross section.

Lateral to the foramen magnum are the posterolaterally directed foramina for the vagus nerve (CN X) and the hypoglossal nerve (CN XII) dorsolateral to that. The vagus nerve pierces through the rim of the foramen magnum, with a round exterior opening and an elongate, pinched opening internally. The foramen for the perilymphatic duct enters the rim of the foramen magnum internally at the corner between the occipital condyle and the

dorsal portion of the rim and exits ventrally adjacent to the vagus foramen. Anterolateral to these foramina, there are two distinct crests. The first, directed anteroventrally, is the crista tuberalis, which forms the posterior border of the lateral opening of the recessus scala tympani. The second, directed laterally, becomes the paroccipital process. The posterior margin of the recessus scala tympani continues ventrally to form a sharp V where it meets the ventral margin of the otooccipital at the contact with the basioccipital. The V-shaped juncture contributes to the posterior of the basal tuber. On the posterior face of the crest, at about its midpoint, anterolateral to the foramina for the hypoglossal and vagus nerves, there are from 1 to 3 tiny foramina for the branches of the accessory nerve (CN XI).

The lateral opening of the recessus scala tympani is an elongate, anteroventrally directed oval, very slightly pinched anteriorly by the posterior curvature of the crista interfenestralis, which forms the anterior border. The ventral rim is open between the crista interfenestralis and the crista tuberalis and their contributions to the sphenoid tubercle and the basal tuber respectively. Anterior to the recessus scala tympani, the otooccipital contacts the posterior of the anterior inferior process of the prootic. The prootic facet is deeply emarginated by the foramen ovale, so that the otooccipital forms the ventral, posterior and dorsal margins of the foramen. The foramen ovale extends nearly to the crista interfenestralis and is overhung by the base of the paroccipital process.

The recessus scala tympani houses a large, posteriorly opening foramen rotundum. Internally, the foramen rotundum opens through the posterior wall of the cochlear cavity, below the recessus utriculi. The ridge between the internal opening of the foramen rotundum and the recessus utriculi separates the cochlear cavity below and the cavum capsularis. Within the cavum capsularis, the recessus utriculi is below the opening of the

horizontal semicircular canal. The horizontal semicircular canal opens again on the prootic facet, just anterior to the paroccipital process. The posterior semicircular canal also has an opening, on the supraoccipital facet, between the foramen magnum and the paroccipital process.

Returning again to the exterior of the otooccipital, the paroccipital process is a posterolaterally directed flange projecting from the contact of the otooccipital with the prootic and supratemporal. The base of the process is subtriangular, but flattens distally into a rectangular, nearly vertically oriented crest. The supratemporal process of the parietal contacts the dorsal side of the paroccipital process from the supratemporal suture to its dorsolateral corner. The supratemporal bone butts against the flattened lateral margin of the process and the squamosal has no direct contact with it. The cephalic condyle of the quadrate articulates with the anteroventral surface of the paroccipital process.

Based on the subterranean habits of *Eremiascincus* one would expect from the predictions of Rieppel (1981), that the paroccipital processes would be shorter than non-sand-swimming relatives. However, The paroccipital processes are similar in proportion to those seen in *Scincus*, *Mabuya*, and *Ctenotus*. The paroccipital processes of all four of those genera are however much shorter than those seen in *Eumeces*. Similarly, although expected only in the burrowers, *Eremiascincus*, *Ctenotus*, *Scincus*, and *Mabuya* have similarly enlarged anterior semicircular canals compared to *Eumeces* and the first three have a relatively large foramen ovale compared to the other two.

Basicranium:

Moving to the ventral side of the braincase, the posterior of the two elements is the basioccipital, and the other is the basisphenoid. The basioccipital resembles an elongate hexagon and is ventrally convex. The contribution of the basioccipital to the occipital condyle is rounded posteriorly and has an obliquely oriented flat facet on either side for articulation with the otooccipitals. The bone is widest in the middle, where it flares out to form the ventrolaterally pointed basal tubers. The basioccipital tapers again anteriorly along its contact with the prootic, and terminates in a straight facet for the basisphenoid containing one shallow median notch. It has well developed basal tubera with epiphyses. The basal tubera start out small in relation to the rest of the basioccipital and grows in proportion in larger individuals. The basioccipital is longer than the basisphenoid, not including the basipterygoid processes. A well-developed crista tuberalis extends from the basal tuber, up the opisthotic, forming the posterolateral opening for the recessus scala tympani, and connecting to the ventromedial border of the base of the paroccipital process. The basioccipital only comprises the ventral-most portion of the opening for the recessus scala tympani. The rest of the opening is within the otooccipital. Thus, the occipital recess is present on the basioccipital in the form of a narrow groove, dorsal to basal tuber.

The basisphenoid is short and bears well-developed, distally expanded basipterygoid processes that have very slightly dorsally concave surfaces that contact the pterygoid. The basisphenoid has a flat posterior facet for the attachment of the basioccipital. This has a median tab that fits into the notch on the opposite side and a thin, triangular lateral lappet on each side, which reach back under the basioccipital. The basisphenoid then expands laterally and dorsally along its contact with the anterior

inferior process of the prootic to form the dorsum sellae medially and the alar process of the sphenoid laterally. The alar process is oriented anterolaterally and overlaps the anterior and anterolateral margins of the anterior inferior process of the prootic. Ventrolateral to the contact between the alar process and the prootic, the ventrolateral crest is pierced by the posterior opening of the vidian canal, which trends anteriorly and exits between the basipterygoid process and the parasphenoid process, anterior to the sella turcica. The dorsum sellae is pierced from the posterior by the two foramina for the abducens nerve (CN VI), and ventrally by the two foramina for the internal carotid artery, which exit laterally and medially respectively on the sella turcica. The alar process of the sphenoid is broad and forms a slight overhang above the lateral head vein.

The basipterygoid processes of the basisphenoid are about the same length as the remainder of the basisphenoid. They have a broad deltoid shaped distal flare, which is dorsomedially interned to articulate with a ventromedial facet on the quadrate process of the pterygoid. Between the basipterygoid processes is a pair of short prongs that make up the parasphenoid process and form the base for the cartilaginous cristae cranii.

A thin, ossified orbitosphenoid is present as a triradiate bone, with two venterocaudal prongs and one rostradorsal. This splinter of thin bone is more commonly lost during rendering of the skull. The parasphenoid process is unossified and is only a very slight spur occurring between the bases for the trabeculae cranii. Contra Evans (2008), no part of the sphenoid or parasphenoid reaches the occipital recess.

Teeth:

Eremiascincus has cylindrical pleurodont teeth with chisel shaped crowns and medial rather than posterior resorption pits. All the teeth have a smooth crown, with a

single cusp, lacking serrations, crenulations, or grooves. Tooth morphology changes slightly, but relatively consistently from the anterior to the posterior of the dentary. At the rostral end of the jaw, the teeth are smaller and the crown is slightly recurved. Posteriorly, the teeth become larger and the crown is tapered somewhat posteriorly and become most conical toward the back of the jaw. As the size of the tooth increases toward the back of the jaw, the crown height remains relatively constant, but the circumference of the tooth increases, while the length of the root varies with the depth of the dental sulcus. This pattern of crown morphology is not as evident in the four smallest individuals. In those, the anterior teeth are still slightly recurved, but not as much as in larger individuals, and the transition to a conical morphology occurs much further forward in the jaw. There are also three specimens that have abnormal teeth, possibly due to errors of replacement, which are discussed below. The morphology of the maxillary teeth change in a similar manner, except that the anterior most teeth are not as recurved as in the dentary, owing to the fact that the premaxillary teeth are the ones that most correspond with the front of the dentary, and the size of the teeth typically peak at tooth position three to five with position four being the most common. Behind position four, the teeth get progressively smaller toward tooth one.

The teeth are set into a shallow pit on the lingual side of the marginal bones and are absent from the pterygoids and vomers. The dentary bears 15 teeth in the smallest individuals and 24 in the largest; the maxilla bears 15 teeth in the smallest individuals and 21 in the largest specimen examined. Regardless of the size of the animal examined, the premaxilla almost always bears four or five teeth for a total of eight or nine teeth. One premaxilla (left ETVP 7135) has only three teeth, but its counterpart has five for a total of

eight. Edmund (1969) points out several studies (Siebenrock 1892; Kingman 1932) that indicate that the right premaxilla almost always bears one more tooth than the left and that the maxilla compensates by having one more on the left. All but one of the specimens of *Eremiascincus* showed the typical asymmetry of the premaxilla. However, only two specimens had one more tooth on the left maxilla than the right. Four of the 15 sets of dentaries had at least one more tooth position on one side of the jaw compared to the other, but the extra tooth was as often on the left dentary as on the right.

The teeth of *Eremiascincus* are replaced at a somewhat regular interval of every fifth tooth in the first 15 teeth. In the smallest specimens, there is a replacement tooth in place, ready to fill the alveolus when the older tooth is lost. In larger specimens, the replacement tooth is missing from the resorption pit, though they are probably lost during the process of skeletonizing the head, when the dental epithelium is eaten or peeled away rather than having a time lag between the loss of one tooth and the start of development of its replacement. Three of the small jaws (left WAMR 146923 and both left and right WAMR 146924) observed showed deformities of the teeth, with crooked crowns and nearly fully formed teeth crammed in the same alveolus as older teeth that lack a resorption pit. In one alveolus of the right dentary of WAMR 146923, there are three teeth in place, one right below the other.

Lower Jaw:

The lower jaw is composed of the dentary, angular, sphenoid, surangular, prearticular, and articular (Figure 2.17). In all specimens examined, the prearticular and articular are completely fused. In subadults, the surangular fuses to the articular-

prearticular, to form the articular complex. The other elements of the lower jaw remain unfused throughout life.

Articular Complex:

The complex is composed of a fused articular, prearticular, and surangular (Figure 2.18). The articular is free of the surangular in early stages of development, but fuses later in life. The angular, however, does not fuse with the other elements of the jaw. The prearticular is fused to the articular early in development and is seen fused in even the smallest individuals examined. The elongate adductor fossa is on the medial side of the articular complex and is composed of a ventral emargination into the prearticular spine of the articular and a dorsal emargination into the surangular.

The articular may be divided into the retroarticular process, the articular condyle and the prearticular spine. The retroarticular process, which bears the insertion of the muscularis pterygoidius, is a long shallow cup made up of a robust central column that has a posterior expansion and a medial flange that brings it flush with the articular condyle, as well as a thin lateral flange. It is obliquely twisted so that there is a major medial component to the orientation of the opening of the fossa and the process as a whole is inflected medially. The oblique twisting of the retroarticular process is a feature shared at the level of the Scleroglossa (Estes et al. 1988: 200), while the posterior broadening of the process, its medial inflection and the presence of a flange on the medial margin are features shared with other members of Scincoidea (Estes et al. 1988: 217).

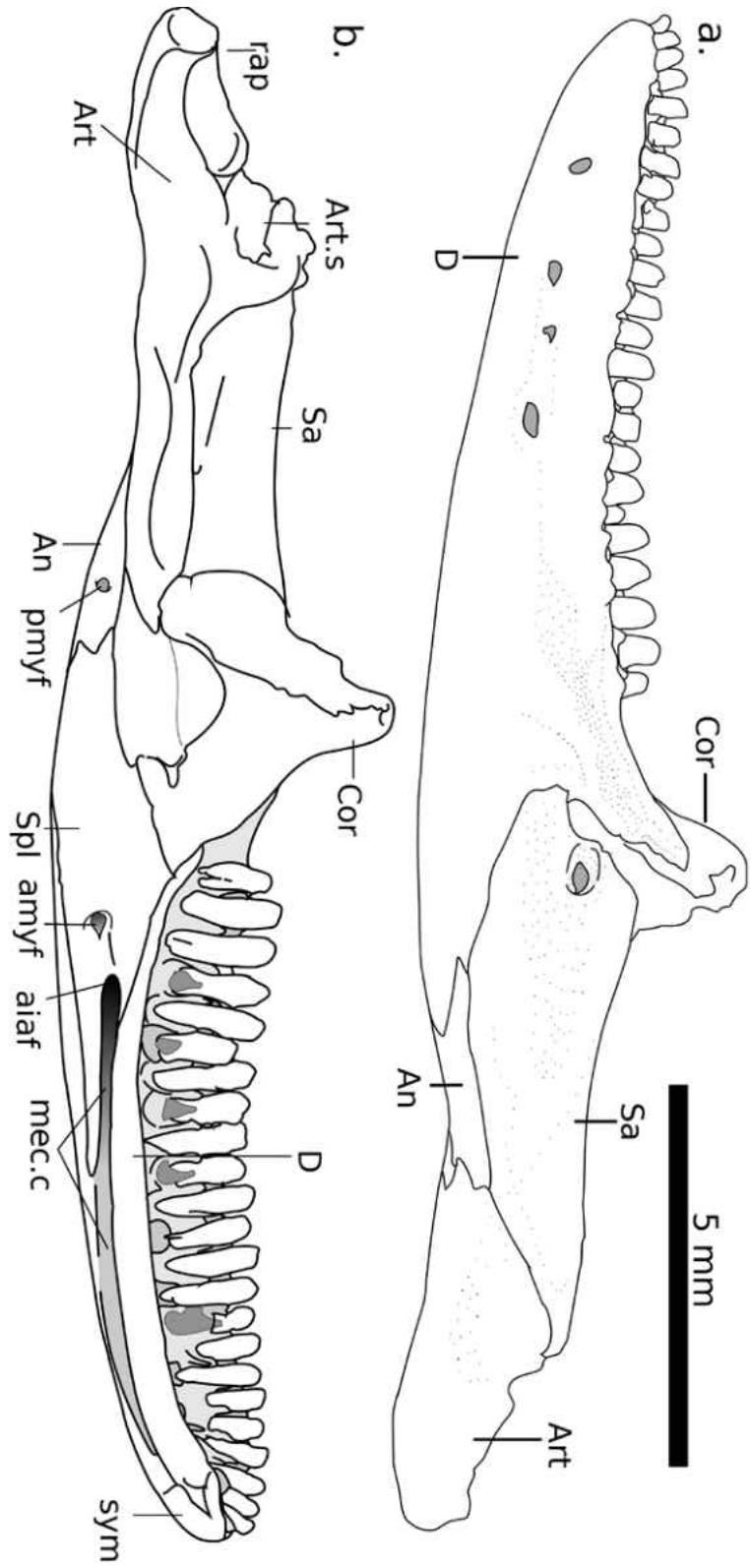


Figure 2.17. Left lower jaw of *Eremiascincus richardsonii* in a) lateral and b) medial views.

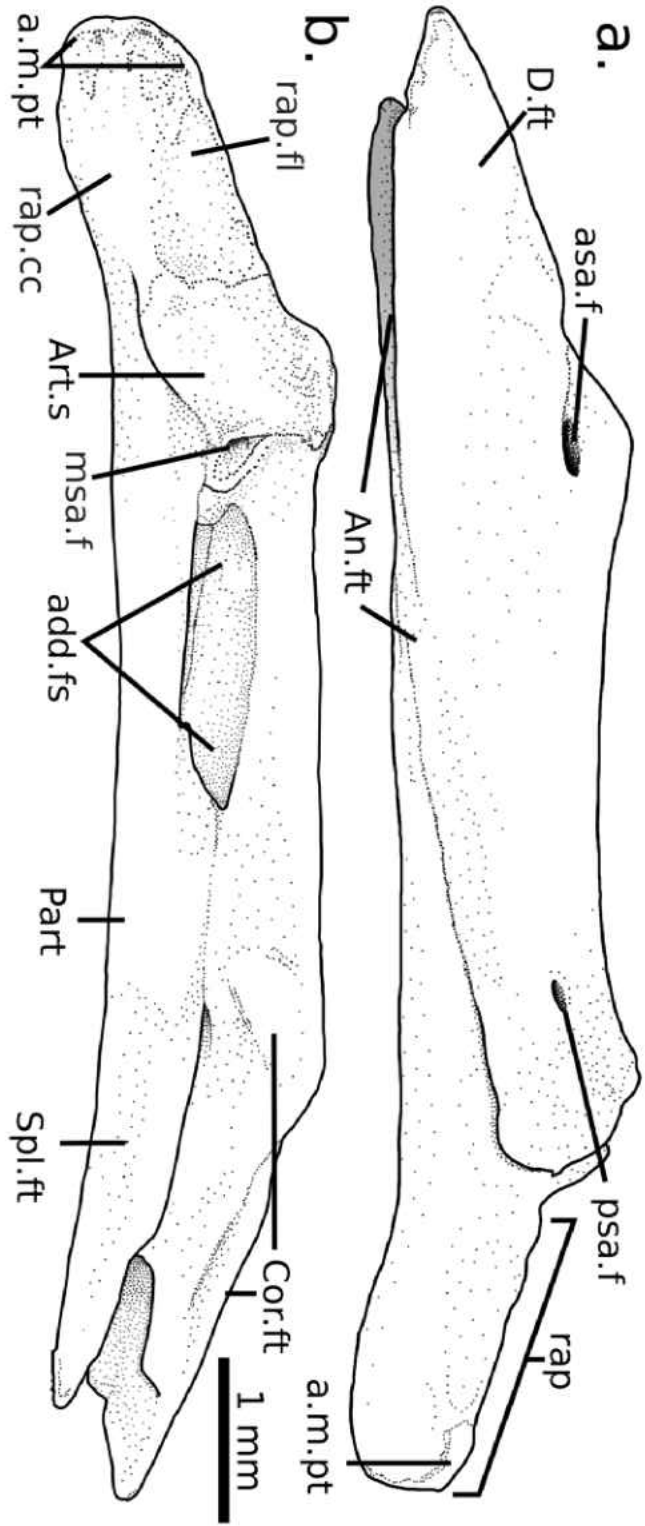


Figure 2.18. Left articular complex of *Eremiascincus richardsonii* in a) lateral and b) medial views.

The articular condyle is somewhat posteriorly directed, is about as long as wide and resembles a pentagon with two parallel sides. It has two small facets posteriorly to accept the articular condyles of the quadrate and a single large protuberance anteriorly that rocks on the anterior side of the articular condyles of the quadrate. There is a small medially directed tubercle immediately anterior to the articular condyle. The prearticular spine is composed of the fused to the prearticular. It is medially grooved for the Meckelian cartilage, and has a facet on the lateral side for the contact with the angular. The prearticular spine dramatically expands about 33% of the way along its length and then tapers to a point anteriorly where it articulates with the posterior process of the dentary, the anteromedial process of the coronoid and the splenial. Posterior to the expansion, the articular spine is smooth and medially concave and forms the ventral margin of the adductor fossa.

The posterior margin of the surangular has a transverse tab that grasps the anterior of the articular condyle of the articular. Anterior to that is the ventral emargination for the adductor fossa. At the posterior edge of the adductor fossa is the posterior surangular foramen, which perforates from the inside of the adductor fossa to the surangular's dorsal margin. The adductor fossa continues anteriorly as a channel between the lateral wall of the surangular and a descending lamina that articulates with the ascending expansion of the articular. Above this descending lamina, there is a triangular dorsal prominence for the articulation of the coronoid. The coronoid prominence is rugose on its medial side for the attachment of the posterior process of the coronoid. Anterior to the coronoid prominence is a facet for the anteromedial process of the coronoid. The anterior surangular foramen pierces the lateral wall of the surangular immediately behind the coronoid facet and exits

the medial wall right behind the descending lamina. Laterally, the anterior surangular foramen opens into a rostrally pointing open groove. The anterior end of the surangular tapers to a point that articulates with the lateral process of the coronoid labially and the posterior notch of the dentary lingually.

Coronoid:

The coronoid forms the dorsal apex of the mandible, rests predominantly on the medial side of the surangular and prearticular, and is the insertion site of both the muscularis adductor mandibulae and the muscularis pseudotemporalis. It is divided from anterior to posterior into four parts, the dentary process, the anteromedial process, the coronoid process and the posterior process (Figure 2.19). On the lateral side of the anteromedial process there is an additional lateral process. As in other skinks, the dentary process and lateral process of the coronoid are overlapped anterodorsally by the large coronoid process of the dentary so that lateral exposure of the lateral process is limited to a narrow wedge between dentary and surangular (Estes et al. 1988). The coronoid process is exposed both medially and laterally, and the posterior process is only exposed medially on the jaw.

The dentary process is a thin spine of bone with a thinner tabular sheet descending from it. This tabular sheet has its own posterior process, the dentary posterior process, which is variably developed from virtually non-existent to a long spine. Anteriorly, the descending tab tapers to a point with the spine of the dentary process. The spine of the dentary process fits into the groove on the ventral side of the dental shelf and extends almost as far forward as the dorsal contact between the splenial and dental shelf. The

lateral side of the descending tab has only a dentary facet. The medial side of the dentary process is divided along its length into a dentary facet and a splenial facet. The spine of the dentary process is entirely obscured from view in the articulated mandible by the dentary and the splenial and the descending tab is only visible posteriomedially where it has a broad, straight contact with the splenial.

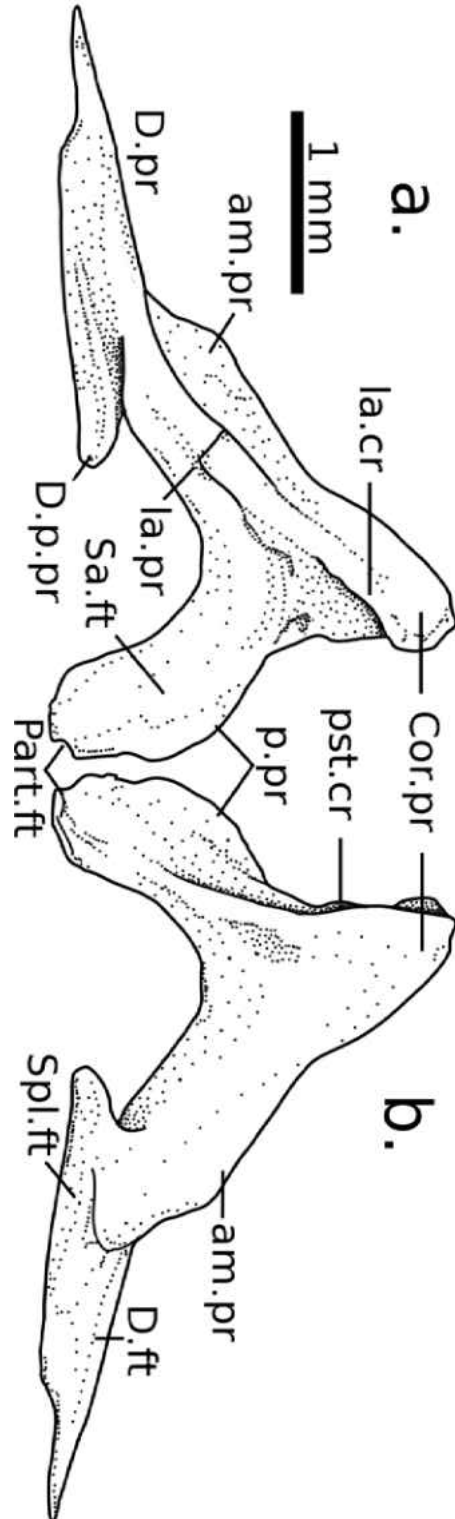


Figure 2.19. Left coronoid of *Eremiascincus richardsonii* in a) lateral and b) medial views.

The remainder of the coronoid is exposed on the medial side of the jaw, though the coronoid process is also exposed laterally. On the medial side, the division between the dentary process and the anteromedial process is distinguished by a change of texture from a faintly striated surface for the suture with the dentary process to a smooth surface. The contact is arrow shaped, with its vertex pointed anteriorly at the contact between the splenial and dentary facets. The anteromedial process has a large facet on its dorsal margin that fits into a ventrally directed groove on the coronoid process of the dentary, a continuation of the groove that grasps the dentary process. The medial side of the anteromedial process is mostly smooth and concave for the attachment of the muscularis pseudotemporalis.

The coronoid process is continuous with the posterior and anteromedial processes, but is distinguished as all of the coronoid that has its lateral side exposed in the articulated jaw. It is tall, triangular, with a slightly convex anterodorsal margin and a straight to slightly concave posterior margin and it is slightly medially inflected. The ventral margin of the coronoid is deeply emarginated, exposing the surangular in medial view. On the lateral side, there is a large lateral crest that runs anteroventrally and terminates in the lateral process. The lateral crest is large but very nearly completely overlapped by the dentary. The large size of the lateral process is a characteristic shared with other scincoides, skinks and cordylids, and the degree of overlap by the dentary is shared among the broader scincomorph group (Estes 1988: pp. 207 & 217). Posterior to this crest is a triangular groove for the muscularis adductor mandibulae externus that attaches to the lateral crest. The medial side of the coronoid process also has a large crest, this one for the attachment

of the muscularis pseudotemporalis. The pseudotemporalis crest runs posteroventrally, all the way down the length of the coronoid process and onto the posterior process.

The posterior process is highly variable in shape, but universally has a major portion that curves to meet the surangular dorsally and the prearticular ventrally. The posterior process may also have an additional triangular secondary process that projects directly posteriorly rather than curving ventrally. This secondary process, where present, overlaps the surangular but does not contact it, instead projecting into the adductor fossa and acting as an extended anchoring point for the basal aponeurosis.

Splénial:

The splénial contacts the dentary, coronoid, prearticular, angular, and surangular. It lies on the medial side of the jaw, starting as a fine point below the apex of the coronoid, expanding mid-length and then tapering rostrally to a narrow splint that partially closes the posterior of the Meckelian canal. There is a small notch in the posterior most point of the splénial where it meets the angular in a sinusoidal suture. Along the posterior half of its dorsal margin, the splénial contacts the descending flange of the surangular. The anterior tip of the splénial is excavated to form the posterior margin anterior inferior alveolar fenestra, which is open anteriorly and is continuous with the lingual exposure of the open Meckelian canal. The entire anterior mylohyoid foramen is within the splénial, located well anterior of the splénial's widest point, but still posterior to the excavation for the anterior inferior alveolar fenestra.

Angular:

The angular remains completely free of fusion with the remainder of the articular complex throughout ontogeny. It is a thin strip of bone, widest at its posterior end that

abruptly narrows and wraps around the ventral margin of the posterior of the jaw. It has a moderate contribution to the labial side, where it grips and is partially overlapped by the angular process of the dentary, moving ventrad anteriorly and having its greatest portion on the ventral margin, and a small contribution to the ventrolingual side, where it contacts the splenial. It is obscured from view by the angular process of the dentary just slightly anteroventral of its splenial contact. The angular also has a notch at its posterior extreme, where it grips the labial side of the articular. The posterior mylohyoid foramen is located entirely within the angular, slightly posteroventral to the contact of the angular with both the articular complex and the splenial.

Dentary:

The dentaries contact one another anteriorly at a 7-shaped symphysis. Each dentary also contacts the splenial, coronoid, surangular, and prearticular, and contains between 17 and 25 tooth positions, with 21, 22, or 23 in most. Overall, the dentary is thin, slightly arched dorsally and curved medially for its entire length (Figure 2.20). There are from 5 to 7 mental foramina on its lateral side. Medially, the dentary is deeply insised by the Meckelian cartilage which is bound dorsally by a large subdental shelf that also contributes to the dorsal margin of the anterior inferior alveolar foramen. The Meckelian canal is open for its entire length, though it is constricted to near closing anterior to the splenial articulation, which comprises about half its length. The open Meckelian canal is characteristic of the *Sphenomorphus* group within the Lygosominae (Greer 1979b). The constriction of the Meckelian fossa is homologous to the apex of the splenial notch. It is well anterior of the inferior alveolar foramen and is between the levels of the 6th and 11th tooth positions.

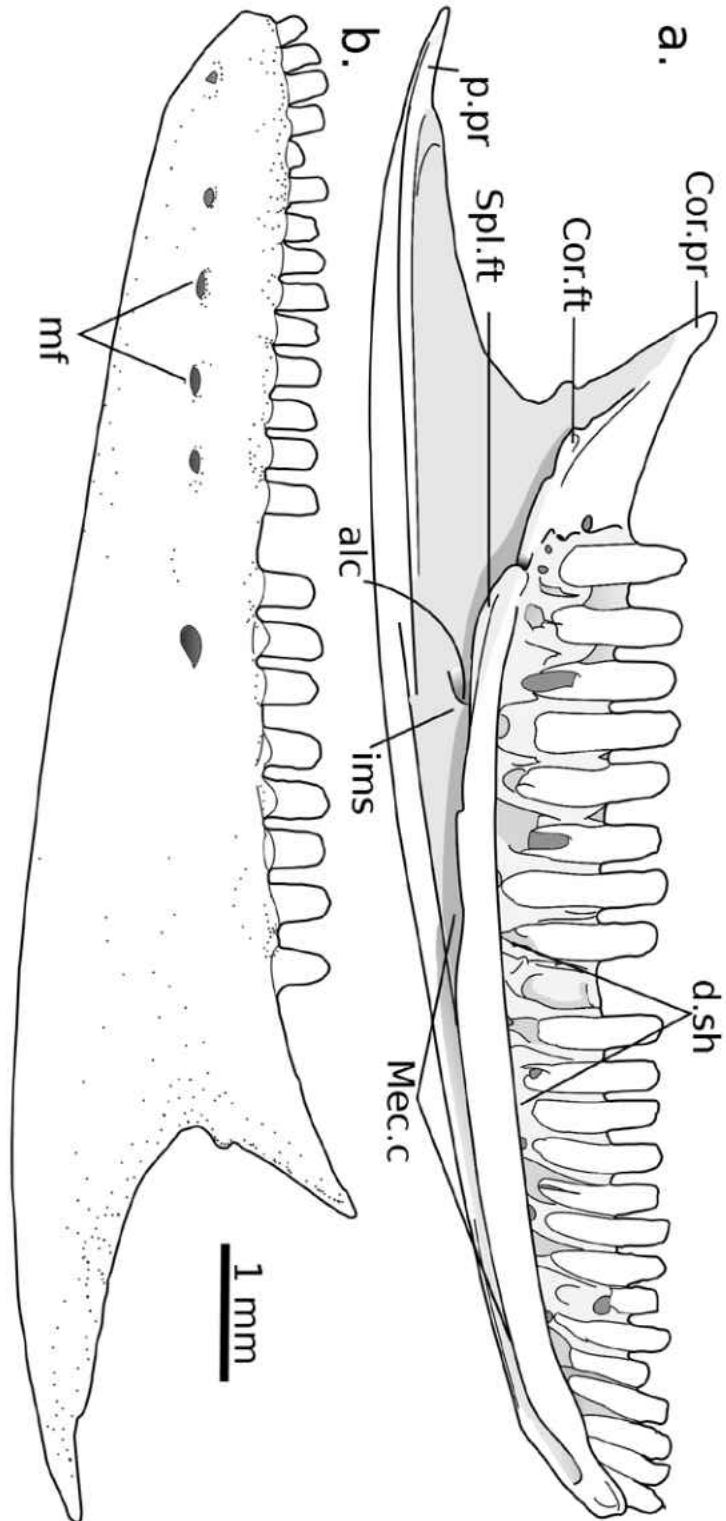


Figure 2.20. Left dentary of *Eremiascincus richardsonii* in a) medial and b) lateral views.

The dental shelf, which constricts the Meckelian canal dorsally, slightly overlaps the ventral edge of the canal laterally, so that the canal is directed inferiorly rather than medially for about the anterior 25% of its length. The groove extends as far anteriorly as the facet of the mental symphysis and its depth increases posteriorly, though this appears due more to the general deepening of the jaw rather than any change in proportion. The dental shelf is continuous with the facets for the splenial and coronoid, appearing to extend the groove posteriorly beyond the posterior opening of the alveolar canal.

The shape of the caudal margin of the internal alveolar septum is variable. The margin is universally, large, elongate and concave, but typically also slanted with the top forward. The top of the internal alveolar septum is typically obscured in medial view by the dental shelf. However, the top is seen from a ventral oblique angle, and is typically located below between tooth positions 2 and 4, while the bottom is between positions 1 and 3. In 5 of the 25 of the dentaries examined, the top of the septum was located directly above its bottom and the posterior margin is acutely concave. In all others, the concavity of the margin of the internal alveolar foramen is more obtuse. The anterior lean of the caudal border may be explained by homology with the caudally projecting prong described by Hutchinson and Mackness (2002) in the jaw of *Tiliqua wilkinsonorum*. If the ventral margin of the prong were fused to the ventral lamina of the dentary, it would give the same appearance as that seen in *Eremiascincus*.

Discussion

Though no new taxonomic distinctions can immediately be drawn from the above description, this is owing most to a lack of similarly detailed descriptions for comparison. *Eremiascincus* displays a suite of derived character states, many of which are characteristic

of the Lygosominae, but also lacks a number of qualities associated with a burrowing lifestyle. The characters that would have been predicted from the taxonomic position of *Eremiascincus* as a Sphenomorphus group skink include: the possession of a fused frontal, up to 9 premaxillary teeth, an open mechelian canal, contact between the ectopterygoid and palatine, medially contacting dorsal and ventral scrolls of the palatine, small size of the descending flanges of the frontal and parietal and medially inflected retroarticular process. *Eremiascincus* shows no particular modification of the braincase, particularly any elongation or enlargement relative to the dermatocranium, as might be anticipated in a face-first burrower (Rieppel 1981). The eyes are still relatively large, and though the jaw is somewhat countersunk, it is not as pronounced as in other burrowers. In order to assess the place of *Eremiascincus* in the context of the evolution of skinks, and in the context of the evolution of burrowing habits, two avenues of research must be done. The first is to build a dataset of direct comparisons of each element across several taxa, which will give insight into identifying characters, as well as trends in morphological evolution associated with ecological shifts. The second avenue will be to examine the skulls of skinks as functional units that are mechanically acted upon during face-first burrowing. It is my hope that the combination of these two avenues of research will yield the insights necessary to separate character states that originate purely from a functional selective pressure, and those characters that arise from taxonomic divergence only.

Acknowledgements

I would like to thank Jim Mead for suggesting that I examine *Eremiascincus* and for collecting the specimens that came from Mt. Gibson station, Western Australia. I would also like to thank Mark Hutchinson of the South Australia Museum for the loan of much

needed articulated specimens. I further appreciate the assistance and input contributed by Sandy Swift, Aaron Abernethy and Sandy Gelnow during the editing process.

Literature Cited

- Camp, C. (1928). Classification of the lizards. *Bulletin of the American Museum of Natural History* **48**: 289-481.
- Conrad, J. (2004). Skull, mandible and hyoid of *Shinisaurus crocodilurus* Ahl (Squamata, Anguimorpha). *Zoological Journal of the Linnean Society* **141**: 399-434.
- Edmund, A.G. (1969). Dentition (pp. 117-200). In: Gans, C., Bellairs, A., and Parsons, T.S. (eds) *Biology of the Reptilia Volume 1, Morphology A*. Academic Press Inc.: London, U.K.
- Estes, R., Gauthier, J. and de Queiroz, K. (1988). Phylogenetic relationships within Squamata (pp 119-282). In: Estes, R., and Pregill, G. (eds) *Phylogenetic Relationships of the Lizard Families: Essays Commemorating Charles L. Camp*. Stanford University Press: Stanford, CA, U.S.A.
- Evans, S.E. (2008). The skull of lizards and Tuatara (pp. 1-347). In: Gans, C., Gaunt, A.S., Adler, K. (eds) *Biology of the Reptilia Vol. 20, Morphology H*. Society for the Study of Amphibians and Reptiles. Ithica, NY, U.S.A.
- Greer, A.E. (1967) A new generic arrangement of some Australian scincid lizards. *Brevoria* **267**: 1-19.
- Greer, A.E. (1970). A Subfamilial Classification of Scincid Lizards. *Bulletin of the Museum of Comparative Zoology* **139 (3)**: 151-184.

- Greer, A.E. (1979a). *Eremiascincus*, a new generic name for some Australian sand swimming skinks (Lacertilia: Scincidae). *Records of the Australian Museum* **32(7)**: 321-338.
- Greer, A.E. (1979b). A Phylogenetic subdivision of Australian skinks. *Records of the Australian Museum* **32(8)**: 339-371.
- Greer, A.E. (1990). The *Glaphyromorphus isolepis* species group (Lacertilia: Scincidae): Diagnosis of the taxon and description of a new species from Timor. *Journal of Herpetology* **24(4)**: 372-377.
- Haas, G. (1973). Muscles of the jaws and associated structures in the Rhynchocephalia and Squamata (pp. 285-490). In: Gans, C. and Parsons, T.S. (eds) *Biology of the Reptilia* Vol. 4. Academic Press: New York, U.S.A.
- Hutchinson, M.N. and Mackness, B.S. (2002). Fossil lizards from the Pliocene Chinchilla Local Fauna, Queensland, with a description of a new species. *Records of the South Australian Museum* **35**: 169-184.
- Kingman, R. H. (1932). A comparative study of the skull in the genus *Eumeces* of the family Scincidae. *Bulletin of the University of Kansas* **20(15)**: 273-295.
- Lakjer, T. (1927). Studien upper die Gaumenregion bei Sauriern im Vergleich mit Anamniern und primitiven Sauropsiden. *Zoologische Jahrbücher, Abteilung für Anatomie und Ontogenie der Tiere* **49**: 57-356.
- Mecke, S., Doughty, P., and Donnel, S. (2009). A news species of *Eremiascincus* (Reptilia: Squamata: Scincidae) from the Great Sandy Desert and Pilbara coast, Western Australia and reassignment of eight species from *Glaphyromorphus* to *Eremiascincus*. *Zootaxa* **2246**: 1-20

- Mittleman, M.B. (1952). A generic synopsis of the lizards of the subfamily Lygosominae. *Smithsonian Misc. Coll* **117 (17)**: 1-35.
- Reeder, T.W. (2003). A phylogeny of the Australian Sphenomorphus group (Scincidae: Squamata) and the phylogenetic placement of the crocodile skinks (Tribolonotus): Bayesian approaches to assessing congruence and obtaining confidence in maximum likelihood inferred relationships. *Molecular Phylogenetics and Evolution* **27**: 384-397.
- Rieppel, O. (1981). The skull and adductor musculature in some burrowing scinciform lizards of the genera *Acontias*, *Typhlosaurus* and *Feylinia*. *Journal of Zoology, London* **195**: 493-528.
- Rieppel, O., Gauthier, J., and Maisano, J. (2008). Comparative morphology of the dermal palate in squamate reptiles, with comments on phylogenetic implications. *Zoological Journal of the Linnean Society* **152**: 131-152.
- Siebenrock, F. (1892). Zur Kenntniss des Kopfskelettes der Scincoiden, Anguiden, und Gerrhosauriden. *Ann. K. K. Naturhist. Mus. Wien* **7**:167-196.
- Storr, G.M. (1964). *Ctenotus*, a new generic name for a group of Australian skinks. *Western Australian Naturalist* **9 (4)**: 84-85.
- Storr, G.M. (1967). The genus *Sphenomorphus* (Lacertilia, Scincidae) in Western Australia and the Northern Territory. *Journal of the Royal Society of Western Australia* **50 (1)**: 10-20.
- Wilson, S., and Swan, G. (2003). *A Complete Guide to Reptiles of Australia*. New Holland Publishers. Sydney, Australia.

CHAPTER 3

Comparing the Cranial Osteology of two Australian Sphenomorphus Group Skinks: *Eremiascincus* and *Ctenotus*

William B. Gel naw

The Don Sundquist Center for Excellence in Paleontology, East Tennessee State University,
Johnson City, Tennessee 37614, United States

Abstract – The variation observed in 10 cranial elements belonging to *Eremiascincus richardsonii* and several species of *Ctenotus* are compared in order to separate the taxonomically informative characters from those that represent intraspecific variation. A total of 127 characters were created to reflect the variation observed, and were subjected to cluster analysis using the parsimony program TNT. The results of the cluster analysis were visualized in MacClade, which has shown to be a valuable tool for quickly assessing taxonomic variation. Using this method, 52 character states were identified that unambiguously differentiated specimens of *Eremiascincus* from *Ctenotus*.

Introduction

The major hurdle to success in paleontology is the ability to confidently identify a particular taxon from an isolated element. Furthermore, the major source of uncertainty is a lack of consensus of what characters are valid for making a confident identification. In the case where the taxa under scrutiny are extinct, the debate over what constitutes a taxonomic character and what reflects intraspecific variation results in a back and forth ebb of lumping taxa together, or splitting them apart, depending on the importance assigned to a character by the author. Where the taxa involved are famous and charismatic, this debate spills even into the popular press, such as has been happening lately with ceratopsian taxonomy (Longrich 2010; Scannella and Horner 2010). Although much of this has been good research, few seem to cite examples of modern taxa as justification for their determination of whether a particular variation in a character state reflects intra- or interspecific variation. Rather than jump directly to charismatic taxa with no modern descendents, this paper will go to first principals by examining a group of modern lizards in the hope of providing information that will lead to their identification as fossils.

Nearly one quarter of all lizard species that are alive today are in the family Scincidae, and of those, about one third, totaling over 370 species, live in Australia (Wilson and Swan 2003). The *Sphenomorphus* group of Australian skinks is dramatically underrepresented in the fossil record, with the bulk of Australian fossil skinks instead attributed to the much more thoroughly described *Egernia* group (Williams 1999; Hutchinson and Mackness 2002; Hutchinson and Scanlon 2009). There are large numbers of undescribed Pleistocene skink fossils from caves throughout Australia (Mead pers. comm.) as well as older, undescribed material from the Mio-Pliocene Riversleigh deposit of

Queensland, Australia (Hutchinson pers. comm.). If a lack of sufficiently diagnostic characters is what has stymied the description of Sphenomorphus group skinks in the fossil record, then it is necessary to examine each genus in the group and establish a catalogue of characters that differentiate them from one another. It is specifically for that reason that establishing what constitutes unambiguous interspecific differences, and what is accounted for by individual variation within a species.

Due to the tremendous scope of work that would be involved in describing all of the variation for all Australian Sphenomorphus skinks, or even a single species group, this paper will focus on two of the most widespread skink genera on the Australian continent. *Eremiascincus* and *Ctenotus* both range throughout the arid interior of Australia, and are similar in size and ecological roles. Furthermore, they are closely related (Reeder 2003). Although several small, tropical species have recently been included in *Eremiascincus* (Mecke et al. 2009), this paper will predominantly focus on *Eremiascincus richardsonii* and *E. fasciolatus* due to their relative abundance in available collections. Also, although *Hemiergus* is more closely related to *Eremiascincus* than *Ctenotus* is, an adult *Hemiergus* is smaller than the smallest examined *Eremiascincus* and size alone would be sufficient to separate the two genera. Similarly, although *Lerista* is more closely related to *Ctenotus* than other genera available in collections, the extremely small size of *Lerista* makes it easily distinguishable by size alone. Discussion of other skinks is included here, and is meant to provide context for *Eremiascincus* and *Ctenotus* within higher taxonomic levels.

The principal objectives of this paper will be two fold. Chiefly, the aim is to establish the framework of a dataset for the analysis of variability among Australian skinks so that they can be identified as fossils. Secondly, this paper will assess the utility of using the

parsimony method utilized by phylogenetics software, to identify characters that are diagnostic for each taxon. The assessment of using phylogenetics software will be supplemented by using Bayes theorem to calculate the probability of achieving a correct identification given each character state.

Materials and Methods

New, qualitative, osteological characters were developed by comparing the disarticulated skulls of 14 *Eremiascincus richardsonii*, 1 *E. fasciolatus*, and 8 *Ctenotus sp.* (Table 3.1). The 23 individuals of the two genera were assessed for 127 characters on 10 cranial elements. The skeletal elements examined for this study were the articular complex (made up of the fused articular and surangular), coronoid, dentary, frontal, maxilla, palatine, parietal, postfrontal, pterygoid, and quadrate. In order to account for lateral asymmetry, and in order to bolster the dataset, left and right elements from one individual were treated separately. The frontal and parietal, which are not paired, are instead recorded twice. The dataset was compiled in MacClade4 (Maddison and Maddison 1992) and then subjected to an unrooted, heuristic parsimony search in the phylogenetics software TNT (Goloboff et al. 2008). All characters were equally weighted and left unordered. If more than one shortest tree was found, then the TNT software would have been used to calculate a strict consensus and a 50% majority rule tree. The resulting shortest tree was exported back to MacClade4 for visualization.

Table 3.1. List of the specimens used for comparison. Snout-vent length given where available. ETVP = East Tennessee State University Laboratory of Vertebrate Paleontology, SAMR = South Australia Museum, WAMR = Western Australia Museum, NA = not available.

Species	Specimen number	SVL (mm)
<i>Eremiascincus richardsonii</i>	WAMR 146922	36
<i>Eremiascincus richardsonii</i>	WAMR 146923	44
<i>Eremiascincus richardsonii</i>	WAMR 146924	47
<i>Eremiascincus richardsonii</i>	ETVP 7127	NA
<i>Eremiascincus richardsonii</i>	ETVP 7128	NA
<i>Eremiascincus richardsonii</i>	ETVP 7129	NA
<i>Eremiascincus richardsonii</i>	ETVP 7130	NA
<i>Eremiascincus richardsonii</i>	ETVP 7131	NA
<i>Eremiascincus richardsonii</i>	ETVP 7132	NA
<i>Eremiascincus richardsonii</i>	ETVP 7133	NA
<i>Eremiascincus richardsonii</i>	ETVP 7134	NA
<i>Eremiascincus richardsonii</i>	ETVP 7135	NA
<i>Eremiascincus richardsonii</i>	ETVP 7136	NA
<i>Eremiascincus richardsonii</i>	ETVP 7137	NA
<i>Ctenotus severus</i>	WAMR 146910	NA
<i>Ctenotus labillardieri</i>	ETVP 7138	NA
<i>Ctenotus schomburgkii</i>	ETVP 7139	NA
<i>Ctenotus severus</i>	WAMR 146912	49
<i>Ctenotus schomburgkii</i>	WAMR 146916	53
<i>Ctenotus severus</i>	WAMR 146913	69
<i>Ctenotus mimetes</i>	WAMR 146909	69
<i>Ctenotus mimetes</i>	WAMR 146927	74
<i>Eremiascincus fasciolatus</i>	SAMR 11125	71
<i>Eremiascincus richardsonii</i>	WAMR 146921	83

Although TNT is designed for phylogenetic analysis, the parsimony search is here intended as a form of cluster analysis that requires no a priori taxonomic information. If the variation of character states is divisible along taxonomic lines, then each genus should fall out either as a separate clade or as one clade nested within the other. The distribution of character state changes on the consensus trees was then used to determine the defining characters of each genus or cluster. Furthermore, it was conjectured that if the ontogenetic series were sufficiently complete, and the steps between individual sizes were sufficiently small, then the cladogram would reflect the similarity of young individuals and the diverging developmental trajectories as they grew. This however assumes that each genus only has one developmental trajectory and that long-branch attraction between similar adult individuals will not cause a departure from reflecting the ontogeny.

Afterwards, using cladistic bracketing as a method of filling in missing character states, the resulting tree was mined for the proportion of individuals showing each character state that fell into each genus. Given these proportions and using Baye's theorem, the probabilities of an individual belonging to either *Eremiascincus* or *Ctenotus* were calculated given that the specimen showed character state 0 and then for character state 1. To simplify calculations, only characters that possessed two alternate states were used. Since the proportion of each taxon in the sample represents what was available in collections rather than a natural population, the null hypothesis used was that populations are equal. If this data set were used as a tool for identifying fossils, in which case actual proportions within a population are largely unknown, it would be fair, at least at first, to treat each taxon as equally likely to occur.

What follows are the characters used in this analysis. There are 10 elements analyzed here, which are arranged alphabetically rather than by functional region. There were 12 characters devised for the articular complex, 12 on the coronoid, 8 on the dentary, 10 on the frontal, 20 on the maxilla, 10 on the palatine, 12 on the parietal, 13 on the postfrontal, 16 on the pterygoid and 13 on the quadrate for a total of 126 characters. Character states are not in any particular order and are not intended to indicate polarity. Figures that accompany each element are not drawn to scale and in some cases include drawings of composites of several real elements drawn as one bone in order to show all the characters and their respective polymorphisms. The character number is labeled in each figure, with the particular state indicated in parentheses. Individual character coding for all specimens is given in Appendix B.

Articular Complex (Figure 3.1):

- ar01. At the posterior end of the retroarticular process, the central column: remains narrow (0); expands laterally (1).
- ar02. The posterior edge of the retroarticular process: is rounded (0); is squared off (1).
- ar03. In dorsal view, the posterior margin of the lateral lamina of retroarticular process: curls somewhat over the process (0); curls, but past the vertical plane (1).
- ar04. Relative to the main body of the mandibular ramus, the retroarticular process is: not or only slightly ventrally deflected in lateral view (0); very ventrally deflected in lateral view (1).
- ar05. The retroarticular process makes up: about 20% of the length of the length of the articular complex or less; about 25% of the length of the articular complex or more (1).

- ar06. Adductor fossa: does not taper anteriorly before closing (0); tapers somewhat to a point (1).
- ar07. Anterior extent of the surangular: roughly equal in length to the prearticular (0); significantly longer than the prearticular (1).
- ar08. Dentary facet: clearly delineated and visible in lateral view (0); indistinct (1).
- ar09. Anterior surangular foramen: visible in lateral view (0); blocked from lateral view by a thin ascending lamina (1).
- ar10. The anterior tip of the surangular: has several rostral projections that together made a broad contact with the dentary (0); has one rostral projection that tapers to a point (1).
- ar11. The articulation for the angular is a: tongue in groove joint (0); broad lap joint (1).
- ar12. Articular and surangular are: not fused (0); Fused (1). This character is intended as a potential indicator of relative maturity.

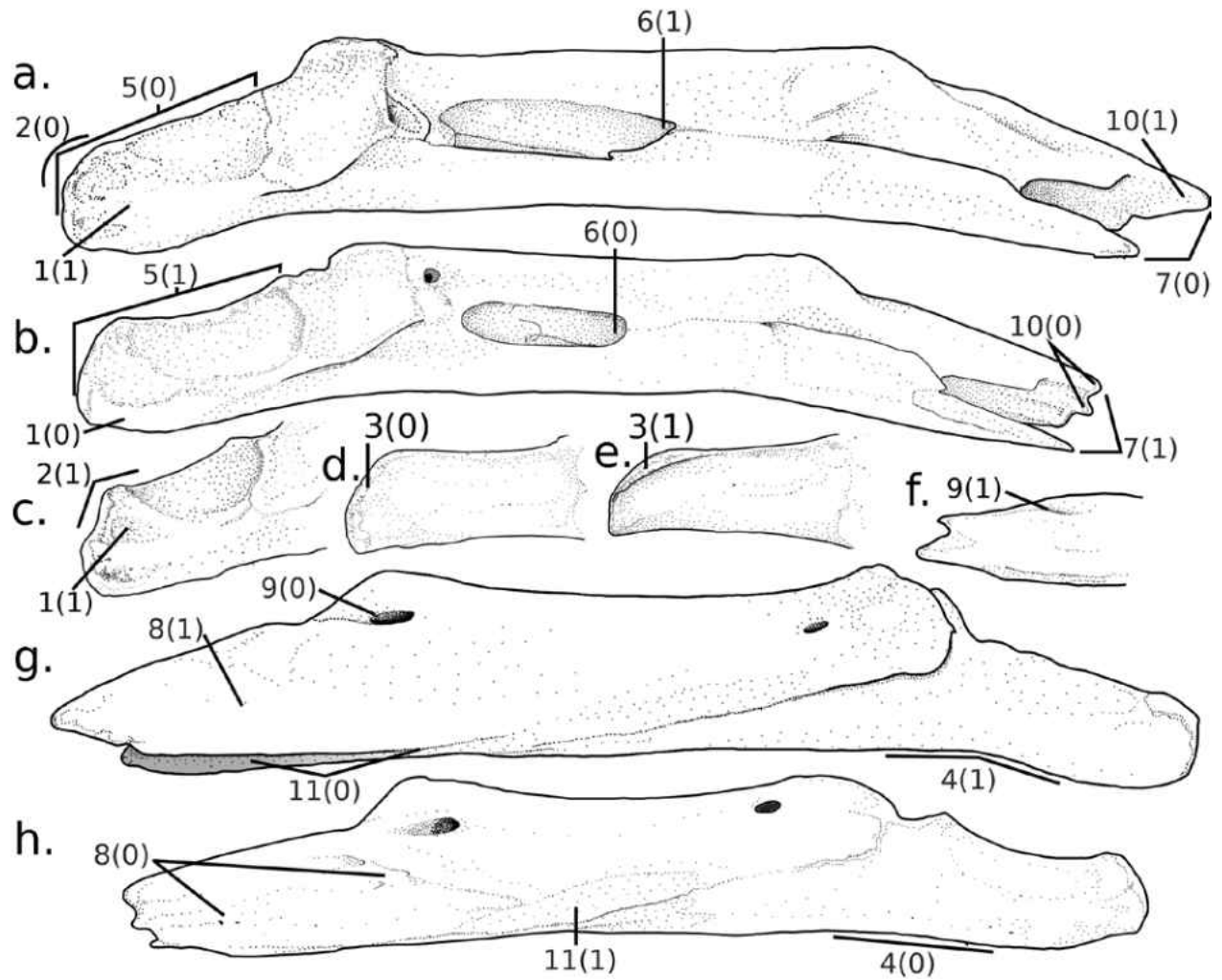


Figure 3.1. The distinguishing characters on a left articular complex a) of *Eremiascincus* in medial view and b) of *Ctenotus* in medial view. C. The left retroarticular process of *Eremiascincus* in medial view. The left retroarticular process of d) *Ctenotus* and e) *Eremiascincus* in dorsal view. F) The anterior tip of the surangular process of *Ctenotus* in lateral view. The left articular complex in lateral view of g) *Eremiascincus* and h) *Ctenotus*. Not drawn to scale.

Coronoid (Figure 3.2):

- co01. Crest delineating the dorsal border of the masseteric fossa: weak to moderate (0); strong (1).
- co02. Dentary process: long and relatively narrow (0); short and relatively deep (1)
- co03. Lateral process: weak (0); moderately developed (1); strongly developed (2).
- co04. Curvature of the surangular process: obtuse (0); acute (1).
- co05. Anterior angle on dorsal margin of the superior dentary facet: weak to non-existent (0); well developed (1).
- co06. Posterior projection of the dentary process: weakly developed (0); well developed (1).
- co07. In medial view, the posteromedial crest is low and close to the surface of the rest of the posterior process (0); high and sharply defined (1).
- co08. Splenial facet on the dentary process: extends to the tip of the posterior dentary process (0); does not extend to the tip of the posterior dentary process (1).
- co09. Line between the splenial facet and the dentary facet: at or below the midline of the dentary process (0); nearer to the top of the dentary process (1).
- co10. Tip of the posterior process points: primarily: downward (0); backward (1).
- co11. Delineation between anteromedial process and the dentary process is distinct (0); indistinct (1).
- co12. Posteromedial crest: lacks an accessory crest (0); has a lateral accessory crest that is present but low (1); has a well-developed and high accessory crest (2).

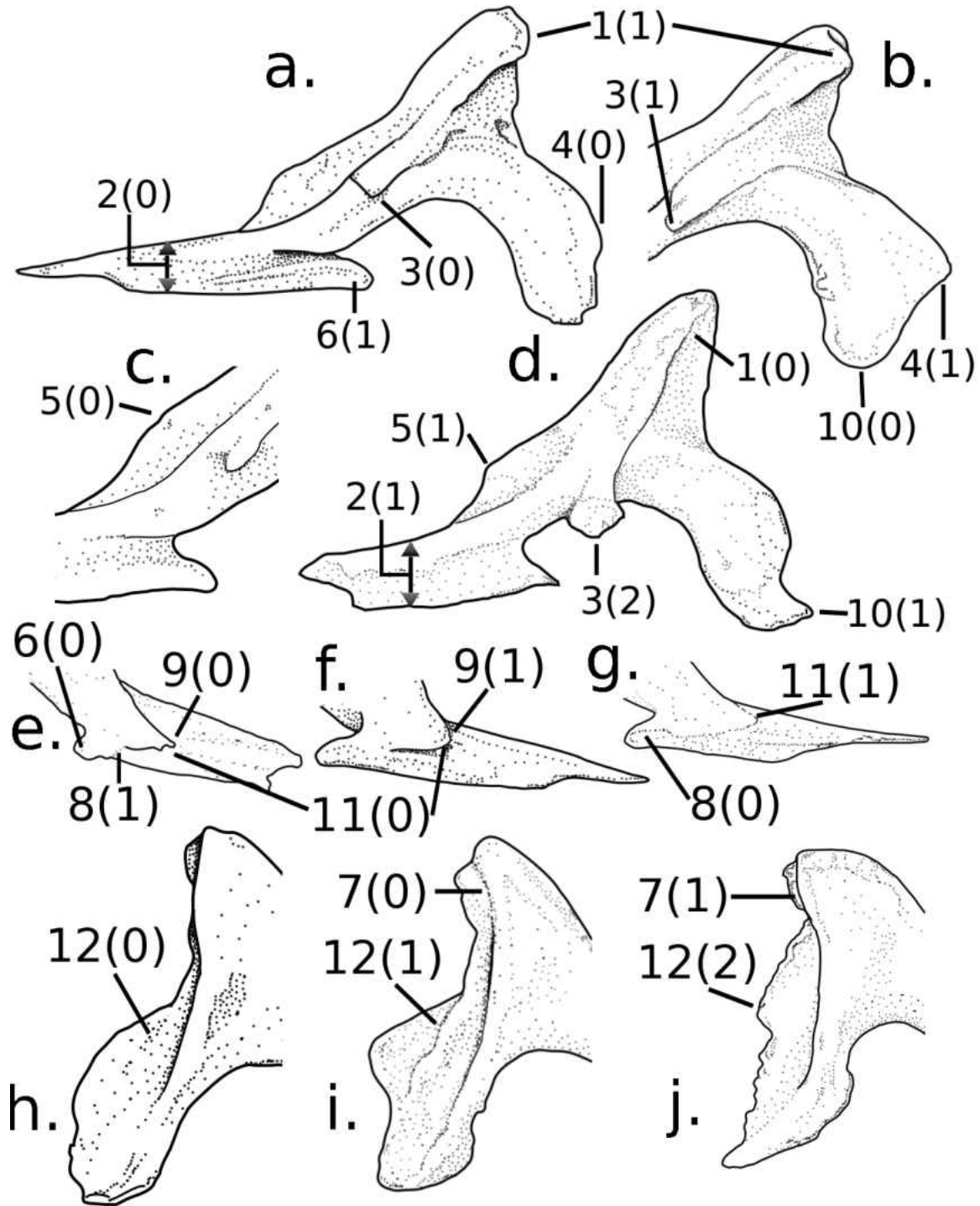


Figure 3.2. The distinguishing characters on a left coronoid a) of *Eremiascincus* in lateral view, b) the coronoid process and posterior process, c) the anteromedial process, d) the coronoid of *Ctenotus*, e, f, g) medial views of the dentary process, h, i, j) medial views of the coronoid process posterior process and posteromedial crest. Not to scale.

Dentary (Figure 3.3):

- d01. Dorsal margin of the posterior/ angular process: concave (0); straight (1); convex (2).
- d02. Posterior tip of the angular process: single to weakly bifid (0); bifid to strongly bifid (1).
- d03. Dorsal margin of dorsal process: concave (0); straight (1); convex (2).
- d04. Tip of the dorsal process: sharp (0); rounded or bifid (1).
- d05. Angle formed by the intersection of the posterior margins of the dorsal and angular processes: less than 90° (0); about 90° (1); greater than 90° (2).
- d06. Gap between the posterior most mental foramen and the next: about the same as other gaps (0); wider than the others (1); narrower than the others (2).
- d07. Coronoid facet: smoothly curves and transitions to the dorsal margin of the Meckelian canal (0); has a distinct obtuse angle to it (1).
- d08. Meckelian groove: unfused (0); closed and/ or fused into a canal.

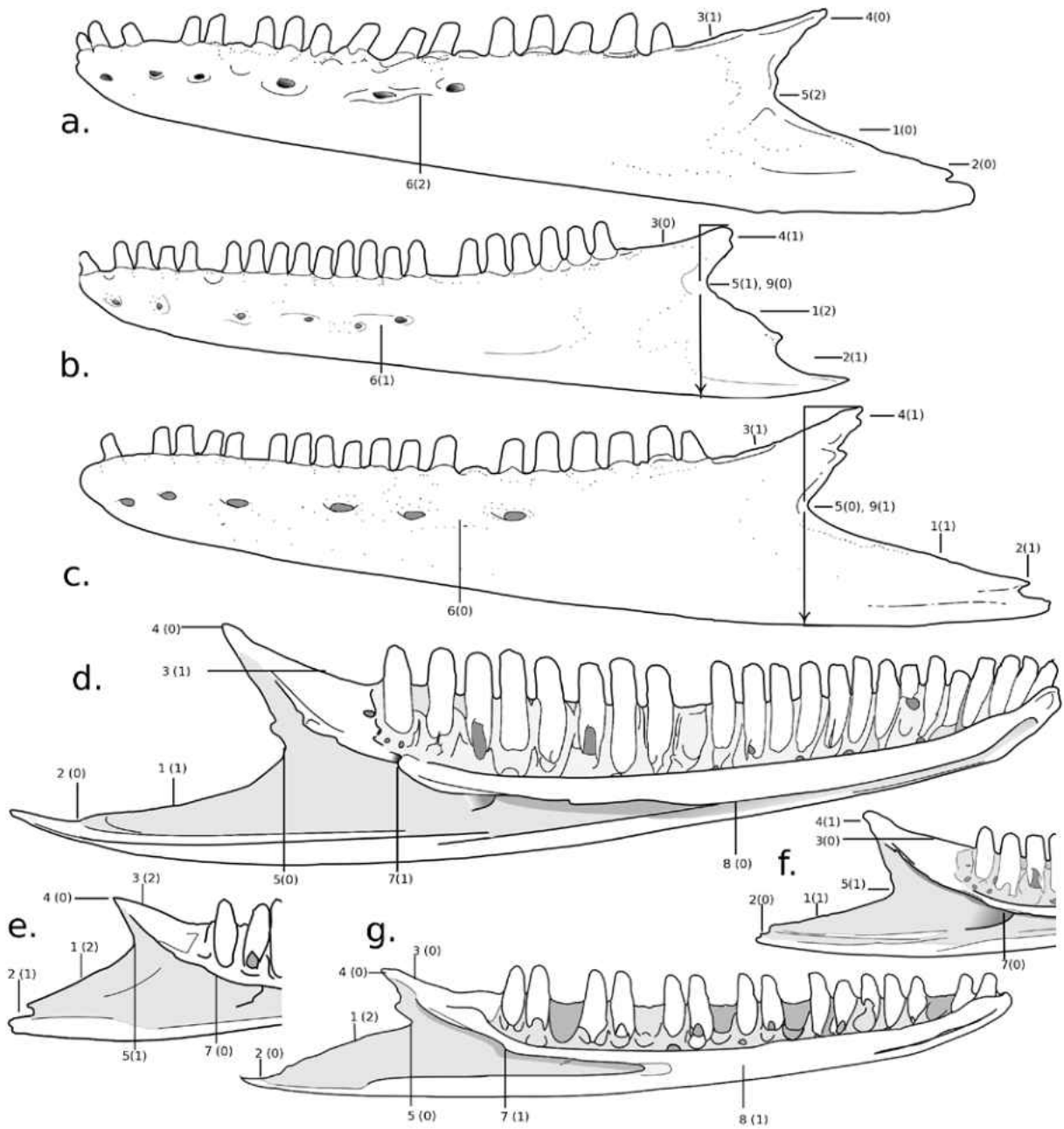


Figure 3.3. The distinguishing characters on a left dentary a) of *Eremiascincus* in lateral view, b) of *Ctenotus* in lateral view, c) of *Eremiascincus* in lateral view, d) of *Eremiascincus* in medial view, e, f) posterior and coronoid processes of the dentary of *Eremiascincus* in medial view, and g) the dentary of *Ctenotus* in medial view. Not drawn to scale.

Frontal (Figure 3.4):

- f01. Anterior margin: flat or concave (0); pointed/ strongly convex (1).
- f02. Maximum width anterior to the orbital constriction: narrow, at about 30% of the frontal's total length (0); wide, at about 40% of the frontal's total length or greater (1).
- f03. Orbital constriction: narrow, at less than 18% of the total length (0); relatively wide, at greater than 18% of the total length (1). The orbital constriction is measured as the narrowest part of the frontal perpendicular to its long axis between the postfrontal facet and the prefrontal facet. This measurement is compared to the total length rather than the anterior width because there was no overlap in the ratio of the former between the genera, and there was overlap in the ratio of the later.
- f04. Posterior margin: straight (0); shaped like a broad W (1).
- f05. Facets for the parietal lapets: difficult to see (0); clearly delineated (1).
- f06. In ventral view, a medial, longitudinal ridge is: absent (0); present (1).
- f07. Crista cranii overlap: 45-52% (0); 52-59% (1); 59-66% (2) of the ventral side of the orbital constriction.
- f08. The anterior angle of the crista cranii: has a tapering or indistinct termination (0); forms a single, well-defined and sharp point (1); has two points that contribute to a tapering effect (2).
- f09. The anterior terminus of the postfrontal facet is poorly defined (0); distinct (1).
- f10. The posterior terminus of the prefrontal facet is poorly defined (0); distinct (1).

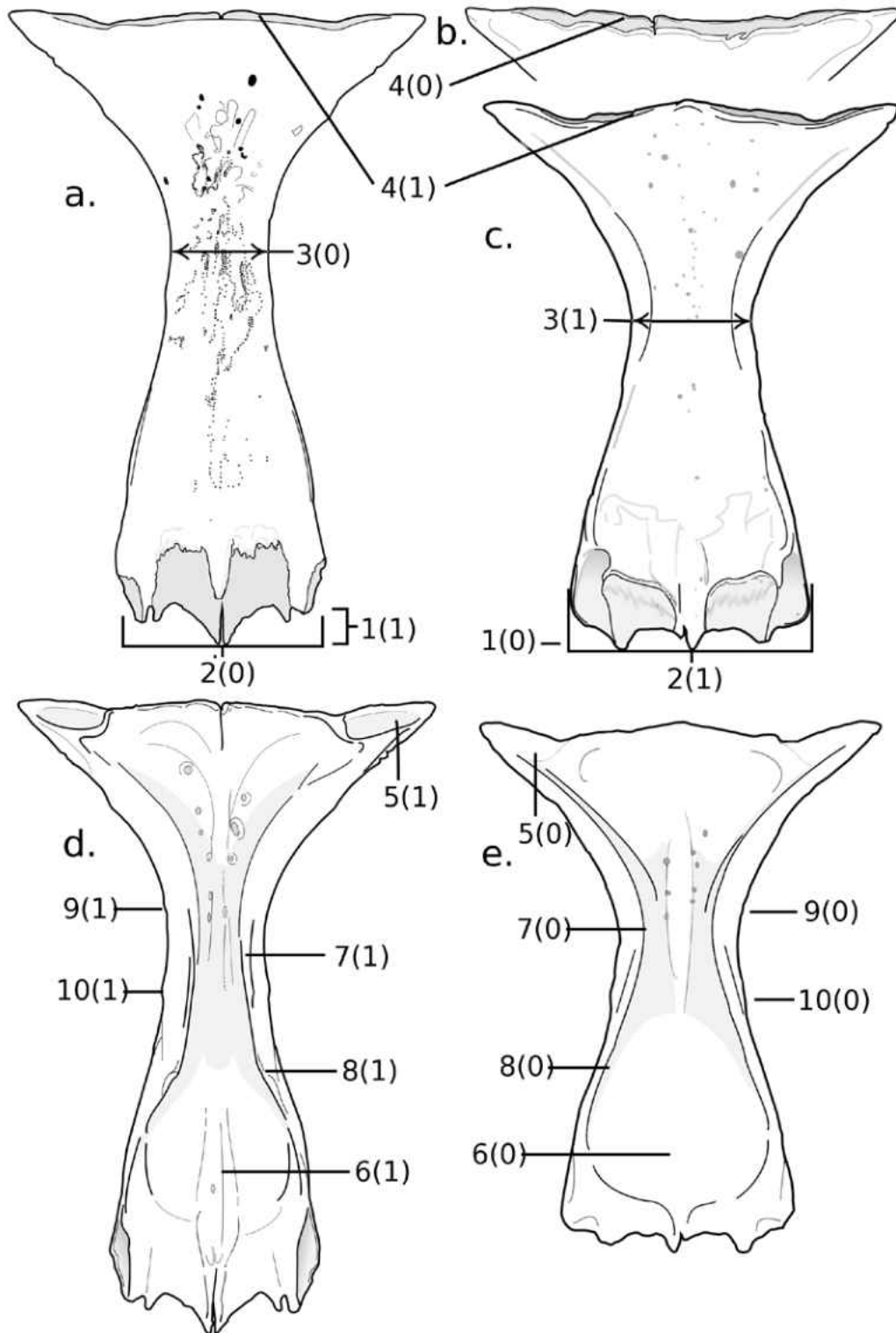


Figure 3.4. The distinguishing characters on a frontal a) of *Eremiascincus* in dorsal view, b) the posterior margin of the frontal of *Eremiascincus* in dorsal view, c) a frontal of *Ctenotus* in dorsal view, d,e) the frontals of *Eremiascincus* and *Ctenotus* in ventral view. Not drawn to scale.

Maxilla (Figure 3.5):

- m01. Number of tooth positions: 15 or fewer (0); 16 or 17 (1); 18 or 19 (2); 20 or 21 (3); 22 or 23 (4); 24 or 25 (5); 26 or more (6).
- m02. Posterior processes: superior longer (0); equal length (1); inferior longer (2).
- m03. Ventral margin of the upper posterior process: sinusoidal (1); straight (2); convex (3).
- m04. Nasal facet: does not overhang or very slightly overhangs the narial opening but lacks a distinct process (0); overhangs the narial opening to a great extent and has a distinct process (1);
- m05. Narial opening has a: long, smoothly curved or straight margin (0); short, strongly curved margin with an anterior drop-off in slope (1).
- m06. Nasal facet: straight (0); convex (1).
- m07. Amount of division of the ascending nasal process: single dorsal apex (0); one small secondary process (1); one large secondary process, sometimes with a small notched, located close to the apex of the ascending nasal process (2); one distinct process spaced far from the apex (3); two distinct secondary processes (4).
- m08. Posterior drop-off of slope behind the frontal facet: gentle to non-existent (0); distinct and large (1).
- m09. Posterior portion of the prefrontal facet: concave (0); straight (1); convex (2).
- m10. Posterior drop-off behind the prefrontal area: gentle to non-existent (0); distinct (1).
- m11. Openings for foramen for the maxillary branch of the trigeminal nerve (cranial nerve V) and superior alveolar canal: separate, not in a common recess (0);

separate but in a common recess (1); form a single elongate opening (2); form a single round opening.

m12. Centre of the opening(s) for foramen for the maxillary branch of the trigeminal nerve (cranial nerve V) and superior alveolar canal: below the centre of the frontal facet (0); below the posterior of the frontal facet (1).

m13. Center of the opening(s) for foramen for the maxillary branch of the trigeminal nerve and superior alveolar canal: above tooth number

m14. Vertex of the choanal shelf: in line with the foramen for the maxillary branch of the trigeminal nerve opening (0); slightly posterior to the foramen for the maxillary branch of the trigeminal nerve opening (1).

m15. Choanal shelf: strongly downturned (0); weakly downturned to straight (1).

m16. Number of large external foramina: 3(0); 4(1); 5(2); 6(3); 7(4).

m17. Ventral margin of the maxilla in lateral view: straight (0); fluted (1).

m18. Jugal facet/groove: somewhat constricts (0); constricts greatly but doesn't close anteriorly (1); closes anteriorly (2).

m19. Medial margins in the gap between premaxillary processes: diverging anteriorly or well rounded (0); parallel and squared off (1).

m20. The septomaxillary process: slender and about as long as the premaxillary process (0); broad and about 75% the length of the premaxillary process (1).

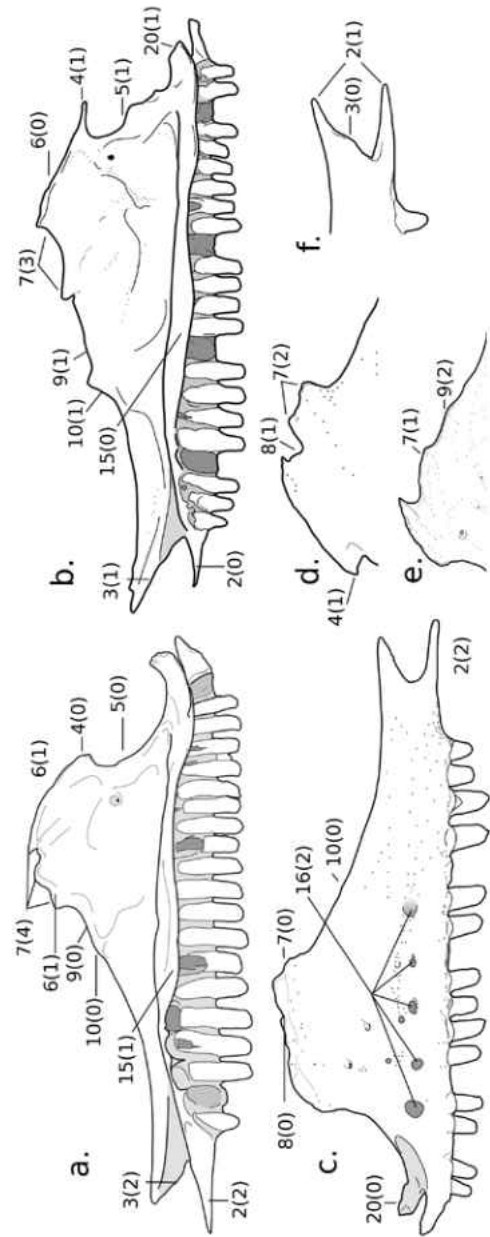


Figure 3.5. The distinguishing characters on a maxilla a) of *Eremiascincus* and b) *Ctenotus* in medial view, c) a maxilla of *Eremiascincus* in lateral view, d, e) ascending nasal processes in lateral view, and f) the posterior processes in lateral view. Not drawn to scale.

Palatine (Figure 3.6):

pa01.Vomerine process: does not extend as far as the anterolateral process of the ventral lamina (0); extends further than the anterolateral process of the ventral lamina (1).

pa02.Anterior margin of the prefrontal facet: runs perpendicular (0); runs somewhat oblique (1) relative to the long axis of the bone.

pa03.Posteromedial process of the ventral lamina: extends about as far posteriorly as the pterygoid process (0); extends dramatically further posteriorly than the pterygoid process (1).

pa04.Dorsal lamina meet along the midline: less than half their length (0); about half their length or more (1).

pa05.The pterygoid process extends about the same distance or a little further posteriorly than the ectopterygoid facet, and there is either no notch or a narrow notch between them (0); The pterygoid process extends much further posteriorly than the ectopterygoid facet and there is a broad notch between them (1).

pa06.Sculpting of dorsal lamina: absent (0); present(1).

pa07.Medial anterior process on the dorsal lamina: projects as far as (0); projects further than (1) the medial ventral process.

pa08.The ratio of the total length to the width is: less than 7:2 (0); greater than 7:2 (1).

pa09.The ectopterygoid facet is: pointed (0); rounded (1); squared off (2).

pa10.The ectopterygoid facet is: narrow (0); broad (1).

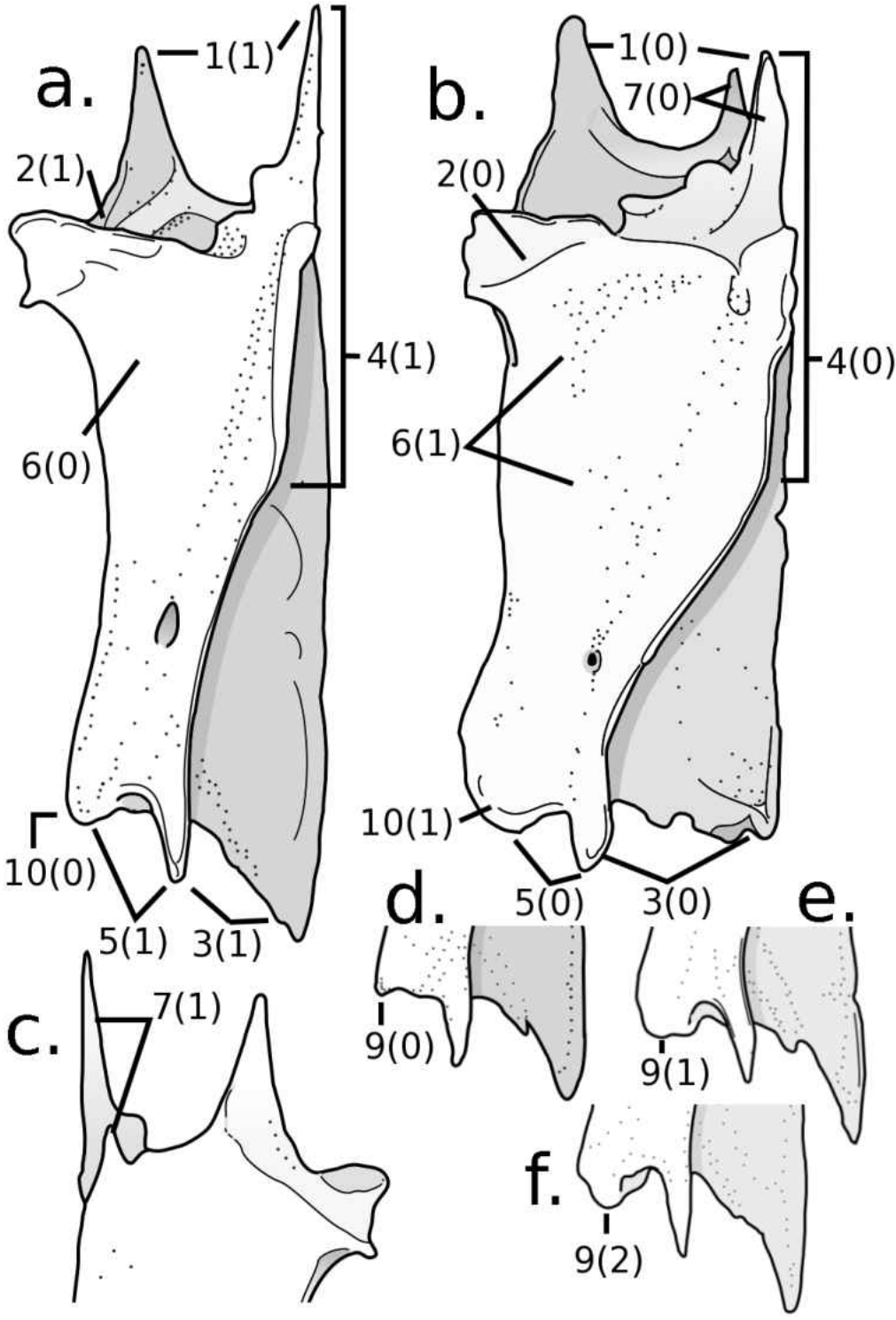


Figure 3.6. The distinguishing characters of a left palatine a) of *Eremiascincus* b) *Ctenotus*, c) the anterior of the left palatine of *Eremiascincus* in ventral view, d, e, f) posterior extent of the left palatine in dorsal view. Not drawn to scale.

Parietal (Figure 3.7):

- p01. Frontal lapets: meet the anterolateral corners of the parietal (0); fail to extend all the way to the corners (1).
- p02. Dermal sculpting: absent (0); present but not raised (1); present and raised (2).
- p03. Anterolateral edge of the parietal, above the frontal lappet is3: concave (0); straight (1); convex (2).
- p04. Ventrolateral crest flares out anteriorly: unevenly, making it 7 shaped (0); evenly, making it Y shaped (1).
- p05. Notch between the posterior processes in dorsal view: gently rounded (0); intermediate, ranging from squared to rounded but having a virtex (1); v-shaped (2).
- p06. Nutritive pits on the underside of the parietal table: absent (0); small (1); large (2).
- p07. Anteromedial margin of the temporal muscle scar: angular (0); rounded (1).
- p08. Anterolateral margin of the temporal muscle scar: an angular turn (0); gently rounded (1).
- p09. Fusion: incomplete with open suture between the two halves of the anterior parietal (0); incomplete but greater than half fused (1); completely fused (2).
- p10. Ventral process: moderate to well developed (0); small (1).
- p11. Lateral flange for the attachment of the pseudotemporalis musculature: poorly developed or absent (0); well developed (1).
- p12. Notch between the posterior processes: parallel with the supratemporal gap (0); posterior to the supratemporal gap (1).

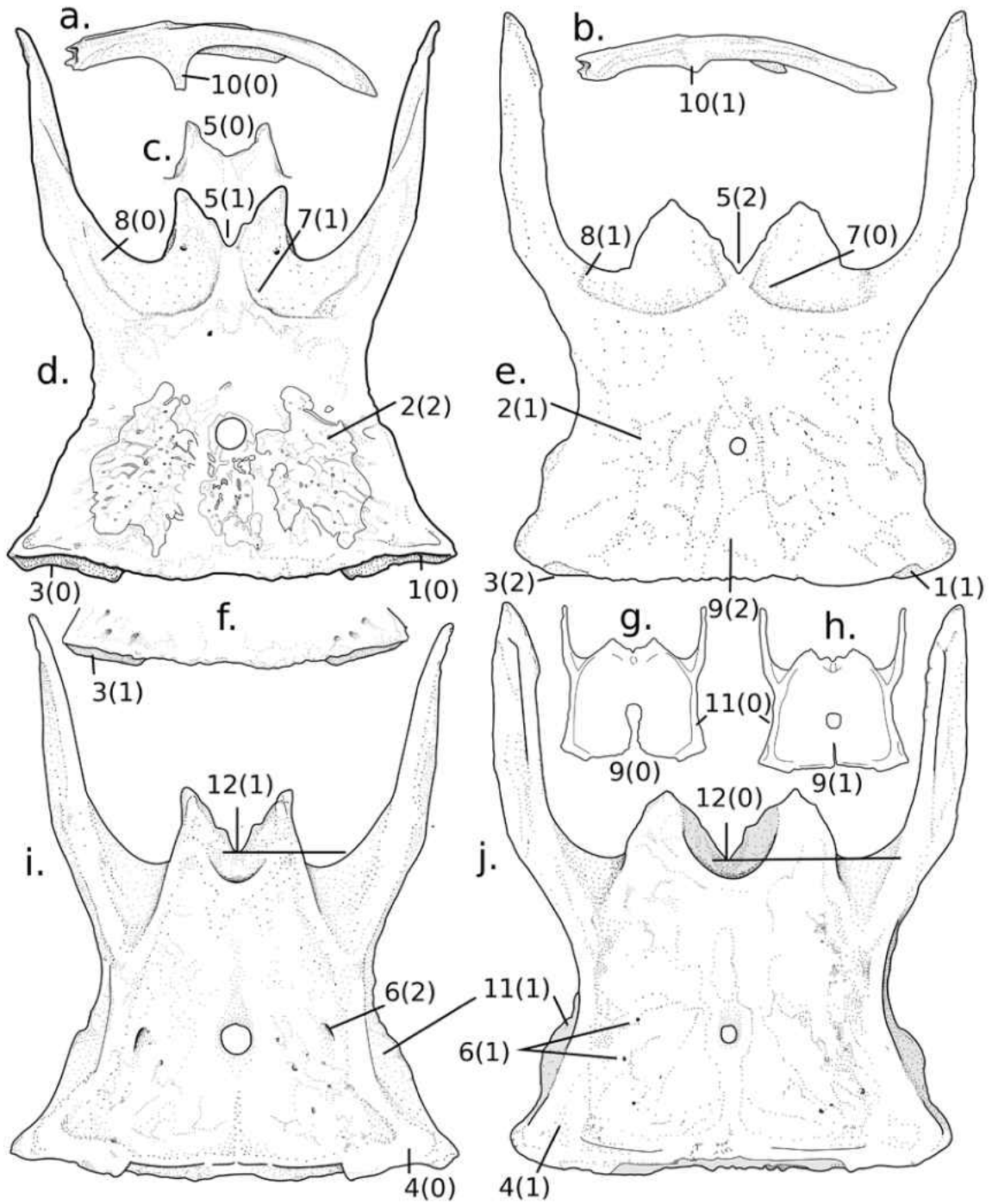


Figure 3.7. Distinguishing characters of the palatine. Parietals on the left belong to *Eremiascincus* and those on the right belong to *Ctenotus*. a, b) left lateral view. c) posterior processes in dorsal view, d, e) parietal in dorsal view, f) anterior margin in dorsal view, g, h, i, j) parietals in ventral view. Not drawn to scale.

Postfrontal (Figure 3.8):

- pof01. Anterior margin: U-shaped (0); anteromedially slanted (1). The
- pof02. Constriction associated with the frontal-parietal contact: narrow (0); wide (1).
- pof03. The medial margin of the postfrontal, posterior to the facet for the overlap of the frontal and parietal and anterior to the margin of the supratemporal fenestra, extends: a short distance (0); far posteriorly (1).
- pof04. The posteromedial margin (the margin of the supratemporal fenestra) is: concave (0); roughly straight (1); convex (2).
- pof05. Frontal-parietal contact with the postorbitofrontal forms a: narrow lap joint (0); broad lap point (1).
- pof06. Posterior point: very acute (0); somewhat obtuse (1).
- pof07. Orbital margin: antero-posteriorly thick (0); thin (1).
- pof08. Posterior margin of the medial orbital process is: mostly straight (0); smoothly curved (1).
- pof09. Separation between the parietal suture and the margin of the supratemporal fenestra: distinct (0); subtle (1).
- pof10. Postfrontal foramen in ventral view: small (0); large (1).
- pof11. The posterior running portion of the postorbitofrontal: narrows towards the supratemporal fenestra (0); retains relatively constant breadth (1); widens (2).
- pof12. Number of postorbital foramina: 1 (0); 2 (1).
- pof13. Postorbital: not fused to the postfrontal (0); fused to the postfrontal (1).

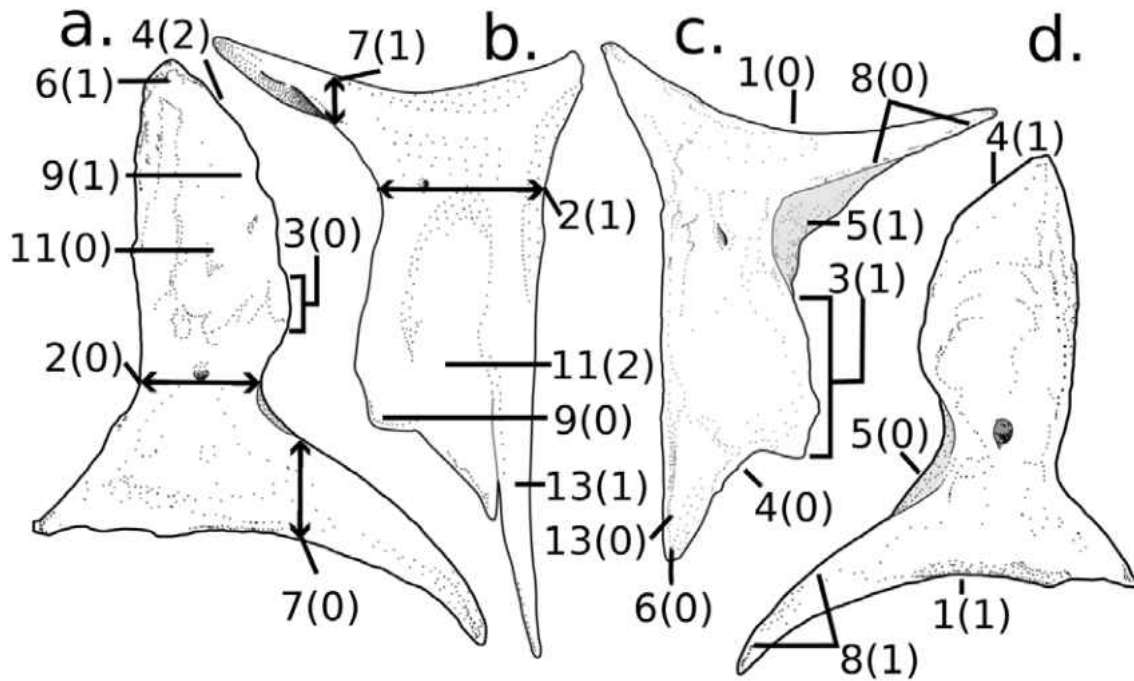


Figure 3.8. The distinguishing characters of a postfrontal a) of *Ctenotus* in dorsal view, b) *Eremiascincus* with a fused postorbital in ventral view, c) *Eremiascincus* in dorsal view and another *Ctenotus* in dorsal view. Not drawn to scale.

Pterygoid (Figure 3.9):

pt01. Ventral transverse crest: sharp and well defined (0); dull and/ or poorly defined (1).

Transverse crest extends from the ectopterygoid facet to the middle of the body of the pterygoid.

pt02. On the anterior edge of the pterygoid, which articulates with the palatines there are/ is: two clearly distinct processes on the lateral side (0); a single or only partially divided process on the lateral side (1).

pt03. Transverse ventral crest turns posteriorly and: continues about half the length of the quadrate process of the pterygoid (0); vanishes shortly after the turn (1); continues roughly the entire quadrate process length (2)

- pt04. Anteromedial angle, which is the anterior extent of the contact of the medial margins of the pterygoids, is: obtuse or forming a gentle curve (0); a sharp angle close to or less than 90° (1).
- pt05. Point of the posterior process: sharp (0); rounded (1).
- pt06. Foramen anterior to the transverse crest: absent (0); 1 foramen (1); 2 foramina (2).
- pt07. Foramen anterior to the transverse crest: absent (0); small (1); large (2).
- pt08. Foramen anterior to the transverse crest surrounded by: no sculpting (0); little sculpting (1); lots of sculpting (2).
- pt09. Ectopterygoid facet: indistinct or barely visible in ventral view (0); well delineated in ventral view (1).
- pt10. Ridge on the lateral side of the fossal columellae: not expanded (0); expanded beyond the body of the posterior process (1).
- pt11. Fossa columellae open posteriorly (0); closed posteriorly (1).
- pt12. Fossa columellae: round or elliptical (0); tear drop or egg shaped (1).
- pt13. Dorsal ectopterygoid facet: does not have a distinct edge (0); has a distinct edge (1).
- pt14. Groove on the dorsal side of the pterygoid expansion: absent (0); present leading posteriorly to the fossa columellae (1).
- pt15. Anterior to the fossa columellae: no foramina (0); one or two distant foramina (1); one foramen near and one or two foramina distant (2).
- pt16. Posterior to the fossa collumellae: no foramen (0); one foramen (1).

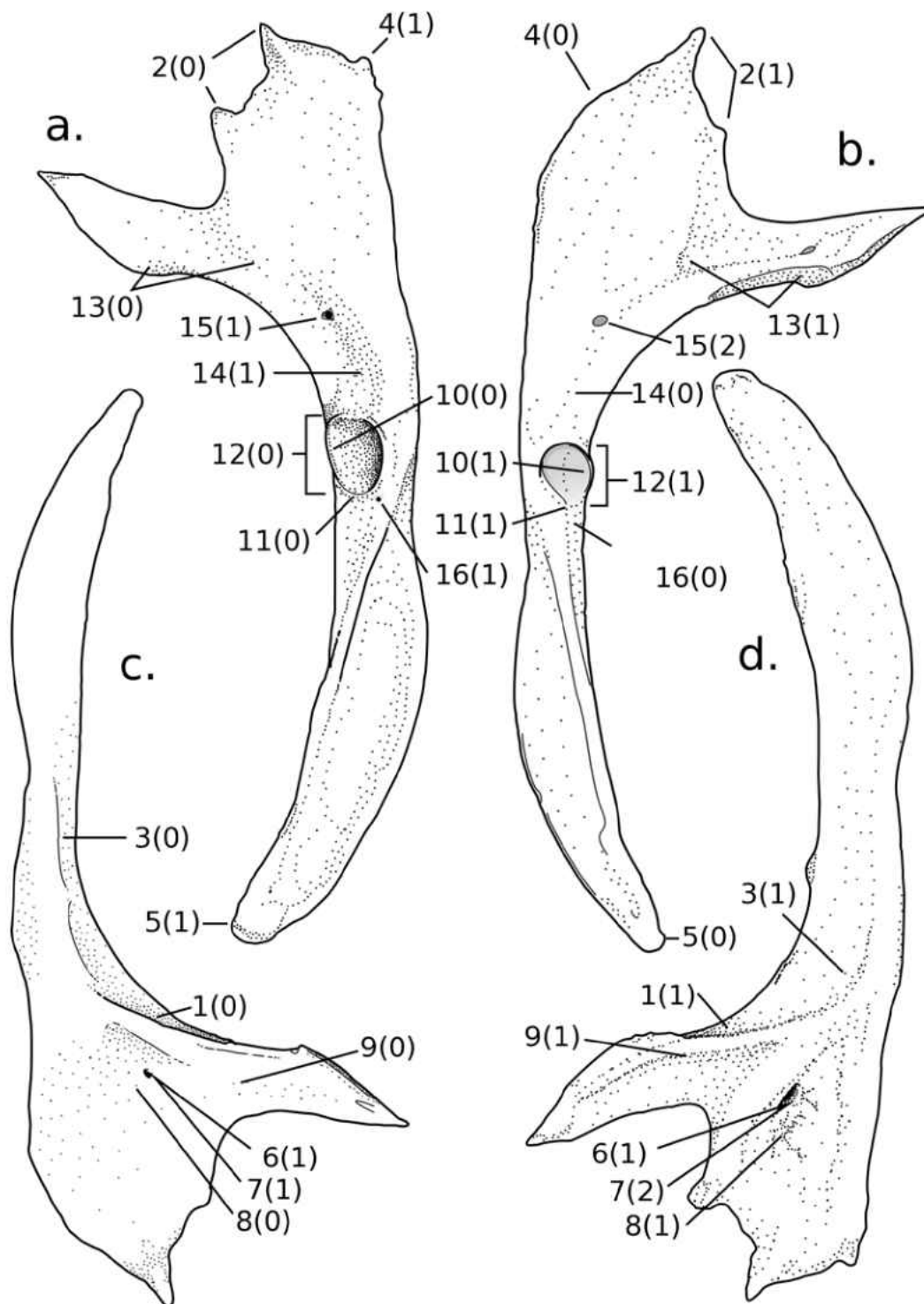


Figure 3.9. Distinguishing characters of a pterygoid. Dorsal view of the pterygoid of a) *Ctenotus* and b) *Eremiascincus*. Ventral view of the pterygoid of c) *Eremiascincus* and d) *Ctenotus*. Not drawn to scale.

Quadrates: (Figure 3.10)

- q01. Apical foramen: lateral to the top of the cephalic condyle (0); at the apex (1).
- q02. Connection between the apical foramen and the squamosal notch: open (0); closed but not fused (1); closed and fused (2).
- q03. Apical foramen: above the pterygoid lamina (0); lateral to it (1).
- q04. Foramen on central column: absent (0); present and small (1); present and large (2).
- q05. Foramen on the anterior side of the mandibular condyle: absent (0); present (1).
- q06. Lateral portion of the mandibular condyle is: the same size as the medial (0); wider than the medial (1).
- q07. Lateral portion of the mandibular condyle extends: the same distance (0) as the medial; extends farther (1) than the medial.
- q08. Thin ridge on the tympanic crest: level with or below (0); above (1) the maximum curvature of the tympanic crest
- q09. In posterior view, the pterygoid lamina starts: below the cephalic condyle (0); at the cephalic condyle (1).
- q10. Pterygoid lamina: does not flare out (0); does (1).
- q11. Foramen on the lateral side of the mandibular condyle: absent (0); present (1).
- q12. Foramen on the medial side of the cephalic condyle: absent (0); present (1).
- q13. Foramen on the posterior side of the mandibular condyle: absent (0); present (1).

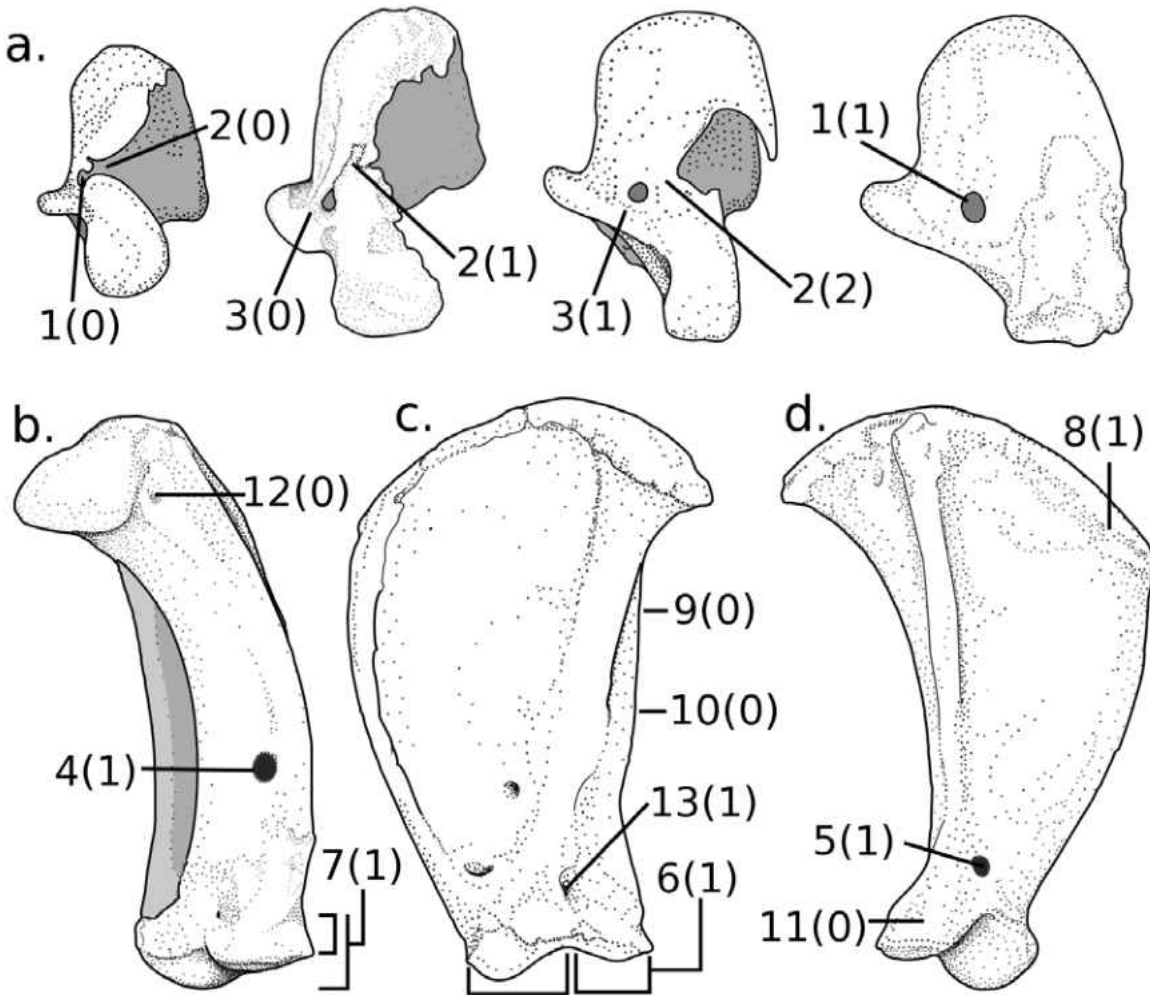


Figure 3.10. Distinguishing characters of the quadrate. Quadrate in a) dorsal, b) medial, c) posterior, and d) anterior views. Not drawn to scale.

Results

When the combined data set of all 46 specimens (left and right sides of 23 individuals) and 127 characters was subjected to a heuristic parsimony search in TNT, it produced only 1 shortest tree, with a length of 712 changes (Figure 3.11). The program TNT mapped *Ctenotus* as a cluster within *Eremiascincus*, but this is not meant as a phylogenetic or taxonomic statement, but merely that three of the individuals of *Eremiascincus* had not developed all the traits that differentiate the two genera.

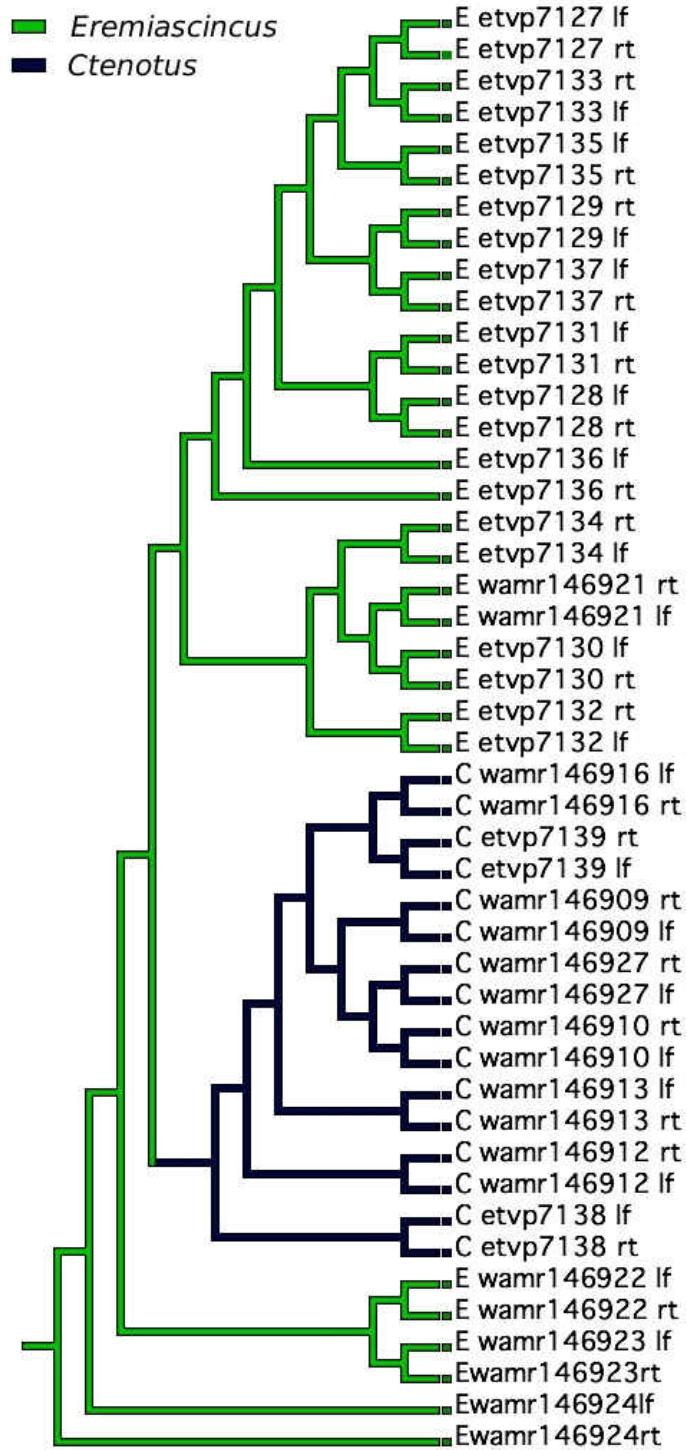


Figure 3.11. Shortest tree derived from analysis of all characters for all element. Tree length = 712 steps. Consistency index = 0.24.

To differentiate the diagnostic power of different characters, it is important to distinguish perfectly diagnostic characters, sufficient diagnostic character states, and necessary character states. Perfectly diagnostic characters are those that have no overlap between taxa for a given character state. For instance, for a two state character, if only *Eremiascincus* possessed character state zero, and only *Ctenotus* has character state one, then that character should be considered perfectly diagnostic. In the case where a particular character state only occurs in one taxon, but not all members of that taxon, then it is sufficient for diagnosis, and the sum of the alternative states are necessary for the diagnosis of the alternative taxon. For instance, only *Ctenotus* displays character state one, but it only occurs in half of specimens, the presence of character state one is indicative of *Ctenotus*, but its absence doesn't rule *Ctenotus* out. Conversely, in the case of a two state character, the presence of character state zero, would be required for the identification of *Eremiascincus*. Character state zero would not necessarily prescribe a diagnosis of *Eremiascincus*, but its absence would negate it as a possibility.

Of the 127 characters assessed, 15 were found to be perfectly diagnostic, as well as 20 characters that have states that are sufficient to diagnose *Ctenotus* and 18 characters that have states that are sufficient to diagnose *Eremiascincus*. None of the characters examined possessed a character state that was necessary for the identification of one taxon, in which the alternative was not sufficient to identify the other taxon. All perfectly diagnostic characters had a consistency index of 1 on the tree, which made it easy to sort them from the remainder of the characters. Only 2 characters had consistency indices of 1 that were not perfectly diagnostic. Of the elements examined, all had several characters

with states that were sufficient to identify either taxon, and only the dentary and the postfrontal lacked any perfectly diagnostic characters.

What follows is the list of diagnostic character states for *Ctenotus* and *Eremiascincus*, broken down by element.

Articular Complex:

In *Ctenotus* only: The retroarticular process remains narrow for its length (ar01 = 0), and in lateral view does not appear strongly ventrally inflected relative to the remainder of the articular complex (ar04 = 0). Also, the retroarticular process makes up about 25% or more of the length of the articular complex (ar05 = 1). At the other end of the element, the surangular process extends forward several projections that together form a broad contact with the dentary (ar10 = 0).

In *Eremiascincus* only: The retroarticular process appears strongly medially inflected in lateral view (ar04 = 1), and the surangular puts forward a single long projection that forms a tapering contact with the dentary (ar10 = 1).

Coronoid:

In *Ctenotus* only: The lateral crest forming the dorsal border of massateric fossa is weakly developed and its edge does not extend below the posterior margin of the coronoid process (co01 = 0). The dentary process is relatively short and deep (co02 = 1). In medial view, the posteromedial crest is low and close to the surface of the remainder of the posterior process (co07 = 0).

In *Eremiascincus* only: The lateral crest that forms the dorsal border of the massateric fossa is moderately to well developed, typically reaching or extending below the line of the posterior margin of the coronoid process (co01 = 1). The dentary process is

relatively long and thin (co02 = 0). The splenial facet extends all the way to the posterior tip of the medial side of the dentary process (co08 = 1) and the line between the splenial and dentary facets lies at or below the midline of the dentary process (co09 = 0). Also, the tip of the posterior process primarily points ventrally (co10 = 0). The line separating the facets on the dentary process from the body of the anteromedial process is indistinct (co11 = 1). And furthermore, only *Eremiascincus* has shown to possess a well-developed accessory crest on the anterior margin of the pseudotemporalis fossa on the posterior process (co12 = 2).

Dentary:

In *Ctenotus* only: There is a mechelien canal that is closed and fused for part of its length (d08 = 1).

In *Eremiascincus* only: The dorsal margin of the posterior process may be concave (d01 = 0).

Frontal:

In *Ctenotus* only: The tips anteromedial and anterolateral processes form a straight line across the frontal (f01 = 0). The maximum width anterior to the constriction of the frontal between the orbits is wide, at about 40% or more of the total length of the frontal (f02 = 1). Similarly, the narrowest portion of the frontal, between the orbits, is relatively wide, being greater than 18% of the total length of the frontal (f03 = 1). The angle formed at the anterior extent of the crista cranii forms two points, contributing to the effect of it tapering down to the level of the rest of the frontal (f08 = 2).

In *Eremiascincus* only: The frontal becomes very narrow between the orbits, at less than 18% of the length of the frontal (f03 = 0). Similarly, in ventral view, the crista cranii

overlap as much as 59- 66% of the width of the frontal (f07 = 2), and anteriorly form a single distinct point (f08 = 1).

Maxilla:

In *Ctenotus* only: There are 24 or more tooth positions (m01 = 4 or 5). The superior posterior process may be longer (m02 = 0). The division of the prefrontal area of the ascending nasal process results in 2 distinct secondary processes behind the apex of the ascending nasal process (m07 =3). The septomaxillary process is broad and about 75% of the length of the premaxillary process (m20 = 1).

In *Eremiascincus* only: The interior posterior process is either the same length or longer than the superior posterior process (m02 = 1 or 2). The nasal facet may be (m06 = 1). The division of the prefrontal area of the ascending nasal process is such that there is one distinct accessory process placed close to the apex, or there are two distinct accessory processes (m07 = 2 or 4). The posterior portion of the prefrontal facet may be convex (m09 = 2). There may be up to 7 large external foramina (m16 = 4). The septomaxillary process is slender and about as long as the premaxillary process (m20 = 0).

Palatine:

In *Ctenotus* only: The vomerine process of the ventral lamina does not extend as far as the anterolateral process (pa01 = 0). The anterior margin of the prefrontal facet runs somewhat oblique to the long axis of the palatine (pa02 = 1). The posteromedial process of the ventral lamina extends about as far as the pterygoid process (pa03 = 0). The dorsal lamina meet along the midline of the nasal cavity for less than half of their length (pa04 = 0). There may be some rugose sculpting of the dorsal lamina (pa06 = 1). The medial anterior process on the dorsal lamina extends about as far as the anteromedial process on

the ventral lamina (pa07 = 0). The ratio of the greatest length to the greatest width is less than 7:2 (pa08 = 0).

In *Eremiascincus* only: The vomerine process of the ventral lamina extends further than the anterolateral process (pa01 = 1). The anterior margin of the prefrontal facet runs perpendicular to the long axis of the palatine (pa02 = 0). The pterygoid process is a long spine that extends much further than the posteromedial process (pa03 = 1). The dorsal lamina meet along the midline of the nasal cavity for about half their length or more (pa04 = 1). The ratio of the greatest length of the palatine to its greatest width is higher than 7:2 (pa08 = 1).

Parietal:

In *Ctenotus* only: The anterolateral margin of the parietal, above the frontal lappet, may be convex (p03 = 2). The ventrolateral crest may flare out anteriorly symmetrically so that it is Y-shaped (p04 = 1). The ventral (epipterygoid) processes extending from the ventrolateral crests are small and weakly developed (p10 = 1).

In *Eremiascincus* only: There is dermal sculpting that is raised above the parietal table (p02 = 2). The nutritive pits on the underside of the parietal table can be large (p06 = 2). There are moderately well developed ventral (epipterygoid) processes extending down from the ventrolateral crests (p10 = 0). Although there is incomplete fusion of the parietal, such that there is still an open groove between the pineal foramen and the anterior margin of the parietal only occurred among *Eremiascincus* in the sample observed, it maps out below the split between *Eremiascincus* and *Ctenotus* and is clearly ontogenetic in nature.

Postfrontal:

In *Ctenotus* only: The posteromedial margin of the postfrontal, which forms the anterior margin of the supratemporal fenestra, is convex (pof04 = 2) and may have a subtle transition from the medial margin that contacts the parietal (pof09 = 1).

In *Eremiascincus* only: The posteromedial margin of the postfrontal is straight (pof04 = 1). There are two postorbital foramina (pof12 = 2).

Pterygoid:

In *Ctenotus* only: The anteromedial angle, where the anterior margins of the pterygoid are separated by the posterior processes of the palatine, form an angle less than or equal to 90 degrees (pt04 = 1). The pterygoid may lack a foramen anterior to the transverse crest (pt06 = 0). There may be a foramen on the dorsal side of the pterygoid, posterior to the fossa collumellae (pt16 = 1).

In *Eremiascincus* only: The anteromedial edge of the pterygoid either forms a gentle curve or an obtuse angle (pt04 = 0). The pterygoid may possess two foramina anterior to the transverse crest (pt06 = 2), though this character is hardly diagnostic since it only occurs on one side of one individual.

Quadrate:

In *Ctenotus* only: The apical foramen is located below the top of the cephalic condyle (q01 = 0) and lateral to the top of the pterygoid lamina (q03 = 1).

In *Eremiascincus* only: The apical foramen is located roughly at the top of the cephalic condyle (q01 = 1) and is directly above the top of the pterygoid lamina (q03 = 0). The foramen on the cephalic condyle is present, and may be large (q04 = 2).

Bayesian Analysis:

Roughly 76% of all the character states described were not completely diagnostic of a single genus, and to one extent or another, represent intrageneric, or intraspecific variation. The characters that are not diagnostic, can still be informative. The results of the Bayesian analysis are given in Table 3.2. The characters that are diagnostic of either *Ctenotus* or *Eremiascincus* using the current dataset are those for which the probability is 1 that the taxon is encountered given a either character state 0 or 1. Those characters have already been identified using the cluster analysis. Excluding the character states that are sufficient to be diagnostic, there are very few characters that confer a high level of confidence in an identification based on them. There is only one character state (m15 = 0) that confers a confidence of 95-99.99% of its identification. As the confidence of identification decreases, the number of character states that can be used for identification at that level of certainty increases dramatically.

Ontogenetic Patterns:

It was expected that juvenile specimens would cluster together at the base of the cladogram due to shared lack of adult characteristics. However, since all *Ctenotus* grouped together, it makes it difficult to assess whether characters are indicative of a taxonomic or ontogenetic change. Several characters did however, show clear ontogenetic patterning. As expected, there were clear increases in the number of tooth positions on both the dentary and maxilla. The articular and surangular fuse as the animal ages. The line delineating the anteromedial process and the dentary processes of the coronoid also becomes more distinct.

Table 3.2: Characters selected by Bayesian analysis. Characters are arranged based on the level of certainty of a specimen being a particular genus given either state 0 or 1 for that character. Probability, derived from the data set, is given to the left. Only characters that would give a greater than 85% confidence of identification are shown.

Probability of:	<i>Eremiascincus</i> given state 0	<i>Ctenotus</i> given state 0	<i>Eremiascincus</i> given state 1	<i>Ctenotus</i> given state 1
1.0	co02 co09 co10 f03 m20 p10 pa01 pt04	ar01 ar04 ar10 co01 co07 f01 pa02 pa03 pa04 pa07 pa08 pof13 q01 q03	p01 q04 co11 co08 p02 q11 m6 ar04 ar10 co01 pa03 pa08 q01 q03	co02 f03 m20 p10 pa01 pt04 ar05 f02 pa06 pof09 d08 m5 p4 pt16
.950-0.999	—	m15	—	—
0.900-0.949	pof01	pt02 m06 pof02 q08 f05 p12	pof10	co09
0.850-0.899	ar05 f02 pa06	ar03 m08 pt13 m18 q10 q11	pa02 pa07 q08 p11	pof01 pt01 m04

On the parietal, the closure of the suture proceeds from the pineal foramen anterior to the margin of the bone. As the lizards age, the dermal sculpting present on the parietal in *Eremiascincus* becomes raised, possibly due to fusion of overlying osteoderms to the skull. In both taxa, the lateral crests on the parietal for the attachment of the pseudotemporalis musculature also becomes more strongly developed. Also, the dorsal

muscle scar for the attachment of the dorsal neck musculature changes from gently rounded and covering most of the posterior process and the base of the supratemporal process, to being somewhat narrower, and having more angular margins medially and laterally. On the ventral side of the parietal, the ventrolateral crests of *Eremiascincus* take on their 7-shaped appearance anteriorly.

On the palatine, the ectopterygoid facet transitions from pointed to either rounded or squared off. Similarly, the tip of the quadrate process on the pterygoid also changes from a sharp point to being rounded. Also on the pterygoid, the appearance of one or two foramina anterior to the fossa collumellae shows the same patterning as other ontogenetic patterns. On the pterygoid, the fossa columellae appears to shrink, as the outer rim ceases to extend beyond the medial margin of the quadrate process.

On the quadrate, the fissure that connects the squamosal notch to the apical foramen starts open and then closes, leaving a line on the surface of the bone and then eventually fuses completely. The pterygoid lamina starts small, with its broadest point just above the mandibular condyle. In some, the pterygoid lamina doesn't reach the cephalic condyle as a juvenile, but expands to reach the cephalic condyle during maturation.

Discussion

As expected, using the parsimony method to analyze the variation in a sample has shown that natural divisions between taxa can be found without any a priori knowledge. Given the success shown here, it stands to reason that once a larger and more taxonomically inclusive dataset is constructed, the correct identification of a specimen of unknown affinity will be as simple as scoring it for what characters are present and re-running the cladistic analysis with the new data. Having such a large pool of characters

from which to draw diagnosis will also be useful in light of the generally incomplete nature of fossil squamates and the brevity of most osteological descriptions connected to a taxonomic description.

A major advantage of using MacClade has been as a visualization tool, in that it has the trace characters feature, which allows one to scroll through each character and quickly see how it is distributed across the specimens. Furthermore, the trace-all-changes tool automatically identified all of the characters that unambiguously identified *Ctenotus*, and placed them on the branch leading to that group. Although the juvenile specimens did not cluster together as expected, the trace changes tool still made it possible to recognize ontogenetic trends.

Given that the scope of this project has so far been limited to two genera, it is not possible at this time to determine how typical it is that roughly a quarter of the total number of character states described are diagnostic. Based on the fact that there are 112 characters of the 127 examined that have polymorphisms that occur in both genera, it is most parsimonious to assume that most of these are polymorphisms that originated before the divergence of the lineages that lead to *Ctenotus* and *Eremiascincus*. If that were true, then a substantial subset of these polymorphisms would be expected in the other taxa that make up the clade containing *Ctenotus* and *Eremiascincus*. This would include *Hemiergis*, *Lerista*, *Eulamprus quoyii*, and *Glaphyromorphus arnhemicus* (Reeder 2003).

In the future, by adding additional taxa to this dataset, as well as new characters when appropriate, one could hypothetically create a metric of selection pressure on each clade based on the rate of appearance and elimination of polymorphisms. Ideally, this would coincide with the calibration of molecular clock estimates for the divergence of each

taxon as fossils are attributed to various taxa based on a character set expanded from the one presented here. In so doing, an expansion of work like this would have the potential to create a synthesis of micro- and macroevolutionary changes that occur in this extremely diverse group of lizards.

Literature Cited

- Goloboff, P.A., Farris, J.S., and Nixon, K.C. (2008). TNT, a free program for phylogenetic analysis. *Cladistics* **24**: 774-786.
- Hutchinson, M.N. and Mackness, B.S. (2002). Fossil lizards from the Pliocene Chinchilla local fauna, Queensland, with description of a new species. *Records of the South Australia Museum* **35**: 169-184.
- Longrich, N. (2010). *Mojoceratops perifania*, a new chasmosaurine ceratopsid from the late Campanian of Western Canada. *Journal of Paleontology* **84(4)**: 681-694.
- Maddison, W. P., and Maddison, D.R. (1992). MacClade: analysis of phylogeny and character evolution. Sinauer, Sunderland, Massachusetts, USA.
- Mecke, S., Doughty, P., and Donnel, S. (2009). A new species of *Eremiascincus* (Reptilia: Squamata: Scincidae) from the Great Sandy Desert and Pilbara coast, Western Australia and reassignment of eight species from *Glaphyromorphus* to *Eremiascincus*. *Zootaxa* **2246**: 1-20
- Reeder, T.W. (2003). A phylogeny of the Australian Sphenomorphus group (Scincidae: Squamata) and the phylogenetic placement of the crocodile skinks (Tribolonotus): Bayesian approaches to assessing congruence and obtaining confidence in maximum likelihood inferred relationships. *Molecular Phylogenetics and Evolution*

27: 384-397.

Scannella, J.B. and Horner, J.R. (2010). *Torosaurus* Marsh 1891, is *Triceratops* Marsh 1889

(Ceratopsidae: Chasmosaurinae): Synonymy through ontogeny. *Journal of*

Vertebrate Paleontology **30(4)**: 1157-1168.

Williams, C. (1999). Fossil lizard identification methods: A case study of three *Egernia*

species. Msc. Thesis. Adelaide University, Adelaide, South Australia.

Wilson, S., and Swan, G. (2003). *A Complete Guide to Reptiles of Australia*. New Holland

Publishers. Sydney, Australia.

CHAPTER 4

Analyzing Skull Shape Through Ontogeny in *Eremiascincus* Using Traditional Morphometrics

William B. Gelnaw

The Don Sundquist Center for Excellence in Paleontology, East Tennessee State University,
Johnson City, Tennessee 37614, United States

Abstract – A comparison of 15 cranial measurements across the available size series of *Eremiascincus* has illuminated the pattern of allometric growth in *Eremiascincus*. There is no significant difference between *E. fasciolatus* and *E. richardsonii* in each of the measurements, and therefore can be combined into a single dataset.

Introduction

The shape of the entire skull of a single type of lizard, or even a group of lizards, has been only rarely quantitatively described in the literature. When skull shape is quantitatively described, it has been for differentiating ecomorphs rather than taxa (Strayton 2005; McBayer and Corbin 2007). In terms of describing head shape in a single taxon, Evans (2008) qualitatively describes the skulls of skinks as being generally narrow and somewhat elongate, yet does not quantify that assessment, likely because the diversity of skinks is so great. Guerra and Montero (2009), in describing the skull of a teoid lizard

(Gymnophthalmidae), also use such broad terms as “relatively elongate and dorsoventrally compressed,” without objectively defining what that means. No mention of the general shape of the head is made by Kingman (1932), El-Toubi (1938), Greer and Cogger (1985) Worthy (1987), or Barahona and Barbadillo (1998) in their respective comparative descriptions of teioid or skink skulls.

Within the context of an osteological description, Conrad (2004) so far gives the best outline for describing the general skull shape of a lizard, though does not go into quantitative specifics. A lizard skull can be subdivided into facial and cranial portions (per Conrad, 2004), separated at the posterior-most point of the ectopterygoid-maxilla contact. Skulls can also be subdivided into rostral, orbital and temporal regions. Conrad (2004) however does not define the limits of the snout, orbit or temporal regions. For the sake of adopting Conrad’s method, I here define the orbital region as the longest distance between the lacrymal notch of the prefrontal and the orbital margin of the postfrontal. The snout is any portion of the skull rostral to the orbit, and the temporal region extends from the orbital margin of the postfrontal to the caudal most point of the supratemporal arch, which in *Eremiascincus* and most other skinks, is on the squamosal.

Ontogeny of lizard skulls has been little described in the literature. Far more has been said about the ontogeny of head shape in dinosaurs than lizards or other reptiles. Of the over 850 publications on eggs, juveniles, embryos and growth series, about 60% concern dinosaurs (Delfino and Sanchez-Villarga 2010). Among reptiles, turtles are moderately well represented in the ontogenetic literature (Bever, 2009). Ontogenies and allometry of many taxa of mammals and fish are also well documented in the literature (Emerson and Bramble 1993). Monteiro and Abe (1997) used geometric morphometrics to

describe the allometry of the skulls of teiid lizards during ontogeny. Powel et al. (2002) described the change in the horns of the horned lizard (*Phrynosoma orbiculare*: Phrynosomatidae). Barahona and Barbadillo (1998), Torres-Carvejal (2003), and Tarazona et al. (2008) correlate the timing of osteological changes with snout-vent length, but give no more discussion of the proportions of the regions of the skull than the authors mentioned above. Therefore, to add to this body of knowledge, the allometry of the skull of *Eremiascincus* will be examined here.

Methods

In order to assess the shape of the skulls and lower jaw, dial calipers were used to take 15 measurements (Figure 4.1) on 14 skulls of *Eremiascincus* (Table 4.1). All parameters were measured to the nearest 0.02 millimeters. All measurements were taken by a single observer using a single set of calipers. For the sake of comparison, the same measurements were also taken on the skulls of 137 other skinks (n = 119), anguids (n = 10), and teiids (n = 8). To reduce the impact of size as a variable in describing the change in shape, all measurements were transformed by dividing them by the length of the skull from the occiput to the tip of the rostrum.

Ontogeny of *Eremiascincus* was assessed by correlating the individual variables in the transformed data set with the total length of the skull. Because of the small sample size (n=12), *Eremiascincus fasciolatus* and *E. richardsonii* are treated as 1 group. To justify lumping the two species together, an independent sample T-test for the difference of means was performed for each variable (Table 4.1). Furthermore, although the two species may actually be different sizes at the same age during development, size was used as the best proxy of age since no other character has been found useful for differentiating age

classes in articulated skulls. Statements regarding a dimension measured in a large group, are stated as the simple mean of that measurement across the sample. No weighting was done to account for over or under-representation of some members of that group.

Table 4.1. Specimens of *Eremiascincus* that were examined. (WAMR = Western Australia Museum; SAMR = South Australia Museum)

Species	Specimen number	Articulation
<i>Eremiascincus richardsonii</i>	WAMR 24144	articulated
<i>Eremiascincus fasciolatus</i>	WAMR 156826	articulated
<i>Eremiascincus richardsonii</i>	SAMR 12717B	articulated
<i>Eremiascincus fasciolatus</i>	SAMR 19862	articulated
<i>Eremiascincus richardsonii</i>	SAMR 14878	articulated
<i>Eremiascincus richardsonii</i>	SAMR 9302	articulated
<i>Eremiascincus richardsonii</i>	SAMR 9301	articulated
<i>Eremiascincus fasciolatus</i>	SAMR 9411	articulated
<i>Eremiascincus richardsonii</i>	SAMR 14866	articulated
<i>Eremiascincus richardsonii</i>	SAMR 1787	articulated
<i>Eremiascincus fasciolatus</i>	SAMR 9333	articulated
<i>Eremiascincus richardsonii</i>	SAMR 24638	articulated
<i>Eremiascincus richardsonii</i>	SAMR 1279A	articulated
<i>Eremiascincus richardsonii</i>	SAMR 24729	articulated

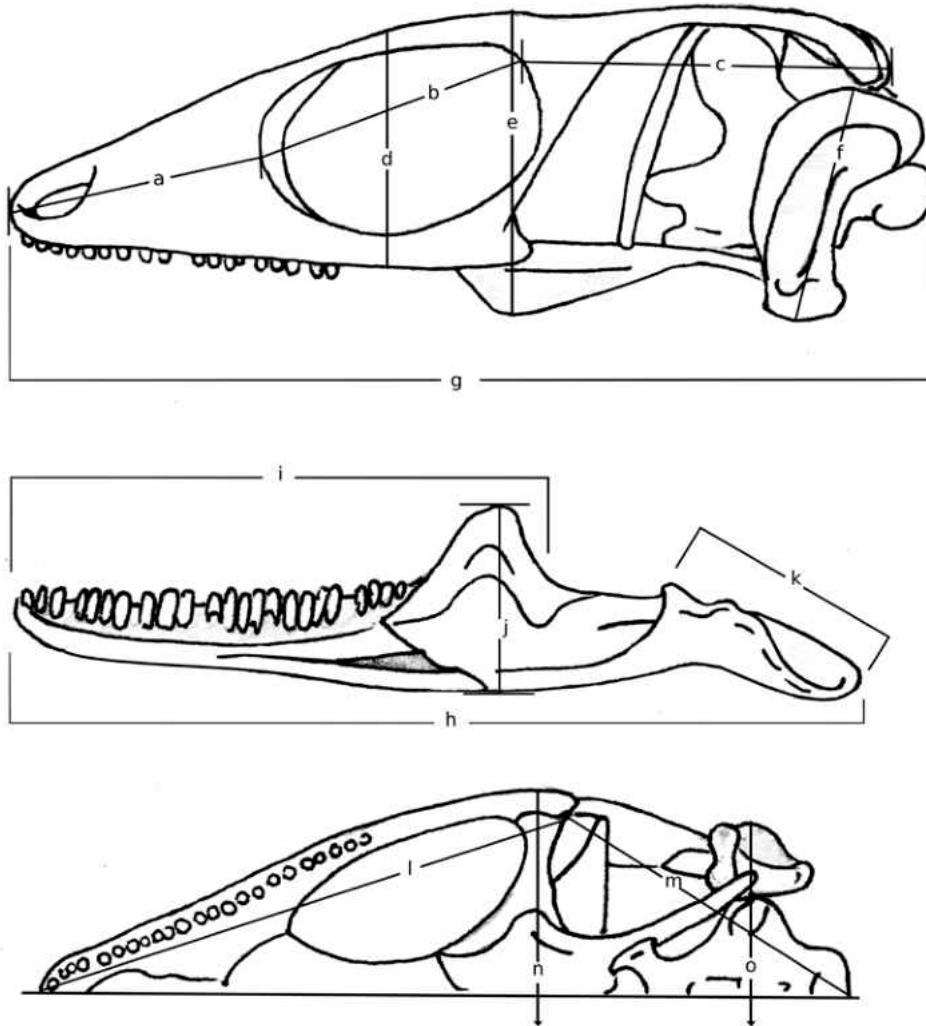


Figure 4.1. Linear measurements of the whole skull of a lizard: a. length of the rostrum, from the tip of the snout to the furthest anterior point of the orbit; b. longest dimension of the orbit; c. length of the temporal region, from the posterior most point of the orbit to the posterior most point of the supratemporal arch; d. height at the center of the orbit; e. maximum height, from the pterygoid flange to the parietal table; f. quadrate length, from cephalic condyle to mandibular condyle; g. occiput to snout tip length; h. length of jaw ramus; i. coronoid to symphysis length, from the anterior tip of the dentary to the posterior edge of the coronoid process of the coronoid bone; j. height at coronoid; k. postarticular region; l. facial region, from snout tip to the posterior edge of where the ectopterygoid meets the maxilla; m. cranial region, from the posterior point where the ectopterygoid meets the maxilla to the tip of the occipital condyle; n. the width of the skull at the jugals; and o. width of the skull at quadrates.

Results and Discussion

Comparisons of the 15 measurements between *Eremiascincus fasciolatus* and *E. richardsonii* showed no significant differences ($P < 0.05$) in the proportions of their skulls (Table 4.2). The data showing the relative proportion of each measurement is given in Figures 4.2 to 4.5, and are divided based on whether they were taken on the ventral, lateral, or dorsal aspects of the skull, or on the lower jaw. A summary of the proportionate change of each measurement through ontogeny is given in Table 4.3.

Table 4.2. Test for differences between *Eremiascincus fasciolatus* and *E. richardsonii*. Independent sample T-test comparing *Eremiascincus fasciolatus* and *E. richardsonii*, as well as combined maximum, minimum and mean values for the two species. In order to account for size differences, each variable was divided by the occipital-snout length of the skull before analysis.

	t-test for Equality of Means			Descriptive statistics		
	t	Sig. (2-tailed)	Mean Difference	Minimum	Maximum	Combined Mean
outside width at the quadrates	-1.387	.196	-.02803	.43	.56	.5030
width at the jugals	-1.362	.203	-.02672	.42	.56	.4960
length of the facial region	-1.498	.165	-.02005	.43	.52	.4901
length of the cranial region	.664	.522	.00764	.53	.60	.5653
length of the orbit	.734	.480	.00654	.30	.34	.3180
length of the temporal region	-1.690	.122	-.02950	.35	.45	.3932
length of the rostrum	-1.007	.338	-.00730	.29	.33	.3111
height of the skull at the orbit	-1.871	.091	-.01176	.23	.27	.2560
length of the quadrate	.116	.910	.00067	.20	.23	.2142
maximum height of the skull	-1.236	.245	-.01963	.28	.39	.3488
length of the lower jaw	-.676	.514	-.01525	.84	.98	.9392
height of the coronoid process	-1.160	.273	-.00961	.16	.21	.1857
length of the lower jaw anterior to the posterior of the coronoid process	-1.290	.226	-.01293	.52	.58	.5515
length of the articular condyle and retroarticular process fo the lower jaw	.379	.712	.00363	.17	.23	.2085

Table 4.3. Table of the slope, y-intercept, and coefficients of correlation of each of the lines of best fit for all 15 dimensions of skull shape.

	Slope	y- intercept	R ²
outside width at the quadrates	0.123	0.296	0.898
width at the jugals	0.109	0.313	0.746
length of the facial region	0.056	0.397	0.406
length of the cranial region	0.028	0.518	0.164
length of the orbit	-0.004	0.324	0.004
length of the temporal region	0.074	0.270	0.398
length of the rostrum	0.026	0.267	0.342
height of the skull at the orbit	0.000	0.256	0.000
length of the quadrate	0.011	0.196	0.103
maximum height of the skull	0.065	0.240	0.419
Jaw ramus length	0.119	0.740	0.764
Length from the posterior of the coronoid process to the symphysis	0.034	0.495	0.282
Coronoid process height	0.046	0.108	0.795
Length of articular and retroarticular	0.036	0.147	0.412

Skulls of both of *Eremiascincus fasciolatus* and *E. richardsonii*, at their widest, are about twice as long as wide, with a somewhat domed cranium and a wedge shaped rostrum. Greer (1979) notes that the snout of *E. fasciolatus* is depressed compared to *E. richardsonii*. The widest points on the skull are at the posterolateral angles of the jugals and at the quadrates, with no significant difference between the two measurements either when transformed ($p=0.633$) or not ($p=0.869$). In all other skinks measured, the skull is an average of 14% wider at the quadrates than the jugal angle ($n= 38$). For comparison, in anguids ($n=10$) and teiids ($n=8$) measured, the skulls at the quadrates were about 7% and 9% wider than at the jugal respectively.

As the skull increases in size, its width (Figure 4.1: measurements n and o) increases relative to its length (Figure 4.2), a pattern also seen in general among other lizards measured, but most strongly in *Eremiascincus*. The height of the skull at the orbit and the length of the quadrates (Figure 4.1: measurements d and f) relative to its length, remains

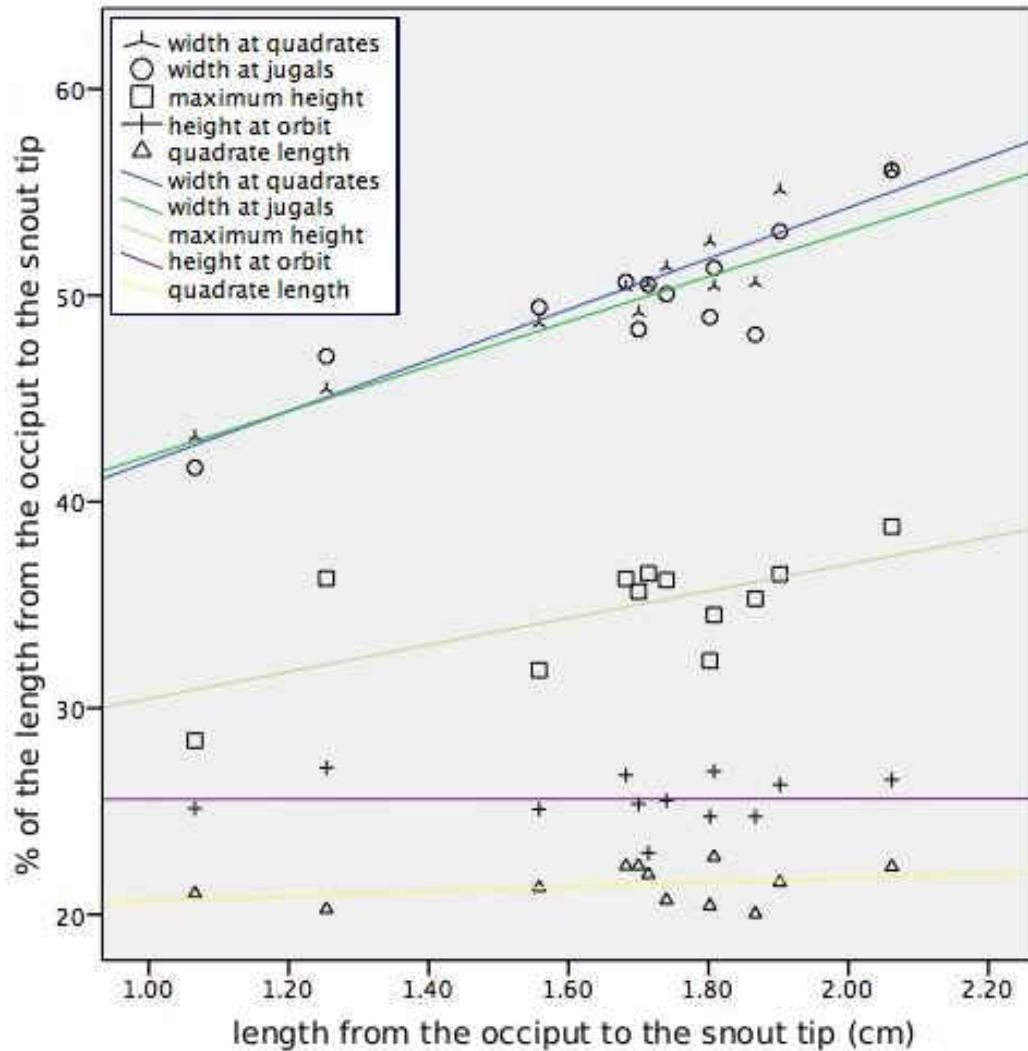


Figure 4.2. Relative widths of the skull of *Eremiascincus* at the quadrates and jugals, as well as depth of the skull measured at the orbit, pterygoid and quadrate. Width at the quadrates: $R^2 = 0.898$. Width at jugals: $R^2 = 0.746$. Maximum height: $R^2 = 0.419$. Height at the orbit: $R^2 = 0.000002$. Quadrate length: $R^2 = 0.103$.

relatively unchanged during growth. Given that the depth of the skull at the orbit and the quadrate increase in direct proportion to the skull length, the comparative increase in the maximum depth of the skull (Figure 4.1: measurement e) seen in Figure 4.2 is probably attributable to the increase of the depth of the pterygoid flanges below the jaw line.

Widening of the skull contributes to an increase in the measured facial, cranial, orbital, rostral and temporal dimensions relative to the midline length. As a consequence, both the

facial and cranial portions of the skull impossibly appear to increase in proportion to the size of the skull. Two methods to correct for this error in the future would be to take measurements parallel to the midline in a photograph, or transform the data using a measured distance from the midline to ectopterygoid-maxilla contact and Pythagorean theorem. The later method would however only reduce error in the measurements of the facial and cranial regions.

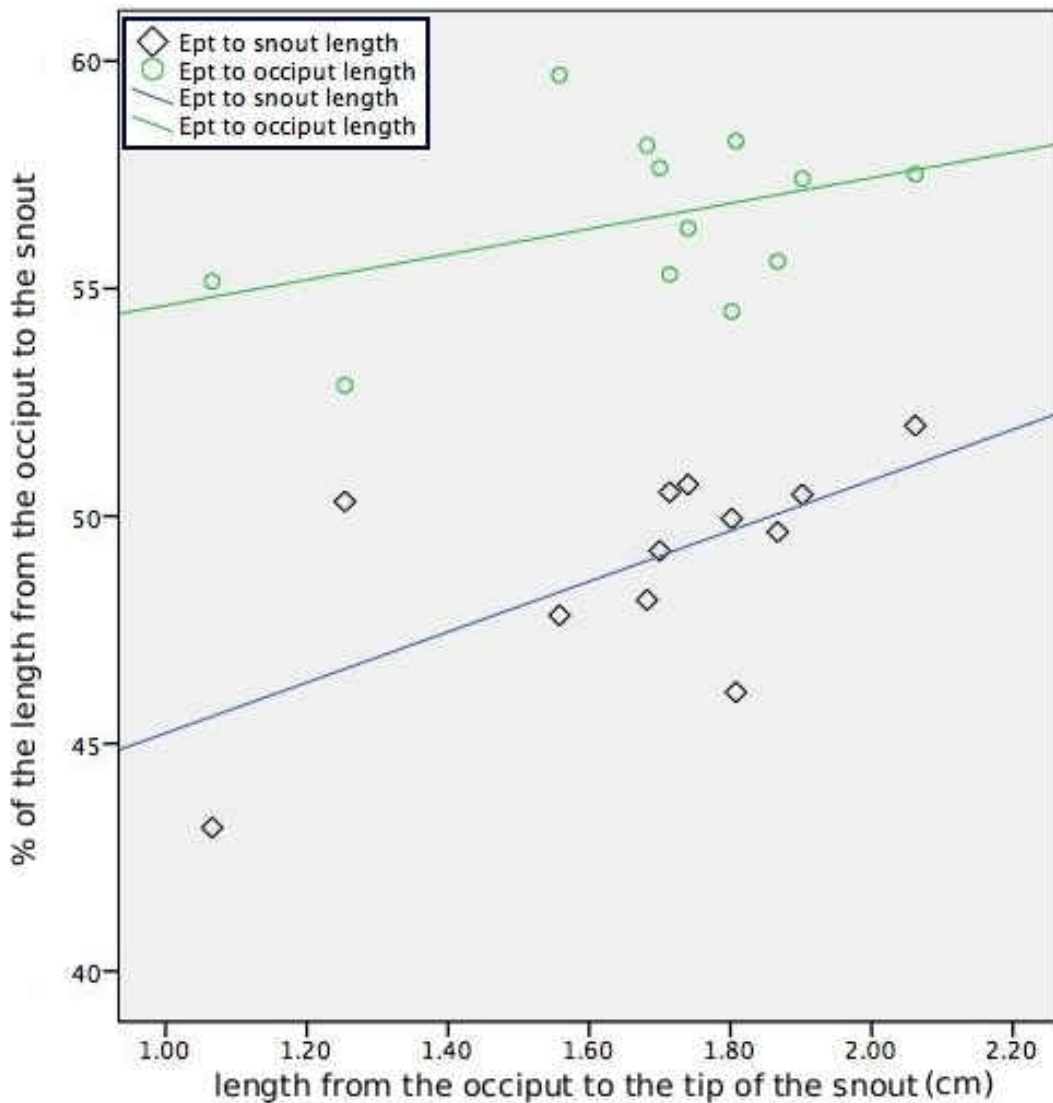


Figure 4.3. Relative lengths of facial and cranial portions of the skull, showing allometric growth with a faster growing facial region. Ectopterygoid to snout length: $R^2 = 0.406$. Ectopterygoid to occiput length: $R^2 = 0.146$.

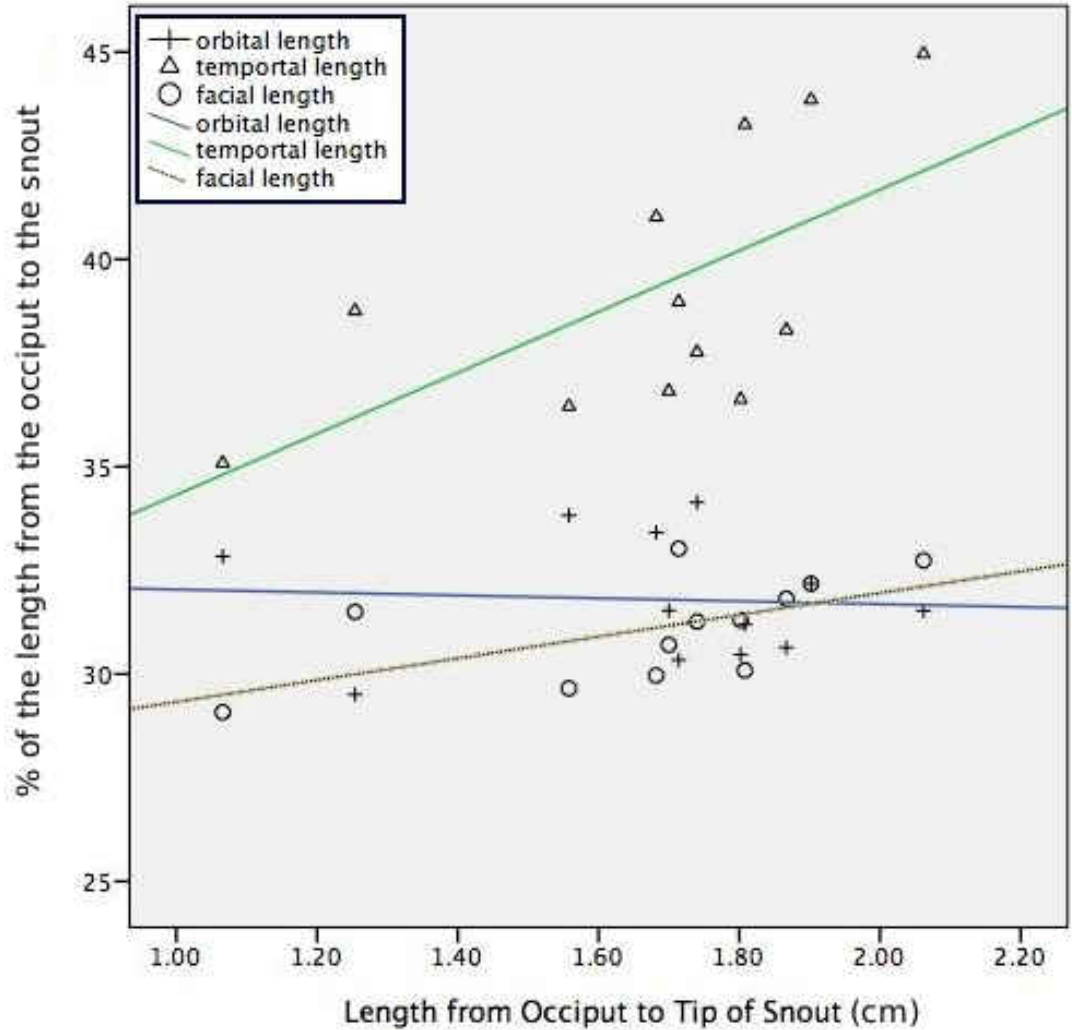


Figure 4.4. Relative lengths of the orbital, temporal and rostral regions of the skull compared to the total length of the skull. Orbit length: $R^2 = 0.004$. Temporal region length: $R^2 = 0.398$. Facial region length: $R^2 = 0.342$.

During ontogeny, the most growth on the ventral side of the skull is in the facial region, whereas it occurs in the temporal region in the dermal roof. In ventral view, the cranium is on average about 9% longer than the facial region. However, the facial region grows somewhat faster than the cranial region throughout life (Figure 4.3). The temporal region is an average of 26% longer than the rostrum and 24% longer than the orbit. Counter to an expected negative allometry (Werner and Seifan, 2006), the relative size of

the orbit does not change significantly as the animal grows ($R^2=0.004$) and remains between 30% and 34% of the total skull length. By comparison, the orbit comprises a mean of about 29% of the skull length in other skinks, 32% in teiids and 27% in anguids.

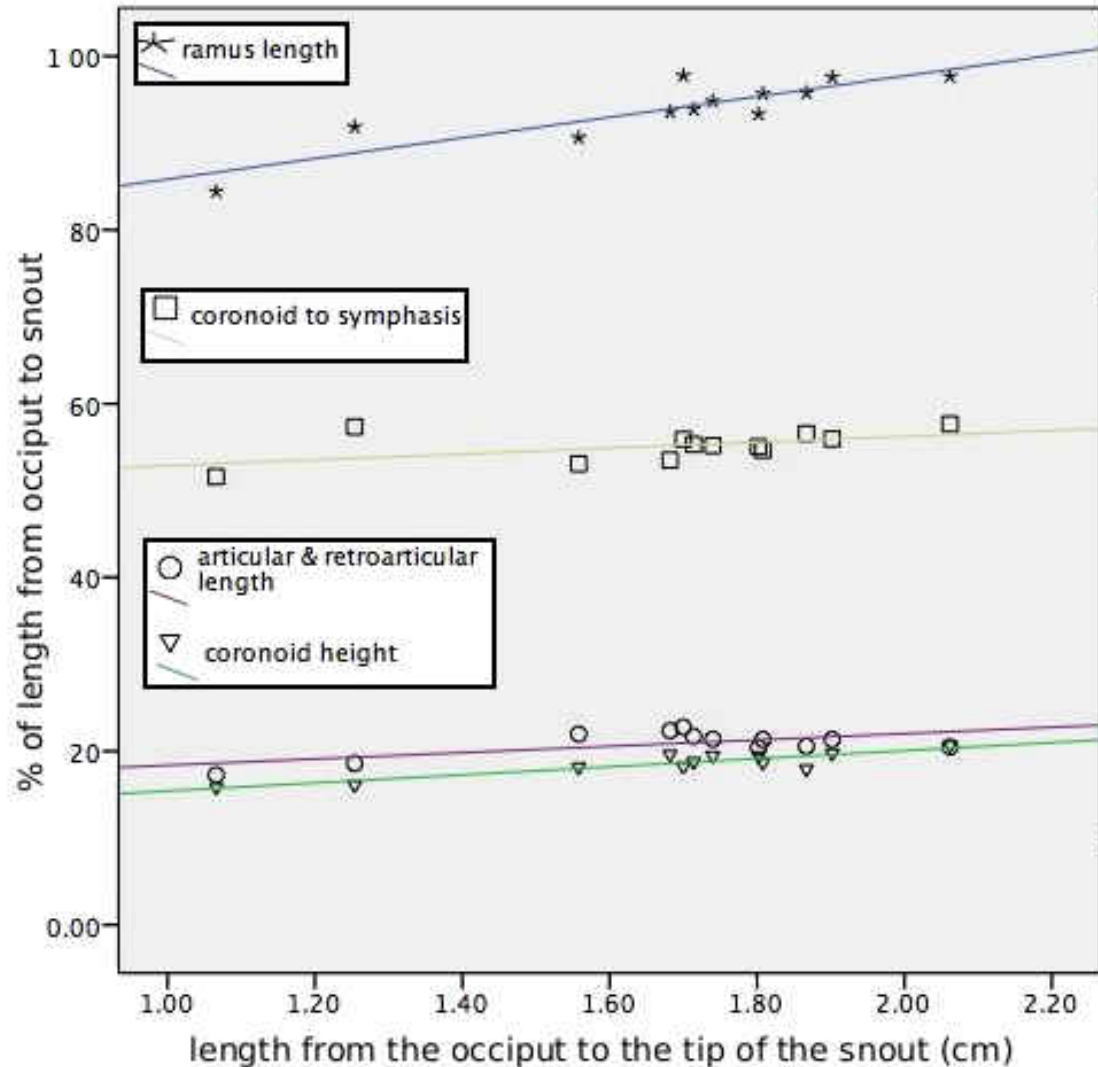


Figure 4.5. Proportions of the lower jaw. The length of the total ramus, the coronoid process anterior and articular facet back as well as the depth of the jaw at the coronoid process. Ramus length: $R^2 = 0.764$. Coronoid height: $R^2 = 0.795$. Coronoid to symphysis length $R^2 = 0.282$. Articular and retroarticular length $R^2 = 0.412$.

Through ontogeny the proportionate length of the rostrum increases slightly, but the greatest change in the dermal roof is in the temporal region (Figure 4.4). The temporal region is about 42% wider than tall and 13% longer than tall. As the skull grows, the

maximum height increases in roughly equal proportion to the widening of the skull, but the quadrate and height at the orbit increases isometrically with the length of the skull. Except in the smallest two individuals examined, the lengthening of the temporal region outpaces the widening of the skull and the increase in height, so that the adult temporal region is comparatively long and low compared to a smaller individual.

Mandibles of *Eremiascincus* are long, slender, and have gently arched ventral margins. The tooth row is on average about 45% the length of the whole jaw ramus (Figure 4.1: measurement h), but the posterior process extends all the way to about the midpoint between the coronoid and the articular facet. Proportions of the lower jaw remain fairly constant relative to one another ($R^2 < 0.5$) and the jaw as a whole increases slightly in size in proportion to the length of the skull (Figure 4.5). The proportional increase in the size of the lower jaw is due also to the widening of the skull.

Literature Cited

- Barahona, F., and Barbadillo, L.J. (1998). Inter- and intraspecific variation in the post-natal skull of some lacertid lizards. *Journal of Zoology, London* **245**: 393-405.
- Bever, G.S. (2009). Postnatal ontogeny of the skull in the extant North American turtle *Sternotherus odoratus* (Cryptodira: Kinosternidae). *Bulletin of the American Museum of Natural History* **330**: 1-97.
- Conrad, J. (2004). Skull, mandible and hyoid of *Shinisaurus crocodilurus* Ahl (Squamata, Anguimorpha). *Zoological Journal of the Linnean Society* **141**: 399-434.
- Delfino, M. and Sanchez-Villagra, M.R. (2010). A survey of the rock record of reptilian ontogeny. *Seminars in Cell & Developmental Biology* **31(4)**: 432-440.

- El-Toubi, M.R. (1938). The osteology of the lizard *Scincus scincus* (Linn.). *Bulletin of the Faculty of Science, Cairo. Fouad I University* **14**: 5-38.
- Emerson, S.B., and Bramble, D.M. (1993). Scaling, allometry, and skull design. In Hanken, J. and B.K. Hall (Eds.). *The Skull. Volume 3. Functional and Evolutionary Mechanisms*: 384-416. University of Chicago Press, Chicago.
- Evans, S.E. (2008). The skull of lizards and Tuatara (pp. 1-347). In: Gans, C., Gaunt, A.S., Adler, K. (eds) *Biology of the Reptilia Vol. 20, Morphology H*. Society for the Study of Amphibians and Reptiles. Ithica, NY, U.S.A.
- Greer, A.E. (1979). *Eremiascincus*, a new generic name for some Australian sand swimming skinks (Lacertilia: Scincidae). *Records of the Australian Museum* **32(7)**: 321-338.
- Greer, A.E. and Cogger, H.G. (1985). Systematics of the reduced-limbed and limbless skinks currently assigned to the genus *Anomalopus* (Lacertilia: Scincidae). *Records of the Australian Museum* **37(1)**: 11-54.
- Guerra, C. and Montero, R. (2009). The skull of *Vanzosaura rubricauda* (Squamata: Gymnophthalmidae). *Acta Zoologica* **89**: 359-371.
- Kingman, R.H. (1932). A comparative study of the skull in the genus *Eumeces* of the family Scincidae. *Bulletin of the University of Kansas* **20(15)**: 273-295.
- McBrayer, L.D. and Corbin, C.E. (2007). Patterns of head shape variation in lizards: morphological correlates of foraging mode. In Reilly, S.M., McBrayer, L.D., and Miles, D.B. (eds) *Lizard Ecology: The Evolutionary Consequences of Foraging Mode*. Cambridge University Press, New York.

- Monteiro, L. R. and Abe, A.S. (1997). Allometry and morphological integration in the skull of *Tupinambis meriana* (Lacertilia: Teiidae). *Amphibia Reptilia* **18**: 397-405.
- Powell, L.G. Russell, A.P., and Ryan, M.J. (2002). Ontogenetic scaling of the cranial horn array in *Phrynosoma orbiculare* (Squamata: Phrynosomatidae). *Journal of Herpetology* **36** (4): 578-589.
- Strayton, C.T. (2005). Morphological evolution of the lizard skull: A geometric morphometrics survey. *Journal of Morphology* **263**: 47-59.
- Tarazona, O.A., Fabrezi, M., and Ramierez-Pinilla, M.P. (2008). Cranial Morphology of *Bachia bicolor* (Squamata: Gymnophthalmidae) and its postnatal development. *Zoological Journal of the Linnean Society* **152**: 775-792.
- Torres-Carvajal, O. (2003). Cranial osteology of the Andean lizard *Stenocercus guentheri* (Squamata: Tropicuridae) and its postembryonic development. *Journal of Morphology* **255**: 94-113.
- Werner, Y.L. and Seifan, T. (2006). Eye size in geckos: asymmetry, allometry, sexual dimorphism, and behavioral correlates. *Journal of Morphology* **267**: 1486-1500.
- Worthy, T.H. (1987). Osteological observations of the larger species of skink *Cyclodina* and the subfossil occurrence of these and the gecko *Hoplodactylus duvaucelii* in the North Island, New Zealand. *New Zealand Journal of Zoology* **14**: 219-229.

CHAPTER 5

Assessing the Phylogenetic Signal of Skull Shape in Skinks from a Morphometric Dataset

William B. Gelnaw

The Don Sundquist Center for Excellence in Paleontology, East Tennessee State University,
Johnson City, Tennessee 37604, United States

Abstract - A set of 15 measurements, taken of 149 skulls of skinks and their close relatives is used to separate the phylogenetic signal from the functional adaptations of skull shape. It is found that traditional morphometrics is only useful for determining a phylogenetic signal when dealing with a small clade. Beyond the species group level, the amount of convergent evolution that has occurred in the skulls of skinks, completely obscures the phylogenetic signal in the shape data.

Introduction

Skinks (Squamata: Scincidae) are one of the most taxonomically diverse groups of terrestrial vertebrates, containing about 1400 species spread across 120 genera, and are on par in terms of diversity with bats or rodents. Skinks have also had multiple and repeated radiations into a number of ecotypes ranging from fully fossorial to fully arboreal (Pianka and Vitt 2003). This makes them prime candidates for investigating how animals radiate

from, or converge on, similar lifestyles and morphologies. With a phylogenetic context in place, one can test whether similarities of mechanical properties of homologous structures are due to parallel or convergent evolution. Furthermore, the ability to recognize subtle morphological differences between populations, and whether they constitute true biological species, is important for finding agreement between the morphological species concept and the biological species concept. By extension, when regarding fossils, one would hope to discern whether the individual fossil is from an extant species, a completely extinct species, or a transitional form between the two.

The degree to which one can infer phylogeny from morphometric data is referred to as the phylogenetic signal. In a continuously evolving group, sister species would be expected to be more similar in shape than distantly related ones. Of course, morphological convergence means that the ability to identify phylogeny from morphometrics is limited. A kangaroo and a deer both have a long skull with a wide diastema and high coronoid process, but that has much more to do with the optimal shape for the feeding apparatus of a browser than the relationship between diprotodonts and cervids. A morphometric comparison of all the orders of Mammalia, showed “almost no consensus with current ordinal level phylogenies as constructed from traditional morphology” (Marcus et al. 2000). Therefore, there seems to be a limited range of morphological evolution that permits taxonomic inference; enough that there are differences between populations, but not so much that there has been secondary convergence.

In a review of the application of morphometric data to phylogenetic inference, MacLeod (2002) concluded that: 1) the concepts of a cladistic character and morphometric variable are essentially the same; 2) morphometric methods can lead to the discovery of

new morphological characters and character states; 3) morphometric analysis can be used to determine if cladistic character states are in fact independent; and 4) partial warp analysis by itself does not perform well as a mode of phylogenetic inference, but that a subdivided relative warp analysis does perform well. To test the subdivided method, MacLeod (2002) used a simulated dataset with a known phylogeny. The subdivided relative warp analysis involved subdividing a shape into a set of functionally significant sections, each defined by a subset of the landmarks, identifying distinct sets of individuals that were separated by the relative warp analyses, and then coding how an individual was placed into those groups for each functional region. That coding was then compiled into a character matrix and phylogeny was inferred using the parsimony method, with the results matching the known phylogeny.

Morphometrics, as a mode of identification has been only infrequently used with lizards, and typically without success. Zug and Gill (1997) used a combination of scalation patterns and 10 measurements of the head, neck, body, and limbs to compare populations of *Emoia murphyi* (Scincidae) on 5 southwest Pacific islands. Their research showed significant sexual dimorphism in one of the populations, but no differences between island populations. However, although they performed multivariate analysis of the scalation characters, the morphometric characters were only subjected to single variate ANOVA. Sumner (2002) examined head length and width in populations of *Glaphyromorphus mjobergi* (Scincidae), but these measures were not used as an identifying quality of the species. Significant sexual dimorphism was also observed in *Anolis carolinensis* (Polychrotidae) by Herrel et al. (2007) using both traditional and geometric morphometrics. *Anolis carolinensis* however was not compared to other species, nor was

there a comparison between populations. Richmond and Reeder (2002) mention “ongoing morphometric studies” of *Plestiodon gilberti* (Scincidae), but the results of those studies largely found sexual dimorphism instead of species boundaries (Richmond pers com.) and were never published.

Much more commonly, researchers have been interested in the functional significance of a change shape, after the phylogenetic signal has been removed. The importance of head shape in lizards as it relates to bite force, and by extension feeding mode and efficiency, has been documented by a number of authors (Herrel et al. 2007; McBrayer 2004; McBrayer and Corbin 2007). Greer and Wadsworth (2003) used skull length as a standard to compare body elongation and limb reduction, but did not incorporate the stoutness of the heads into their analysis, and so didn’t account for cranial elongation. McBrayer (2004) did an excellent job of describing head shape quantitatively and relating it to bite force and feeding ecology in a lacertid, incorporating many measurements into his analysis. Strayton (2005) performed a broad morphometric comparison of 441 species across 17 families of lizards, using 11 landmarks placed on the lateral view of the skull. Strayton (2005) and McBrayer and Corbin (2007) both showed that when a wide taxonomic cross section is considered, differences in skull shape reflect a strong phylogenetic signal, separating iguanians from scleroglossans, that signal is overlain by a secondary functional one.

Although there are shortcomings to traditional morphometrics (Marcus 1988; Bookstein 1991), particularly that variables are more likely to be interdependent and that less actual data is collected than possible (Zelditch et al. 2004), this method was used for the broad scale comparison of lizard skulls because of the relative ease of using calipers

compared to photographing skulls then digitizing landmarks in 3 dimensions. Also, because collections at a large number of institutions were used, it was far easier to bring calipers than the camera equipment and stand needed to photograph such small objects. Furthermore, since the coordinates of a landmark used in a final analysis are dependent on the alignment, which will change given any differences in the dataset, sharing data with other authors in the future will be better served by publishing the actual measurements (Appendix C).

One of the particular shortcomings of using traditional morphometrics here is that it is more difficult to subdivide the skull into functional regions, without using the same measurement several times. Therefore, the subdivided method for phylogenetic inference cannot be directly tested on this dataset. Instead, the entire skull shape will be used to determine if taxonomy can be inferred from head shape, and more specifically, at what taxonomic level *Eremiascincus* can be differentiated from other lizards. Lastly, the functional signal in the dataset will be examined to make inferences about changes in head shape as a consequence of an ecological shift through evolution.

Materials and Methods

In order to assess the shape of the skulls, dial calipers were used to take 15 measurements (Figure 5.1) on 217 lizard skulls. All parameters were measured to the nearest 0.02 millimeters, and were taken by a single observer using a single set of calipers. Specimens with obvious deformities, or missing data were excluded from the analysis. Since *Eremiascincus* is the lizard of primary interest here, specimens measured were chosen either for similarity of lifestyle or closeness of relationship. As such, the vast majority of specimens in this study were skinks (n=171). There were also 31 anguids, 14

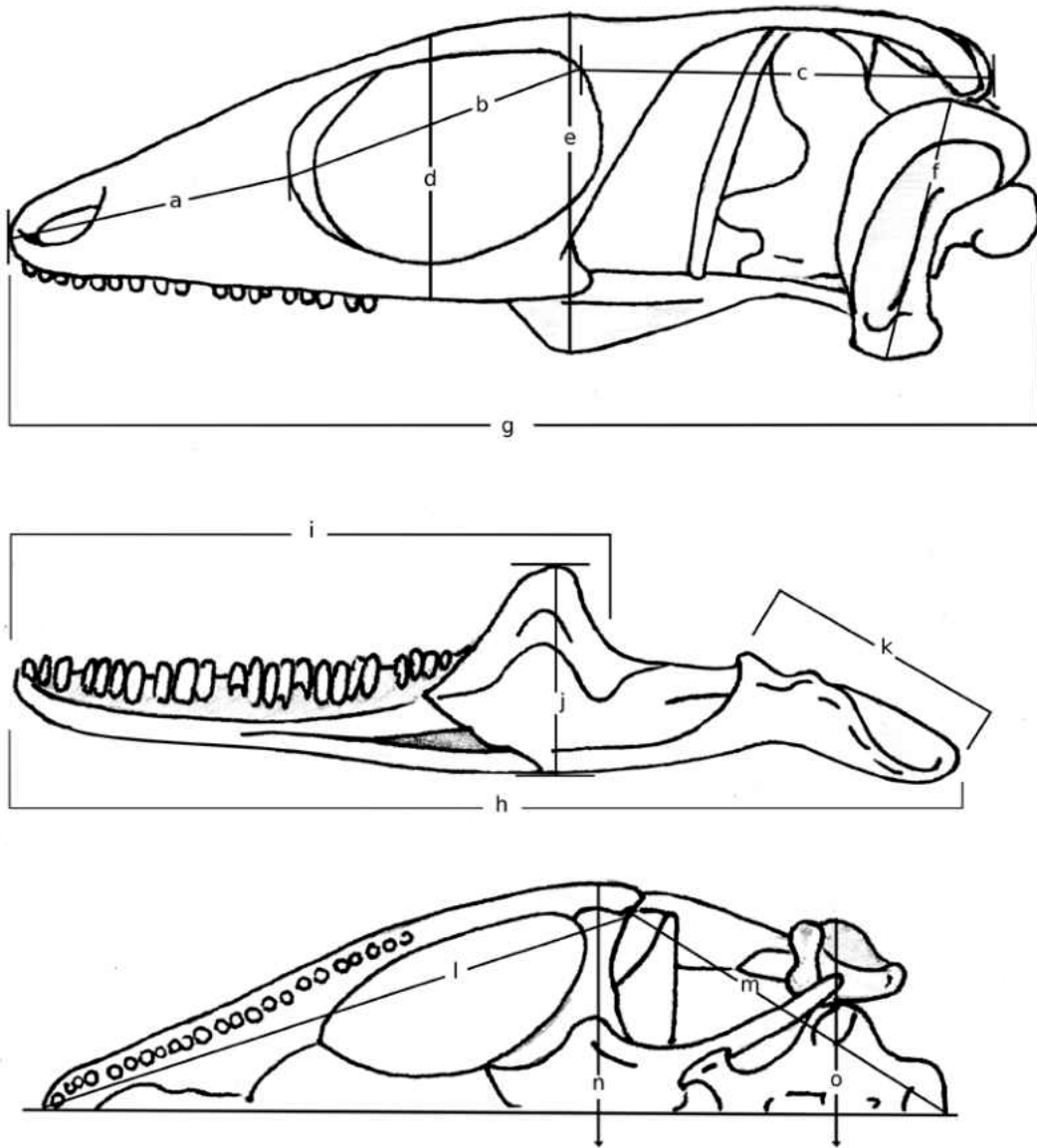


Figure 5.1. Linear measurements of the whole skull of a lizard: a. rostrum; b. orbit length; c. length of the temporal region; d. height at orbit; e. maximum height; f. quadrate length; g. occiput to rostrum tip length; h, length of jaw ramus; i. coronoid to symphysis length; j. height at coronoid; k. postarticular region; l. facial region length; m. cranial region length; n. width at jugals; o. width at quadrates.

teiids, and 1 xantusiid measured. Members of families other than Scincidae were included in order to provide an outgroup comparison for skinks as a whole. Teiids and a xantusiid were selected because of their close relationship to skinks, whereas anguids were used due to their similar ecology (Conrad 2008). Cordylids and gerrosaurids were considered because of their close relationship but rejected since the fusion of dermal ossicles to the skull made it impossible to take several measurements (Conrad 2008). Among the skinks measured, there are 8 genera within the Scincinae, 1 in the Acontinae and 17 genera in the Lygosominae. For most taxa, only adult lizards skulls were used, and those that had obvious deformities were excluded. However, because this thesis focuses on *Eremiascincus*, juveniles of that genus were included to determine if they would fall out in morphospace with their adult congeners.

To examine variability in shape only, absolute size of the animal was removed from the dataset by dividing each linear measurement by total length of the skull, thus also eliminating one variable. Because the use of PCA and discriminant analyses assume equal variance of the included variables, the coefficient of variation was calculated for each of the size transformed variables and found to consistently be between 0.09 and 0.19. As such, all variables were retained for further analysis. All statistical analyses were carried out using SPSS 17.0 (PASW Inc., USA).

Placement of *Eremiascincus* in the lizard skull morphospace was assessed by illustrating its place in the morphospace of successively more taxonomically constrained groups. First, a principal component analysis (PCA) was carried out using all individuals together so as to illustrate the morphospace occupied by skinks compared to the other families (Figure 5.2). Second, skinks (n=171) were separated from the other lizards, and

analyzed using PCA. For the sake of grouping points, skinks were divided up based on whether they belong to the Scincinae, Acontinae or Lygosominae. Within the Lygosominae, specimens were divided into the *Egernia* group, *Sphenomorphus* group, *Mabuya* group, *Eugongylous* group, or *Lygosoma* group (Figure 5.3). Although Reeder (2003) placed *Tribolonotus* as uncertain between being either the sister taxon to the *Egernia* group, or the *Mabuya* group, it is grouped in this paper with the *Egernia* group for the sake of simplifying the representation of the data.

Finally, *Eremiascincus richardsonii* (n = 7) was compared to *E. fasciolatus* (n=5) using first a PCA then a discriminant function analysis. Since the goal of the discriminant function analysis was to determine if it is possible to distinguish the two species from their skulls alone, both the original data set (Figure 5.5b) and size-transformed data (Figure 5.5a) set were analyzed. In addition, an independent t-test for the equality of means was performed for each of the transformed variables to determine if there was a simpler way to tell the two species apart.

At the family level, a high degree of correspondence is expected between the phylogenetic and functional signals because the majority of anguids available for measurement were either sand swimmers or semi-fossorial, and the majority of teiids examined were terrestrial. Therefore, a comparison between the phylogenetic and functional signal will be carried out here only within the skinks. To visually assess the phylogenetic signal, a phylogeny of the skinks used was laid over the plot of the first two principal components. To simplify the graph, the centroid for the first two principal component scores was calculated for each species. For genera that have all of its members in a single functional group, the centroid was calculated for the entire genus instead of

individual species. Nodes and branches of the cladogram are plotted onto the morphospace so that the largest natural groups could be plotted before branches of the cladogram crossed. It is drawn this way to illustrate the largest natural groups that could evolve without necessarily crossing the shape space occupied by another, existing taxon. However, the length of each branch from a centroid to the node connecting two centroids, or the branch length between two nodes, was visually optimized to minimize overlap of branches, a purely aesthetic decision.

The phylogenetic hypothesis used (Figure 5.6) is based on a combination of trees derived from molecular data. Arrangement of *Plestiodon anthracinus*, *P. septentrionalis*, *P. skiltonianus*, *P. lynxe*, *P. gilberti*, *Eumeces managuae*, *Novoeumeces algeriensis*, *E. schneideri*, and *Scincus scincus* on the tree was taken from Schmitz et al. (2004). Placement of *P. fasciatus*, *P. septentrionalis*, *P. tetragrammus*, *P. inexpectatus*, *P. obseletus*, *P. longirostris*, and *P. laticeps* within the tree is taken from Richmond (2006). Where the cladograms of Schmitz et al. (2004) and Richmond (2006) disagree on the relative positions of *P. inexpectatus*, *P. obeletus*, and *P. laticeps*, Richmond's (2006) clade was used because it was more taxonomically inclusive for closely related species. Placement of *P. marginatus* is based on its inclusion in the *P. latiscutatus* group (Honda et al. 2008). The arrangement of the lygosomine skinks in this analysis was based on analyses by Reeder (2003) and Gardner et al. (2008). Placement of *Acontias*, *Ophiomorus*, *Brachymeles*, and *Chalcides* on the tree was derived from the work of Brandley et al. (2005). *Plestiodon copei* and *P. dicei* were not found in previously published phylogenies. Consequently, here they are arbitrarily grouped with *Plestiodon lynxe* based on the fact that they are all Mexican taxa.

To assess functional shifts in morphospace, the skinks are here divided into 7 categories on the basis of substrate use. Categories are: sand-swimmer, fossorial, semi-fossorial, surface dweller, crevice dweller, arboreal, and semi-aquatic. References and assignments to each category are listed in Table 5.1. A sand swimmer is defined as having fossorial locomotion through a loose substrate, including sand, loam or leaf litter, by means of an undulating motion and do not maintain an open tunnel. Fossorial is maintaining an open burrow and foraging underground. Semi-fossorial is maintaining a living burrow but foraging outside of it. Terrestrial is foraging above ground and not maintaining a living burrow. A crevice dweller is one that occupies crevices in rocks, logs or other hard substrates that the lizard cannot change the dimensions of. Arboreal lizards are those that rest and forage predominantly in trees and semi-aquatic are those that primarily forage in the water. For cases where no data was available on habit, the lizard was assumed to have the same habit as its closest congener. Functional shifts in morphospace were made phylogenetically independent by only comparing sister taxa. There are 14 nodes on the tree that show a change from one ecotype to another. Direction of change that represents greater fossoriality was noted. Loading of each variable on the principal components was used to evaluate the kind of change in the skull represented by the change in morphospace.

In several cases, the taxonomic name used here differs from the name used on the museum tag associated with the specimen. In particular, East Asian and American *Eumeces* have been updated here to *Plestiodon* (Schmitz et al. 2004), and *Mabuya maculata* has been updated to *Trachylepis maculata* (Mausfeld and Vrcibradic 2002). Furthermore, the genus *Novoeumeces* was replaced with *Eumeces* following the current literature (eg. Kastle et al. 1996)

Although each measurement was size transformed to reduce the impact of total size on the calculation of the principal components, it does not eliminate the impact of shape changes that are the product of skull miniaturization. Because fossorial lizards are typically small (Rieppel 1984), skull miniaturization will be treated as an alternative hypothesis for explaining the variation in shape data. To determine whether size is a major contributing factor to the variation in the shape data, each of the extracted principal components were correlated against the total length of the skull, from occiput to snout, and the coefficient of determination was used to determine the proportion of variation in the PCA scores determined by size.

Results

There is only a weak phylogenetic signal in the dataset examined here. In the PCA of all taxa measured, the first principal component accounts for 42.0% of the variation in the data, and the second principal component accounts for an additional 17.0% of the variation. Figure 5.2 shows the plot of the first 2 principal component scores for all taxa and shows no clear separation between anguids, skinks or teiids. Morphospace containing anguids is almost entirely subsumed by the area containing skinks. Similarly, about half of the morphospace containing teiids is also occupied by skinks. Given this data set, one would be able to potentially rule out either anguids or teiids as identifications, but not positively identify members of either group. When only skinks are considered (Figure 5.3), there is still very little taxonomic utility to the groupings in the axes of the first two principal components. In the PCA of only skinks, the first principal component accounts for 43.6% of the variation in the data, and the second principal component accounts for another 16.7%. All 7 subgroups of skinks cross the origin of both axes at some point, and

only the *Egernia* group does not overlap all of the 6 remaining groups, although it does overlap 4 of them.

Separation of the subgroups within skinks is not substantially improved by the discriminant function analysis, which also separates the *Egernia* group to one side of the origin on the first discriminant axis (Figure 5.4a), but clumps all the other taxa together. The *Egernia* group is not even completely separated from the other skinks because some of them also cross onto the positive side of the origin on the first discriminant axis. When the discriminant function is re-run excluding members of the *Egernia* group, the remaining taxa still largely overlap one another (Figure 5.4b). Therefore, a skink skull belonging to something other than a member of the *Egernia* group, would be identifiable only if it fell out in one of the extremes of the ranges of one of the remaining groups.

When the specific level was considered, the discriminant function did however prove somewhat useful for distinguishing *Eremiascincus fasciolatus* from *E. richardsonii* (Figure 5.5a). Single-variate statistics failed to differentiate the two species (Gelnaw 2011), and there was still a large amount of overlap when they were subjected to principal component analysis. In the discriminant analysis, the dataset of size-transformed measurements had incomplete separation, with one individual of *E. fasciolatus* plotting on the *E. richardsonii* side of the origin. When the un-transformed dataset was subjected to the discriminant function analysis, there was complete separation (Figure 5.5b), suggesting that size, when considered after shape, can improve the identification of members of the genus.

Table 5.1. List of species used in the analysis with their respective substrate use classification and the literature source of that classification. Centroid refers to data points in Figures 5.7-10. A. arboreal; C. crevice dweller; F. fossorial; Sa. semi-aquatic; Sf. semi-fossorial; Ss. sand swimmer; T. terrestrial; NDA = no data available.

Centroid	Species	Category	Reference
1	<i>Acontias litoralis</i>	F	Pianka and Vitt 2003
2	<i>Brachymeles boulengeri</i>	SS	Siler et al. 2010
3	<i>Carlia ailanpalai</i>	Sf	Cogger 1992
4	<i>Chalcides ocellatus</i>	SS	Andrews et al. 1987
5	<i>Corucia zebrata</i>	A	Harmon 2002
6	<i>Ctenotus robustus</i>	T	Cogger 1992
7	<i>Egernia cunninghami</i>	C	Cogger 1992
7	<i>Egernia stokesi</i>	C	Cogger 1992
8	<i>Emoia kuekenhali</i>	NDA	
8	<i>Emoia trossula</i>	A	Zug et al. 1988
9	<i>Eremiascincus richardsonii</i>	Ss	Greer 1979
10	<i>Eremiascincus fasciolatus</i>	Ss	Greer 1979
13	<i>Plestiodon copei</i>	C	Lemo-Espinal et al. 1997; Van Devender and Van Devender 1975
14	<i>Plestiodon dicei</i>	NDA	
15	<i>Plestiodon fasciatus</i>	C	Smith 1946
17	<i>Plestiodon inexpectatus</i>	T	Smith 1946; Andrews et al., 1987
18	<i>Plestiodon laticeps</i>	A	Smith 1946
19	<i>Plestiodon longirostris</i>	T	Gocmen et al. 2002
20	<i>Plestiodon lynxe</i>	NDA	
21	<i>Plestiodon marginatus</i>	NDA	
23	<i>Eumeces schneideri</i>	Sf	Kastle et al. 1996, pg 351; Gocmen et al. 2002
27	<i>Lamprolepis smaragdina</i>	A	Perry and Buden 1999
28	<i>Lampropholis guichenoti</i>	Sf	Howard et al. 2003
29	<i>Leiolopisma zelandica</i>	Sf	Barwick 1959
29	<i>Leiolopisma festium</i>	NDA	
30	<i>Lipinia noctua</i>	A	Zweifel 1979
31	<i>Lygosoma fernandi</i>	Sf	Akani et al. 2009
32	<i>Mabuya rudis</i>	Sf	Inger 1959
32	<i>Mabuya multifasciata</i>	T	Inger and Colwell 1977
32	<i>Trachylepis maculata</i>	NDA	
32	<i>Mabuya carinata</i>	NDA	
32	<i>Mabuya macularia</i>	T	Inger et al. 1987
32	<i>Mabuya trilineata</i>	NDA	
32	<i>Mabuya bistrata</i>	C	Murphy 1997
32	<i>Mabuya fasciata</i>	NDA	
32	<i>Mesaspis monticola</i>	C	Roegiers and McCuen 2001
33	<i>Eumeces algeriensis</i>	Sf	Kastle et al. 1996: pg 349
34	<i>Ophiomorus brevipes</i>	F	Szczerbak 2003
11	<i>Plestiodon anthracinus</i>	Sf	Smith 1946
12	<i>Plestiodon brevilineatus</i>	Sf	Smith 1946
16	<i>Plestiodon gilberti</i>	sf	Lemm 2008
22	<i>Plestiodon obselatus</i>	C, f	Smith 1946; Caron and Swann, 2008

25	<i>Plestiodon skiltonianus</i>	F	Ryan 2008
26	<i>Plestiodon tetragrammus</i>	Sf	Fitzgerald 2008
35	<i>Scincopus fasciatus</i>	Ss	Kastle, et al. 1996: pg 357
36	<i>Scincus scincus</i>	Ss	Maladen et al. 2009
37	<i>Sphenomorphus jagori</i>	Ss	Diesmos 2007
38	<i>Tiliqua spp.</i>	T	Cogger 1992
39	<i>Tribolonotus mesaminius</i>	Sa	Pianka and Vitt 2003
40	<i>Tropidophorus grayi</i> & <i>T. brookei</i>	Sa	Barbour 1921

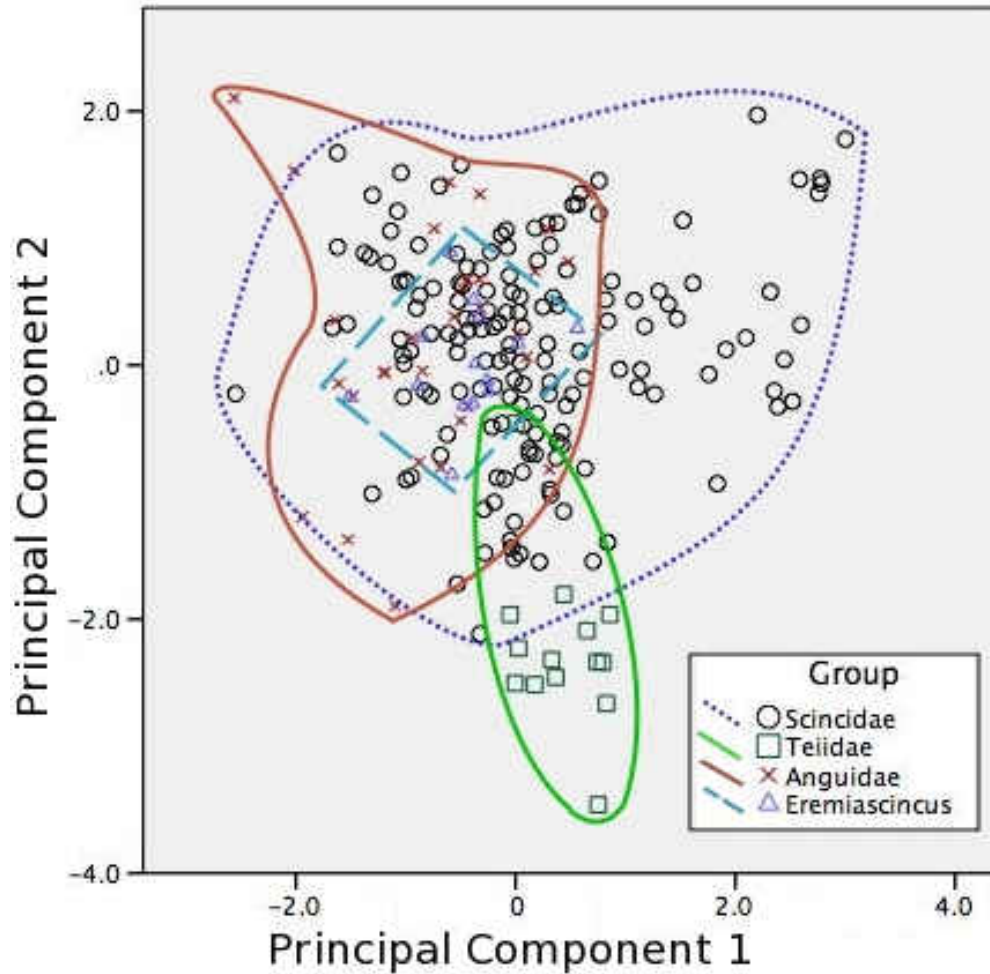


Figure 5.2. Plot of the first two principle component scores for all anguids, teiids and skinks measured. Each family is outlined separately in order to show the limits of their range in morphospace. *Eremiascincus* is outlined separately from other skinks in order to show its place in morphospace within the family.

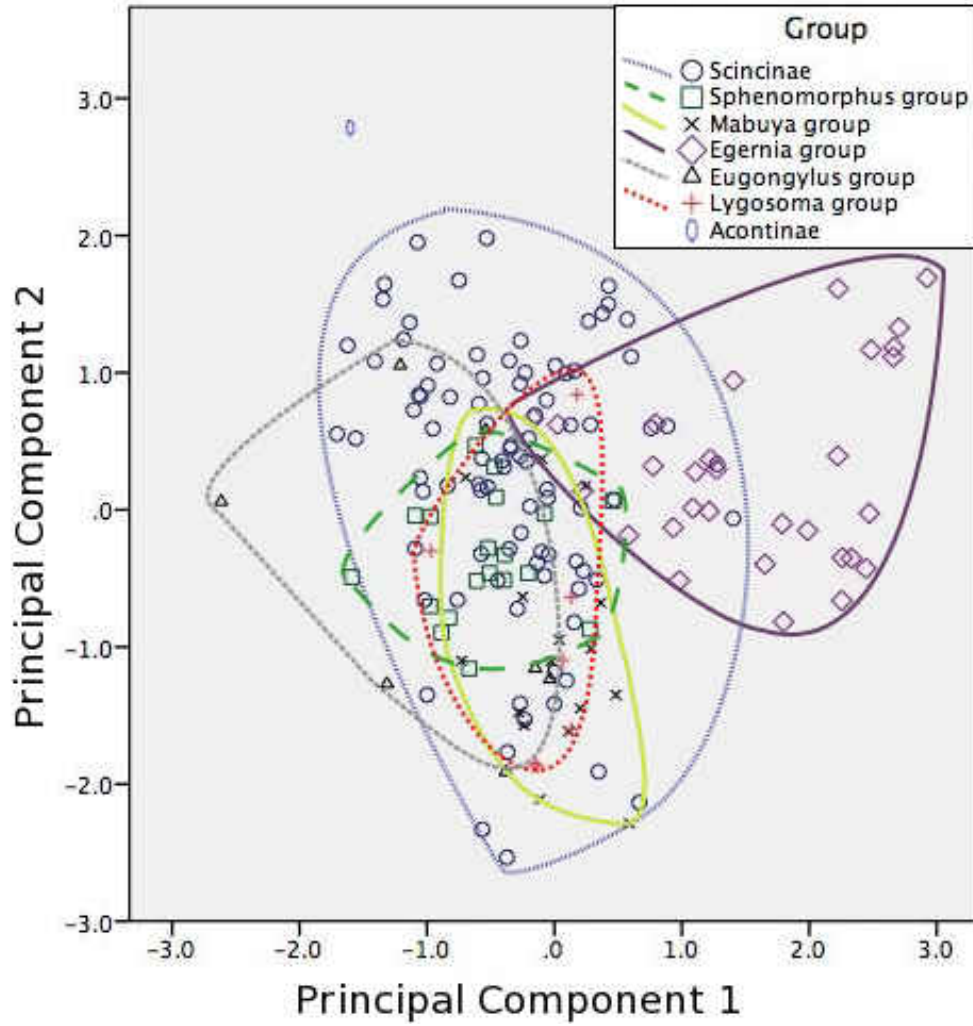
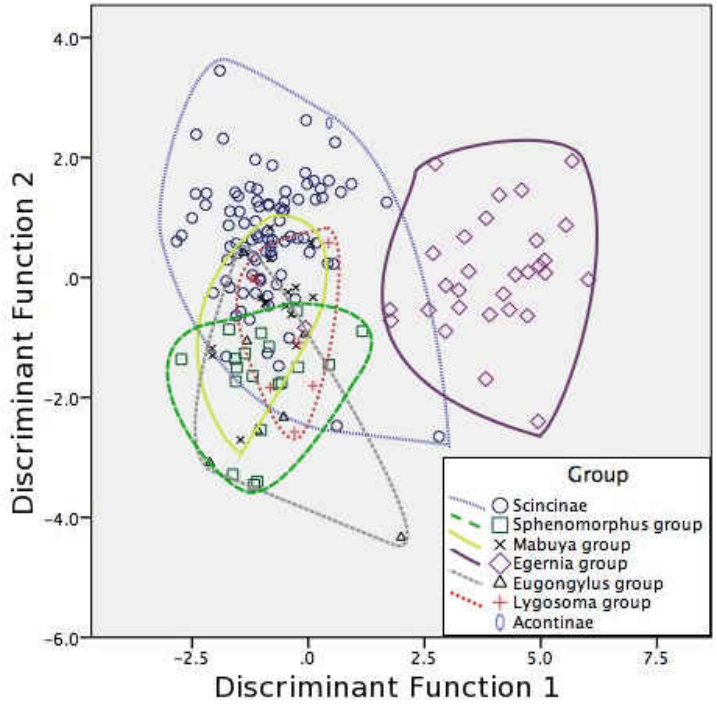
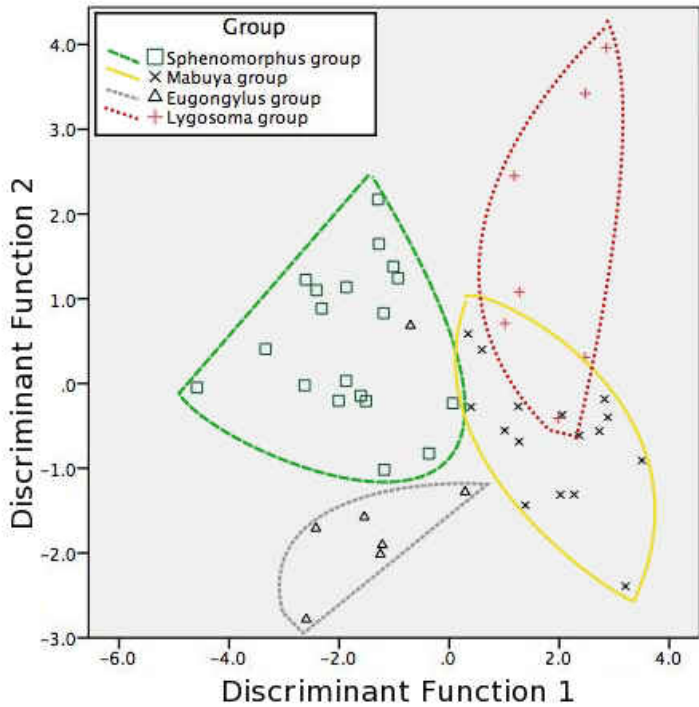


Figure 5.3. Plot of the first two principal component scores for all skinks measured. Outlines have been drawn to delineate the limits of morphospace occupied by each subgroup within the family.

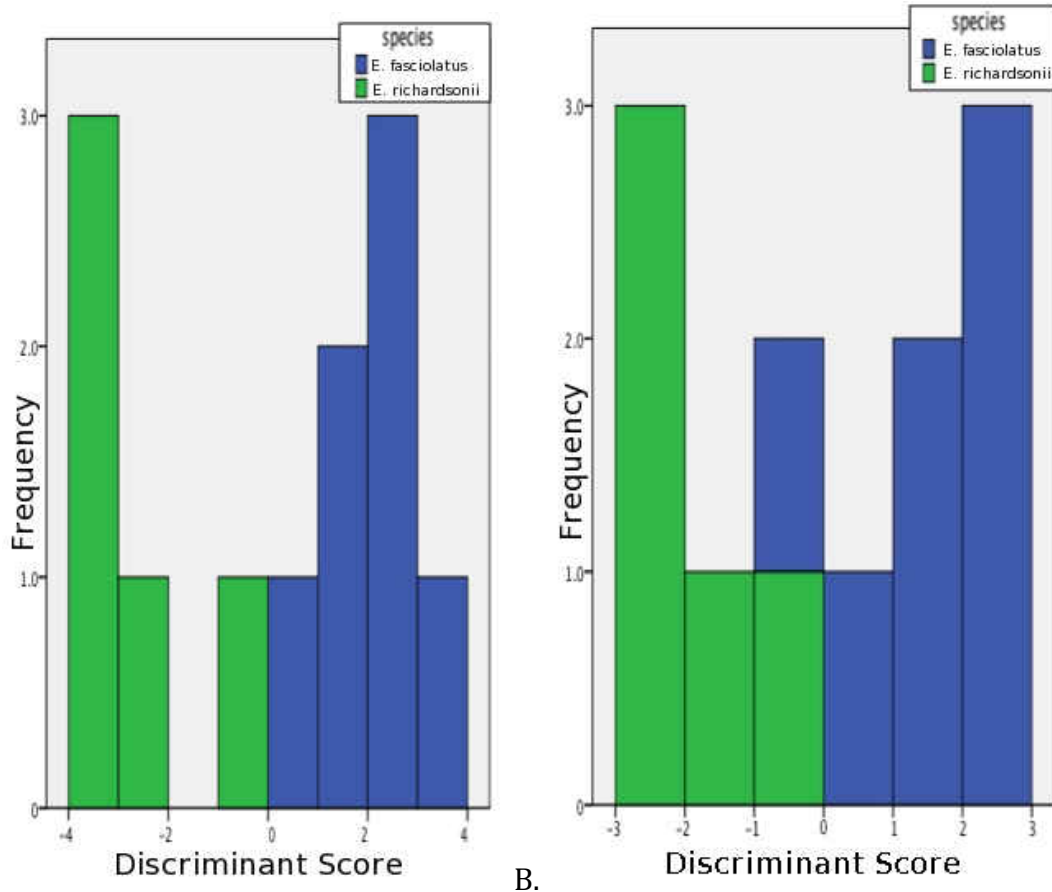


A.



B.

Figure 5.4. Separating groups of skinks on the basis of discriminant scores. A) Plot of the first two discriminant scores for all skinks in the dataset. B) Plot of the first two discriminant scores for all skinks, excluding members of the Scincinae, Acontinae, and the *Egernia* group.



A. Plot of the discriminant function of the untransformed. And B) transformed linear data sets differentiating *Eremiascincus richardsonii* and *E. fasciolatus*.

Using the cross-validation, the discriminant function separating *Eremiascincus richardsonii* from *E. fasciolatus* was rerun with casewise removal of a single specimen, which was then placed into a predicted group. Of the 12 specimens, 6 were incorrectly identified when treated as an unknown in the transformed dataset and 7 were incorrectly identified in the untransformed dataset. Of those incorrectly identified in either dataset, only 2 were incorrectly identified in both. With such a small data set (n=12), removal of a single specimen dramatically affects the discriminant function. Because of the complete separation around the origin line when all 12 individuals are included, I am optimistic that

a more robust dataset in the future will produce accurate separation of unidentified specimens.

When the phylogeny of skinks is mapped onto the plot of the first two principal components, rather than each group radiating from a single point or groups branching off from within a sister group, the plot is a tangled mess (Figure 5.7), with most transitions from one habit to another passing through the middle of the plot, rather than around the periphery. Close to the middle of the plot of the first two principal components, the ability of a clade to change direction or even undergo a reversal is greater than at the periphery, where selection appears to constrain evolution to a tangent away from the center of the graph. Not only this, but large scale changes are also most possible at the center, where the difference between sister taxa is greatest.

As taxa are stripped away, so that the plot represents largest natural groups that can be drawn without crossing branches of the phylogenetic tree, inferring phylogeny is still largely out of the question, but patterns of evolution do emerge. It worked out that Lygosominae (Figure 5.8), North American scincines (Figure 5.9) and Afro-Eurasian scincines (Figure 5.10) were each groups that could be plotted without crossing phylogenetic tree branches. This implies support of a hypothesis that competitive exclusion prevents skinks from crossing from one niche to another through morphospace, but is far from a test of it.

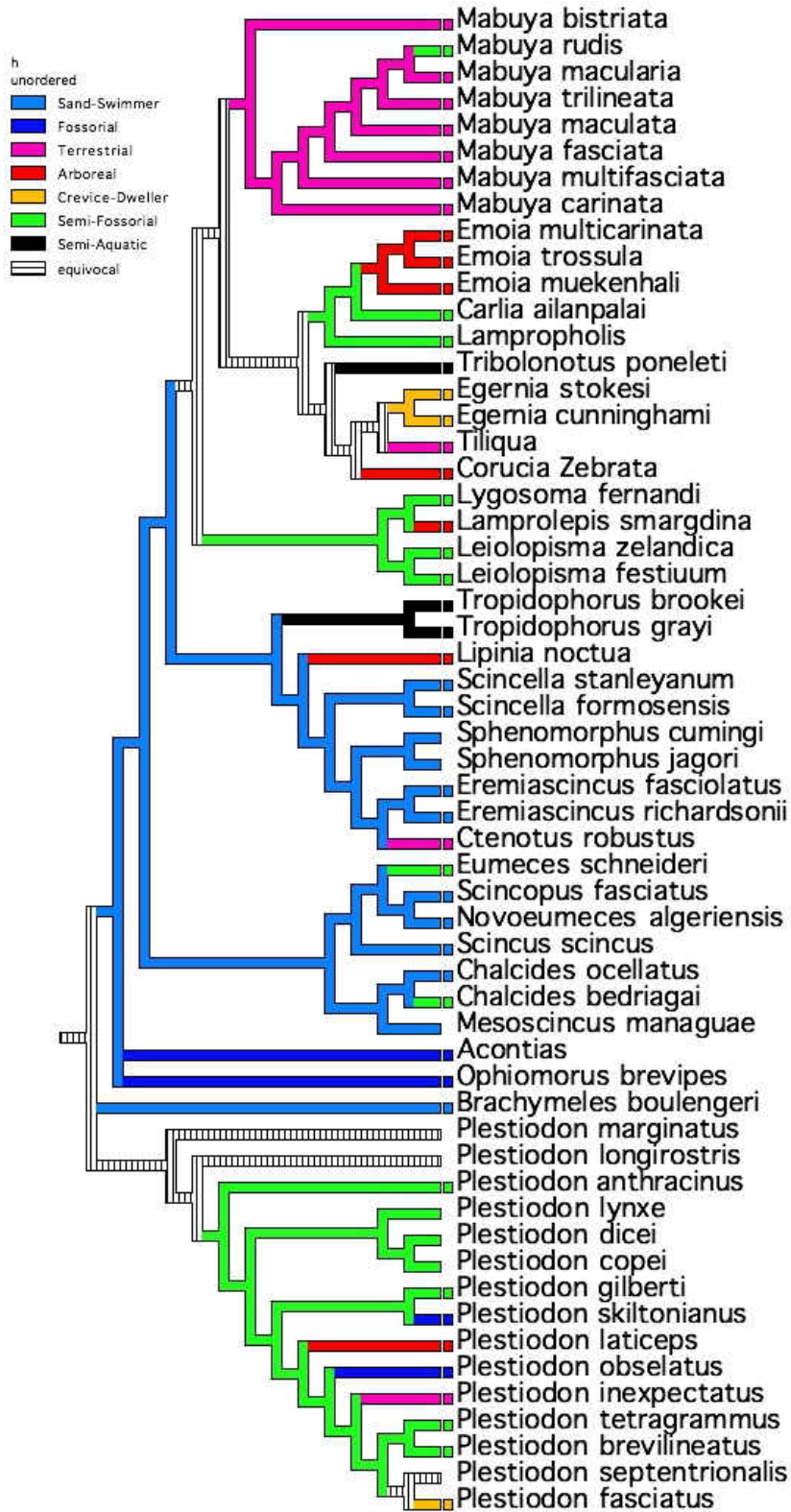


Figure 5.6. Combined phylogenetic tree of skinks used in the morphometric analysis.

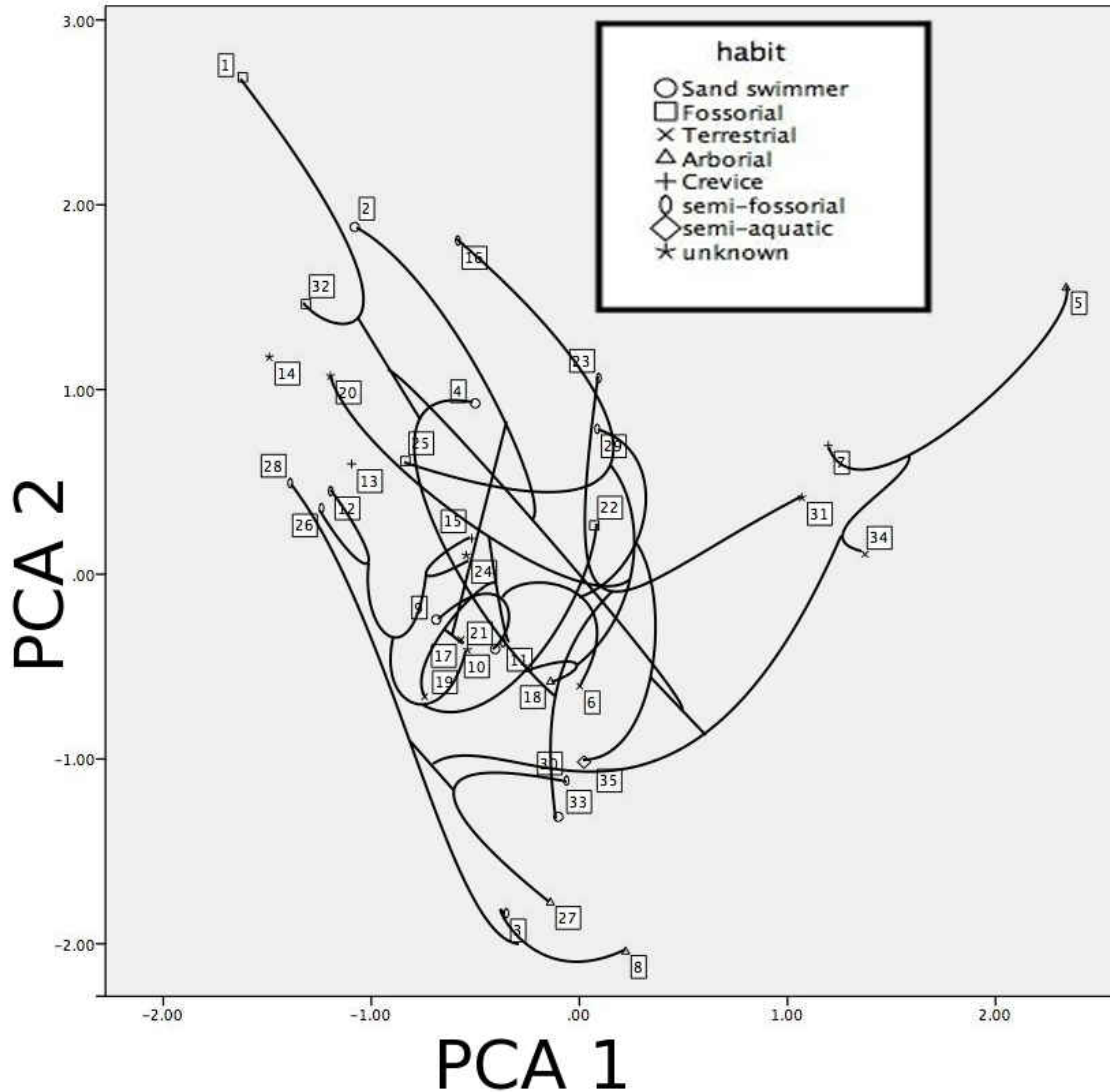


Figure 5.7. Phylogeny of skinks plotted onto the first two principal components of the cranial measurements. Points represent the centroids of each species that is a separate ecotype from its congeners, and each genus that is a single ecotype. Numbers affiliated with the points refer to the number of the centroid in Table 5.1.

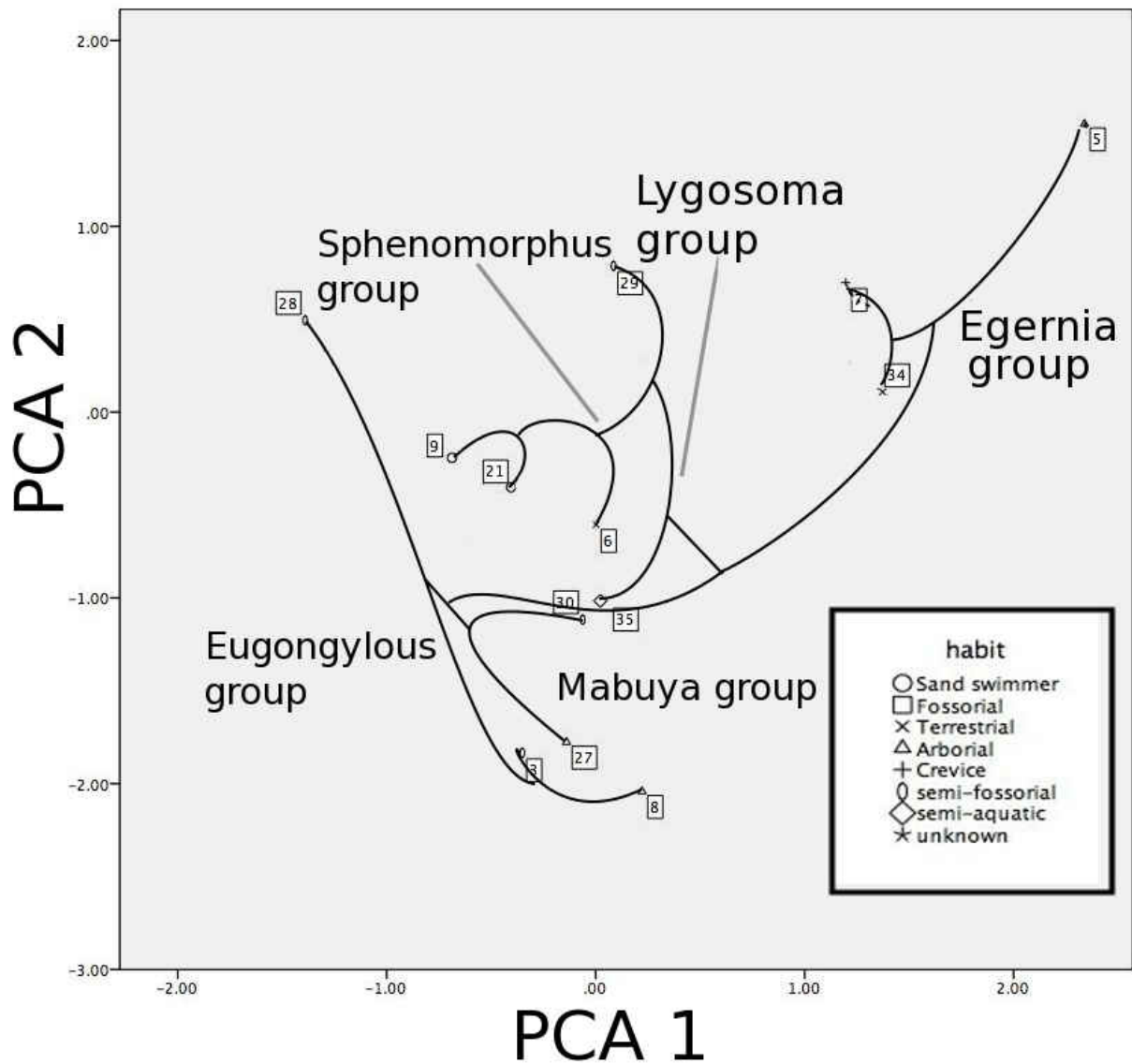


Figure 5.8. Phylogeny of the Lygosominae plotted onto the first two principal components of their cranial measurements.

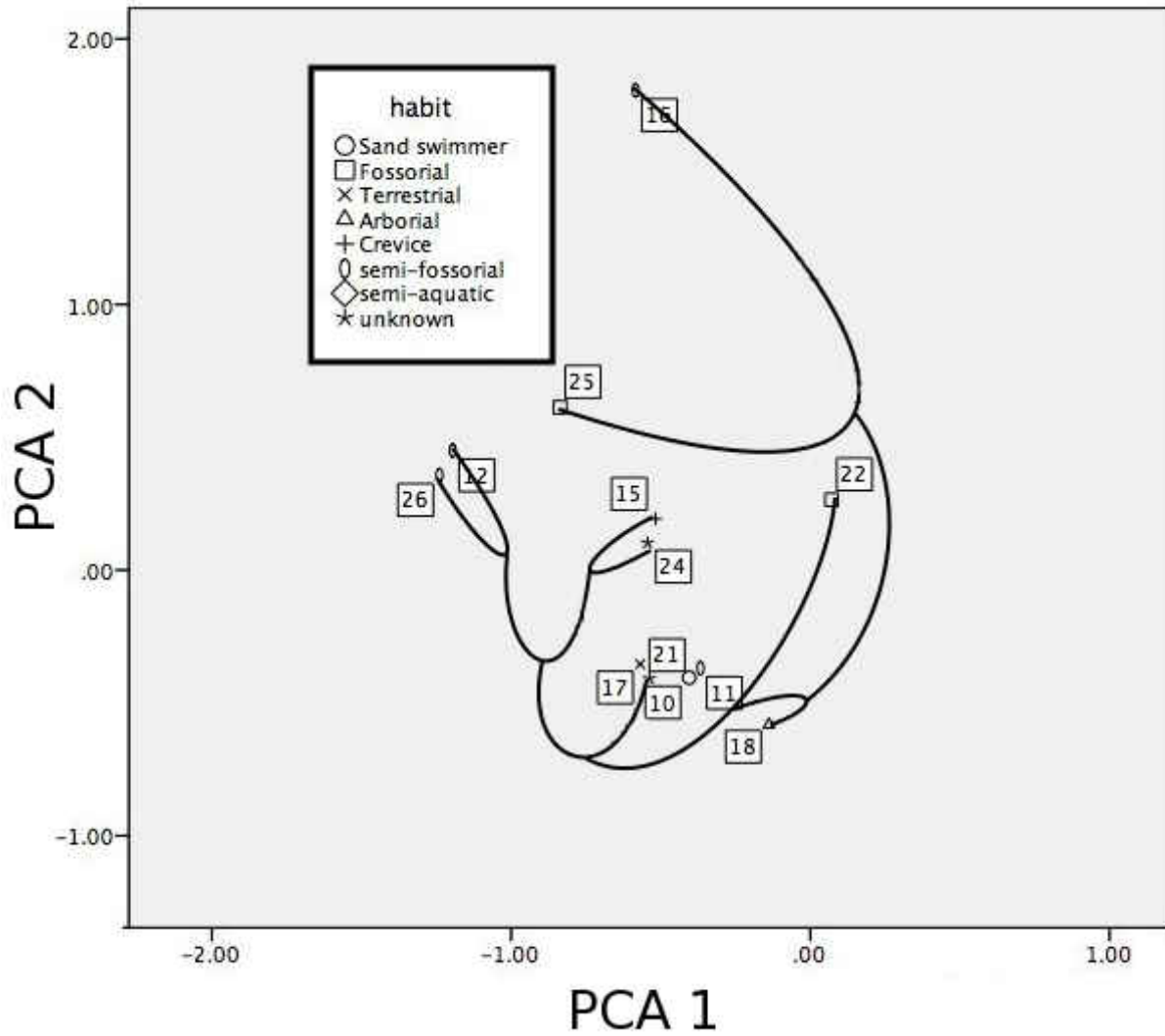


Figure 5.9. Phylogeny of *Plestiodon* plotted over the first two principal components of their cranial measurements.

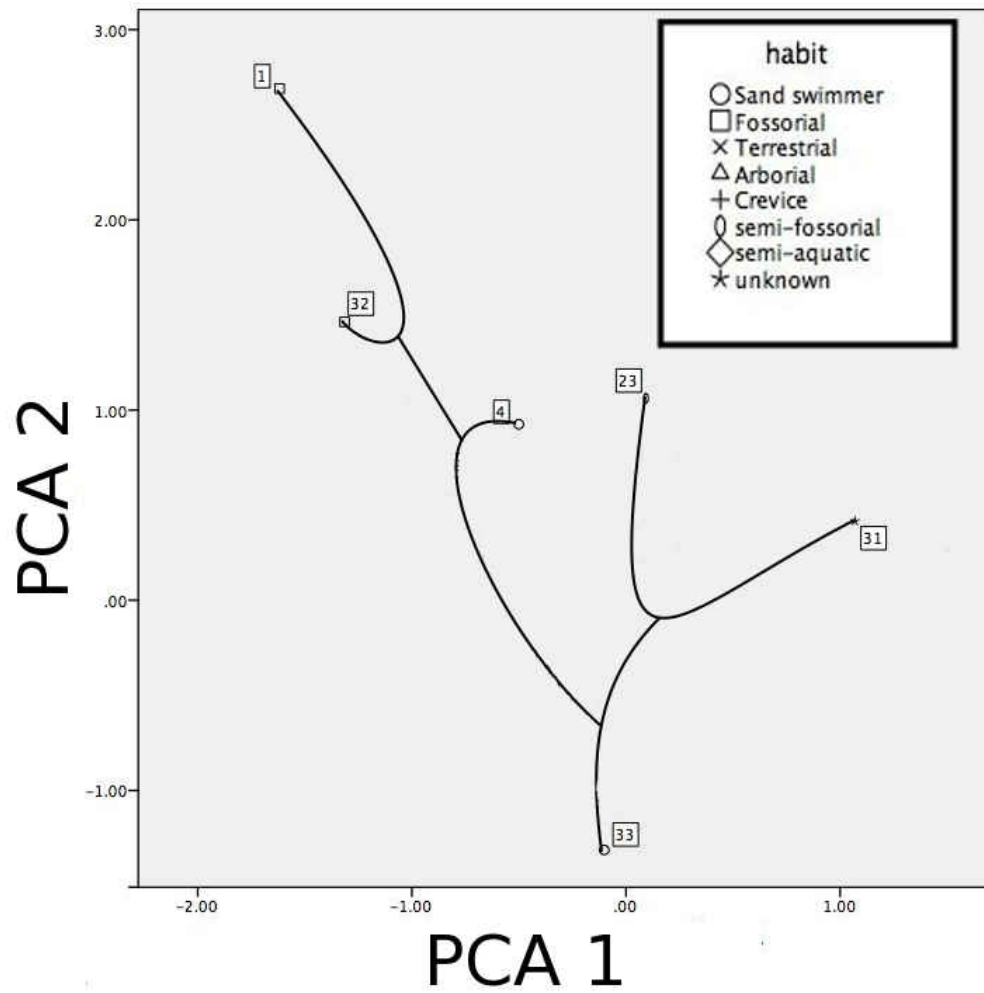


Figure 5.10. Phylogeny of the Afro- Eurasian skinks plotted over the first 2 principal components of their cranial measurements.

Table 5.2. Individual loading of each variable on the first four principal components. Variables are arranged in order from greatest loading to smallest. Loadings of less than 0.3 are excluded from the table.

	Component			
	1	2	3	4
Maximum height	.858	---	---	---
Height at the orbit	.825	---		
Width at the jugals	.822	---	---	---
Width between the quadrates	.821	---	---	---
Length of the lower jaw anterior to the posterior of the coronoid process	.820	-.342	---	---
Outside width at the quadrates	.811	.384	---	---
Height of the coronoid process	.698	.421	---	---
Length of the facial region	.669	-.653	---	---
Length of the quadrate	.660	---	.316	
Length of the rostrum	.604	---	---	.601
Length of the cranial region	-.360	.766	---	---
Length of the temporal region	.649	.663	---	---
Length of the articular condyle and retroarticular process of the lower jaw	---	---	.819	---
Length of the orbit	---	-.551	.619	-.459
Length of the lower jaw	.335	---	.300	.520

There were 15 comparisons made at transitions across a node from one habit to another. In most cases, increased fossoriality was associated with a decrease in the first principal component and an increase in the second. Examining the loading of each principal component (Table 5.2), the first is most heavily loaded by the three variables related to the height of the skull followed by the three variables indicating its width, two related to the height and position of the coronoid process and finally the length of the

anterior of the skull, in the facial region and rostrum. Loading of the second component is strongest in two variables relating to the length of the posterior of the skull, followed by the length of the facial region and of the orbit, which has a negative loading. Because an increase in fossoriality is affiliated with increased temporal length in the first component and decreased temporal length in the second component, the variable should perhaps be disregarded. However, a lengthening of the posterior of the skull in more fossorial taxa is still supported by the length of the cranial region on the ventral side of the skull.

Total skull length showed a strong correlation the first principal component ($R^2 = 0.732$). Only the terrestrial skinks deviated substantially more than the other groups from the line of best fit between skull length and the first principal component. When they were removed from the regression, the coefficient of determination increased marginally ($R^2 = 0.83$). The second principal component however, showed only a weak correlation ($R^2 = 0.028$) with skull length. For comparison, when the non size-transformed dataset is used to generate the principal component scores, the first principal component accounts for 97.5% of the total variance in the data, and the total skull size accounts for nearly all ($R^2 = 0.993$) of the variation in the first principal component. Therefore, the direct impact of size on the dataset has largely been removed, and the impact of size on the shape of skink skulls is accounted for by the first principal component. Consistent with the finding that a size was tied to skull shape, in 14 of the 15 comparisons made, the more fossorial skink was either smaller than, or within the size range of its less fossorial sister taxon. The only exception was that the fully fossorial *Plestiodon obsoletus* was larger than any of the members of the clade containing *P. inexpectatus*, *P. fasciatus*, and *P. tetragrammus*. Therefore, in nearly all cases, as animals became increasingly fossorial, the skull as a whole shrinks. As a

consequence of miniaturization, the skull becomes lower, narrower, and proportionately shorter in the temporal and facial regions, but not the orbit. On the lower jaw, the coronoid process in tern becomes lower and moves anteriorly.

Although another hypothesis to explain the variation in the second principal component may be devised in the future, after accounting for phylogeny and skull miniaturization, a change in fossoriality seems to be the best explanation for the shift in morphospace. For the most part, as one crosses a node toward a more fossorial habit, the facial region and orbit become proportionately smaller, and the posterior of the skull, in the temporal and cranial regions, become longer. There are however several counterexamples that may elucidate assumptions about fossoriality itself. *Scincus scincus*, a sand-swimmer, had a lower principal component score than the clade containing *Eumeces schneideri* and *Novoeumeces algeriensis*, which are semi-fossorial. *Lygosoma fernandi*, also semi-fossorial, showed a higher second principal component score than the clade containing *Ctenotus* and *Eremiascincus*, the later being a sand-swimmer. This suggests that the semi-fossorial habit should be considered the more fossorial state compared to sand-swimming.

There are also three more counterexamples to the more fossorial skink having a higher second principal component score than cannot easily be eliminated by rearranging which habit is considered more fossorial. Among the *Egernia* group skinks examined, *Egernia*, a crevice-dweller, has a lower second principal component score than *Corucia*, which is fully arboreal. *Tiliqua* also showed a lower second principal component score than the clade containing *Egernia* and *Corucia*. *Plestiodon gilberti*, classified here as semi-fossorial has a lower second principal component score than *Plestiodon skiltonianus*, which

is fully fossorial. In all three counterexamples, the more fossorial skink still had a lower first principal component score.

Discussion

As a predictive tool for either taxonomy or habit, the morphometric dataset is limited in its utility to taxonomically constrained subsets of the data. As a tool for identifying a specimen of completely unknown affinity, traditional morphometrics of the whole skull is apparently useless here. Gross morphological convergence sufficiently complicates the dataset that one would need to examine only a very taxonomically constrained subset of the data in order to get a positive identification of an unknown. Even within the largest natural groups that could be drawn without crossing phylogenetic branches, there were sharp reversals in the direction of evolution of each of the subclades. Taxonomic constraint of the data would come from qualitative characters, and the qualitative dataset has already shown to be sufficient to differentiate two similar and closely related genera (Chapter 3). As for estimations of habit, even knowing the sister group of a given taxon and the habit of that sister group, the dataset given here would only provide a relative statement about whether the specimen in question was more or less fossorial.

Taxonomic value of the morphometric dataset appears to be greatest at the smallest taxonomic level, particularly where no other characters have been developed for differentiating the closely related species. In the qualitative dataset, no characters were derived for differentiating *Eremiascincus fasciolatus* from *E. richardsonii*. Furthermore, in the ontogenetic study of *Eremiascincus* (Gelnaw 2010), single-variable t-tests were also unable to discern the two species, but the application of the discriminant function was

successful in separating them. In a vacuum of other methods, multivariate statistics can therefore be used, but only with extreme caution. Multivariate statistics could be applied to existing datasets that have failed to produce distinction between the taxa of interest. The morphometric dataset of Zug and Gill (1997), that found no significant differences between populations of *Emoia murphyi* based on single variable comparisons and a PCA, would be ideal to test the utility of the discriminant function analysis, since the subjects are already taxonomically constrained. If successful, the discriminant function analysis would provide a way for differentiating the populations without costly re-sampling from the wild.

Future work using traditional morphometrics will naturally be more thorough as additional samples and variables are added to this dataset. Small sample size of anguids and teiids was possibly a hindrance to their identification. However, if one assumes that the collections of those lizards measured represent a random taxonomic sample of the group, then the centroid of the sample should be close to the centroid of the group as a whole. A large sample size would in that case only further increase the overlap of the three groups in morphospace, possibly to the extent of not being able to rule any one out as identifications of a sample of unknown affinity. Also, the separation of the *Egernia* group by the first discriminant function analysis was possibly due to the over representation in the dataset of *Tiliqua* and *Corucia*, which are both highly specialized for being robust, much more so than another *Egernia* group member, such as *Egernia pulchra* or *E. saxatilis*. A more taxonomically diverse sampling would probably have produced more overlap in the resulting discriminant function analysis.

In spite of its shortcomings as a tool for taxonomic inference, the technique is somewhat useful as a tool for interpreting evolutionary trends in a known phylogeny.

When each pair of sister taxa were examined independently, there was a clear separation between the effects of skull miniaturization, and those of optimizing skull shape for fossoriality. The question remains though whether reduced head size is a consequence of a fossorial habit, or they have a common cause. There are at least four possibilities: 1) head size could be reduced relative to the body, in order to streamline the body and reduce drag through the soil; 2) small body size is preadaptive to increase fossoriality because the animal is able to wedge itself into smaller spaces and has less drag in soil; 3) shape changes associated with miniaturization of the skull also confer increased strength or reduced drag for face-first burrowing; or 4) fossoriality exerts a selective pressure for smaller body size because prey items are smaller or less abundant. Although an association between relative body elongation and fossorial habits is well documented (Schmitz et al. 2004; Brandley et al. 2008; Carranza et al. 2008), the first two possibilities are difficult to assess for this dataset because snout-vent length was not available for most specimens examined, and body width was not available for any of them. The third option, that the shape change associated with skull miniaturization is helpful for burrowing, is countered by the loading of the first two principal components. In the first component, when skink skulls shrink, the temporal region decreases in proportion to the total length, leaving the orbit relatively unchanged. Conversely, in the second component, the relative size of the orbit shrinks, and the temporal region increases in length. It is possible that the relative shrinking of the rostrum and facial region when the skull is miniaturized, gives a selective mechanical advantage for burrowing since it also impacts the second principal component in the same way. Countering the fourth possibility, that there is a feeding advantage to a smaller head, Andrews et al. (1987) examined the ecological cost of feeding in a fossorial *Chalcides*

compared to a terrestrial *Plestiodon inexpectatus*, and found that for a given mass of lizard, *Chalcides* expended more energy and time to eat a prey item of a given size, and was generally restricted to smaller prey items.

While this dataset is informative, the existence of several counter-examples to the trend of temporal and cranial elongation, and orbital shortening suggest that more work needs to be done to either find the cause of these counterexamples or produce a dataset that does not produce them in the first place. Classification of the lizards in this study into only seven groups is probably an oversimplification of the way that these animals use the substrates that they live on or in. For example, *Gerrhonotus infernalis* is known to be frequently arboreal, but also forage in leaf litter and spend inactive periods under rocks and logs (Greene et al. 2008), which means that it could easily be placed into 3 of the 7 categories. By comparison, the closely related *Elgaria multicaudata* also occupies 4 of the 7 categories, additionally being described as good swimmers (Beck 2008). In order to further tease out functional from phylogenetic signals in the data, future work should include two things: 1) a mode of ordination for substrate use so that multiple forms of substrate use by a single species are accounted for, and 2) a much more exhaustive taxonomic sampling so that each of the many new categories have a reasonable level of representation. Perhaps instead of ordination, another metric for comparison would be percent of time spent burrowing or density of the thickest substrate that the lizard moves through. As for the measurements themselves, future datasets should include a metric for the angle of attack of the rostrum. In this dataset, a blunt snout and a shovel shaped snout are treated as equivalent so long as all other variables remain the same. The problem there lies in measuring the angle on such small skulls.

A good next step in this line of investigation will be to look at a single genus that has a wide range of morphologies. For example, both *Brachymeles* and *Larista* are skink genera that contain members with a full range from fully terrestrial forms with well-developed limbs, to legless burrowers. When good phylogenetic hypotheses for these groups are developed, having such a limited taxonomic breadth would hopefully eliminate convergence as a confounding factor, enabling a researcher to focus specifically on the mechanisms for the evolution of fossoriality.

Literature Cited

- Andrews, R.M., Pough, F.H., Collazo, A., and A. de Queiroz. (1987). The ecological cost of morphological specialization: feeding by a fossorial lizard. *Oecologia* **73**: 139-145.
- Beck, D.D. (2008). Southern Alligator Lizard. (pp. 484-487). In: Jones, L.L.C., and Lovich, R.E. (eds) *Lizards of the American South West*. Rio Nuevo Publishers, Tucson, Arizona.
- Bookstein, F.L. (1991). *Morphometric tools for landmark data: geometry and biology*. Cambridge, UK: Cambridge University press.
- Brandley, M.C., Schmitz, A., and Reeder, T.W. (2005). Partitioned Bayesian analysis, partition choice, and phylogenetic relationships of scincid lizards. *Systematic Biology* **54(3)**: 373-390.
- Brandley, M.C., Huelsenbeck, J.P., and Wiens, J.J. (2008). Rates and patterns in the evolution of snake-like body form in squamate reptiles: evidence for repeated re-evolution of lost digits and long-term persistence of intermediate body forms. *Evolution* **62(8)**: 2042-2064.

- Carranza, S., Arnold, E.N., Geniez, P.H., Roca, J., and Mateo, J.A. (2008). Radiation, multiple dispersal and parallelism in the skinks *Chalcides* and *Sphenops* (Squamata: Scincidae), with comments on *Scincus* and *Scincopus* and the age of the Sahara desert. *Molecular Phylogenetics and Evolution* **46**: 1071-1094.
- Cogger, H.G. (1992). *Reptiles and Amphibians of Australia*. Cornell University Press, Ithica.
- Conrad, J.L. (2008). Phylogeny and systematics of Squamata (Reptilia) based on morphology. *Bulletin of the American Museum of Natural History* **310**: 1-182.
- Diesmos, A.C. (2007). Conservation of Herpetofaunal Communities in Fragmented Lowland Rainforests in the Phillippines. Final Technical Report. Rutherford Small Grant for Nature Conservation 171/07/04
- Gardner, M.G., Hugall, A.F., Donnellan, S.S., Hutchinson, M.N., and Foster, R. (2008). Molecular systematics of social skinks: phylogeny and taxonomy of the *Egernia* group (Reptilia: Scincidae). *Zoological Journal of the Linnean Society* **154**: 781-794.
- Gelnaw, W.B. (2011). Analyzing skull shape through ontogeny in *Eremiascincus* using traditional morphometrics. In: On the cranial osteology of *Eremiascincus*, and its use for identification. M.Sc. Thesis. East Tennessee State University.
- Gocmen, B., Senol, A., and Mermer, A. (2002). A new record of Schneider's Skink, *Eumeces schneideri* Daudin, 1802 (Sauria: Scincidae) from Cypress.
- Greene, H.W., Ralidis, P.M., and Acuna, E.W. (2010). Texas Alligator Lizard (pp. 492-495). In: *Lizards of the American South West*, eds. L.L.C. Jones and R.E. Lovich. Rio Nuevo Publishers, Tucson, Arizona.

- Greer, A.E. (1979). *Eremiascincus*, a new generic name for some Australian sand swimming skinks (Lacertilia: Scincidae). *Records of the Australian Museum* **32(7)**: 321-338.
- Greer, A.E and Wordsworth, L. (2003). Body shape in skinks: the relationship between relative hind limb length and relative snout-vent length. *Journal of Herpetology* **37(3)**: 554-559.
- Harmon, L.J. (2002). Some observations of the natural history of the prehensile-tailed skink, *Corucia zebrata* in the Solomon Islands. *Herpetological Review* **33(3)**: 177-179.
- Herrel, A., McBrayer, L.D., and Larson, P.M. (2007). Functional basis for sexual differences in bite force in the lizard *Anolis carolinensis*. *Biological Journal of the Linnean Society* **91**: 111-119.
- Honda, M., H. Ota, Kobayashi, M., Nabhitabhata, J., Yong, H., and Hikida, T. (2000). Phylogenetic relationships, character evolution and biogeography of the subfamily Lygosominae (Reptilia: Scincidae) inferred from mitochondrial DNA sequences. *Molecular Phylogenetics and Evolution* **15(3)**: 452-461.
- Honda, M., T. Okamoto, Hikida, T., and Ota, H. (2008). Molecular phylogeny of the endemic five-lined skink (*Plestiodon marginatus*) (Reptilia: Scincidae) of the Ryukyu archipelago, Japan, with special reference to the relationship of a Northern Tokara population. *Pacific Science* **62(3)**: 351-362.
- Howard, R., Williamson, I., and Mather P. (2003). Structural aspects of microhabitat selection by the skink *Lampropholis delicata*. *Journal of Herpetology* **39(3)**: 613-617.

- Inger, R.F. and Colwell, R.K. (1977). Organization of contiguous communities of amphibians and reptiles in Thailand. *Ecological Monographs* **47(3)**: 229-253.
- Kastle, W., Schleich, H.H., and Habisch, K. (1996). *Amphibians and Reptiles of North Africa: biology, systematics, field guide*. Koelz Scientific Publishers, Germany.
- Lemo-Espinal, J. A., Smith, G.R., and Ballinger, R.E. (1997). Observations on the body temperatures and natural history of some Mexican reptiles. *Bulletin of the Maryland Herpetological Society* **33(4)**: 159-164.
- MacLeod, N. (2002). Phylogenetic signals in morphometric data. In: MacLeod, N. and Forey, P.L. (eds) *Morphology, Shape and Phylogeny*. Taylor and Francis, Inc., New York and London.
- Marcus, L.F. (1988). Traditional Morphometrics (pp 77-122). In: Rolf, F.J. and Bookstein, F.L (eds) *Proceedings of the Michigan Morphometrics Workshop*. University of Michigan Museum of Zoology.
- Marcus, L.F., Hingst-Zaher, E., and Zaher, H. (2000). Application of landmark morphometrics to skulls representing the orders of living mammals. *Hystrix* **11**: 27-47.
- Mausfeld, P. and Vrcibradic, D. (2002). On the nomenclature of the skink (*Mabuya*) endemic to the western Atlantic archipelago of Fernando de Noronha, Brazil. *Journal of Herpetology* **36(2)**: 292-295.
- McBrayer, L.D. (2004). The relationship between skull morphology, biting performance and foraging mode in Kalahari lacertid lizards. *Zoological Journal of the Linnean Society* **140**: 403-416.

- McBrayer, L.D. and Corbin, C.E. (2007). Patterns of head shape variation in lizards: morphological correlates of foraging mode. In: S.M. Reilly, S.M., McBrayer, L.D., and Miles, D.B. (eds) *Lizard Ecology: The Evolutionary Consequences of Foraging Mode*. Cambridge University Press, New York.
- Pianka, E.R. and Vitt, L.J. (2003). *Lizards: Windows to the Evolution of Diversity*. University of California Press, Berkeley, California.
- Reeder, T.W. (2003). A phylogeny of the Australian *Sphenomorphus* group (Scincidae: Squamata) and the phylogenetic placement of the crocodile skinks (*Tribolonotus*): Bayesian approaches to assessing congruence and obtaining confidence in maximum likelihood inferred relationships. *Molecular Phylogenetics and Evolution* **27**: 384-397.
- Richmond, J.Q. and Reeder, T.W. (2002). Evidence for parallel ecological speciation in scincid lizards of the *Eumeces skiltonianus* species group (Squamata: Scincidae). *Evolution* **56** (7): 1498-1513
- Richmond, J.Q. (2006). Evolutionary basis for parallelism in North American scincid lizards. *Evolution & Development* **8** (6): 477-490.
- Rieppel, O. (1984). Miniaturization of the lizard skull: its functional and evolutionary implications. *Symposium of the Zoological Society of London* **52**: 503-520.
- Schmitz, A., Mausfield, P., and Embert, D. (2004). Molecular studies on the genus *Eumeces* Wiegmann, 1834: phylogenetic relationships and taxonomic implications. *Hamadryad* **28**: 73-89.

- Siler, C.D., Diesmos, A.C., and Brown, R.M (2010). New loam-swimming skink, genus *Bracymeles* (Reptilia: Squamata: Scincidae) from Luzon and Catanduanes Islands, Philippines. *Journal of Herpetology* **44(1)**: 49-60.
- Smith, H.M. (1946). Handbook of Lizards: lizards of the United States and Canada. Comstock Publishing Associates, Ithica and London.
- Strayton, C.T. (2005). Morphological evolution of the lizard skull: a geometric morphometrics survey. *Journal of Morphology* **263**: 47-59.
- Sumner, J. (2002). Morphometric and reproductive notes on the rare wet tropics skink, *Glaphyromorphus mjobergi*. *Memoirs of the Queensland Museum* **48(1)**: 146.
- Tihen, J.A. (1949). The genera of the Gerrhonotine lizards. *The American Midland Naturalist* **41(3)**: 580-601.
- Whiting, A.S., Bauer, A.M., and Sites Jr., J.W. (2003). Phylogenetic relationships and limb loss in sub-Saharan African scincine lizards (Squamata: Scincidae). *Molecular Phylogenetics and Evolution* **29**: 582-598.
- Zeldritch, M.L., Swiderski, D.L., Sheets, H.D., and Fink, W.L. (2004). *Geometric morphometrics for biologists: a primer*. Elsevier Academic Press, San Diego.
- Zug, G.R. and Gill, B.J. (1997). Morphological variation of *Emoia murphyi* (Lacertilia: Scincidae) on islands of the southwest Pacific. *Journal of the Royal Society of New Zealand* **27(2)**: 235-242.
- Zug, G.R., Springer, V.G., Williams, J.T., and Johnson, D. (1988). The vertebrates of Rotuma and surrounding waters. *Atoll Research Bulletin* **316**: 1-25.
- Zweifel, R.G. (1979). Variation in the scincid lizard *Lipinia noctua* and notes on other *Lipinia* from the New Guinea region. *American Museum Novitates* **2676**: 1-21.

CHAPTER 6

Using Geometric Morphometrics to Distinguish Individual Elements of *Eremiascincus* from *Ctenotus*

William B. Gelnaw

The Don Sundquist Center for Excellence in Paleontology, East Tennessee State University,
Johnson City, Tennessee 37614, United States

Abstract – Geometric morphometrics successfully differentiated the closely related skinks *Eremiascincus* and *Ctenotus* based on only isolated elements, as might be found in the fossil record. Sets of 9 elements were compared between groups of the two genera, using a total of 113 landmarks. Principal component analysis, a discriminant function analysis, and a stepwise discriminant analysis of the dataset was tested for efficacy of distinguishing an individual of one taxon or the other, and the stepwise discriminant was found to be best.

Introduction

Fossil lizard skulls do not lend themselves well to existing techniques of morphometric comparison, and so need a modified methodology that suits the special needs of comparing squamates. So far, morphometric comparisons between lizard taxa have only been made of living taxa, using complete skulls (McBrayer 2004; Strayton 2005;

McBrayer and Corbin 2007), and although they have had success in teasing apart ecological distinctions, frequent convergence has meant that a phylogenetic signal is best found in an already taxonomically constrained sample (Gelnaw 2010). Furthermore, diagenetic biases against lizard skulls remaining articulated dramatically reduce the practicality of applying whole-skull techniques. Lizards are especially susceptible to disarticulation because the contacts between elements of the skulls of lizards are most commonly lap joints or butt joints, and infrequently the stronger sutured or fused joints (Conrad 2004; Evans 2008). Weigelt (1927) noted that the oral cavity and the anus are the two openings through which insects and other scavengers access the insides of the animal, resulting in frequent disarticulation of the lower jaw, and by extension other loose elements around the oral cavity. Even when an entire skull is preserved as a fossil, it is often deformed due to torsion, cracking, elastic warping or flattening, again rendering whole-skull morphometric data sets useless. Since for lizards, disarticulated elements are more commonly preserved intact, it makes sense to construct a dataset appropriate to their identification.

Macleod (2002) demonstrated that independently comparing functional subunits of an animal's shape can produce phylogenetically informative characters. Using geometric morphometrics to compare disarticulated cranial elements, the actual subunits of the skull, is a natural progression. In a literature search, there was only one publication (Hocknull 2002) and one thesis (Williams 1999) account of using morphometrics to identify isolated cranial elements from lizards. Hocknull (2002) used four traditional morphometric measures as criteria to differentiate members of five genera of Australian agamids, but distilled the measurement of the width of the ascending nasal process to general terms such as narrow and wide. Williams (1999) used traditional morphometrics to examine

frontals, parietals, dentaries, and maxillae of skinks in the *Egernia* group, and found it useful for identifying fossils of *Egernia* to the specific level. There has, however, been no documented use of geometric morphometrics on individual elements of lizard skulls.

Geometric morphometrics offers an advantage over traditional morphometrics in that it effectively measures variation in all measures between all landmarks placed on a shape, rather than a small subset of those measures as in traditional morphometrics. A comparison of *Eremiascincus* and *Ctenotus* is used here to test the utility of geometric morphometrics to differentiate closely related genera of lizards. Because of the success of the qualitative characters at differentiating these two taxa, it is expected that geometric morphometrics should have success as well (Gelnaw, this volume). Furthermore, it is the hope that differences in shape will provide insight for additional qualitative characters that can be used in future parsimony based analyses. Because characters are derived from landmark coordinates via principal component analysis or discriminant function analysis, each character is independent of the next, and therefore satisfies the assumption of independence, which is central to cladistic analysis. Consequentially, the correspondence between the results of this analysis and the qualitative characters described by Gelnaw (this volume) will be examined in detail to determine if any sets of characters previously described should be collapsed into a single, multifaceted character in future analysis.

Materials and Methods

Specimens of *Eremiascincus* and *Ctenotus* used are listed in Table 6.1. To bolster sample size and account for asymmetries of the skulls, left and right elements of each individual were treated as separate specimens. For consistency of landmark placement, the mirror image of all left elements was used so that it corresponded with the right side.

Broken specimens that were missing somewhere to place a landmark, were excluded from analyses. Digital photographs of each element were taken using a 3.2mp camera attached to a Lyca Z16 APO lens. The multifocus feature of the software Automontage (Syncroscopy 2008) was used to achieve greater depth of field by taking multiple photos of the specimen at different depths of field and combining the focused areas of each one into a single image. The images were then cropped, rotated so that each specimen was in a standard orientation (described below), and converted from tiff into jpg format in the program GIMP (Free Software Foundation 2010). Landmarks were placed on each photo using TPSdig, the landmark data for each specimen combined for each element in tpsUTIL and then superimposed and aligned with its counterparts using the Procrustes fit (Rohlf and Slice 1990) method in tpsSUPER. Most landmarks are type II and some are type III. Because the elements are isolated, there are no type I landmarks.

Landmark Placement:

Landmarks for each bone are illustrated and described in Figures 6.1 through 6.9. The following also lists the number of samples and landmarks for each bone.

Coronoid: (n=38: *Eremiascincus* = 26; *Ctenotus* = 12) 10 landmarks placed on the lateral side (Figure 6.1).

Dentary: (n=40: *Eremiascincus* = 26; *Ctenotus* = 14) 16 landmarks placed on the medial side (Figure 6.2). The dentary is oriented so that the dorsal edge of the first and last alveolus are on the same level.

Frontal: (n=23: *Eremiascincus* = 15; *Ctenotus* = 8) 9 landmarks placed on the left side of the ventral view. The frontal was rotated so that the line of symmetry is oriented vertically (Figure 6.3).

Table 6.1. Specimens used for comparison, with snout-vent length where available. ETVP = East Tennessee Laboratory of Vertebrate Paleontology, SAMR = South Australia Museum, WAMR = Western Australia Museum, NA = not available.

Species	Specimen number	SVL (mm)
<i>Eremiascincus richardsonii</i>	WAMR 146922	36
<i>Eremiascincus richardsonii</i>	WAMR 146923	44
<i>Eremiascincus richardsonii</i>	WAMR 146924	47
<i>Eremiascincus richardsonii</i>	ETVP 7127	NA
<i>Eremiascincus richardsonii</i>	ETVP 7128	NA
<i>Eremiascincus richardsonii</i>	ETVP 7129	NA
<i>Eremiascincus richardsonii</i>	ETVP 7130	NA
<i>Eremiascincus richardsonii</i>	ETVP 7131	NA
<i>Eremiascincus richardsonii</i>	ETVP 7132	NA
<i>Eremiascincus richardsonii</i>	ETVP 7133	NA
<i>Eremiascincus richardsonii</i>	ETVP 7134	NA
<i>Eremiascincus richardsonii</i>	ETVP 7135	NA
<i>Eremiascincus richardsonii</i>	ETVP 7136	NA
<i>Eremiascincus richardsonii</i>	ETVP 7137	NA
<i>Ctenotus severus</i>	WAMR 146910	NA
<i>Ctenotus labillardieri</i>	ETVP 7138	NA
<i>Ctenotus schomburgkii</i>	ETVP 7139	NA
<i>Ctenotus severus</i>	WAMR 146912	49
<i>Ctenotus schomburgkii</i>	WAMR 146916	53
<i>Ctenotus severus</i>	WAMR 146913	69
<i>Ctenotus mimetes</i>	WAMR 146909	69
<i>Ctenotus mimetes</i>	WAMR 146927	74
<i>Eremiascincus fasciolatus</i>	SAMR 11125	71
<i>Eremiascincus richardsonii</i>	WAMR 146921	83

Maxilla: (n = 39: *Eremiascincus* = 28; *Ctenotus* = 11) 12 landmarks placed on the medial side. The maxilla is oriented so that the ventral edges of the first and last alveolus are on the same level (Figure 6.4).

Palatine: (n=39: *Eremiascincus* = 25; *Ctenotus* = 14) 17 landmarks placed on the dorsal view. The palatine was oriented with the anterior to the left (Figure 6.5).

Parietal: (n=19: *Eremiascincus* = 13; *Ctenotus* = 6) 18 landmarks placed on the left half of the ventral side. The parietal is rotated so that the line of symmetry is oriented vertically. (Figure 6.6).

Postfrontal: (n=24: *Eremiascincus* = 15; *Ctenotus* = 9) 8 landmarks placed on the dorsal side (Figure 6.7).

Pterygoid: (n=41: *Eremiascincus* = 25; *Ctenotus* = 16) 12 landmarks placed on the dorsal side. The long axis of the pterygoid was oriented horizontally, with the anterior to the left (Figure 6.8).

Quadrate: (n=36: *Eremiascincus* = 27; *Ctenotus* = 9) 14 landmarks placed on the posterior view. The quadrate was oriented so that the lateral edge of the cephalic condyle was in the same vertical plane as the lateral edge of the mandibular condyle (Figure 6.9).

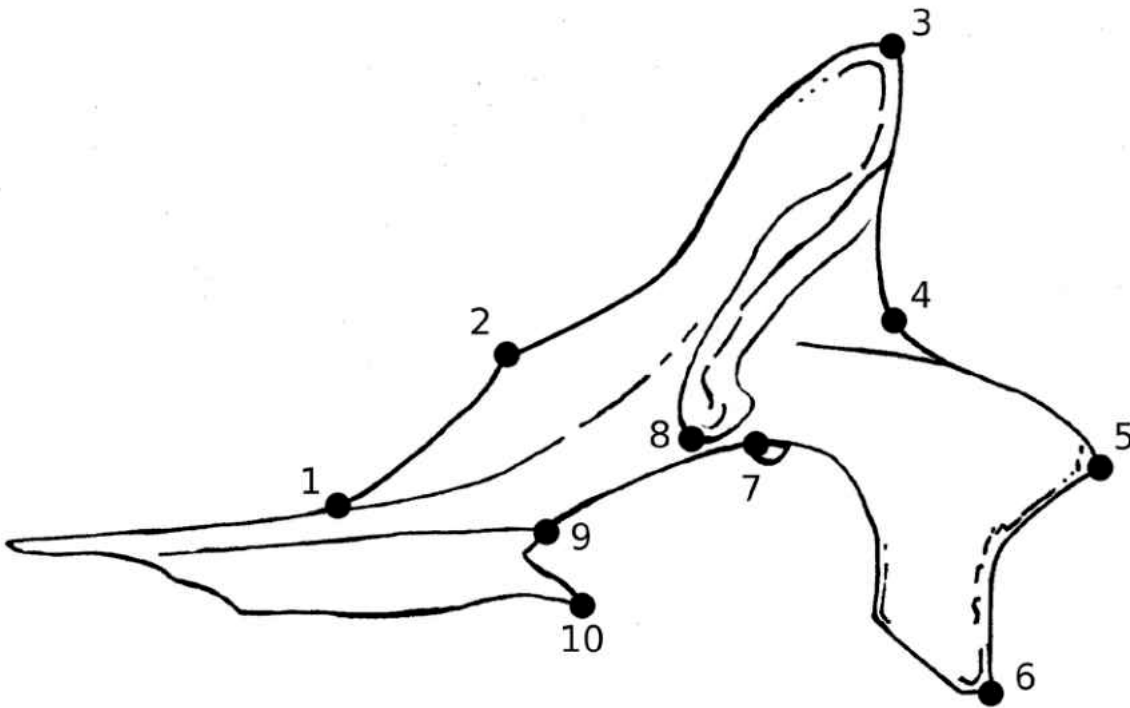


Figure 6.1. Coronoid landmarks: C1) At the junction between the anteromedial process, the lateral process and the coronoid process, forming the anterior most point of the superior dentary facet. C2) At the point of maximum curvature on the anterior face of the coronoid process. C3) At the apex of the coronoid process. C4) At the point of maximum curvature between the apex of the coronoid process and the posterior process. C5) At the vertex of the posterior process. C6) At the inferior vertex of the posterior process. C7) In standard view, the apex of the curvature on the inferior margin of the coronoid, located between the inferior process and the anterior sprcess. C8) At the anterior most projection of the lateral process. C9) At the posterior most extent of the inferior dentary facet on the anteromedial process; C10) The vertex of the posterior spine of the anteromedial process. Even when a true spine is absent, there is still a sharp homologous angle.

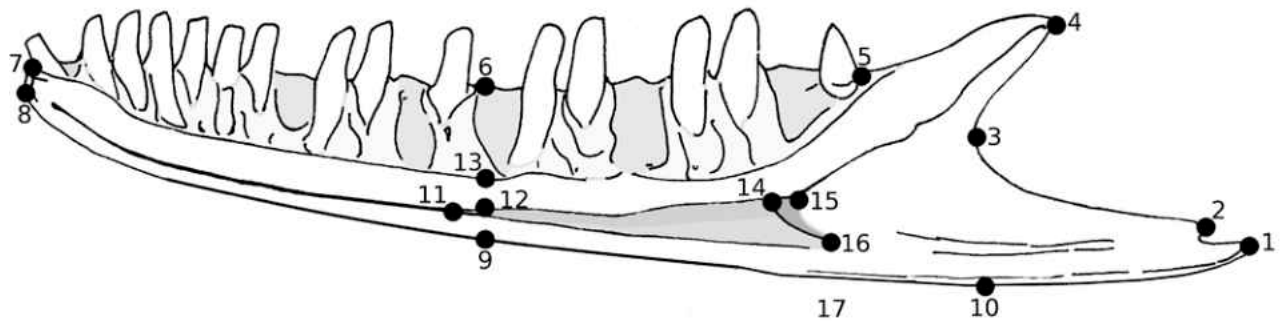


Figure 6.2. Dentary landmarks: D1) Vertex of the inferior posterior process. D2) Vertex of the superior posterior process. D3) Anteriormost inflection between the coronoid process and the posterior process. D4) Apex of the coronoid process. D5) posterodorsal margin of the posterior most alveolus. 6) The midpoint on the dorsal margin of the dentary, half way between points D5 and D7. D7) The anterodorsal point of the anterior most alveolus. D8) Anteriorventral corner of the mental symphysis. D9) The ventral margin of the dentary, directly below point D6. D10) The ventral most point of the dentary in standard position. D11) The constriction of the mechelian canal, where it closes or most constricts. D12) The dorsal margin of the mechelian canal, directly below point D6. D13) The ventral margin of the dental sulcus, directly below point D6. D14) The top of the infraalveolar septum. D15) The angle of the dental margin posterior to the infra-alveolar foramen. D16) The bottom of the infra-alveolar septum.

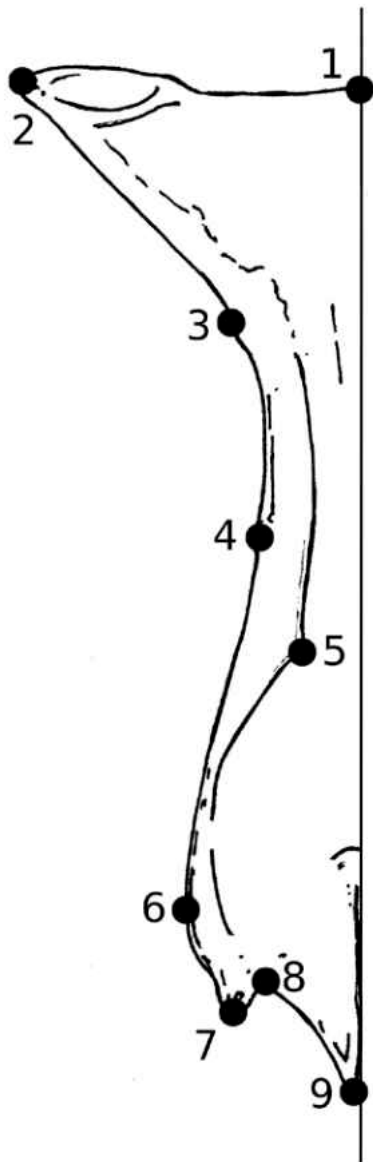


Figure 6.3. Frontal landmarks: F1) On the midline of the parietal facet. F2) Lateral corner of the parietal facet. F3) Anterior extent of the postfrontal facet. F4) Posterior extent of the prefrontal facet. This is also the narrowest point of the frontal. F5) The anterior most extend of the descending process. F6) The widest part of the frontal in front of the bone's midpoint. F7)The vertex of the anterolateral process. F8) The notch between the anterolateral process and anteromedial process. F9) The vertex of the anteromedial process.

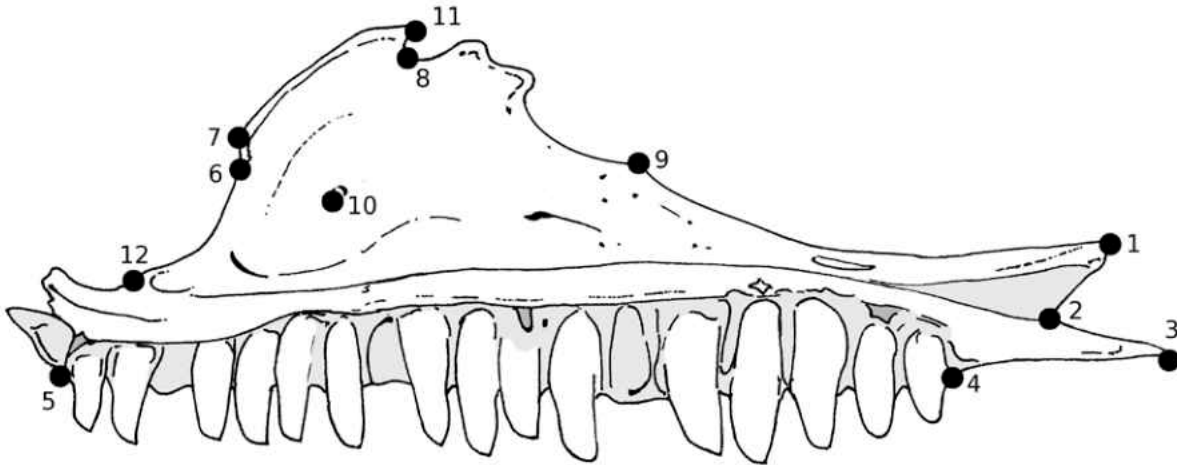


Figure 6.4. Maxilla landmarks. Mx1) The vertex of the superior posterior process. Mx2) Junction between the superior and inferior posterior processes. Mx3) The vertex of the inferior posterior process. Mx4) The posteroventral corner of the posterior most alveolus. Mx5) The anteroventral corner of the anterior most alveolus. Mx6) Maximum convexity on the anterior margin of the ascending nasal process. Mx7) The vertex of the anterior nasal process. Mx8) Vertex of the notch directly below or posterior to the apex of the ascending nasal process. Mx9) Angle at the junction between the orbital margin and the prefrontal facet. Mx10) The center of the foramen on the ascending nasal process. Mx11) Apex of the ascending nasal process.

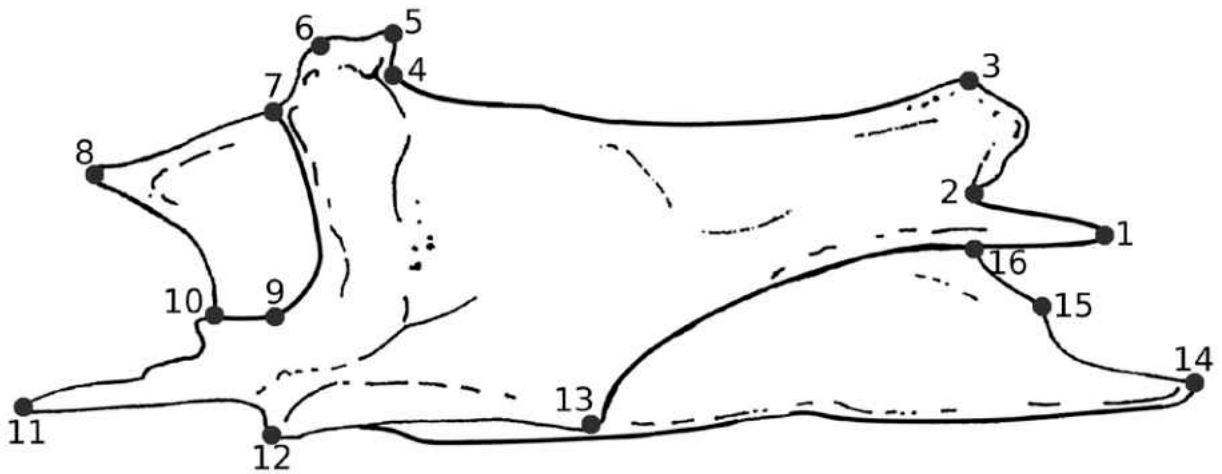


Figure 6.5. Palatine landmarks. Pa01) The vertex of the posteromedial process of the dorsal lamina. Pa02) The vertex of the posteromedial notch of the dorsal lamina. Pa03) The vertex of the lateral pterygoid process. Pa04) Posteromedial angle of the maxillary process. Pa05) Posterolateral angle of the maxillary process. Pa06) Anterolateral angle of the maxillary process. Pa07) The intersection between the anterior margin of the dorsal lamina and the lateral margin of the lateral vomerine process in the vertical plane. Pa08) The vertex of the lateral vomerine process. Pa09) Angle lateral to the anteromedial process of the dorsal lamina. Pa10) Where the anterior margin of the dorsal lamina and the lateral margin of the medial vomerine process intersect in the vertical plane. Pa11) The vertex of the medial vomerine process. Pa12) Anterior most point of contact between the ventral lamina of the palatines on the midline, marked by an angle on the medial margin. Pa13) Posterior most point of contact between the dorsal lamina on the midline, marked by a lateral inflection of the bone. Pa14) The vertex of the medial pterygoid process. Pa15) The vertex of the accessory pterygoid process. Pa16) Intersection of the posteromedial process of the dorsal lamina and the posterior margin of the ventral lamina in the vertical plane. Pa17) Posterior foramen in the dorsal lamina.

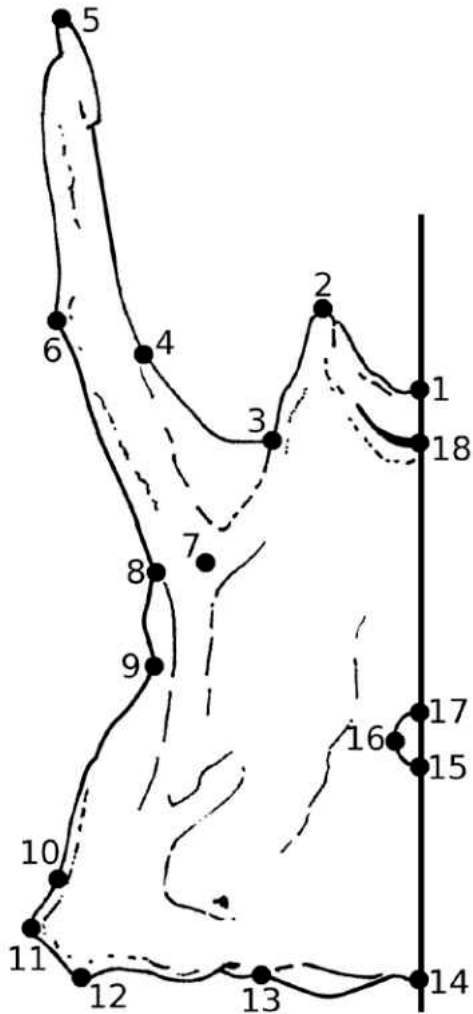


Figure 6.6. Parietal landmarks. P01) On the line of symmetry, at the posterior edge of the parietal. P02) Posterior edge of the parietal. P03) Junction between the posterior process and the supratemporal process. P04) The medial side of the supratemporal process, on the inside margin of the inflection. P05) The apex of the supratemporal process. P06) The outside of the inflection of the supratemporal process. P08) The posterior edge of the descending parietal process. P09) The posteriormost point of the lateral lamina. P10) The narrowest point of the parietal table. P11) The anterior most point of the lateral lamina. P12) The lateral most point on the anterior margin of the parietal. P13) The medial corner of the frontal tab. P14) The corner meeting the frontal tab and the parietal table. P15) On the line of symmetry, at the anterior margin of the parietal. P16) The anterior most point of the parietal foramen. P17) The lateral most point of the parietal foramen. P18) The posterior most point of the parietal foramen. P19) The anterior most point of the sulcus for the ascending process of the prootic.

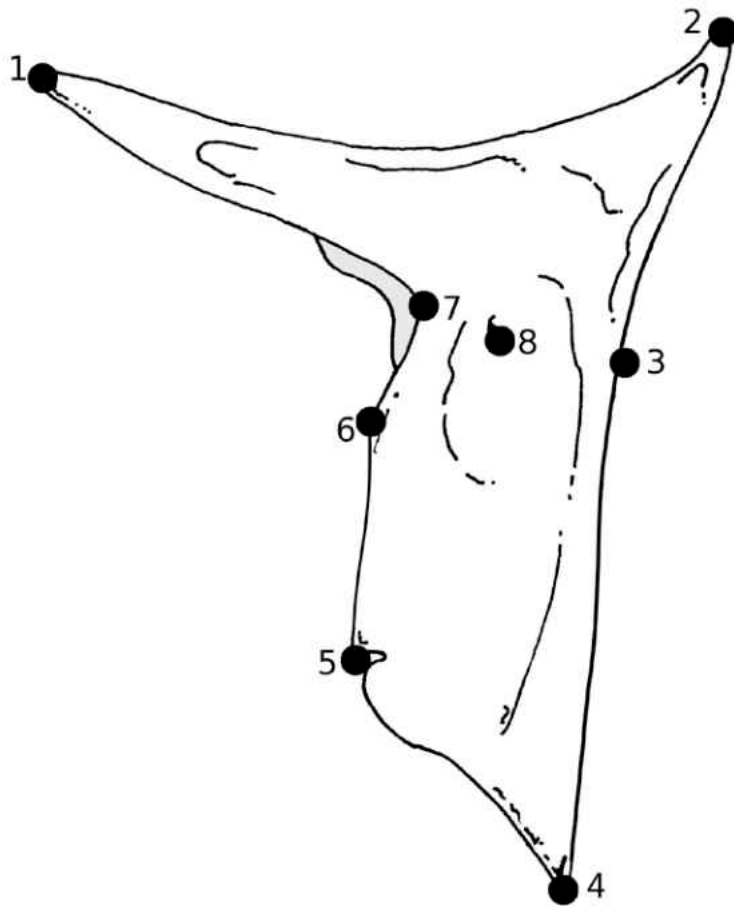


Figure 6.7: Postfrontal landmarks. Pof01) Vertex of the medial process. Pof02) Vertex of the lateral angle. Pof03) Maximum concavity on the lateral margin of the bone. Pof04) Vertex of the posterior process. Pof05) Angle at the anterior extent of the superior temporal fenestra. Pof06) Angle immediately posterior to the fronto-parietal notch. Pof07) Vertex of the frontoparietal notch. Pof08) Postfrontal foramen.

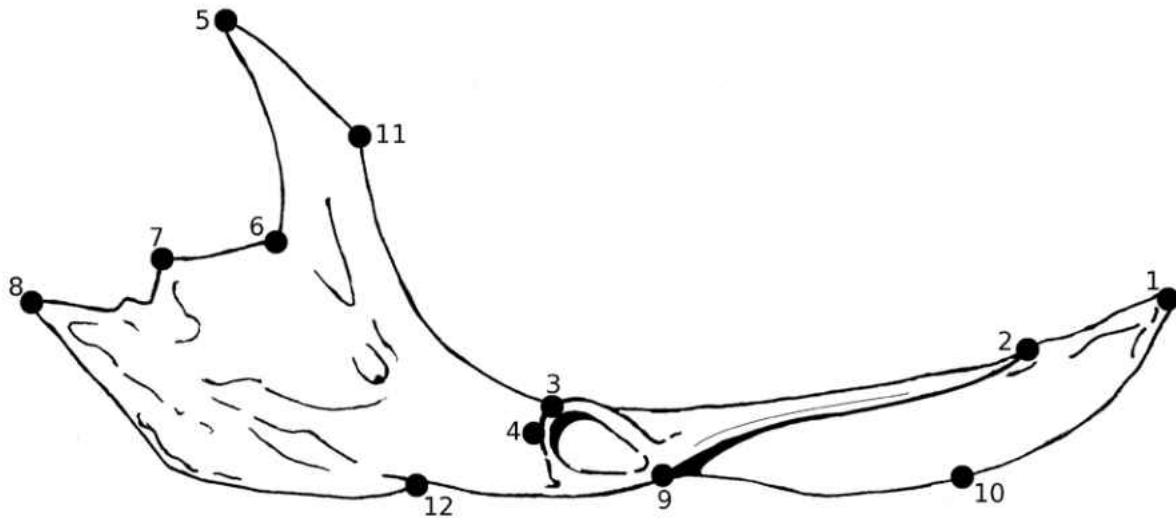


Figure 6.8. Pterygoid landmarks. Pt01) Vertex of the quadrate process. Pt02) Lateral margin of the quadrate process where the curl crosses the lateral edge. Pt03) The junction between the anterior edge of the fossa columellae and the lateral margin. Pt04) The anterior most point of the fossa columellae. Pt05) Vertex of the ectopterygoid process. Pt06) Vertex of the angle between the ectopterygoid process and the palatine process. Pt07) Vertex of the anterolateral palatine process. Pt08) Vertex of the anteromedial palatine process. Pt09) The junction between the curl of the quadrate process and the medial margin. Pt10) Maximum curvature on the medial margin of the quadrate process. Pt11) Posterior angle of the pterygoid flange. Pt12) The point of maximum curvature on the inflection of medial margin.

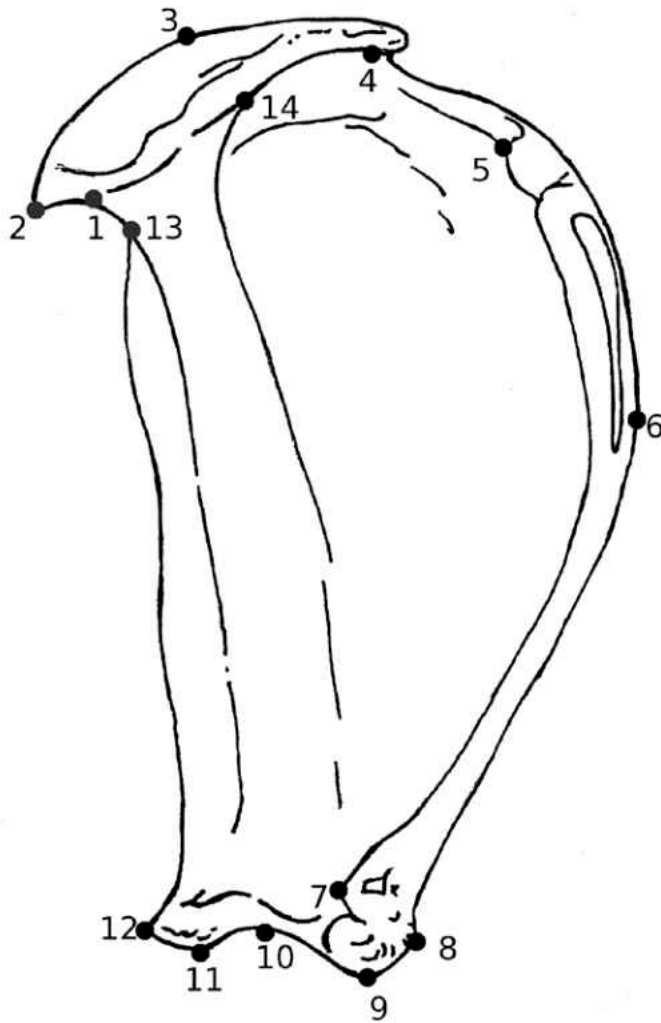


Figure 6.9: Landmarks on the quadratum. Q01) Junction between the medial edge of the central column and the cephalic condyle. Q02) Medial most extent of the cephalic condyle. Q03) Dorsal most extent of the cephalic condyle. Q04) Margin of the conch along the line of fusion with the cephalic condyle. Q05) Medial extent of the squamosal surface. Q06) Lateral most extent of the conch. Q07) Junction between the tympanic crest and the mandibular condyle. Q08) Lateral extent of the lateral mandibular condyle. Q09) Ventral extent of the lateral mandibular condyle. Q10) Maximum dorsal curvature of the mandibular condyle. Q11) Ventral extent of the medial mandibular condyle. Q12) Medial extent of the medial mandibular condyle. Q13) Junction between the pterygoid lamina and the central column. Q14) Junction between the lateral edge of the central column and the cephalic condyle.

Statistical Analyses:

All statistical analyses were carried out using the SPSS 17 statistics package (PASW, 2008). The degree of separation between the shapes of elements belonging to *Eremiascincus* and *Ctenotus* was examined using three techniques: A principal component analysis (PCA), a discriminant function analysis and a stepwise discriminant function analysis. Separation in the data represented by the PCA was visually inspected with the plot of the first two principal components for each element, and divided into three categories: complete separation; small amount of overlap; or large amount of overlap.

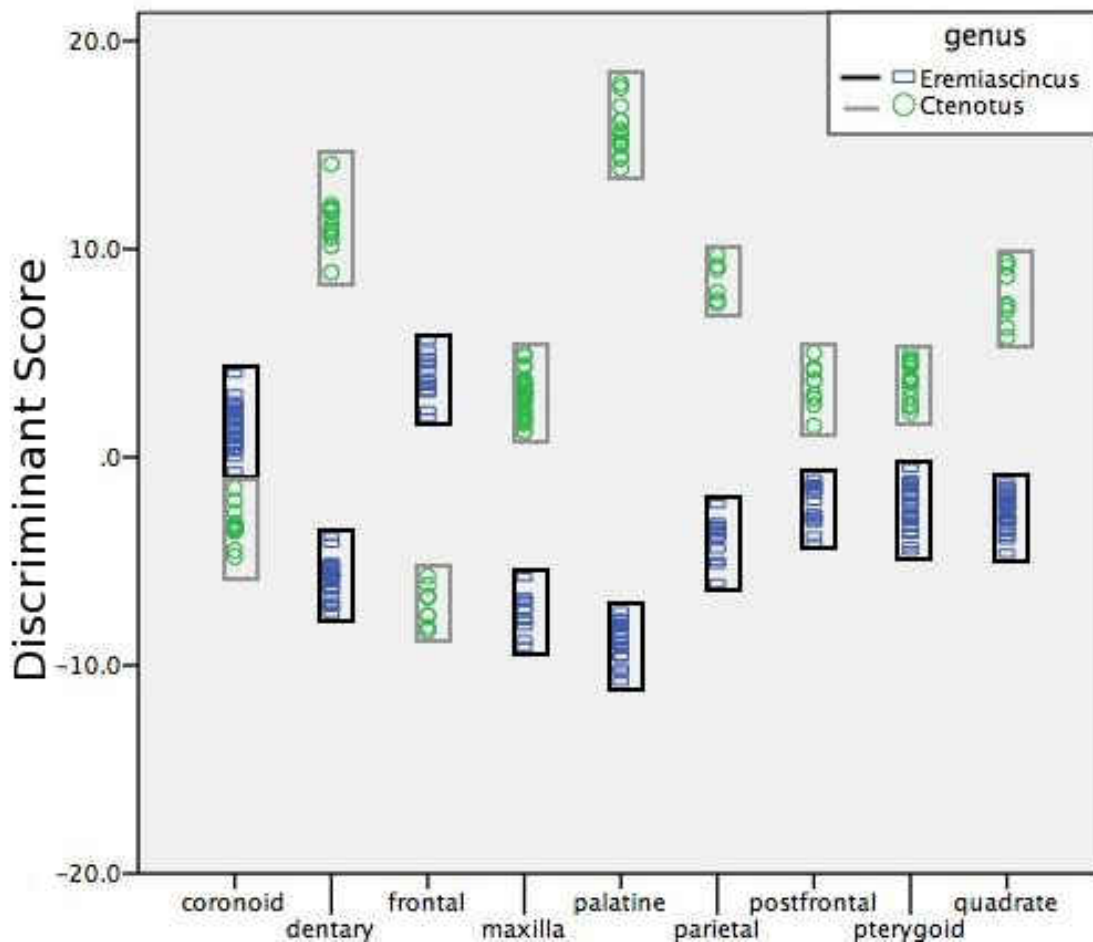


Figure 6.10. Discriminant scores of *Eremiascincus* and *Ctenotus* for each of the 9 elements examined.

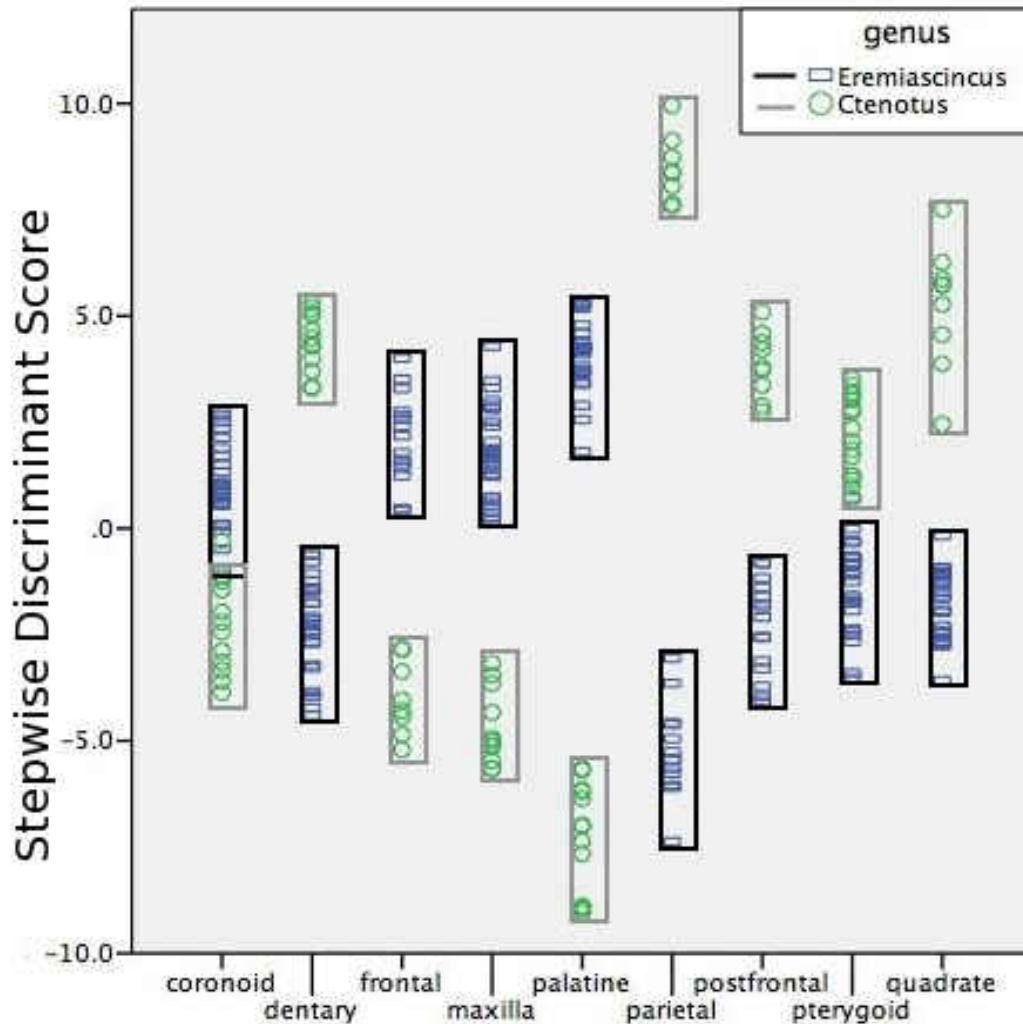


Figure 6.11. Stepwise discriminant scores of *Eremiascincus* and *Ctenotus* for each of the 9 elements examined.

Even though a PCA may be sufficient to discern *Eremiascincus* from *Ctenotus*, a discriminant function and stepwise discriminant function analyses were still carried out to determine which method was the most useful for differentiating the two genera. Utility of the discriminant function and stepwise discriminant function analyses to differentiate the two genera was further tested by cross-validation, using the leave-one-out method. In cross validation, the analysis is re-run repeatedly, each time excluding one of the specimens, which is treated as an unknown. Degree of success of each type of analysis is

given as the percent of each taxon that is correctly identified when treated as an unknown.

Plots of the discriminant scores for each of the taxa in the discriminant function and stepwise discriminant function analyses are given in Figures 6.10 and 6.11 respectively.

Following Williams (1999), the dataset is also tested for an ontogenetic affect on the ability to differentiate the taxa. Linear regression is used to correlate the scores resulting from whichever analysis is most successful at telling *Eremiascincus* from *Ctenotus*, with the length of the frontal, which is used as a proxy for total size. Regression coefficients and coefficients of determination are given for each element in each genus is given in Table 6.2.

Table 6.2. Regression coefficients (B) and coefficients of determination (R^2) for the stepwise discriminant scores correlated with the length of the frontal in mm.

	<i>Eremiascincus</i>		<i>Ctenotus</i>	
	B	R^2	B	R^2
Coronoid	0.039	0.002	-0.658	.412
Dentary	-0.049	0.002	0.297	.268
Frontal	-0.073	.008	-0.151	.046
Maxilla	-0.443	.29	-0.417	.319
Palatine	-0.113	.032	0.442	.188
Parietal	0.085	.01	0.236	.143
Postfrontal	0.119	.024	-0.451	.579
Pterygoid	0.051	.003	-0.044	.003
Quadrate	0.000	<0.001	0.036	<0.001

Results

When 9 types of elements were compared between *Eremiascincus* and *Ctenotus* using geometric morphometrics, principal component analysis was moderately successful at differentiating the 2 genera. Discriminant and stepwise discriminant function analyses

were effective at correctly identifying the genus to which each specimen belonged, when that specimen was treated as an unknown and removed from the dataset. In all cases, the stepwise method more accurately identified unknowns than the discriminant method.

Coronoid:

There were 10 landmarks placed on the coronoid. The first principal component explains 21% of the variance in the data and the second principal component explains an additional 14.9% of the variance. Not until the 11th principal component is a cumulative 95% of the data explained. Possibly as a consequence of explaining so little of the data, the first 2 principal components show large amounts of overlap between the 2 genera in the plot of the principal component scores (Figure 6.12).

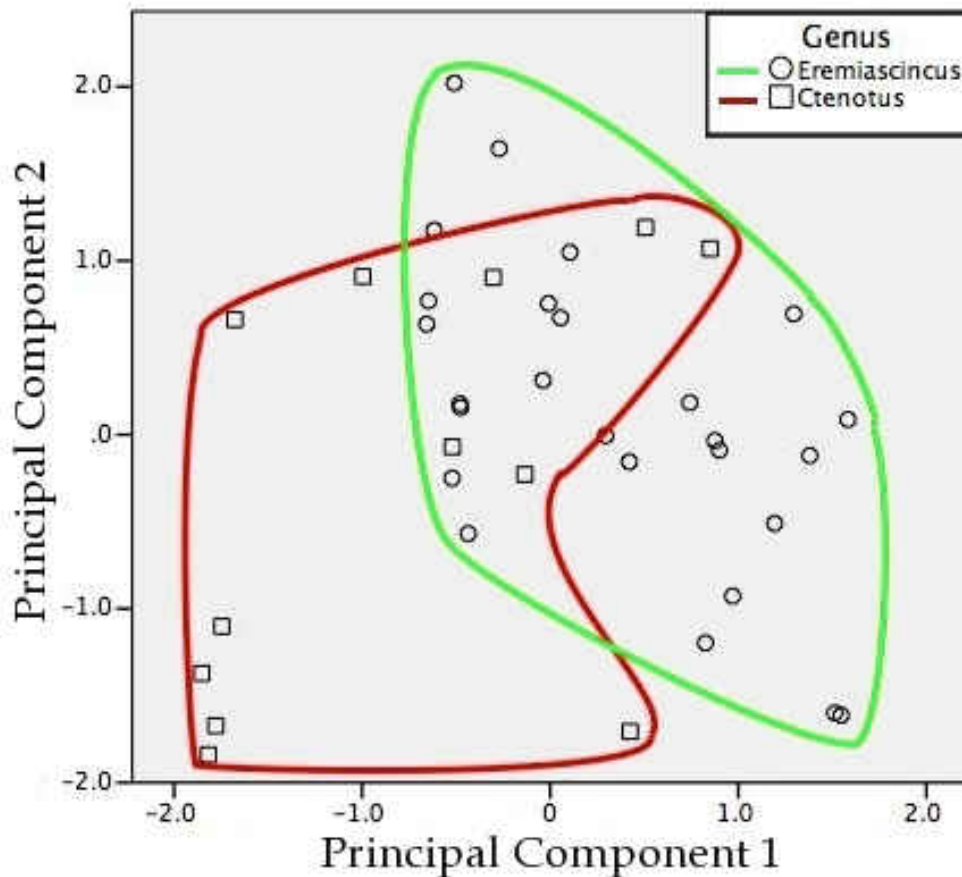


Figure 6.12. Plot of the first two principal components coronoid landmark data.

In the discriminant function analysis of 10 landmarks, cross validation correctly identified *Eremiascincus* correctly 84.6% of the time, and *Ctenotus* in 83.3% of cases. The stepwise discriminant function correctly identified *Eremiascincus* 92.3% of the time, and *Ctenotus* correctly 91.7% of the time. In the discriminant analysis, 3 variables (x11, x12, y12) fail the tolerance test. In the stepwise discriminant function, 4 variables were extracted for use. These variables were y4, y9, y10, and x8. Therefore, one can discern *Eremiascincus* from *Ctenotus* in the stepwise discriminant analysis because: the point of maximum curvature on the posterior of the coronoid process tends to be lower in *Ctenotus*; the ventral extent of the lateral process is more anteriorly placed in *Eremiascincus*; the junction between the descending lamina of the dentary process and the main body of the dentary process is lower in *Eremiascincus* than *Ctenotus*, and the vertex of the posterior process on the descending flange of the dentary process is also lower in *Eremiascincus* than it is in *Ctenotus*.

Dentary:

There were 16 landmarks placed on the dentary. The first principal component explains 22.7% of the variance in the data and the second principal component explains an additional 17.8% of the variance. Not until the 14th principal component is a cumulative 95% of the data explained. In spite of explaining so little of the data, the first 2 principal components still produce distinct groups for each genus in the plot of the principal canonical variables (Figure 6.13).

In an analysis of 16 landmarks, the discriminant function correctly identified *Eremiascincus* correctly 37.5% of the time, and *Ctenotus* in 41.7% of cases. Stepwise

discriminant function analysis correctly identified both *Eremiascincus* and *Ctenotus* 100% of the time. In the discriminant analysis, 16 of the 50 variables fail the tolerance test. In the stepwise discriminant function, 5 variables are extracted for use. These variables were x3, y4, x5, y6, and x14. From this, one finds that *Ctenotus* and *Eremiascincus* are differentiated because: *Ctenotus* has a posterior facet that is placed more posteriorly than in *Eremiascincus*; the coronoid process extends higher in *Eremiascincus*; in *Ctenotus* the posterior edge of the tooth row is more posterior on the jaw than in *Eremiascincus*; *Eremiascincus* has a higher coronoid process; *Eremiascincus* has a higher midpoint of the tooth row, indicating that it is less curved than in *Ctenotus*; and *Ctenotus* tend to have the top of their intramandibular septum is more anteriorly placed than in *Eremiascincus*.

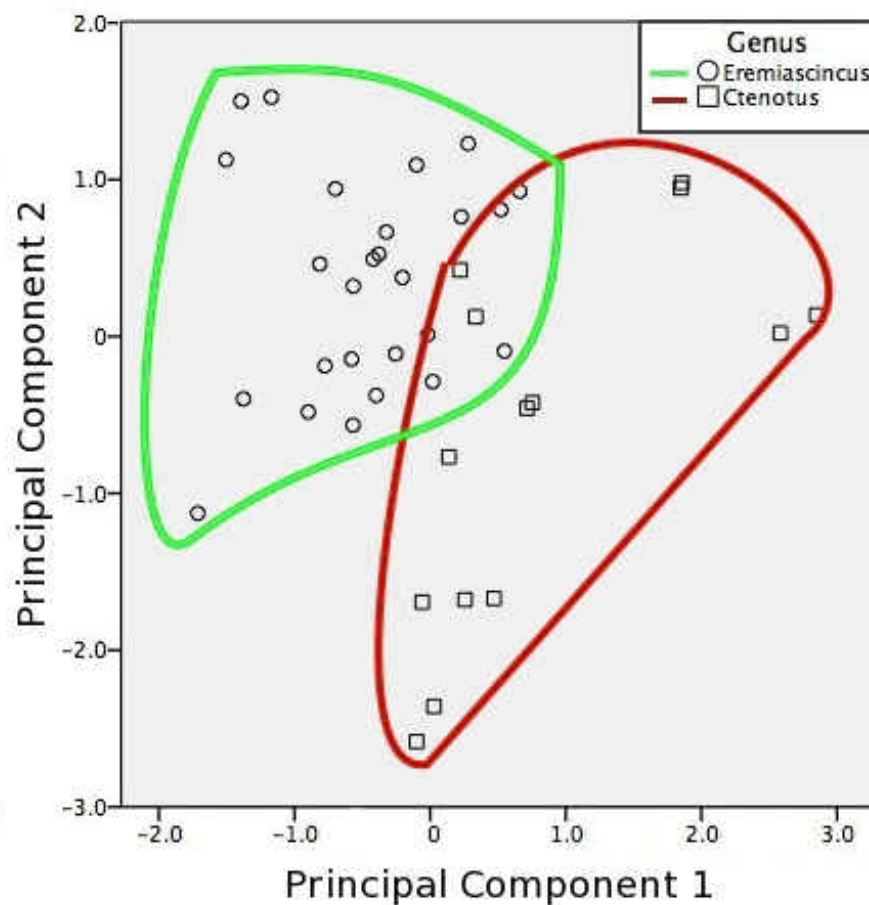


Figure 6.13. Plot of the first two principal components for dentary landmark data.

Frontal:

Principal components 1 and 2 cumulatively accounted for only 48.2% of the total variance. It takes the first 8 principal components together to break the 95% threshold. In spite of the low amount of variance explained by the first 2 principal components, they do separate the 2 genera moderately well (Figure 6.14).

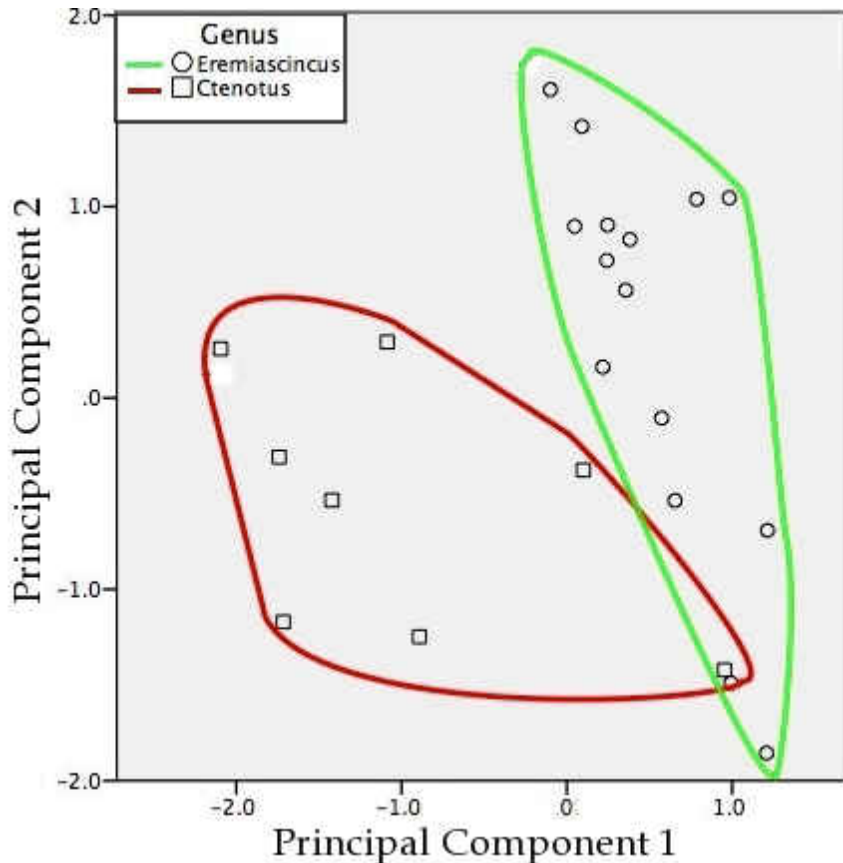


Figure 6.14. Plot of the first two principal components of frontal landmark data.

In an analysis of 9 landmarks, the discriminant function correctly identified *Eremiascincus* correctly 93% of the time, and *Ctenotus* in 66.7% of cases. Stepwise discriminant function correctly identified *Eremiascincus* and *Ctenotus* 100% of the time. In the discriminant function analysis, 3 of the landmarks failed the test of significance (x8, y8, y9). Of the original 18 variables, the stepwise discriminant function extracted 3 for use in

the analysis. These were x5, x6, and x9. Therefore, *Eremiascincus* can be discerned from *Ctenotus* because: *Eremiascincus* has more medially inflected cristae cranii; *Eremiascincus* is narrower than *Ctenotus* anterior of the orbital constriction; and *Eremiascincus* has a longer medial nasal process.

Maxilla:

The first 2 principal components describe 43% of the variance in the data and the 95% threshold is not achieved until the 12th principal component. A plot of the first to principal components completely separates the landmarks of *Ctenotus* and *Eremiascincus* (Figure 6.15). However, they are not separated strictly by one of the axes or the other, suggesting that there is still some correlation between the two variables.

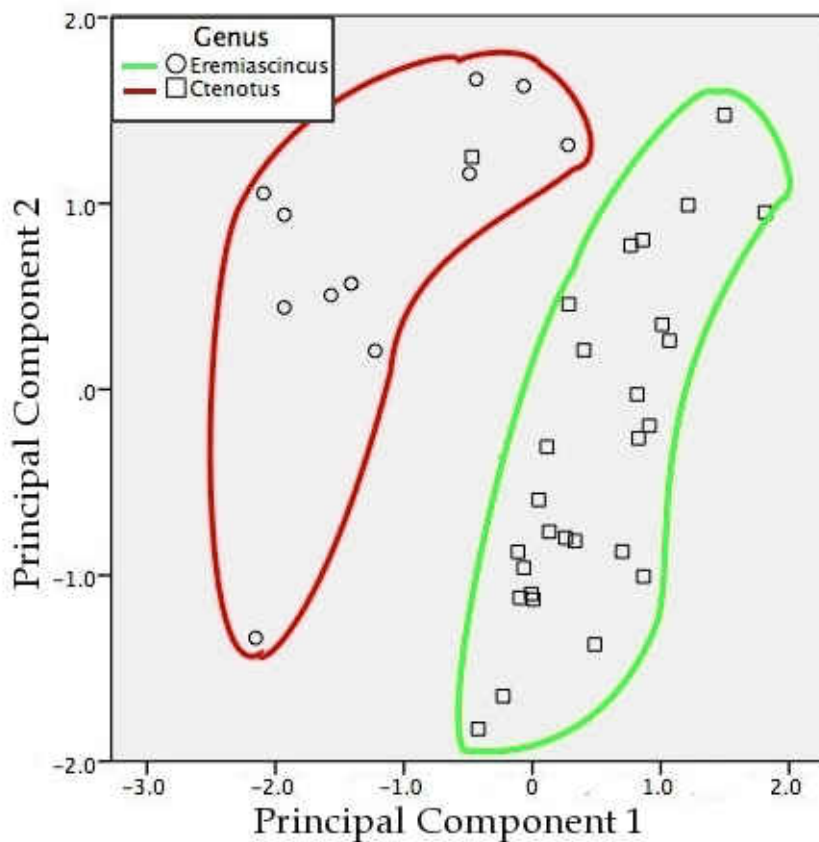


Figure 6.15. Plot of the first two principal components of maxilla landmark data.

In an analysis of 12 landmarks, the discriminant function correctly identified *Eremiascincus* correctly 100% of the time, and *Ctenotus* in 90.9% of cases. Stepwise discriminant function analysis correctly identified *Eremiascincus* and *Ctenotus* 100% of the time. In the discriminant function, 4 of the 24 variables (x11, y11, x12, y12) failed the tolerance test. Stepwise discriminant analysis extracted 4 variables. These variables were x3, y2, x4, and y4. Since landmark 4 relates to the placement of the posterior extent of the tooth, and all of the images of the maxilla were rotated prior to analysis so that the anterior and posterior ends of the tooth row would be horizontal relative to one another, the vertical displacement of the posterior of the tooth row must be an artifact of the application of procrustes fit to the dataset. Although it is an artifact, the vertical variation of the posterior of the tooth row will be treated as a viable here for the sake of consistency of method. Therefore, one can discern *Eremiascincus* from *Ctenotus* because: *Eremiascincus* has a longer inferior posterior process; the notch between the inferior and superior posterior processes is higher in *Eremiascincus*; the tooth row extends further posteriorly on the maxilla in *Ctenotus* than *Eremiascincus*; and the posterior end of the tooth row is lower in *Ctenotus* than *Eremiascincus*.

Palatine:

Principal component 1 explains 25.1% of the variance in the data and the second principal component explains an additional 11.6% of the variance. Not until the 16th principal component is a cumulative 95% of the data explained. In spite of explaining so little of the data, the first principal component still produces distinct groups for each genus in the plot of the canonical variables (Figure 6.16). The second principal component does not appear to contribute to the separation of the data of *Ctenotus* and *Eremiascincus*.

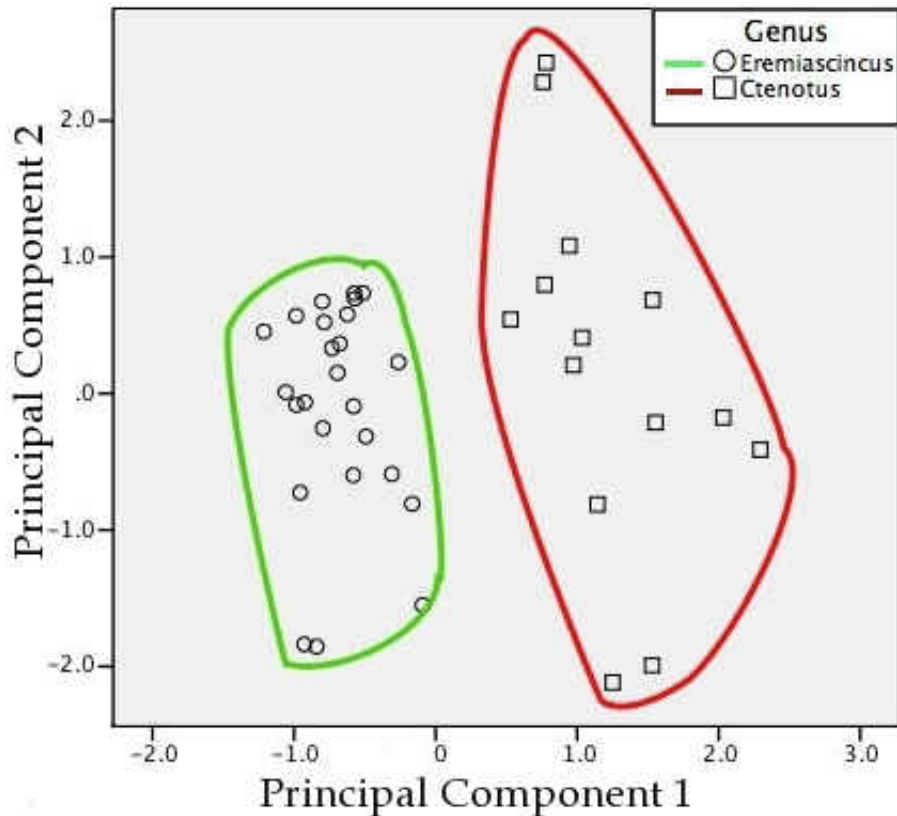


Figure 6.16. Plot of the first two principal components of palatine landmark data.

In the analysis of 17 landmarks, the discriminant function correctly identified *Eremiascincus* correctly 96% of the time, and *Ctenotus* in 85.7% of cases. Stepwise discriminant function analysis correctly identified *Eremiascincus* and *Ctenotus* 100% of the time. In the discriminant analysis, 3 variables (x15, x17, y17) fail the tolerance test. In the stepwise discriminant function, 8 variables were extracted for use. These variables were x8, x14, y10, y11, y13, y15, y16, and y17. Although y17 failed the tolerance test in the regular discriminant function analysis, it was included in the stepwise, indicating that its significance to the dataset increases dramatically as other landmarks are stripped away. From the stepwise discriminant analysis, one can discern the palatine of *Eremiascincus* from that of *Ctenotus* because: *Eremiascincus* has a shorter antero-lateral process on the

ventral lamina; the postero-medial process of the ventral lamina extends further posteriorly on *Eremiascincus* than *Ctenotus*; the lateral margin of the antero-medial process of the dorsal lamina extends further laterally in *Eremiascincus*; the vertex of the antero-medial process of the dorsal lamina is also more laterally placed in *Eremiascincus*; the posterior corner of the portion of the dorsal lamina that approaches the midline, approaches the midline more closely in *Ctenotus*; the secondary postero-medial process is more medially placed in *Eremiascincus*; the medial margin of the postero-lateral process on the dorsal lamina is more medially placed in *Eremiascincus*, and the foramen in the dorsal lamina is somewhat more medially placed in *Eremiascincus*.

Parietal:

Principal component 1 accounts for 50.2% of the variance in the data and the second accounts for an additional 13.7%. Not until the tenth principal component is the 95% threshold achieved. Although *Eremiascincus* and *Ctenotus* are well separated for the most part by the first principal component (Figure 6.17), there are two specimens that fall distinctly in the grouping of the other genus. These 2 specimens are WAMR 146910 and Jim 37-1.

In the analysis of 20 landmarks, the discriminant function correctly identified *Eremiascincus* correctly 53.8% of the time, and *Ctenotus* in 75% of cases. Stepwise discriminant function analysis correctly identified *Eremiascincus* and *Ctenotus* 100% of the time. In the discriminant function analysis, of the 40 original variables, 23 failed the tolerance test and were excluded. Also, of the original 40 variables, 5 were extracted and used by the stepwise discriminant analysis. These variables were y3, x5, y2, x8, and y8. From these, one can discern *Eremiascincus* from *Ctenotus* because: the apex of the notch

between the posterior process and the surpatemporal process is more posteriorly placed in *Eremiascincus*; the tip of the supratemporal is more laterally placed in *Eremiascincus*; the tip of the posterior process extends further posteriorly in *Eremiascincus*; and the point where the supratemporal process and the parietal table meet on the lateral margin of the bone is placed more antero-medially in *Eremiascincus*.

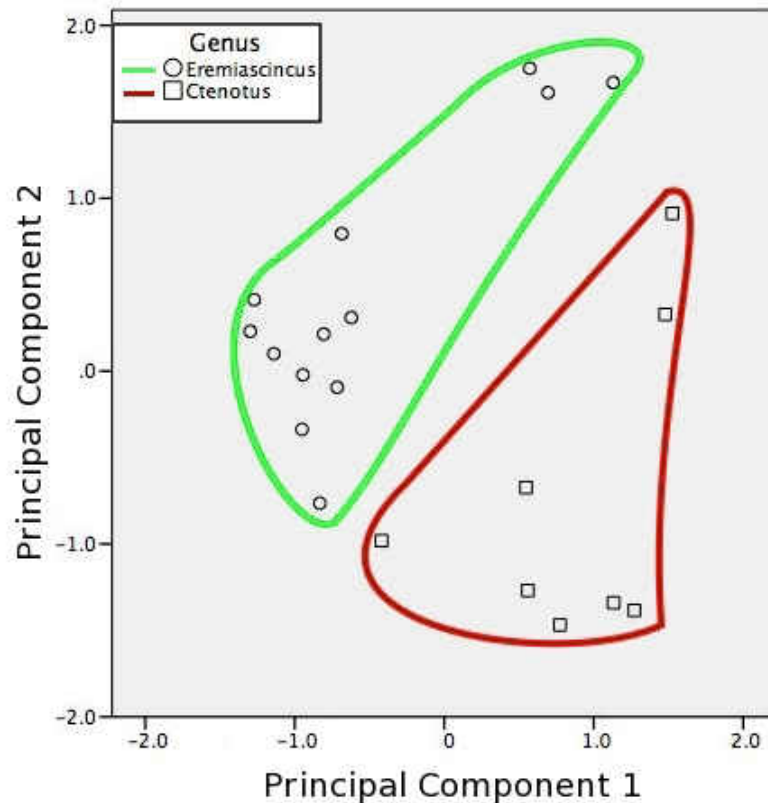


Figure 6.17. Plot of the first two principal components of parietal landmark data.

Postfrontal:

Principal component 1 explains 27.4% of the variance in the data and the second principal component explains an additional 23.6% of the variance. Not until the 8th principal component is a cumulative 95% of the data explained. Possibly as a consequence of explaining so little of the data, the first 2 principal components show large amounts of overlap between the 2 genera in the plot of the canonical variables (Figure 6.18).

In the analysis of 8 landmarks, the discriminant function correctly identified *Eremiascincus* correctly 80% of the time, and *Ctenotus* in 77.8% of cases. The stepwise discriminant function correctly identified *Eremiascincus* 86.7% of the time, and *Ctenotus* correctly 100% of the time. In the discriminant analysis, 3 variables (y7, x8, y8) fail the tolerance test. In the stepwise discriminant function, 3 variables were extracted for use. These variables were y3, x5, and y5. Therefore, one can differentiate the postfrontal of *Eremiascincus* from *Ctenotus* because: the lateral inflection on the lateral margin of the postfrontal is located more anteriorly in *Eremiascincus*; and the posteromedial corner of the postfrontal, which forms the anterior margin of the supratemporal fenestra, is located more antero-medially in *Eremiascincus* than in *Ctenotus*.

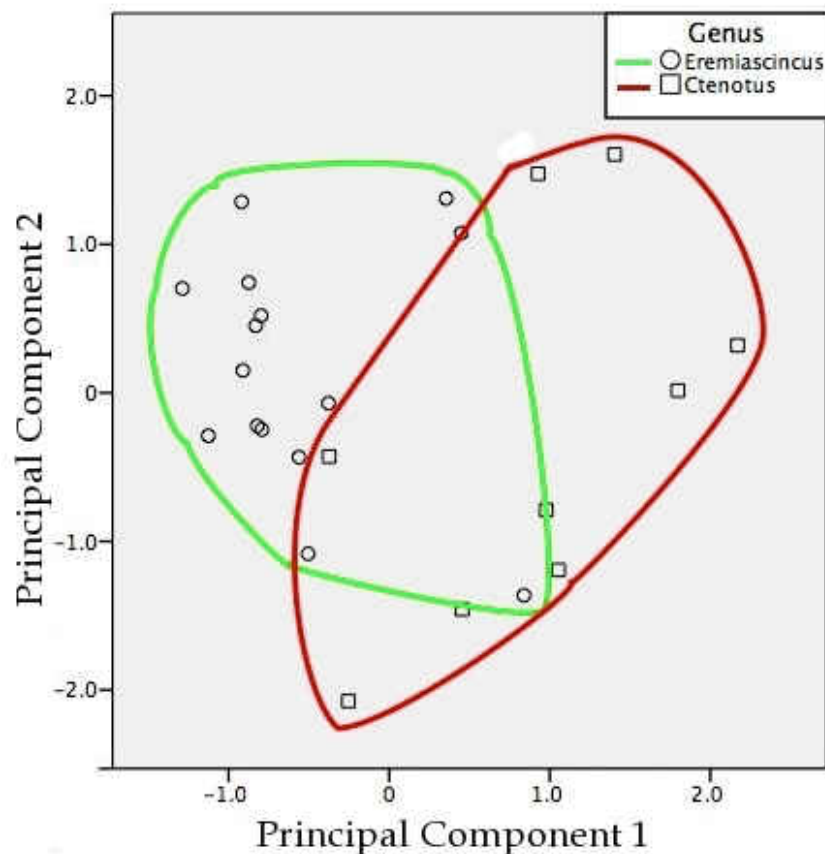


Figure 6.18: Plot of the first two principal components of postfrontal landmark data.

Pterygoid:

Principal component 1 explains 37.5% of the variance in the data and the second principal component explains an additional 16.8% of the variance. Not until the 11th principal component is a cumulative 95% of the data explained. Possibly as a consequence of explaining so little of the data, the first 2 principal components show large amounts of overlap between the 2 genera in the plot of the canonical variables (Figure 6.19).

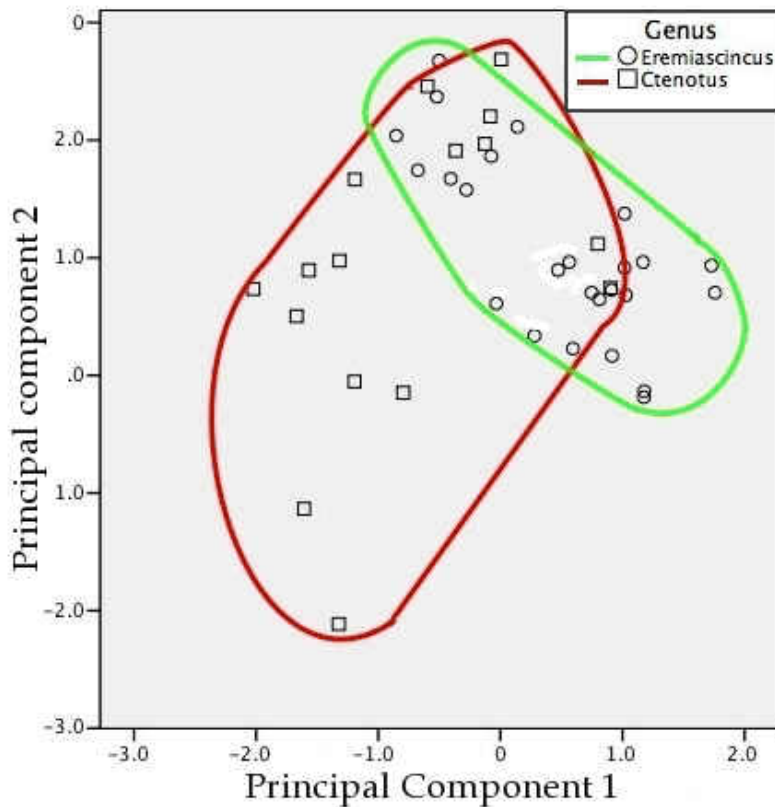


Figure 6.19. Plot of the first two principal components of pterygoid landmark data.

In the analysis of 12 landmarks, the discriminant function correctly identified *Eremiascincus* correctly 92% of the time, and *Ctenotus* in 93.8% of cases. The stepwise discriminant function correctly identified *Eremiascincus* 96% of the time, and *Ctenotus* correctly 100% of the time. In the discriminant analysis, 3 variables (x11, x12, y12) fail the tolerance test. In the stepwise discriminant function, 3 variables were extracted for use.

These variables were y_3 , y_4 , and y_9 . Therefore, *Eremiascincus* can be discerned from *Ctenotus* because the fossa columellae of *Eremiascincus* is medially displaced on the pterygoid relative to that in *Ctenotus*.

Quadrate:

The first principal component explains 27.2% of the variance in the data and the second principal component explains an additional 23.6% of the variance. Not until the 11th principal component is a cumulative 95% of the data explained. A plot of the first 2 canonical variables shows excellent separation of the 2 genera in to distinct data clusters, though not separated by the origin (Figure 6.20).

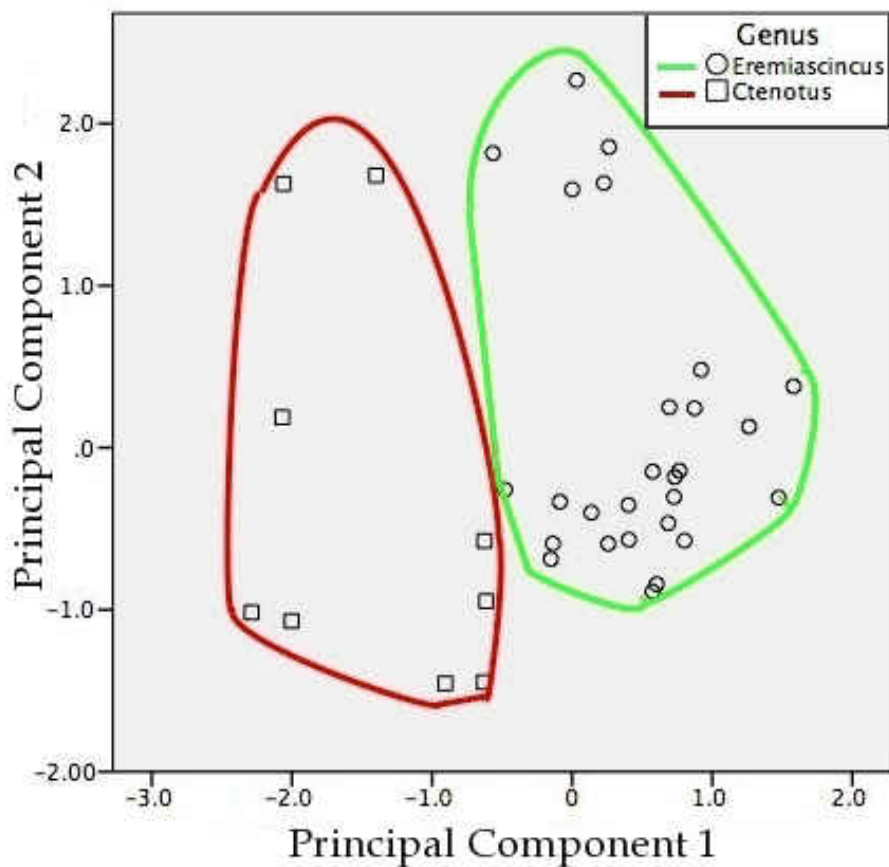


Figure 6.20. Plot of the first two principal components of quadrate landmark data. It shows separation of the two genera, primarily in the first principal component, but not across the origin.

In the analysis of 14 landmarks, the discriminant function correctly identified *Eremiascincus* correctly 88.9% of the time, and *Ctenotus* in 77.8% of cases. The stepwise discriminant function correctly identified *Eremiascincus* and *Ctenotus* correctly all the time. In the discriminant analysis, 3 variables (y13, x14, y14) fail the tolerance test. In the stepwise discriminant function, 6 variables were extracted for use. These variables were x2, x4, x6, x13, y5, and y11. Therefore, one can differentiate *Eremiascincus* from *Ctenotus* using the stepwise-discriminant function, because: the cephalic condyle in *Eremiascincus* is medio-laterally wider for its height; the tympanic crest extends somewhat more laterally in *Ctenotus*; the dorsal extent of the pterygoid lamina is placed more laterally in *Ctenotus*; the medial inflection of the tympanic crest is lower on the quadrate on *Eremiascincus*; and the medial lobe of the mandibular condyle is more dorsally placed in *Eremiascincus* than in *Ctenotus*.

Ontogeny:

Unlike the findings of Williams (1999) for species of *Egernia*, the shape differences between *Eremiascincus* and *Ctenotus* are fully expressed in the youngest individuals, and do not increase appreciably through ontogeny. Although there is a positive correlation between the length of the frontal and discriminant scores greater than 0, and a negative correlation with scores less than 0, the low R^2 values indicate that the total variance in discriminant scores, explained by that correlation, is negligible in most cases. Chapter 3 demonstrated that there are ontogenetic changes in the proportions of the skull of *Eremiascincus*, but the lack of correlation shows that these ontogenetic changes are not responsible for the differences that differentiate the individual elements of the skull from their counterparts in *Ctenotus*.

Discussion

What is most immediately apparent from the results is that given a specimen with an unknown identity, once it has been narrowed down to either *Ctenotus* or *Eremiascincus*, morphometrics can be used to decide which it is. Furthermore, of the statistical methods used on this dataset, the stepwise discriminant function was by far the most useful. Only 4 of the 9 elements showed complete separation in the PCA, and of those, 2 were separated by a combination of the first two principal components, suggesting some residual correlation between them. An additional 3 elements showed moderate, but incomplete separation. Discriminant function analysis was consistently an improvement over the use of principal components, but not a substantial one. Of all of the elements examined, when using the discriminant function, only the maxillae of *Eremiascincus* were correctly identified during cross validation. The stepwise discriminant function however was a tremendous improvement in all cases. When using the stepwise discriminant function, 6 of the 9 elements examined were correctly identified as *Eremiascincus* or *Ctenotus* in 100% of cases. Of the remaining 3 elements, specimens of *Ctenotus* were always correctly identified in 2 of them. In all other cases, where there was not 100% correct identification during cross validation, at least 85% of cases were correctly identified.

Morphometric comparisons however require having a sufficiently large dataset and is very time consuming in terms of taking the photos, placing the landmarks and performing the statistical analyses. It is of interest therefore to use the results of morphometric analyses to generate qualitative characters that can be identified with the naked eye. Many of the qualitative characters used in the previous analysis are already shape related. For example, stating that a process is long is equivalent to saying that the

point defining its vertex is placed further along one or both axes relative to the points at the base of the process, compared to a shorter process in which the vertex is not so far removed. Furthermore, the stepwise discriminant function isolated those landmarks that are necessary and sufficient to discern *Eremiascincus* from *Ctenotus*, which is the same as the goal of the Bayesian analysis of the qualitative characters. Therefore, one would expect at least some degree of correspondence between the most useful qualitative and morphometrics results. Obviously though, there cannot be perfect correspondence because many of the qualitative characters differentiate presence and absence features, which cannot be differentiated by this type of morphometrics analysis.

One of the central assumptions of the analysis of the qualitative characters is addressed by the correspondence between qualitative and morphometric characters. Missing data in the previous analysis was filled in using cladistic bracketing based on parsimony analysis. Given that one of the assumptions of a parsimony analysis is that each character evolves independently, it is important not to base multiple characters on the same shape change. Therefore, it would be superfluous to add characters based on the results of morphometrics if those changes are homologous with an existing qualitative character. Furthermore, if one of the characters produced by morphometric analyses is homologous with multiple qualitative characters, then the later should be replaced by the former in future work. Furthermore, although traditional morphometrics of the entire skull showed to have only a miniscule phylogenetic signature, the ability of geometric morphometrics to test phylogeny has not yet been assessed and it is possible that characters derived from geometric morphometrics could be used in a phylogenetic context, whether as raw data or as qualitative characters derived from morphometric analyses. In

such a case, if one were going to combine data sets or choose to treat them as separate modes of inference, it would be especially important not to violate the assumption of the independence of characters.

In both the qualitative and quantitative analyses of the coronoid, the placement of the lateral process was identified as a character. The moderately to strongly developed lateral process of *Ctenotus* is reflected by the posterior placement of the anterior end of the process in the morphometric analysis. As the process becomes more strongly developed, it grows posterolaterally, increasing the angle of insertion of the muscularis adductor mandibuli externus. Of these characters, only a deep dentary process was sufficient to discern members of *Ctenotus*.

On the dentary, the first 5 qualitative characters relate to the posterior end of the element, as do the first 3 landmarks extracted by the stepwise discriminant analysis. The angle measured on the notch between the coronoid and angular processes of the dentary was divided into 3 discrete states based on whether it was greater than, equal to, or less than 90 degrees. The angle was however insufficient to discriminate *Eremiascincus* from *Ctenotus*. Since landmarks were placed at the tips of the angular and coronoid processes, as well as at the apex of the notch between them, a significant difference in the angle could have been inferred from a particular movement of the landmarks with respect to one another. However, the posterior placement of the apex of the notch between the processes in *Ctenotus* is coupled with a ventral position of the tip of the coronoid process, which produces no consistent difference from the angle in *Eremiascincus*, which has an anteriorly placed apex of the notch and a dorsally extended coronoid process.

A more posterior placement of the back of the dentary tooth row, combined with the more ventrally placed tip of the coronoid process, means that *Ctenotus* has an altogether shorter coronoid process than *Eremiascincus*, a character state that could be added to future cladistic analyses. The posterior position of the back of the tooth row also relates to the number of teeth in the dentary. *Ctenotus* has the longer tooth row, with from 16 to 26 dentary tooth positions, with no particular range occurring more frequently than the others in the small sample size. Tooth counts in the dentary of *Eremiascincus* largely overlaps those of *Ctenotus*, having from 15 to 24 tooth positions. Using the relative length of the tooth row as a character could supplant the less useful tooth count for differentiating *Eremiascincus* from *Ctenotus*.

Placement of the intramandibular septum and curvature of the dentary tooth row would each also make a decent candidate for a qualitative character. However, both are difficult to judge with the naked eye, and the placement of the top of the intramandibular septum would require a frame of reference, such as the tooth position that it occurs under. The tooth position that the intramandibular septum falls under would itself also be dependent on other factors, so it seems that, at least for now, the two characters are best excluded from qualitative analyses.

For the frontal, all 3 of the variables extracted by the stepwise discriminant function correspond directly with qualitative characters used in the Bayesian analysis. Qualitative characters relating to the width of the frontal, anterior to the orbital constriction, and inflection of the cristae cranii were already defined numerically, but neither was deemed sufficient to differentiate *Eremiascincus* from *Ctenotus*. Length of the medial anterior process was however deemed necessary but not sufficient to differentiate *Eremiascincus*

and *Ctenotus*. Thus, in both the qualitative and quantitative analyses, the combination of characters is required to perfectly differentiate the two genera.

With regard to the maxilla, only 1 of the 4 extracted landmark variables, the position of the tip of the inferior posterior process, is directly homologous with 1 of the existing qualitative characters. By itself, the difference in height of the point at the vertex of the notch between the inferior and superior processes would suggest a difference in the thicknesses of both processes. However, that the position of the posterior of the tooth row moves dorsally when the vertex of the notch moves up indicates that only the thickness of the superior posterior process is changing. Therefore, future qualitative analyses could include a character homologous to this change. The position of the posterior end of the tooth row is related to the number of teeth in the row, but not directly homologous. Furthermore, although there is typically a difference in the number of teeth in adults of *Eremiascincus* from adults of *Ctenotus*, the change in number through ontogeny obscures the difference in the qualitative analysis. In *Eremiascincus*, there are from 16 to 21 tooth positions, with 19 and 20 as the most common counts. In *Ctenotus* examined, the range is wider, from 14 to 24 maxillary tooth positions, with 21 and 23 as the most frequent counts. Having a more posteriorly placed end of the tooth row accounts for differences in the number of teeth between *Eremiascincus* and *Ctenotus* at each size. Furthermore, it shows that the tooth row must be expanded to hold more teeth, rather than making each tooth smaller.

In the case of the palatine, there is no longer the all-or-nothing homology between landmarks extracted by the stepwise analysis and qualitative characters used in the Bayesian analysis. Only the position of the tip of the anterolateral process of the ventral

lamina is directly homologous between the two analyses. Location of the tip of the posteromedial process of the ventral lamina relates to whether that process is longer or the same length as the posteromedial process of the dorsal lamina. Furthermore, antero-posterior placement of the tip of the medial vomerine process on the dorsal lamina determines the relative length of that process to the anteromedial and anterolateral processes on the ventral lamina. Lengths of both the anteromedial and posteromedial processes relate to the total length to width ratio, and the proportion of the total length that the dorsal lamina meet along the midline.

Overlap by the dorsal lamina relative to the ventral lamina of the palatine, is also determined by the position of the posterior corner of the meeting of the dorsal lamina along the midline. It was expected that if this landmark was extracted, then it would vary along the anteroposterior direction, thereby changing the amount of overlap. However, the landmark instead varied mediolaterally, which indicates that either the dorsal lamina possibly is not contacting the midline at that corner in *Eremiascincus* or the mediolateral variation in the placement of that landmark is an artifact of procrustes rotation. That the qualitative characters relate to multiple significant landmark variables and each landmark can relate to multiple qualitative characters, indicates that the assumption of independence was violated by the characters chosen for the palatine. Therefore, in future analyses, it would be advisable to replace or supplement the non-independent variables with ones derived from the morphometric data set. Given that the Bayesian analysis found that many of the qualitative palatine characters were useful for differentiating *Eremiascincus* from *Ctenotus*, and given that the character states can be easily discerned visually, the qualitative characters should not automatically be discarded.

In the case of the parietal however, the Bayesian analysis only found 1 character to be sufficient to differentiate *Eremiascincus* from *Ctenotus*, and it is unrelated to any of the landmarks extracted by the stepwise discriminant analysis. Furthermore, only 1 of the landmarks extracted by the stepwise discriminant analysis, at the apex of the notch between the posterior and supratemporal processes, relates directly to one of the qualitative characters, which compares the depth of that notch to the depth of the notch between the posterior processes. In *Eremiascincus*, in which the apex of the notch between the posterior and supratemporal processes is posteriorly placed, the tip and the lateral edge of the base of the supratemporal process are posteriorly and anteromedially placed respectively, meaning that *Eremiascincus* has a longer and broader process than *Ctenotus*. By adding this one more character state, the number of characters sufficient to differentiate *Eremiascincus* from *Ctenotus* is effectively doubled.

The postfrontal and the pterygoid are the extreme examples of lacking correspondence between the morphometric and qualitative results. None of the 3 landmark variables extracted for each bone had a direct homology with qualitative characters used. Results of morphometric comparison do however suggest the addition of 3 new characters with states that could be identified with the naked eye: placement of the lateral inflection of the lateral margin, and length of the broad portion of the posterior process of the postfrontal, and the medial or central placement of the fossa columnellae. The first of the 3 likely relates to the anterior extent of the postorbital in the articulated skull, and the second to the size of the supratemporal fenestra. Unfortunately, at the time of writing, no articulated *Ctenotus* skulls were available for comparison to verify these 2 suppositions. Lastly, the third character would require a frame of reference to assess it,

such as a line drawn between the tips of the palatine and quadrate processes of the pterygoid.

Finally, the quadrate also shows a low degree of correspondence between morphometric and qualitative characters. Only 1 of the 6 landmark variables extracted, the ventral extent of the medial lobe of the mandibular condyle, has direct homology with a qualitative character. Although it was expected that an important distinction would occur at the point where the dorsal extent of the pterygoid lamina meets the central column of the quadrate, it was expected to show a difference on the dorsoventral axis, not the mediolateral axis as was extracted. However, this is also not completely unexpected. As the pterygoid lamina expands dorsally along the central column, the column thickens and moves medially, forcing the point where the pterygoid lamina meets it to also move laterally. It is possible that the more lateral placement of the lateral edge of the cephalic condyle may relate to the degree of closure of the apical foramen, but without further examination, they will be regarded as independent for now.

Over all, there is a moderate degree of homology between existing qualitative characters and the results of the morphometric comparisons. Consequentially, a number of characters may be added to a qualitative analysis, and still others will replace existing characters, particularly on the palatine. Until success has been shown when more taxa are added to the analysis, qualitative characters will still need to be used to taxonomically constrain the hypothesis of identity for fossil specimens. When a specimen of uncertain identity has been restricted to either *Ctenotus* or *Eremiascincus*, morphometric data can be used by itself, or as qualitative characteristics that incorporate the results of morphometric analyses, to correctly identify the specimen in nearly all cases. Successive datasets and

techniques will be successful if they require less a priori knowledge the group to which a specimen belongs.

Literature Cited

- Bookstein, F.L. (1991). *Morphometric tools for landmark data: geometry and biology*.
Cambridge, UK: Cambridge University press.
- Conrad, J. (2004). Skull, mandible and hyoid of *Shinisaurus crocodilurus* Ahl (Squamata, Anguimorpha). *Zoological Journal of the Linnean Society* **141**: 399-434.
- Evans, S.E. (2008). The skull of lizards and Tuatara (pp. 1-347). In: Gans, C., Gaunt, A.S., Adler, K. (eds) *Biology of the Reptilia Vol. 20, Morphology H*. Society for the Study of Amphibians and Reptiles. Ithica, NY, U.S.A.
- Free Software Foundation. 2010. GNU Image Manipulation Program: GIMP.
[Www.gimp.org](http://www.gimp.org)
- Gelnaw, W.B. (2011). Systematics and skink skull shape: assessing a phylogenetic signal from morphometric data. In: *On the Skull of Eremiascincus*. M.Sc. Thesis. East Tennessee State University.
- Hocknull, S.A. (2002). Comparative maxillary and dentary morphology of the Australian dragons (Agamidae: Squamata): a framework for fossil identification. *Memoirs of the Queensland Museum* **48(1)**: 125-145.
- Marcus, L.F. (1988). Traditional Morphometrics (pp 77-122). In: Rolf, F.J. and Bookstein, F.L (eds) *Proceedings of the Michigan Morphometrics Workshop*. University of Michigan Museum of Zoology.

- McBrayer, L.D., 2004. The relationship between skull morphology, biting performance and foraging mode in Kalahari lacertid lizards. *Zoological Journal of the Linnean Society* 140: 403-416
- McBrayer, L.D. and Corbin, C.E. (2007). Patterns of head shape variation in lizards: morphological correlates of foraging mode. In Reilly, S.M, McBrayer, L.D. and Miles, D.B. *Lizard Ecology: The Evolutionary Consequences of Foraging Mode*. Cambridge University Press.
- MacLeod, N. (2002). Phylogenetic signals in morphometric data (pp 100-138). In: MacLeod N, Forey, P.L. (eds) *Morphology, Shape and Phylogeny*. Taylor and Francis, London.
- PASW, Inc. 2008. SPSS 17.0
- Rohlf, F.J. and Slice, D. (1990). Extensions of the Procrustes method for the optimal superimposition of landmarks. *Systematic Zoology* 39: 40-59.
- Rohlf, F.J. (2010). TPSDig, TPSUtil, and TPSSuper. <http://life.bio.sunysb.edu/morph>. 02/10/2010.
- Strayton, C.T. (2005). Morphological evolution of the lizard skull: A geometric morphometrics survey. *Journal of Morphology* 263: 47-59.
- Syncroscopy (2008). Automontage. Advanced Imaging Concepts, Inc.
- Weigelt, J. (1927). *Recent Vertebrate Carcasses and their Paleobiological Implications*. Translated by J. Schaefer. University of Chicago Press, Chicago.
- Williams, C. (1999). Fossil lizard identification methods: a case study of three *Egernia* species. Thesis for Bachelor of Science Degree with Honors. Zoology Department, Adelaide University, Adelaide, South Australia.

Zeldritch, M.L., Swiderski, D.L., Sheets, H.D., and Fink, W.L. 2004. Geometric morphometrics for biologists: a primer. Elsevier Academic Press, San Diego.

REFERENCES

- Andrews RM, Pough FH, Collazo, A, de Queiroz A. 1987. The ecological cost of morphological specialization: feeding by a fossorial lizard. *Oecologia*. 73: 139-145.
- Barahona F, Barbillo LJ. 1998. Inter- and intraspecific variation in the post-natal skull of some lacertid lizards. *Journal of Zoology London*. 245: 393-405.
- Baverstock PB, Donnellan SC. 1990. Molecular evolution in Australian dragons and skinks: a progress report. *Memoirs of the Queensland Museum*. 29: 323-331
- Beck DD. 2008. Southern Alligator Lizard. (pp. 484-487). In: Jones, L.L.C., and Lovich, R.E. (eds) *Lizards of the American South West*. Rio Nuevo Publishers, Tucson, Arizona.
- Bookstein FL. 1991. *Morphometric tools for landmark data: geometry and biology*. Cambridge, UK: Cambridge University press.
- Boulenger GA. 1887. *Catalogue of lizards in the British Museum (Natural History)*. Vol. 3, 2nd edition. Tailor and Francis, London.
- Brandley MC, Schmitz A, Reeder TW. 2005. Partitioned Bayesian analysis, partition choice, and phylogenetic relationships of scincid lizards. *Systematic Biology*. 54(3): 373-390.
- Brandley M.C., Huelsenbeck, J.P., Wiens J.J. 2008. Rates and patterns in the evolution of snake-like body form in squamate reptiles: evidence for repeated re-evolution of lost digits and long-term persistence of intermediate body forms. *Evolution*. 62(8): 2042-2064.
- Camp C. 1928. Classification of the lizards. *Bulletin of the American Museum of Natural History* 48: 289-481.

- Carranza S., Arnold E.N., Geniez P.H., Roca J., Mateo J.A. 2008. Radiation, multiple dispersal and parallelism in the skinks *Chalcides* and *Sphenops* (Squamata: Scincidae), with comments on *Scincus* and *Scincopus* and the age of the Sahara desert. *Molecular Phylogenetics and Evolution*. 46: 1071-1094.
- Cogger H.G. 1992. *Reptiles and Amphibians of Australia*. Cornell University Press, Ithica.
- Conrad J. 2004. Skull, mandible and hyoid of *Shinisaurus crocodilurus* Ahl (Squamata, Anguimorpha). *Zoological Journal of the Linnean Society*. 141: 399-434.
- Conrad J.L. 2008. Phylogeny and systematics of Squamata (Reptilia) based on morphology. *Bulletin of the American Museum of Natural History*. 310: 1-182.
- Diesmos A.C. 2007. Conservation of Herpetofaunal Communities in Fragmented Lowland Rainforests in the Phillippines. Final Technical Report. Rutherford Small Grant for Nature Conservation 17 1/07/04.
- Edmund AG. 1969. Dentition (pp. 117-200). In: Gans, C., Bellairs, A., and Parsons, T.S. (eds) *Biology of the Reptilia Volume 1, Morphology A*. Academic Press Inc.: London, U.K.
- Estes R. 1984. Fish, amphibians, and reptiles from the Etadunna Formation, Miocene of South Australia. *Australian Zoologist*. 21: 335-343.
- Estes R, Gauthier J, de Queiroz, K. 1988. Phylogenetic relationships within Squamata (pp 119-282). In: Estes, R., and Pregill, G. (eds) *Phylogenetic Relationships of the Lizard Families: Essays Commemorating Charles L. Camp*. Stanford University Press: Stanford, CA, U.S.A.

- Evans SE. 2008. The skull of lizards and Tuatara (pp. 1-347). In: Gans, C., Gaunt, A.S., Adler, K. (eds) *Biology of the Reptilia Vol. 20, Morphology H*. Society for the Study of Amphibians and Reptiles. Ithica, NY, U.S.A.
- Fasham MJR. 1977. A comparison of non-metric multidimensional scaling, principal components and reciprocal averaging for the ordination of simulated coenoclines and coenoplanes. *Ecology*. 58: 551-561.
- Free Software Foundation. 2010. GNU Image Manipulation Program: GIMP.
[Www.gimp.org](http://www.gimp.org) 05/15/2008.
- Gardner MG, Huggall AF, Donnellan SS, Hutchinson MN, Foster R. 2008. Molecular systematics of social skinks: phylogeny and taxonomy of the Egernia group (Reptilia: Scincidae). *Zoological Journal of the Linnean Society*. 154: 781-794.
- Gocmen B, Senol A, Mermer A. 2002. A new record of Schneider's Skink, *Eumeces schneideri* Daudin, 1802 (Sauria: Scincidae) from Cypress.
- Goloboff PA, Farris JS, Nixon KC. 2008. TNT, a free program for phylogenetic analysis. *Cladistics* 24: 774-786.
- Greene HW, Ralidis PM, Acuna EW. 2010. Texas Alligator Lizard (pp. 492-495). In: *Lizards of the American South West*, eds. L.L.C. Jones and R.E. Lovich. Rio Nuevo Publishers, Tucson, Arizona.
- Greer AE. 1967. A new generic arrangement of some Australian scincid lizards. *Brevoria*. 267: 1-19.
- Greer AE. 1970. A Subfamilial Classification of Scincid Lizards. *Bulletin of the Museum of Comparative Zoology*. 139 (3): 151-184.

- Greer AE. 1979a. *Eremiascincus*, a new generic name for some Australian sand swimming skinks (Lacertilia: Scincidae). Records of the Australian Museum 32 (7): 321-338.
- Greer AE. 1979b. A Phylogenetic subdivision of Australian skinks. Records of the Australian Museum. 32 (8): 339-371.
- Greer AE. 1983. The Australian scincid lizard genus *Calypotis* De Vis: resurrection of the name, description of four new species, and discussion of relationships. Records of the Australian Museum. 35: 29-59.
- Greer AE. 1989. Biology and Evolution of Australian Lizards. Surrey Beatty & Sons Pty LTD., New South Wales.
- Greer AE. 1990. The *Glaphyromorphus isolepis* species group (Lacertilia: Scincidae): Diagnosis of the taxon and description of a new species from Timor. Journal of Herpetology. 24(4): 372-377.
- Greer AE, Wordsworth L. 2003. Body shape in skinks: the relationship between relative hind limb length and relative snout-vent length. Journal of Herpetology. 37(3): 554-559.
- Haas G. 1973. Muscles of the jaws and associated structures in the Rhynchocephalia and Squamata (pp. 285-490). In: Gans, C. and Parsons, T.S. (eds) Biology of the Reptilia Vol. 4. Academic Press: New York, U.S.A.
- Hand SJ, Dawson L, Augee ML. 1988. *Macroderma koppa*, a new Tertiary species of false vampire bat (Microchiroptera: Megadermatidae) from Wellington Caves, New South Wales. Records of the Australian Museum. 40: 343-351.
- Harmon LJ. 2002. Some observations of the natural history of the prehensile-tailed skink, *Corucia zebrata* in the Solomon Islands. Herpetological Review. 33(3): 177-179.

- Herrel A, McBrayer LD, Larson PM. 2007. Functional basis for sexual differences in bite force in the lizard *Anolis carolinensis*. *Biological Journal of the Linnean Society*. 91: 111-119.
- Hocknull S.A. 2000. Remains of an Eocene skink from Queensland. *Alcheringa*. 24: 63-64.
- Hocknull S.A. 2002. Comparative maxillary and dentary morphology of the Australian dragons (Agamidae: Squamata): a framework for fossil identification. *Memoirs of the Queensland Museum* 48(1): 125-145.
- Hollenshead M, Mead JI, Swift S. 2011. Late Pleistocene *Egernia* group skinks (Squamata: scincidae) from Devils Lair, Western Australia. *Alcheringa*. 35(1): 31-51.
- Honda M, Ota H, Kobayashi M, Hikida T. 1999. Phylogenetic relationships of Australian skinks of the *Mabuya* group (Reptilia: Scincidae) inferred from mitochondrial DNA sequences. *Genes and Genetic Systems*. 74(4): 135-139.
- Honda M, Ota H, Kobayashi M, Nabhitabhata J, Yong H, Hikida T. 2000. Phylogenetic relationships, character evolution and biogeography of the subfamily Lygosominae (Reptilia: Scincidae) inferred from mitochondrial DNA sequences. *Molecular Phylogenetics and Evolution*. 15(3): 452-461.
- Honda M, Okamoto T, Hikida T, Ota H. 2008. Molecular phylogeny of the endemic five-lined skink (*Plestiodon marginatus*) (Reptilia: Scincidae) of the Ryukyu archipelago, Japan, with special reference to the relationship of a Northern Tokara population. *Pacific Science*. 62(3): 351-362.
- Howard R, Williamson I, Mather P. 2003. Structural aspects of microhabitat selection by the skink *Lampropholis delicata*. *Journal of Herpetology*. 39(3): 613-617.

- Hutchinson MN. 1992. Origins of the Australian scincid lizards: a preliminary report on the skinks of Riversleigh. The Beagle, Records of the Northern Territories Museum of Arts and Sciences. 9: 61-69.
- Hutchinson MN, Mackness BS. 2002. Fossil lizards from the Pliocene Chinchilla local fauna, Queensland, with description of a new species. Records of the South Australia Museum. 35: 169-184.
- Hutchinson MN, Scanlon J. 2009. New and unusual Plio-Pleistocene lizard (Reptilia: Scincidae) from Wellington Caves, New South Wales, Australia. Journal of Herpetology. 43(1): 139-147.
- Inger RF, Colwell RK. 1977. Organization of contiguous communities of amphibians and reptiles in Thailand. Ecological Monographs. 47(3): 229-253.
- Kastle W, Schleich HH, Habisch K. 1996. Amphibians and Reptiles of North Africa: biology, systematics, field guide. Koelz Scientific Publishers, Germany.
- Kingman RH. 1932. A comparative study of the skull in the genus *Eumeces* of the family Scincidae. Bulletin of the University of Kansas. 20(15): 273-295.
- Lakjer T. 1927. Studien upper die Gaumenregion bei Sauriern im Vergleich mit Anamniern und primitiven Sauropsiden. Zoologische Jahrbücher, Abteilung für Anatomie und Ontogenie der Tiere. 49: 57-356.
- Lemo-Espinal JA, Smith GR, Ballinger RE. 1997. Observations on the body temperatures and natural history of some Mexican reptiles. Bulletin of the Maryland Herpetological Society. 33(4): 159-164.
- Longrich N. 2010. *Mojoceratops perifania*, a new chasmosaurine ceratopsid from the late Campanian of Western Canada. Journal of Paleontology. 84(4): 681-694.

- MacLeod N. 2002. Phylogenetic signals in morphometric data. In: MacLeod, N. and Forey, P.L. (eds) *Morphology, Shape and Phylogeny*. Taylor and Francis, Inc., New York and London.
- Maddison WP, Maddison DR. 1992. *MacClade: analysis of phylogeny and character evolution*. Sinauer, Sunderland, Massachusetts, USA.
- Marcus LF. 1988. Traditional Morphometrics (pp 77-122). In: Rolf, F.J. and Bookstein, F.L (eds) *Proceedings of the Michigan Morphometrics Workshop*. University of Michigan Museum of Zoology.
- Marcus LF, Hingst-Zaher E, Zaher H. 2000. Application of landmark morphometrics to skulls representing the orders of living mammals. *Hystrix*. 11: 27-47.
- Martin J, Hutchinson MN, Meredith R, Case JA, Pledge NS. 2004. The oldest genus of scincid lizard (Squamata) from the Tertiary Etadunna Formation of South Australia. *Journal of Herpetology*. 38(2): 180-187.
- Mausfeld P, Vrcibradic D. 2002. On the nomenclature of the skink (*Mabuya*) endemic to the western Atlantic archipelago of Fernando de Noronha, Brazil. *Journal of Herpetology*. 36(2): 292-295.
- McBrayer LD. 2004. The relationship between skull morphology, biting performance and foraging mode in Kalahari lacertid lizards. *Zoological Journal of the Linnean Society*. 140: 403-416.
- McBrayer LD, Corbin CE. 2007. Patterns of head shape variation in lizards: morphological correlates of foraging mode. In: S.M. Reilly, S.M., McBrayer, L.D., and Miles, D.B. (eds) *Lizard Ecology: The Evolutionary Consequences of Foraging Mode*. Cambridge University Press, New York.

- Mecke S, Doughty P, Donnel S. 2009. A news species of *Eremiascincus* (Reptilia: Squamata: Scincidae) from the Great Sandy Desert and Pilbara coast, Western Australia and reassignment of eight species from *Glaphyromorphus* to *Eremiascincus*. *Zootaxa*. 2246: 1-20
- Mittleman MB. 1952. A generic synopsis of the lizards of the subfamily Lygosominae. *Smithsonian Misc. Coll.* 117 (17): 1-35.
- Molnar RE. 1991. Fossil Reptiles in Australia (Pp. 605-702). In: Vickers-Rich, P., Monaghan, J.M., Baird, R.F., and Rich, T.H. (eds) *Vertebrate Paleontology of Australia*. Monash University Publications Committee, Melbourne.
- PASW, Inc. 2008. SPSS 17.0
- Pianka ER, Vitt LJ. 2003. *Lizards: Windows to the Evolution of Diversity*. University of California Press, Berkeley and Los Angeles, CA.
- Pledge NS. 1992. The Curramulka local fauna: a new late Tertiary fossil assemblage from Yorke Peninsula, South Australia. *Beagle, Records of the Northern Territory Museum of Arts and Sciences*. 9: 115-142.
- Price GJ, Webb GE. 2006. Late Pleistocene sedimentology, taphonomy and megafauna extinction on the Darling Downs, southeastern Queensland. *Australian Journal of Earth Sciences*. 53 (6): 947-970.
- Reeder TW. 2003. A phylogeny of the Australian *Sphenomorphus* group (Scincidae: Squamata) and the phylogenetic placement of the crocodile skinks (*Tribolonotus*): Bayesian approaches to assessing congruence and obtaining confidence in maximum likelihood inferred relationships. *Molecular Phylogenetics and Evolution*. 27: 384-397.

- Richmond JQ, Reeder TW. 2002. Evidence for parallel ecological speciation in scincid lizards of the *Eumeces skiltonianus* species group (Squamata: Scincidae). *Evolution*. 56 (7): 1498-1513.
- Richmond JQ. 2006. Evolutionary basis for parallelism in North American scincid lizards. *Evolution & Development*. 8 (6): 477-490.
- Rieppel O. 1981. The skull and adductor musculature in some burrowing scincomorph lizards of the genera *Acontias*, *Typhlosaurus* and *Feylinia*. *Journal of Zoology*, London. 195: 493-528.
- Rieppel O, Gauthier J, Maisano J. 2008. Comparative morphology of the dermal palate in squamate reptiles, with comments on phylogenetic implications. *Zoological Journal of the Linnean Society*. 152: 131-152.
- Rohlf FJ, Slice D. 1990. Extensions of the Procrustes method for the optimal superimposition of landmarks. *Systematic Zoology*. 39: 40-59.
- Scannella JB, Horner JR. 2010. *Torosaurus* Marsh 1891, is *Triceratops* Marsh 1889 (Ceratopsidae: Chasmosaurinae): Synonymy through ontogeny. *Journal of Vertebrate Paleontology*. 30(4): 1157-1168.
- Schmitz A, Mausfield P, Embert D. 2004. Molecular studies on the genus *Eumeces* Wiegmann, 1834: phylogenetic relationships and taxonomic implications. *Hamadryad*. 28: 73-89.
- Shea GM, Hutchinson MN. 1992. A new species of *Tiliqua* (Lacertilia: Scincidae) from the Miocene of Riversleigh. *Memoirs of the Queensland Museum*. 32: 303-310.
- Siebenrock F. 1892. Zur Kenntniss des Kopfskelettes der Scincoiden, Anguiden, und Gerrhosauriden. *Ann. K. K. Naturhist. Mus. Wien*. 7:167-196.

- Siler CD, Diesmos AC, Brown RM. 2010. New loam-swimming skink, genus *Bracymeles* (Reptilia: Squamata: Scincidae) from Luzon and Catanduanes Islands, Philippines. *Journal of Herpetology*. 44(1): 49-60.
- Smith HM. 1946. *Handbook of Lizards: lizards of the United States and Canada*. Comstock Publishing Associates, Ithica and London.
- Storr GM. 1964. *Ctenotus*, a new generic name for a group of Australian skinks. *Western Australian Naturalist*. 9(4): 84-85.
- Storr GM. 1967. The genus *Sphenomorphus* (Lacertilia, Scincidae) in Western Australia and the Northern Territory. *Journal of the Royal Society of Western Australia*. 50 (1): 10-20.
- Strayton CT. 2005). Morphological evolution of the lizard skull: a geometric morphometrics survey. *Journal of Morphology*. 263: 47-59.
- Sumner, J. (2002). Morphometric and reproductive notes on the rare wet tropics skink, *Glaphyromorphus mjobergi*. *Memoirs of the Queensland Museum*. 48(1): 146.
- Syncroscopy. (2007). *Auto-Montage Pro*. Beacon House, Nuffield Road, Cambridge, UK.
- Tihen, J.A. (1949). The genera of the Gerrhonotine lizards. *The American Midland Naturalist*. 41(3): 580-601.
- Weigelt, J. (1927). *Recent Vertebrate Carcasses and their Paleobiological Implications*. Translated by J. Schaefer. University of Chicago Press, Chicago.
- Williams, C. (1999). *Fossil lizard identification methods: A case study of three *Egernia* species*. Msc. Thesis. Adelaide University, Adelaide, South Australia.

- Whiting AS, Bauer AM, Sites Jr. JW. 2003. Phylogenetic relationships and limb loss in sub-Saharan African scincine lizards (Squamata: Scincidae). *Molecular Phylogenetics and Evolution*. 29: 582-598.
- Wilson S, Swan G. 2003. *A Complete Guide to Reptiles of Australia*. New Holland Publishers. Sydney.
- Zeldritch ML, Swiderski DL, Sheets HD, Fink WL. 2004. *Geometric morphometrics for biologists: a primer*. Elsevier Academic Press, San Diego.
- Zug GR, Gill BJ. 1997. Morphological variation of *Emoia murphyi* (Lacertilia: Scincidae) on islands of the southwest Pacific. *Journal of the Royal Society of New Zealand*. 27(2): 235-242.
- Zug GR, Springer VG, Williams JT, Johnson D. 1988. The vertebrates of Rotuma and surrounding waters. *Atoll Research Bulletin*. 316: 1-25.
- Zweifel RG. 1979. Variation in the scincid lizard *Lipinia noctua* and notes on other *Lipinia* from the New Guinea region. *American Museum Novitates*. 2676: 1-21.

APPENDIXES

APPENDIX A: Key to abbreviations

add.fs	adductor fossa
adnm	attachment site for the dorsal neck musculature
aiaf	anterior inferior alveolar fenestra
aip	anterior inferior process of the prootic
alc	alveolar canal
al.pr	anterolateral process
am.pr	anteromedial process
a.m.pt	attachment for the posterior branch of the muscularis pterygoidius.
amyf	anterior mylohyoid foramen
Ang	angular
An.ft	angular facet
anp	ascending nasal process
ap.f	apical foramen
apl	palatine articulation
Art	Articular
Art.s	articular surface
asa.f	anterior surangular foramen
ascc	anterior semicircular canal
as.pr	ascending process
avc	anterior opening of the vidian canal
Bo	basioccipital
Bpt	basipterygoid
Bpt.ft	basipterygoid facet
b.tb	basilar tuber
cc	cranial carotid canal
cch	conch
c.cl	central column
ce.co	cephalic condyle
ch.s	choanal shelf
Cor	Coronoid
Cor.ft	coronoid facet
Cor.pr	coronoid process
cr.pro	crista prootica
cr.cr	crista cranii
cr.pf	crista postfovealis
cr.se	crista sellaris
cr.tr	crista trabecularis
D	Dentary
D.ft	dentary facet
d.lm	dorsal lamina
D.pr	dentary process

D.p.pr	dentary posterior process
dpt.pr	dorsal pterygoid process of the ectopterygoid
ds	dermal sculpting
d.sh	dental shelf
Ec	ectopterygoid
Ec.ft	ectopterygoid facet
Eo	exoccipital
Ep	epipterygoid
eth	ethmoid foramen
ex.n	external nares
F	frontal
fe	fenestra exochoanalis
F.ft	frontal facet
F.lp	frontal lappet
f.Mx5	foramen for the maxillary branch of the trigeminal nerve
f.Op.5	foramen for the ophthalmic branch of the trigeminal nerve
FP.ft	frontal-parietal facet
F.pr	frontal process
fs.c	fossa columellae
fv	fenestra vomeronasalis
f.mg	foramen magnum
f.o	fenestra ovalis
ic	internal choanae
ims	intramandibular septum
in.pr	incisive process
it.f	infratemporal fenestra
io.f	infraorbital fenestra
J	jugal
J.f	jugal foramen
J.ft	jugal facet
L	lacrymal
la.cr	lateral crest
la.pr	lateral process
lrst	lateral opening of the recessus scala tympani
lsc	lateral semicircular canal
ma.co	mandibular condyle
mcr	medial crest
mec.c	mechelien canal
mf	mental foramina
mgr	medial groove
msa.f	medial surangular foramen
Mx	maxilla
Mx.5	path for the maxillary branch of the trigeminal nerve
Mx.ft	maxillary facet
Mx.pr	maxillary process
N	nasal

N.ft	nasal facet
n.m	nasal margin
N.pr	nasal process
nu.f	nutritive foramen
O	orbit
occ	occipital condyle
o.m	orbital margin
on.fl	orbitonasal flange
P	parietal
Pa	palatine
Pa.f	palatine foramen
Part	prearticular
Part.ft	prearticular facet
pdp	process descendens parietalis
pf	pineal foramen
Pfr	Postfrontal
Pfr.ft	postfrontal facet
Pfr.f	postfrontal foramen
pm.pr	posteromedial process
Pmx	premaxilla
pmyf	posterior mylohyoid foramen
Po	Postorbital
Pocc	paroccipital
Pocc.ft	facet for paroccipital process
Pocc.s	Paroccipital surface
ppas	pit for the processus ascendens
p.pr	posterior process
p.pr.inf	inferior posterior process
p.pr.sup	superior posterior process
Prf	prefrontal
Prf.ft	prefrontal facet
Prf.ft.a	anterior portion of the prefrontal facet
Prf.ft.p	posterior portion of the prefrontal facet
Pro.al	alar process of the prootic
ps	parashenoid
psa.f	posterior surangular foramen
pssc	posterior semicircular canal
pst.cr	pseudotemporalis crest
Pt	pterygoid
Pt.fl	pterygoid flange
Pt.ft	pterygoid facet
Pt.lm	pterygoid lamina
Pt.pr	pterygoid process
Pt.s	Pterygoid surface
pvc	posterior opening of the vidian canal
Px.ft	premaxillary facet

Px.pr	premaxillary process
Px.pr.l	lateral premaxillary process
Px.pr.m	medial premaxillary process
pys	pyriform space
Q	quadrate
Q.pr	quadrate process
rap	retroarticular process
rap.cc	central column of the retroarticular process
rap.fl	dorsolateral flange of the retroarticular process
Sa	surangular
Sa.ft	surangular facet
sac	superior alveolar canal
Sm.pr	septomaxillary process
Socc	supraoccipital
sofo	suborbital foramen
Sp	sphenoid
Spl	splenic
Spl.ft	splenic facet
Sq	squamosal
Sq.ft	squamosal facet
Sq.n	squamosal notch
sscc	superior semicircular canal
St	supratemporal
St.ft	supratemporal facet
St.s	supratemporal surface
Stp	stapes
St.pr	supratemporal process
St.f	supratemporal fenestra
sym	symphysis
T1	first tooth
tcr	transverse crest
ty.cr	tympanic crest
Vo	vomer
VI	Path for the abducens nerve (cranial nerve VI)
VIII	foramen for the acoustic nerve (cranial nerve VIII)
vl.alp	Anterolateral process of the ventral lamina
vl.amp	Anteromedial process of the ventral lamina
vf	vomerine foramine
v.lm	ventral lamina
vl.pmp	posteromedial process of the ventral lamina
V.pr	vomerine process
vpt.pr	ventral pterygoid process of the ectopterygoid
X	path of the vagus nerve (cranial nerve X)
XII	Patch of the hypoglossal nerve (cranial nerve XII)

APPENDIX B:

Dataset Used in the Cladistic Analysis

Characters: 1 ar01, 2 ar02, 3 ar03, 4 ar04, 5 ar05, 6 ar06, 7 ar07, 8 ar08, 9 ar09, 10 ar10, 11 ar11, 12 ar12, 13 co01, 14 co02, 15 co03, 16 co04, 17 co05, 18 co06, 19 co07, 20 co08, 21 co09, 22 co10, 23 co11, 24 co12, 25 d01, 26 d02, 27 d03, 28 d04, 29 d05, 30 d06, 31 d07, 32 d08, 33 f01, 34 f02, 35 f03, 36 f04 37 f05, 38 f06, 39 f07, 40 f08, 41 f09, 42 F10, 43 m01, 44 m02, 45 m03, 46 m04, 47 m05, 48 m06, 49 m07, 50 m08, 51 m09, 52 m10, 53 m11, 54 m12, 55 m13, 56 m14, 57 m15, 58 m16, 59 m17, 60 m18, 61 m19, 62 m20, 63 p01, 64 p02, 65 p03, 66 p04, 67 p05, 68 p06, 69 p07, 70 p08, 71 p09, 72 p10, 73 p11, 74 p12, 75 pa01, 76 pa02, 77 pa03, 78 pa04, 79 pa05, 80 pa06, 81 pa07, 82 pa08, 83 pa09, 84 pa10, 85 po5, 86 pof01, 87 pof02, 88 pof03, 89 pof04, 90 pof05, 91 pof06, 92 pof07, 93 pof08, 94 pof09, 95 pof10, 96 pof11, 97 pof12, 98 pof13, 99 pt01, 100 pt02, 101 pt03, 102 pt04, 103 pt05, 104 pt06, 105 pt07, 106 pt08, 107 pt09, 108 pt10, 109 pt11, 110 pt12, 111 pt13, 112 pt14, 113 pt15, 114 pt16, 115 q01, 116 q02, 117 q03, 118 q04, 119 q05, 120 q06, 121 q07, 122 q08, 123 q09, 124 q10, 125 q11, 126 q12, 127 q13

E_wamr146924 rt

10110?1001?01010011001110010211010011110002120011110212012111001001111
100111111?110011110101101110????????????????1002110111101

E_wamr146924 lf

10110?1001?01000011001110?101010100111100021200111212011130010010011111
00111111?110011110101101110????????????????1002000111111

E_wamr146923rt

1?110?0001?01000001001111?100210100000211111200121003131120110010011001
00111110?1100101000011011?001?001010011100?1002110110000

E_wamr146923_lf

1?110?0001?010000010011120100010100000211111210121003021120110010011001
00111110?1120101000011011?001?001111111110?1001110111111

E_wamr146922_rt

11110??001?010010011011010100010100111100101000111201120130110010011000
00111110?110011000111100100????????????????1001110100101

E_wamr146922_lf

11110??001?010010010011010100110100111100101100111202111131110010011000
00111110?11001????????????????????????????100111110100?

E_wamr146921_rt

1001010101011011001111020111011010011100003100011110213011110012002111
201011111011212011010100112001?01120101010101??111011110?

E_wamr146921_lf

1001010101011011001111020111000010011100003201011120203012010012002111
201011111011212011010100112001?001111101010011?111011110?

E_etvp7136_rt

1?11001001111010011100011001100010011121012100011100212002110002101211
201111111011201?????????????0110?11110011010120111111110

E_etvp7136_lf

1?1100100111101001110001100110101001112101210001110011201311?002101211
201111111011201011100110001001101112100110101101111111111

E_etvp7130_rt

1011011011111011001100121110200010001021012200011110213012111002100101
201111111011110011100110010011101110110010??1201111111100

E_etvp7130_lf

1111011001111011001100022010101010001021012210001100203113111002100101
201111111011110011?1?100112010100110110010??1201100111100

E_etvp7135_rt

11110110111110211111010100100010100011210112000?4120202013011001001211
2011?111?0?1?01?????????????001?001120001101?1?????????????

E_etvp7135_lf

11110110111110211111010120100010100011210112000?4120203013011001001211
2011?111?0?1?01011010100111?01?0011201?1101011?111?10111?

E_etvp7127_rt

11110?????1010011011001101101110100111111131200141102120121100020022112
011?111?011?02?????????????01?012020001111?11?110010111?

E_etvp7127_lf

11110?????101001101101111110010100111111131200141002130130100020022112
01111111011202?????????????????01?0110200?1111?11?111111101?

E_etvp7132_rt

111100100111101011110111100001101000112111????1????????????0020001012011
?1111011200????????????01?001010101111011?111111101?

E_etvp7132_lf

11110010011110101111011110000101000112111????1????????????0020001012011
?1111011200????????????01?0010111?1111011?110011111?

E_etvp7131_rt

11110??10110101111101101001111010001121112200012020113013110002100011
20111110011200????????????010011121??110??1102111011110

E_etvp7131_lf

11110??101101011011101101000101010001121112200012020112011110002100011
2011111001120001101110011100100111210?110??1102111011110

E_etvp7133_rt

101101?1010110111110000101101110100011211132100141102130131100?????????
???11?0?1?1????????????????????????????????120201111110

E_etvp7133_lf

101101?1010110111110000101101010100011211132110121202131131100?????????
?1111101121????????????????????????????????11?111111001?

E_etvp7134_rt

1111011001111001011101011110001010001121012110012110212011110002000201
20111111011210011010100012001?0011111?1102?1102110111111

E_etvp7134_lf

111101100111101101110101111001101000112101211101211020201211?002000201
20111111011110011010100012001?0110110?100201101110101111

E_etvp7128_rt

1?11001101101010111100110010220010001111012200012120103013111002100211
2011111101120001001110011100110011011?11110120211111110

E_etvp7128_lf

1?1100110110101011110011001021010001111012210000010102112111002100211
2011111101110001011110011100110010011?110101202110111111

E_etvp7137_rt

1111011001111010101100011010001010001021113220014120113112110002001111
2011111101100101101010010200100110010?1111?1202111111100

E_etvp7137_lf

111101101111010101100011010001010001021113220014100113111110002001111
2011111101100101101010010200120110110?1111?1102110111100

E_etvp7129_rt

?0???111011110100011001110200010100011210122000141201130141100020001112
011111101121001110010011000100010011?100101102011111101

E_etvp7129_lf

1011011101111010001100111110021010001121012200014100112112110002000111
20111111101111001110010011100110110110?110201102011101100

C_wamr146927_rt

0000101000010121110011002111001001110102104021100010013103111111212110
210000001100212101211111011100011100000000?021100000000

C_wamr146927_lf

0000101000010120110011002110121001110102104021103000013102111111212110
21000000110021210121111101110001110000000?021100000000

C_wamr146916_rt

0000010010010110111011012011200101110000003021001010213110110111012000
210100?1010011211121011100101001102110?000110211000001000

C_wamr146916_lf

0000010010010110111011012020100101110000003010001010213112010111012000
210100010100112111210111001011?1102100?000210211100001000

C_wamr146913_rt

00001011000101210100110?1020100111111100003011101002213101111101002001
11000000111021201120111111101?111111001101?0211110011011

C_wamr146913_lf

00001011000101210100110?2020001111111100003001101000213102111101002001
110000001110212?????????????01?11111100100200211110011001

C_wamr146912_rt

01101?????001211110110121201100011001100120111000113121001011011011001
10100000100111101000110011010011020010000?0011110000000

C_wamr146912_lf

01101?????001211110110121011000011001100110211000103121001011011011001
10100000100211101000110011011010020110000?0011010000000

C_wamr146910_rt

00001000101101211100110111100101011100001140111000012131000?1111112101
211000000100112100201111001000?11111000101100211101011010

C_wamr146910_lf

00001000101101211100110111100101011100001150111000113031001?1111112101
211000000100112100201111001000?11111110101100211101011010

C_wamr146909_rt

10001001001101210010110?2101111101101112104021101101203103111111012011
11000??01100212?????????????00110111000010?10211100110000

C_wamr146909_lf

10001001000101210010110?2101111101101112104011101111203103011111012011
11000??01100212100000110001000?10111101000??0211100110000

C_etvp7139_rt

000010011011011001001100200000110011011210?02000??20?????01?11110000121
000??1010011011?0101?????1121?3?2000002210210110000010

C_etvp7139_lf

000010011011011001001100200000110011011210301000000020111211111100001
210000?10100?10?????????????0121111101110110211110000000

C_etvp7138_rt

11101?1100?001100110110020010110111101000000010010001100030011110010?12
10101011000001111000100010010110??00?0100000011010?00000

C_etvp7138_lf

11101?1100?001100110110020010210111101000000210011011100020011110010?12
10101011000001111000100010010110??0010?001?0111110?00000

APPENDIX C:
Linear Measurements of Lizard Skulls

Accession #	Species	Skull Length	Width at Quadrates	Facial Region Length
Jim 0920	<i>Acontias percivali</i>	1.671	0.754	0.69
UCMP123066	<i>Ameiva sp.</i>	5.334	2.633	3.237
UCMP137832	<i>Ameiva sp.</i>	1.296	0.606	0.734
UCMVZ204290	<i>Anguis fragilis</i>	1.314	0.575	0.602
UCMVZ33828	<i>Anniella pulchra</i>	1.075	0.46	0.427
UCMVZ69473	<i>Anniella pulchra</i>	0.925	0.407	0.398
LACM127179	<i>Barisia gadovi</i>	1.946	1.093	0.969
LACM127180	<i>Barisia gadovi</i>	2.163	1.298	1.102
LACM127183	<i>Barisia moreleti</i>	1.955	0.99	0.862
LACM127184	<i>Barisia moreleti</i>	1.381	0.682	0.644
USNM305967	<i>Brachymeles boulengeri</i>	1.27	0.719	0.572
UCMP141140	<i>Callopiastes maculatus</i>	3.372	1.87	1.999
UCMP141141	<i>Callopiastes maculatus</i>	3.307	1.899	1.946
USNM323689	<i>Carlia ailanpalai</i>	1.424	0.683	0.793
CAS100777	<i>Carlia fusca</i>	1.402	0.758	0.736
UF56315	<i>Celestus warreni</i>	5.066	3.245	2.606
LACM127198	<i>Chalcides bedriagais</i>	0.988	0.534	0.502
LACM127199	<i>Chalcides bedriagais</i>	1.028	0.556	0.531
CNHM 154619	<i>Chalcides ocellatus</i>	1.676	0.885	0.828
CNHM 167941	<i>Chalcides ocellatus</i>	1.802	1.026	0.876
USNM313453	<i>Chalcides ocellatus</i>	1.926	1.09	0.92
LACM132298	<i>Cnemidophorus burti</i>	2.879	1.408	1.511
LACM132302	<i>Cnemidophorus burti</i>	2.828	1.452	1.514
LACM132303	<i>Cnemidophorus burti</i>	3.152	1.8	1.652
LACM132307	<i>Cnemidophorus burti</i>	2.412	1.15	1.176
LACM132375	<i>Cnemidophorus tigris</i>	1.752	0.812	0.881
LACM132375	<i>Cnemidophorus tigris</i>	2.312	1.174	1.196
UCMP118925	<i>Cnemidophorus tigris</i>	2.277	1.122	1.295
CNHM 257163	<i>Corucia zebrata</i>	4.461	3.903	2.509
LACM137467	<i>Corucia zebrata</i>	4.87	4.168	2.571
UCMP137850	<i>Corucia zebrata</i>	4.786	4.039	2.61
UF70431	<i>Corucia zebrata</i>	5.218	4.554	2.89
UF75985	<i>Corucia zebrata</i>	5.015	4.309	2.727
UF87979	<i>Corucia zebrata</i>	4.89	4.202	2.685
CAS47453	<i>Cryptoblepharus poecilopleurus</i>	0.985	0.484	0.507
WAMR 50361	<i>Ctenotus robustus</i>	2.086	1.048	1.064
WAMR 50689	<i>Ctenotus robustus</i>	2.252	1.152	1.172
CNHM 31041	<i>Egernia cunninghami</i>	4.186	2.928	2.182
UCMP138689	<i>Egernia major</i>	5.278	3.009	2.88
CNHM 51707	<i>Egernia stokesi</i>	3.66	2.68	1.897
UCMVZ39254	<i>Elgaria coerulea</i>	2.07	1.172	1.228
UCMVZ62154	<i>Elgaria coerulea</i>	1.938	1.01	0.958
LACM127194	<i>Elgaria multicarinata</i>	1.18	0.546	0.546
LACM127195	<i>Elgaria multicarinata</i>	2.245	1.208	1.06

Accession #	Species	Skull Length	Width at Quadrate s	Facial Region Length
LACM127196	<i>Elgaria multica rinata</i>	2.318	1.292	1.18
LACM159075	<i>Elgaria multica rinatus</i>	2.264	1.194	0.988
LACM163884	<i>Elgaria multica rinatus</i>	2.78	1.446	1.239
LACM130787	<i>Elgaria multica rinatus</i>	2.577	1.284	1.29
LACM166679	<i>Elgaria multica rinatus</i>	1.61	0.748	0.722
UF99219	<i>Elgaria multica rinatus</i>	2.393	1.197	1.169
CNHM 134594	<i>Emoia kueken thali</i>	1.72	0.868	0.988
CAS100684	<i>Emoia longicauda</i>	1.706	0.82	0.985
CNHM 236132	<i>Emoia sp.</i>	3.115	1.627	1.784
USNM249742	<i>Emoia trossula</i>	1.762	0.78	1.056
R14866	<i>Eremiascincus fasciolatus</i>	1.74	0.894	0.882
R156826	<i>Eremiascincus fasciolatus</i>	1.558	0.758	0.745
R19862	<i>Eremiascincus fasciolatus</i>	1.066	0.46	0.46
R24638	<i>Eremiascincus fasciolatus</i>	1.7	0.836	0.837
R24729	<i>Eremiascincus fasciolatus</i>	1.867	0.945	0.927
R9333	<i>Eremiascincus fasciolatus</i>	1.808	0.912	0.834
R9411	<i>Eremiascincus fasciolatus</i>	1.714	0.866	0.866
WAMR 24144	<i>Eremiascincus fasciolatus</i>	1.796	1.004	0.903
R12717B	<i>Eremiascincus richardsonii</i>	1.035	0.474	0.498
R1279a	<i>Eremiascincus richardsonii</i>	1.902	1.048	0.96
R143878E	<i>Eremiascincus richardsonii</i>	1.254	0.57	0.631
R1787	<i>Eremiascincus richardsonii</i>	2.062	1.157	1.072
R9301	<i>Eremiascincus richardsonii</i>	1.802	0.948	0.9
R9302	<i>Eremiascincus richardsonii</i>	1.682	0.848	0.81
UF99209	<i>Eumeces algeriensis</i>	3.19	2.111	1.728
MCB191	<i>Eumeces schneideri</i>	2.971	1.834	1.484
MCB56	<i>Eumeces schneideri</i>	2.468	1.384	1.178
MCB57	<i>Eumeces schneideri</i>	3.061	1.825	1.494
MCB59	<i>Eumeces schneideri</i>	3.166	1.904	1.49
MCB60	<i>Eumeces schneideri</i>	2.686	1.624	1.296
MCB63	<i>Eumeces schneideri</i>	2.473	1.424	1.172
MCB64	<i>Eumeces schneideri</i>	2.676	1.562	1.328
MCB78	<i>Eumeces schneideri</i>	2.696	1.539	1.3
MCB84	<i>Eumeces schneideri</i>	2.822	1.6	1.333
MCB85	<i>Eumeces schneideri</i>	3.021	1.78	1.482
FB 1139	<i>Gerrhonotus kingi</i>	2.257	1.165	1.146
FB1230	<i>Gerrhonotus multica rinata</i>	3.254	1.856	1.1
FB6666	<i>Gerrhonotus multica rinata</i>	2.554	1.495	1.266
UCMP123070	<i>Gerrhonotus multica rinata</i>	2.5	1.348	1.27
LACM127239	<i>Gymnophthalmus pleei</i>	0.868	0.489	0.488
USNM507550	<i>Lamprolepis smaragdina</i>	2.336	1.164	1.331
USNM507551	<i>Lamprolepis smaragdina</i>	2.146	1.108	1.218
CAS92966	<i>Lamprolepis smaragdina</i>	2.544	1.328	1.464
CAS83885	<i>Lampropholis guichenoti</i>	0.902	0.486	0.46
REE2101	<i>Leiopisma festium</i>	1.954	0.9	0.81

Accession #	Species	Skull Length	Width at Quadrates	Facial Region Length
REE2103	<i>Leiolopisma festium</i>	1.438	0.773	0.668
REE2096	<i>Leiolopisma zelandica</i>	1.57	0.858	0.746
CAS50270	<i>Libinia noctua</i>	0.995	0.528	0.498
CNHM 12763	<i>Lygosoma fernandi</i>	2.294	1.374	1.131
LACM166601	<i>Lygosoma laterale</i>	0.882	0.437	0.458
JIm 1465	<i>Mabuya bibroni</i>	2.194	1.154	1.187
USNM292407	<i>Mabuya bistrata</i>	1.936	1.003	1.072
CAS-nonumber	<i>Mabuya capensis</i>	2.045	1.248	1.046
REE312	<i>Mabuya carinata</i>	2.027	1.024	1.012
WBG09101	<i>Mabuya fasciata</i>	2.343	1.311	1.316
WBG09102	<i>Mabuya fasciata</i>	2.371	1.351	1.341
WBG09103	<i>Mabuya fasciata</i>	2.468	1.426	1.374
UF71580	<i>Mabuya macularia</i>	1.218	0.718	0.622
CNHM 229940	<i>Mabuya maculata</i>	1.224	0.724	0.686
CNHM 171520	<i>Mabuya multifasciata</i>	2.301	1.404	1.292
CNHM 229939	<i>Mabuya multifasciata</i>	1.91	0.94	1.03
UF61708	<i>Mabuya multifasciata</i>	2.25	1.31	1.228
UF61710	<i>Mabuya multifasciata</i>	2.553	1.494	1.433
CNHM 120270	<i>Mabuya rudis</i>	2.251	1.196	1.3
CNHM 150823	<i>Mabuya rudis</i>	2.245	1.178	1.345
CNHM 98525	<i>Mabuya sp (mexico)</i>	1.356	0.692	0.713
LACM172703	<i>Mabuya sp.</i>	2.242	1.25	1.16
LACM172704	<i>Mabuya sp.</i>	2.13	1.148	1.176
UF99194	<i>Mabuya trilineata</i>	1.957	0.984	1.108
LACM163897	<i>Mesaspis monticola</i>	1.461	0.832	0.696
UCMVZ191063	<i>Mesaspis monticola</i>	1.3	0.627	0.6
UCMVZ191064	<i>Mesaspis monticola</i>	1.224	0.677	0.584
UCMVZ81319	<i>Mesaspis monticola</i>	1.745	0.916	0.825
UCMVZ116570	<i>Ophiodes intermedius</i>	1.807	0.729	0.95
UCMVZ92988	<i>Ophiodes intermedius</i>	1.336	0.498	0.664
CNHM 141550	<i>Ophiomorus brevipes</i>	1.076	0.547	0.483
FB6666	<i>Ophisaurus apodus</i>	3.216	1.435	1.642
UCMP131083	<i>Ophisaurus apodus</i>	4.288	1.919	2.208
UCMP140693	<i>Ophisaurus apodus</i>	3.612	1.585	1.866
LACM127197	<i>Ophisaurus ventralis</i>	1.988	0.822	0.958
LACM130792	<i>Ophisaurus ventralis</i>	1.966	0.828	0.87
UCMVZ79249	<i>Ophisaurus ventralis</i>	1.582	0.612	0.773
UCMVZ95960	<i>Ophisaurus ventralis</i>	2.243	0.873	1.073
LACM127208	<i>Plestiodon anthracinus</i>	1.306	0.742	0.604
UF99701	<i>Plestiodon anthracinus</i>	1.098	0.627	0.548
REE692	<i>Plestiodon brevilineatus</i>	1.292	0.716	0.622
REE819	<i>Plestiodon brevilineatus</i>	1.226	0.655	0.56
REE1559	<i>Plestiodon copei</i>	1.128	0.608	0.524
REE1600	<i>Plestiodon copei</i>	1.37	0.742	0.636
REE1017	<i>Plestiodon dicei pineus</i>	1.064	0.544	0.502

Accession #	Species	Skull Length	Width at Quadrates	Facial Region Length
REE1053	<i>Plestiodon dicei pineus</i>	1.164	0.656	0.527
UCMVZ175940	<i>Plestiodon egregius</i>	1.047	0.511	0.543
LACM127209	<i>Plestiodon fasciatus</i>	1.547	0.912	0.88
LACM127210	<i>Plestiodon fasciatus</i>	0.93	0.49	0.523
UF13010-1	<i>Plestiodon fasciatus</i>	1.312	0.732	0.63
UF130111-2	<i>Plestiodon fasciatus</i>	1.468	0.878	0.717
USNM332755	<i>Plestiodon inexpectatus</i>	1.396	0.771	0.715
REE1331	<i>Plestiodon laticeps</i>	2.402	1.308	1.265
UF11817	<i>Plestiodon laticeps</i>	1.284	0.685	0.707
UF14279	<i>Plestiodon laticeps</i>	2.44	1.566	1.3
UF42388	<i>Plestiodon laticeps</i>	2.362	1.47	1.236
UF99700	<i>Plestiodon laticeps</i>	1.976	1.186	1.042
USNM009242	<i>Plestiodon laticeps</i>	2.786	1.871	1.445
USNM217505	<i>Plestiodon longirostris</i>	1.923	0.966	0.992
REE1148	<i>Plestiodon lynxe lynxe</i>	1.199	0.672	0.526
REE1236	<i>Plestiodon lynxe lynxe</i>	1.077	0.579	0.472
USNM17851	<i>Plestiodon marginatus</i>	1.362	0.83	0.698
USNM17852	<i>Plestiodon marginatus</i>	1.305	0.752	0.645
USNM17853	<i>Plestiodon marginatus</i>	1.33	0.688	0.646
FB609	<i>Plestiodon obsoletus</i>	2.212	1.256	1.133
USNM220269	<i>Plestiodon obsoletus</i>	2.114	1.05	1.092
JIm 1616	<i>Plestiodon septentrionali</i>	1.307	0.737	0.638
LACM136234	<i>Plestiodon skiltonianus</i>	1.482	0.86	0.642
REE1293	<i>Plestiodon tetragrammus</i>	1.298	0.66	0.59
REE856	<i>Plestiodon tetragrammus</i>	1.272	0.7	0.574
REE1362	<i>Plestiodon gilberti</i>	2.174	1.368	0.984
UCMVZ58177	<i>Plestiodon gilberti</i>	1.276	0.712	0.637
UCMVZ58200	<i>Plestiodon gilberti</i>	1.703	1.024	0.864
UCMVZ64199	<i>Plestiodon gilberti</i>	1.681	0.968	0.81
UCMVZ64200	<i>Plestiodon gilberti</i>	1.937	1.36	0.996
UCMVZ64201	<i>Plestiodon gilberti</i>	1.304	0.714	0.636
UCMVZ64202	<i>Plestiodon gilberti</i>	2.157	1.396	1.067
UCMVZ78204	<i>Plestiodon gilberti</i>	1.642	1	0.808
UCMVZ78205	<i>Plestiodon gilberti</i>	1.508	0.902	0.721
UCMVZ79241	<i>Plestiodon gilberti</i>	1.809	1.108	0.876
UCMVZ79242	<i>Plestiodon gilberti</i>	1.412	0.8	0.708
UCMP118717	<i>Plestiodon laticeps</i>	2.29	1.382	1.173
UCMVZ137649	<i>Plestiodon laticeps</i>	2.777	1.925	1.494
UCMVZ137633	<i>Plestiodon obsoletus</i>	1.993	1.111	1.058
UCMVZ79243	<i>Plestiodon obsoletus</i>	2.142	1.222	1.077
REE128	<i>Plestiodon obsoletus</i>	2.344	1.478	1.134
CAS_no_#	<i>Eumeces schneideri</i>	3.2	1.89	1.67
UCMVZ58178	<i>Plestiodon skiltonianus</i>	1.476	0.842	0.707
UCMVZ64197	<i>Plestiodon skiltonianus</i>	1.545	0.883	0.72
UCMVZ64198	<i>Plestiodon skiltonianus</i>	1.482	0.759	0.654

Accession #	Species	Skull Length	Width at Quadrates	Facial Region Length
UCMVZ78202	<i>Plestiodon skiltonianus</i>	1.431	0.826	0.701
UCMVZ78203	<i>Plestiodon skiltonianus</i>	1.406	0.894	0.688
UCMVZ79085	<i>Plestiodon skiltonianus</i>	1.51	0.962	0.722
UCMVZ79303	<i>Plestiodon skiltonianus</i>	1.33	0.737	0.658
UCMVZ79304	<i>Plestiodon skiltonianus</i>	1.421	0.863	0.74
MCB128	<i>Plestiodon skiltonianus</i>	1.424	0.788	0.682
MCB132	<i>Plestiodon skiltonianus</i>	1.232	0.71	0.583
MCB156	<i>Plestiodon skiltonianus</i>	0.958	0.523	0.463
CAS25035	<i>Scincella formosensis</i>	0.946	0.488	0.49
CAS96400	<i>Scincella stanleyanum</i>	1.062	0.562	0.528
UCMP140676	<i>Scincopus fasciatus</i>	2.244	1.185	1.288
UCMVZ128951	<i>Scincopus fasciatus</i>	3.692	2.386	1.998
UCMVZ129983	<i>Scincus scincus</i>	2.272	1.146	1.258
UF67798	<i>Scincus scincus</i>	2.12	1.01	1.224
UF99577	<i>Scincus scincus</i>	1.884	0.94	1.054
UCMP137844	<i>Tiliqua gigas</i>	4.986	2.746	2.539
UF45647	<i>Tiliqua gigas</i>	5.01	3.117	2.79
CNHM 22498	<i>Tiliqua nigrolutea</i>	4.513	3.08	2.466
CNHM 23149	<i>Tiliqua nigrolutea</i>	4.541	3.104	2.536
CNHM 22361	<i>Tiliqua rugosa</i>	4.213	3.358	2.406
CNHM 22442	<i>Tiliqua rugosa</i>	5.31	3.979	2.833
CNHM 22470	<i>Tiliqua rugosa</i>	5.48	3.998	3.08
CNHM 22490	<i>Tiliqua rugosa</i>	4.944	3.697	2.746
CNHM 31353	<i>Tiliqua rugosa</i>	5.05	3.755	2.851
UF99164	<i>Tiliqua rugosa</i>	5.225	4	2.903
CNHM 22091	<i>Tiliqua scincoides</i>	5.356	3.261	2.677
CNHM 22092	<i>Tiliqua scincoides</i>	4.836	3.094	2.502
CNHM 22779	<i>Tiliqua scincoides</i>	4.277	2.677	2.259
CNHM 229975	<i>Tiliqua scincoides</i>	4.928	2.89	2.733
CNHM 51702	<i>Tiliqua scincoides</i>	5.628	3.247	2.916
CNHM 51710	<i>Tiliqua scincoides</i>	5.379	2.812	2.751
CNHM 57520	<i>Tiliqua scincoides</i>	5.071	3.021	2.637
CNHM 73343	<i>Tiliqua scincoides</i>	4.34	3.056	2.398
REE1833	<i>Tiliqua scincoides</i>	3.342	2.033	1.741
REE487	<i>Tiliqua scincoides</i>	5.168	3.004	2.468
CAS94010	<i>Tribolonotus poneleti</i>	1.296	0.746	0.624
CNHM 145993	<i>Tropidophorus brookei</i>	2.255	1.178	1.227
CAS62004	<i>Tropidophorus misaminius</i>	2.028	1.134	1.131
UCMP137865	<i>Tupinambis nigripunctatus</i>	4.784	2.432	2.834
UCMP140937	<i>Tupinambis nigripunctatus</i>	3.344	1.665	1.984
LACM76850	<i>Tupinambis nigropunctatus</i>	5.12	2.85	2.964
UF50670	<i>Tupinambis teguixin</i>	6.424	3.529	3.913

Accession #	Cranial Region Length	Orbit Length	Temporal Region Length	Rostral Region Length	Orbit Height
Jim 0920	1.052	0.238	0.868	0.507	0.357
UCMP123066	2.216	1.417	2.118	2.448	1.507
UCMP137832	0.64	0.484	0.385	0.441	0.402
UCMVZ204290	0.753	0.303	0.587	0.424	0.307
UCMVZ33828	0.714	0.157	0.5	0.296	0.213
UCMVZ69473	0.562	0.182	0.584	0.287	0.184
LACM127179	1.132	0.51	0.95	0.588	0.434
LACM127180	1.25	0.562	1.168	0.62	0.533
LACM127183	1.234	0.506	1.008	0.573	0.48
LACM127184	0.821	0.364	0.676	0.398	0.3
USNM305967	0.784	0.252	0.584	0.378	0.276
UCMP141140	1.628	1.047	1.258	1.255	0.924
UCMP141141	1.641	1.063	1.213	1.228	0.854
USNM323689	0.742	0.488	0.523	0.441	0.394
CAS100777	0.783	0.506	0.538	0.42	0.423
UF56315	3.02	0.968	2.728	1.748	1.277
LACM127198	0.586	0.218	0.42	0.302	0.233
LACM127199	0.574	0.223	0.45	0.31	0.252
CNHM 154619	0.948	0.448	0.706	0.559	0.451
CNHM 167941	1.099	0.473	0.807	0.552	0.492
USNM313453	1.13	0.472	0.812	0.592	0.476
LACM132298	1.452	0.958	0.922	1.256	0.8
LACM132302	1.428	0.936	0.914	1.237	0.726
LACM132303	1.582	1.008	1.16	1.41	0.852
LACM132307	1.292	0.796	0.762	1.065	0.66
LACM132375	0.945	0.586	0.536	0.708	0.425
LACM132375	1.218	0.732	0.745	0.956	0.608
UCMP118925	1.112	0.726	0.718	0.937	0.602
CNHM 257163	2.54	1.276	2.435	1.561	1.418
LACM137467	2.694	1.48	2.686	1.73	1.658
UCMP137850	2.862	1.368	2.888	1.65	1.612
UF70431	3.06	1.539	3.01	1.835	1.542
UF75985	2.876	1.476	2.728	1.706	1.617
UF87979	2.858	1.47	2.757	1.576	1.628
CAS47453	0.533	0.3	0.365	0.312	0.212
WAMR 50361	1.14	0.612	0.793	0.734	0.546
WAMR 50689	1.186	0.645	0.874	0.816	0.646
CNHM 31041	2.38	1.244	1.926	1.472	1.262
UCMP138689	2.868	1.7	2.382	1.924	1.449
CNHM 51707	2.105	1.06	1.85	1.184	1.044
UCMVZ39254	0.966	0.595	0.995	0.667	0.519
UCMVZ62154	1.115	0.566	0.87	0.594	0.468
LACM127194	0.7	0.366	0.46	0.372	0.264
LACM127195	1.348	0.7	1.036	0.746	0.506
LACM127196	1.3	0.601	1.126	0.782	0.598

Accession #	Cranial Region Length	Orbit Length	Temporal Region Length	Rostral Region Length	Orbit Height
LACM159075	1.454	0.67	1.051	0.68	0.446
LACM163884	1.75	0.774	1.386	0.89	0.65
LACM130787	1.466	0.754	1.17	0.771	0.571
LACM166679	0.979	0.506	0.652	0.504	0.338
UF99219	1.338	0.676	1.056	0.81	0.56
CNHM 134594	0.901	0.586	0.68	0.556	0.518
CAS100684	0.865	0.565	0.633	0.56	0.41
CNHM 236132	1.638	1.121	1.101	1.084	1.06
USNM249742	0.869	0.502	0.657	0.628	0.428
R14866	0.98	0.594	0.657	0.544	0.444
R156826	0.93	0.527	0.568	0.462	0.391
R19862	0.588	0.35	0.374	0.31	0.268
R24638	0.98	0.536	0.626	0.522	0.431
R24729	1.038	0.572	0.715	0.594	0.462
R9333	1.053	0.564	0.782	0.544	0.487
R9411	0.948	0.52	0.668	0.566	0.394
WAMR 24144	1.051	0.577	0.718	0.521	0.449
R12717B	0.567	0.316	0.376	0.311	0.27
R1279a	1.092	0.612	0.834	0.612	0.5
R143878E	0.663	0.37	0.486	0.395	0.34
R1787	1.186	0.65	0.927	0.675	0.547
R9301	0.982	0.549	0.66	0.564	0.446
R9302	0.978	0.562	0.69	0.504	0.45
UF99209	1.764	0.97	1.505	1.141	0.974
MCB191	1.768	0.974	1.437	0.955	0.704
MCB56	1.494	0.8	1.068	0.79	0.503
MCB57	1.868	0.837	1.455	1.067	0.743
MCB59	1.9	0.846	1.524	1.173	0.723
MCB60	1.597	0.87	1.284	0.858	0.648
MCB63	1.468	0.728	1.098	0.842	0.657
MCB64	1.58	0.858	1.133	0.882	0.648
MCB78	1.589	0.834	1.203	0.873	0.607
MCB84	1.71	0.89	1.384	0.864	0.7
MCB85	1.849	0.934	1.452	0.988	0.734
FB 1139	1.3	0.546	1.24	0.707	0.514
FB1230	1.873	0.911	1.586	1.01	0.786
FB6666	1.417	0.636	1.299	0.922	0.682
UCMP123070	1.387	0.715	1.143	0.818	0.628
LACM127239	0.463	0.222	0.39	0.304	0.2
USNM507550	1.2	0.713	0.836	0.822	0.602
USNM507551	1.096	0.684	0.776	0.722	0.543
CAS92966	1.264	0.625	1	0.97	0.624
CAS83885	0.467	0.286	0.374	0.268	0.222
REE2101	0.927	0.396	0.662	0.55	0.314
REE2103	0.882	0.356	0.596	0.479	0.295
REE2096	0.941	0.43	0.662	0.509	0.368
CAS50270	0.578	0.306	0.394	0.298	0.213

Accession #	Cranial Region Length	Orbit Length	Temporal Region Length	Rostral Region Length	Orbit Height
CNHM 12763	1.42	0.702	1.019	0.69	0.674
LACM166601	0.51	0.246	0.362	0.254	0.209
JIm 1465	1.216	0.648	0.954	0.758	0.562
USNM292407	0.998	0.57	0.741	0.641	0.522
CAS-nonumber	1.202	0.684	0.852	0.663	0.58
REE312	1.199	0.585	0.844	0.639	0.407
WBG09101	1.228	0.752	0.91	0.761	0.641
WBG09102	1.356	0.77	0.936	0.787	0.588
WBG09103	1.39	0.801	0.957	0.826	0.656
UF71580	0.742	0.371	0.538	0.375	0.33
CNHM 229940	0.654	0.432	0.487	0.348	0.331
CNHM 171520	1.252	0.743	0.893	0.74	0.645
CNHM 229939	1.086	0.688	0.647	0.6	0.537
UF61708	1.25	0.718	0.881	0.712	0.612
UF61710	1.345	0.837	0.984	0.832	0.737
CNHM 120270	1.18	0.766	0.735	0.72	0.606
CNHM 150823	1.18	0.766	0.839	0.77	0.648
CNHM 98525	0.722	0.41	0.478	0.4	0.321
LACM172703	1.292	0.72	0.858	0.718	0.62
LACM172704	1.134	0.676	0.832	0.672	0.572
UF99194	1.012	0.656	0.73	0.698	0.466
LACM163897	0.865	0.377	0.738	0.448	0.358
UCMVZ191063	0.79	0.384	0.608	0.36	0.56
UCMVZ191064	0.714	0.364	0.546	0.339	0.361
UCMVZ81319	0.989	0.479	0.877	0.484	0.463
UCMVZ116570	0.997	1.42	0.732	0.541	0.483
UCMVZ92988	0.685	0.351	0.557	0.402	0.316
CNHM 141550	0.65	0.19	0.466	0.366	0.251
FB6666	1.712	0.836	1.49	1.055	0.881
UCMP131083	2.336	1.088	1.913	1.493	1.17
UCMP140693	1.986	0.955	1.75	1.222	1.01
LACM127197	1.102	0.481	0.997	0.596	0.498
LACM130792	1.204	0.511	0.868	0.624	0.42
UCMVZ79249	0.9	0.351	0.72	0.499	0.36
UCMVZ95960	1.276	0.55	0.382	0.664	0.529
LACM127208	0.804	0.374	0.513	0.432	0.352
UF99701	0.664	0.365	0.405	0.338	0.294
REE692	0.759	0.358	0.511	0.461	0.264
REE819	0.758	0.334	0.522	0.348	0.246
REE1559	0.684	0.32	0.46	0.344	0.232
REE1600	0.82	0.378	0.612	0.41	0.302
REE1017	0.682	0.28	0.458	0.323	0.197
REE1053	0.776	0.345	0.504	0.334	0.218
UCMVZ175940	0.554	0.243	0.422	0.361	0.235
LACM127209	0.68	0.344	0.718	0.552	0.387
LACM127210	0.47	0.247	0.36	0.271	0.222
UF13010-1	0.766	0.376	0.568	0.428	0.337

Accession #	Cranial Region Length	Orbit Length	Temporal Region Length	Rostral Region Length	Orbit Height
UF130111-2	0.83	0.44	0.605	0.459	0.341
USNM332755	0.79	0.406	0.558	0.449	0.341
REE1331	1.388	0.81	0.911	0.756	0.585
UF11817	0.676	0.442	0.527	0.41	0.36
UF14279	1.374	0.78	0.965	0.784	0.682
UF42388	1.301	0.753	0.969	0.765	0.61
UF99700	1.092	0.632	0.764	0.668	0.518
USNM009242	1.594	0.844	1.162	0.952	0.672
USNM217505	1.034	0.528	0.75	0.675	0.446
REE1148	0.75	0.354	0.528	0.33	0.272
REE1236	0.692	0.31	0.444	0.329	0.2
USNM17851	0.761	0.455	0.535	0.43	0.388
USNM17852	0.74	0.409	0.518	0.412	0.38
USNM17853	0.772	0.418	0.514	0.407	0.37
FB609	1.224	0.579	0.963	0.798	0.614
USNM220269	1.242	0.647	0.898	0.698	0.574
JIm 1616	0.742	0.368	0.53	0.412	0.349
LACM136234	0.952	0.39	0.67	0.468	0.37
REE1293	0.782	0.34	0.498	0.401	0.248
REE856	0.795	0.426	0.49	0.407	0.294
REE1362	1.416	0.626	0.936	0.722	0.484
UCMVZ58177	0.751	0.36	0.51	0.454	0.304
UCMVZ58200	0.986	0.509	0.729	0.576	0.41
UCMVZ64199	0.964	0.472	0.676	0.554	0.425
UCMVZ64200	1.1	0.589	0.94	0.66	0.531
UCMVZ64201	0.77	0.37	0.507	0.436	0.308
UCMVZ64202	1.224	0.608	0.974	0.706	0.56
UCMVZ78204	0.962	0.45	0.684	0.54	0.398
UCMVZ78205	0.846	0.416	0.623	0.502	0.36
UCMVZ79241	1.047	0.464	0.788	0.658	0.45
UCMVZ79242	0.794	0.638	0.586	0.448	0.378
UCMP118717	1.274	0.643	0.978	0.79	0.586
UCMVZ137649	1.538	0.821	1.22	0.937	0.714
UCMVZ137633	1.116	0.59	0.803	0.717	0.556
UCMVZ79243	1.2	0.627	0.89	0.692	0.572
REE128	1.439	0.71	1.007	0.758	0.534
CAS_no #	1.773	0.903	1.498	1.168	0.908
UCMVZ58178	0.86	0.393	0.646	0.517	0.37
UCMVZ64197	0.925	0.394	0.675	0.511	0.38
UCMVZ64198	0.821	0.35	0.593	0.447	0.338
UCMVZ78202	0.85	0.439	0.614	0.5	0.4
UCMVZ78203	0.84	0.34	0.659	0.491	0.368
UCMVZ79085	0.927	0.41	0.682	0.512	0.396
UCMVZ79303	0.789	0.357	0.556	0.428	0.361
UCMVZ79304	0.825	0.39	0.612	0.467	0.343
MCB128	0.894	0.403	0.575	0.472	0.296

Accession #	Cranial Region Length	Orbit Length	Temporal Region Length	Rostral Region Length	Orbit Height
MCB132	0.726	0.304	0.504	0.396	0.262
MCB156	0.592	0.254	0.414	0.298	0.194
CAS25035	0.523	0.303	0.361	0.265	0.239
CAS96400	0.6	0.378	0.417	0.311	0.276
UCMP140676	1.153	0.604	0.817	0.896	0.604
UCMVZ128951	2.043	1.292	1.556	1.181	1.104
UCMVZ129983	1.194	0.588	0.88	0.924	0.61
UF67798	1.078	0.627	0.714	0.866	0.531
UF99577	0.969	0.538	0.65	0.738	0.571
UCMP137844	2.782	1.341	2.433	1.719	1.405
UF45647	2.708	1.384	2.37	1.839	1.484
CNHM 22498	2.49	1.283	2.119	1.639	1.498
CNHM 23149	2.427	1.092	2.226	1.774	1.511
CNHM 22361	2.252	1.278	2.13	1.46	1.339
CNHM 22442	2.878	1.388	2.617	2	1.594
CNHM 22470	2.924	1.63	2.756	1.901	1.837
CNHM 22490	2.584	1.474	2.382	1.795	1.731
CNHM 31353	2.62	1.172	2.602	1.945	1.734
UF99164	2.787	1.494	2.6	1.762	1.721
CNHM 22091	3.051	1.357	2.755	1.974	1.488
CNHM 22092	2.631	1.262	2.365	1.784	1.298
CNHM 22779	2.36	1.181	2.077	1.572	1.28
CNHM 229975	2.585	1.353	2.497	2.394	1.634
CNHM 51702	3.081	1.558	2.666	2.03	1.47
CNHM 51710	3.022	1.414	2.52	1.828	1.346
CNHM 57520	2.747	1.316	2.581	1.765	1.3
CNHM 73343	2.4	1.094	2.3	1.562	1.402
REE1833	1.83	0.893	1.652	1.26	0.868
REE487	2.989	1.467	2.61	1.825	1.146
CAS94010	0.746	0.409	0.612	0.34	0.345
CNHM 145993	1.189	0.73	0.949	0.651	0.652
CAS62004	1.151	0.732	0.845	0.543	0.578
UCMP137865	2.252	1.458	1.66	1.817	1.478
UCMP140937	1.586	1.106	1.102	1.244	0.97
LACM76850	2.514	1.61	1.75	2.008	1.35
UF50670	2.976	1.914	2.21	2.552	1.806

Accession #	Quadrate Length	Maximum Skull Depth	Width at Jugals	Jaw Ramus Length	Coronoid Height
Jim 0920	0.262	0.532	0.61	1.425	0.356
UCMP123066	0.802	1.905	2.154	5.727	1.258
UCMP137832	0.287	0.444	0.605	1.2	0.219
UCMVZ204290	0.233	0.376	0.533	1.163	0.197
UCMVZ33828	0.164	0.31	0.427	0.924	0.169
UCMVZ69473	0.141	0.273	0.366	0.74	0.148
LACM127179	0.432	0.633	0.844	1.914	0.349
LACM127180	0.526	0.87	1.087	2.216	0.41
LACM127183	0.439	0.678	0.919	1.896	0.387
LACM127184	0.342	0.408	0.667	1.32	0.268
USNM305967	0.261	0.358	0.624	1.123	0.24
UCMP141140	0.6	1.142	1.7	3.463	0.731
UCMP141141	0.624	1.066	1.631	3.341	0.707
USNM323689	0.339	0.46	0.685	1.331	0.218
CAS100777	0.336	0.488	0.746	1.318	0.21
UF56315	1.068	1.73	2.99	5.287	1.062
LACM127198	0.198	0.303	0.431	0.856	0.178
LACM127199	0.188	0.313	0.448	0.895	0.173
CNHM 154619	0.352	0.6	0.774	0.61	0.372
CNHM 167941	0.358	0.665	0.827	1.739	0.394
USNM313453	0.394	0.638	0.9	1.784	0.409
LACM132298	0.473	0.994	1.334	2.93	0.627
LACM132302	0.486	0.976	1.354	2.924	0.625
LACM132303	0.6	1.194	1.526	3.251	0.797
LACM132307	0.42	0.823	1.089	2.46	0.501
LACM132375	0.36	0.535	0.802	1.718	0.283
LACM132375	0.402	0.796	1.092	2.292	0.47
UCMP118925	0.4	0.774	1.04	2.27	0.438
CNHM 257163	1.229	1.806	2.915	4.462	1.248
LACM137467	1.325	2.012	3.282	4.858	1.406
UCMP137850	1.259	2.03	3.347	4.937	1.421
UF70431	1.403	2.224	3.427	5.358	1.44
UF75985	1.41	1.993	3.235	5.038	1.348
UF87979	1.292	1.985	3.21	1.894	1.416
CAS47453	0.188	0.28	0.426	0.867	0.114
WAMR 50361	0.488	0.717	1.001	2.053	0.418
WAMR 50689	0.539	0.807	1.102	2.216	0.486
CNHM 31041	1.026	1.624	2.368	4.276	0.927
UCMP138689	1.33	2.138	2.673	5.448	1.165
CNHM 51707	0.924	1.434	2.131	3.799	0.841
UCMVZ39254	0.469	0.686	0.949	2.02	0.422
UCMVZ62154	0.44	0.6	0.874	1.778	0.391
LACM127194	0.268	0.319	0.532	1.08	0.172
LACM127195	0.484	0.776	1.112	2.21	0.422
LACM127196	0.5	0.78	1.126	2.283	0.475

Accession #	Quadrate Length	Maximum Skull Depth	Width at Jugals	Jaw Ramus Length	Coronoid Height
LACM159075	0.494	0.642	1.106	2.198	0.452
LACM163884	0.602	0.858	1.318	2.754	0.498
LACM130787	0.552	0.704	1.176	2.433	0.511
LACM166679	0.328	0.475	0.724	1.49	0.242
UF99219	0.491	0.67	1.061	2.263	0.454
CNHM 134594	0.414	0.614	0.89	1.656	0.296
CAS100684	0.365	0.478	0.786	1.602	0.249
CNHM 236132	0.709	1.179	1.686	3.067	0.606
USNM249742	0.351	0.561	0.78	1.728	0.25
R14866	0.36	0.63	0.871	1.65	0.339
R156826	0.332	0.496	0.77	1.412	0.283
R19862	0.224	0.303	0.444	0.9	0.169
R24638	0.38	0.606	0.822	1.662	0.31
R24729	0.374	0.659	0.898	1.788	0.335
R9333	0.412	0.624	0.928	1.73	0.338
R9411	0.376	0.626	0.866	1.609	0.322
WAMR 24144	0.403	0.617	0.945	0.682	0.35
R12717B	0.272	0.295	0.472	0.902	0.164
R1279a	0.41	0.694	1.01	1.856	0.376
R143878E	0.254	0.455	0.59	1.152	0.202
R1787	0.46	0.8	1.156	2.014	0.426
R9301	0.368	0.582	0.882	1.682	0.351
R9302	0.376	0.61	0.852	1.574	0.33
UF99209	0.76	1.308	1.355	3.326	0.911
MCB191	0.713	1.134	1.617	3.084	0.776
MCB56	0.592	0.839	1.275	2.472	0.562
MCB57	0.724	1.188	1.608	3.162	0.726
MCB59	0.735	1.178	1.688	3.259	0.834
MCB60	0.632	1.103	1.507	2.736	0.68
MCB63	0.552	0.892	1.318	2.474	0.572
MCB64	0.648	0.983	1.424	2.728	0.671
MCB78	0.649	0.98	1.33	2.758	0.645
MCB84	0.614	0.949	1.371	2.774	0.576
MCB85	0.668	1.177	1.586	3.073	0.815
FB 1139	0.453	0.652	1.155	2.231	0.399
FB1230	0.743	1.044	1.574	3.322	0.735
FB6666	0.544	0.9	1.248	2.35	0.538
UCMP123070	0.552	0.8	0.739	2.472	0.452
LACM127239	0.202	0.266	0.43	0.812	0.177
USNM507550	0.456	0.79	1.114	2.314	0.406
USNM507551	0.411	0.692	1.063	2.148	0.368
CAS92966	0.478	0.869	1.312	2.557	0.479
CAS83885	0.234	0.298	0.474	0.81	0.126
REE2101	0.324	0.482	0.733	1.522	0.29
REE2103	0.302	0.416	0.677	1.314	0.223
REE2096	0.384	0.463	0.772	1.51	0.281

Accession #	Quadrate Length	Maximum Skull Depth	Width at Jugals	Jaw Ramus Length	Coronoid Height
CAS50270	0.222	0.272	0.446	0.886	0.148
CNHM 12763	0.576	0.84	1.275	2.14	0.477
LACM166601	0.219	0.266	0.385	0.763	0.116
JIm 1465	0.448	0.679	1.086	2.11	0.378
USNM292407	0.412	0.576	0.954	1.842	0.341
CAS-nonumber	0.485	0.702	1.075	1.919	0.464
REE312	0.424	0.695	0.992	1.956	0.368
WBG09101	0.478	0.777	1.226	2.304	0.41
WBG09102	0.461	0.756	1.26	2.363	0.413
WBG09103	0.465	0.838	1.261	2.4	0.43
UF71580	0.296	0.38	0.654	1.122	0.194
CNHM 229940	0.304	0.382	0.604	1.146	0.164
CNHM 171520	0.515	0.776	1.194	2.256	0.448
CNHM 229939	0.446	0.612	0.944	1.891	0.316
UF61708	0.482	0.843	1.26	2.248	0.4
UF61710	0.54	0.908	1.41	2.6	0.465
CNHM 120270	0.451	0.764	1.171	2.186	0.384
CNHM 150823	0.5	0.802	1.303	2.267	0.384
CNHM 98525	0.322	0.412	0.643	1.24	0.212
LACM172703	0.512	0.767	1.18	1.238	0.412
LACM172704	0.446	0.716	1.13	2.071	0.372
UF99194	0.351	0.564	0.972	1.916	0.35
LACM163897	0.336	0.49	0.721	1.398	0.247
UCMVZ191063	0.302	0.451	0.676	1.261	0.246
UCMVZ191064	0.284	0.448	0.647	1.166	0.23
UCMVZ81319	0.398	0.585	0.836	1.685	0.327
UCMVZ116570	0.315	0.565	0.786	1.509	0.262
UCMVZ92988	0.232	0.374	0.45	1.27	0.225
CNHM 141550	0.184	0.352	0.46	0.885	0.176
FB6666	0.588	1.001	1.274	3.024	0.623
UCMP131083	0.675	1.38	1.822	3.898	0.723
UCMP140693	0.643	1.3	1.69	3.361	0.59
LACM127197	0.387	0.61	0.767	1.844	0.341
LACM130792	0.36	0.58	0.775	1.772	0.337
UCMVZ79249	0.305	0.459	0.6	1.402	0.251
UCMVZ95960	0.395	0.656	0.914	2.023	0.398
LACM127208	0.332	0.414	0.632	1.224	0.225
UF99701	0.23	0.34	0.59	0.956	0.18
REE692	0.252	0.36	0.626	1.19	0.16
REE819	0.222	0.36	0.586	1.088	0.189
REE1559	0.22	0.345	0.551	1.031	0.16
REE1600	0.247	0.436	0.66	1.313	0.204
REE1017	0.204	0.299	0.472	0.93	0.155
REE1053	0.202	0.311	0.584	1.086	0.186
UCMVZ175940	0.164	0.313	0.5	0.954	0.172
LACM127209	0.307	0.412	0.8	1.463	0.248

Accession #	Quadrate Length	Maximum Skull Depth	Width at Jugals	Jaw Ramus Length	Coronoid Height
LACM127210	0.198	0.278	0.412	0.795	0.132
UF13010-1	0.274	0.419	0.618	1.212	0.21
UF130111-2	0.28	0.435	0.731	1.362	0.254
USNM332755	0.273	0.431	0.708	1.276	0.236
REE1331	0.494	0.803	1.212	2.32	0.413
UF11817	0.262	0.468	0.64	1.202	0.219
UF14279	0.457	0.836	1.387	2.35	0.521
UF42388	0.453	0.762	1.283	2.29	0.471
UF99700	0.374	0.614	1.053	1.88	0.385
USNM009242	0.477	0.907	1.587	2.746	0.526
USNM217505	0.361	0.56	0.866	1.848	0.351
REE1148	0.224	0.366	0.586	1.112	0.204
REE1236	0.228	0.324	0.501	0.968	0.176
USNM17851	0.248	0.478	0.732	1.253	0.228
USNM17852	0.254	0.442	0.675	1.211	0.226
USNM17853	0.224	0.387	0.604	1.191	0.221
FB609	0.51	0.826	1.177	1.5	0.469
USNM220269	0.448	0.76	1.137	1.975	0.435
JIm 1616	0.272	0.428	0.658	1.201	0.223
LACM136234	0.313	0.48	0.758	1.401	0.252
REE1293	0.238	0.362	0.589	1.126	0.172
REE856	0.249	0.388	0.612	1.174	0.21
REE1362	0.367	0.728	1.231	1.193	0.476
UCMVZ58177	0.264	0.382	0.635	1.123	0.214
UCMVZ58200	0.324	0.525	0.902	1.636	0.306
UCMVZ64199	0.342	0.552	0.831	1.573	0.3
UCMVZ64200	0.404	0.717	1.13	2.079	0.392
UCMVZ64201	0.298	0.379	0.63	1.162	0.228
UCMVZ64202	0.388	0.792	1.142	2.193	0.444
UCMVZ78204	0.319	0.556	0.854	1.585	0.314
UCMVZ78205	0.292	0.514	0.772	1.433	0.286
UCMVZ79241	0.351	0.638	0.96	1.767	0.337
UCMVZ79242	0.28	0.451	0.714	1.32	0.248
UCMP118717	0.397	0.794	1.269	2.241	0.495
UCMVZ137649	0.514	0.965	1.558	2.838	0.543
UCMVZ137633	0.42	0.661	1.11	1.963	0.412
UCMVZ79243	0.416	0.738	1.116	2.044	0.44
REE128	0.448	0.81	1.362	2.271	0.524
CAS_no_#	0.709	1.29	1.724	3.321	0.914
UCMVZ58178	0.272	0.468	0.721	1.394	0.259
UCMVZ64197	0.296	0.495	0.803	1.439	0.27
UCMVZ64198	0.263	0.41	0.63	1.251	0.227
UCMVZ78202	0.288	0.472	0.757	1.323	0.262
UCMVZ78203	0.26	0.465	0.702	1.31	0.228
UCMVZ79085	0.28	0.55	0.928	1.485	0.302
UCMVZ79303	0.25	0.448	0.736	1.238	0.23

Accession #	Quadrate Length	Maximum Skull Depth	Width at Jugals	Jaw Ramus Length	Coronoid Height
UCMVZ79304	0.261	0.447	0.736	1.35	0.256
MCB128	0.267	0.455	0.708	1.308	0.234
MCB132	0.18	0.398	0.592	1.17	0.214
MCB156	0.2	0.292	0.47	0.852	0.154
CAS25035	0.238	0.288	0.45	0.836	0.121
CAS96400	0.256	0.323	0.446	0.947	0.161
UCMP140676	0.472	0.808	1.107	2.152	0.524
UCMVZ128951	0.832	1.323	3.334	3.67	0.87
UCMVZ129983	0.49	0.849	1.11	2.173	0.54
UF67798	0.431	0.727	1	1.998	0.468
UF99577	0.417	0.672	0.89	1.823	0.442
UCMP137844	1.313	2.09	2.766	4.95	1.026
UF45647	1.266	2.207	3.264	5.051	1.132
CNHM 22498	1.023	1.992	2.972	4.482	1.035
CNHM 23149	1.074	2.041	3.05	4.616	1.022
CNHM 22361	0.935	1.918	3.035	4.322	1.008
CNHM 22442	1.133	2.129	2.124	5.4	1.201
CNHM 22470	1.266	2.542	3.873	5.694	1.252
CNHM 22490	1.132	2.285	3.167	5.238	1.142
CNHM 31353	1.206	2.329	3.273	5.436	1.111
UF99164	1.274	2.304	3.036	5.438	1.098
CNHM 22091	1.172	2.092	3.28	5.4	1.021
CNHM 22092	1.112	1.795	3.046	5.034	1.004
CNHM 22779	1	1.096	2.531	4.494	0.906
CNHM 229975	1.045	2.154	3.37	5.151	1.053
CNHM 51702	1.295	2.02	3.185	5.728	1.1
CNHM 51710	1.192	2.002	3.021	5.434	1.062
CNHM 57520	1.162	2.073	2.836	5.207	1.04
CNHM 73343	1.076	1.98	2.864	4.486	0.995
REE1833	0.803	1.37	1.744	3.396	0.778
REE487	1.252	1.782	1.862	5.29	1.036
CAS94010	0.284	0.438	0.723	1.216	0.278
CNHM 145993	0.513	0.808	1.067	2.242	0.433
CAS62004	0.45	0.755	1.071	1.912	0.389
UCMP137865	0.914	1.577	2.341	4.932	1.074
UCMP140937	0.651	1.092	1.106	3.247	0.602
LACM76850	0.9	1.824	2.534	5.432	1.048
UF50670	1.2	2.101	3.101	6.943	1.403

VITA

WILLIAM B. GELNAW

- Personal Data: Date of Birth: August 28, 1983
- Place of Birth: Lomita, California
- Marital Status: Single
- Education: Public Schools, Orange County, California
- B.Sc. with honors in Paleontology, University of Alberta,
Edmonton, Alberta 2005.
- M.S. Biology, East Tennessee State
University, Johnson City, Tennessee 2011
- Professional Experience: Educational Interpreter, Royal Tyrrell Museum of
Paleontology, Drumheller, Alberta
- Educational Interpreter, Mammoth Site of Hot Springs
South Dakota, Hot Springs, South Dakota. 2004
- Collections Assistant, University of Alberta Museums,
Edmonton, Alberta. 2005.
- Paleontologist, SWCA Inc., Pasadena, California; Vernal,
Utah; and Denver, Colorado. 2005-2008.
- Graduate Assistant, East Tennessee State University,
Johnson City, Tennessee 2008-2010
- Conference Abstracts: Gelnow, W., and Mead, J. 2010. The first characters
useful for identifying fossil scolecophidian
vertebrae to the family level. Society of
Vertebrate paleontology 70th Anniversary
Meeting Program and Abstracts.